



**HAL**  
open science

# Apport de l'imagerie TDM et IRM quantitative à l'étude des modifications structurales et fonctionnelles respiratoires dans les maladies obstructives chroniques des voies aériennes chez l'homme

Ilyes Benlala

► **To cite this version:**

Ilyes Benlala. Apport de l'imagerie TDM et IRM quantitative à l'étude des modifications structurales et fonctionnelles respiratoires dans les maladies obstructives chroniques des voies aériennes chez l'homme. Médecine humaine et pathologie. Université de Bordeaux, 2019. Français. NNT : 2019BORD0291 . tel-03048828

**HAL Id: tel-03048828**

**<https://theses.hal.science/tel-03048828>**

Submitted on 9 Dec 2020

**HAL** is a multi-disciplinary open access archive for the deposit and dissemination of scientific research documents, whether they are published or not. The documents may come from teaching and research institutions in France or abroad, or from public or private research centers.

L'archive ouverte pluridisciplinaire **HAL**, est destinée au dépôt et à la diffusion de documents scientifiques de niveau recherche, publiés ou non, émanant des établissements d'enseignement et de recherche français ou étrangers, des laboratoires publics ou privés.

THÈSE PRÉSENTÉE  
POUR OBTENIR LE GRADE DE  
**DOCTEUR DE**  
**L'UNIVERSITÉ DE BORDEAUX**

ÉCOLE DOCTORALE SCIENCES DE LA VIE ET DE LA SANTÉ  
SPÉCIALITÉ BIOIMAGERIE

Par Ilyes BENLALA

**Apport de l'imagerie TDM et IRM quantitative à l'étude des  
modifications structurales et fonctionnelles respiratoires dans les  
maladies obstructives chroniques des voies aériennes chez  
l'homme**

Sous la direction de : François LAURENT  
(Co-directeur : Gaël DOURNES)

Soutenue le 03 Décembre 2019

Membres du jury :

M. FERRETTI, Gilbert

M. BOURDIN, Arnaud

M. PADOVANI, Bernard

Mme. BORDENAVE, Laurence

M. BERGER, Patrick

M. LAURENT, François

PU-PH, Université de Grenoble

PU-PH, Université de Montpellier

PU-PH, Université de Nice

PU-PH, Université de Bordeaux

PU-PH, Université de Bordeaux

PU-PH, Université de Bordeaux

Président/Rapporteur

Rapporteur

Examineur

Examineur

Invité

Directeur de thèse

## **Apport de l'imagerie TDM et IRM quantitative à l'étude des modifications structurales et fonctionnelles respiratoires dans les maladies obstructives chroniques des voies aériennes chez l'homme**

**Résumé :** Les maladies bronchiques obstructives chroniques constituent un problème majeur de santé publique. Leur pathogénie est caractérisée par l'inflammation chronique et le remodelage des voies aériennes. L'étude en imagerie des différents éléments structuraux des poumons (bronches, bronchioles, vaisseaux...) est primordiale dans la définition, le phénotypage, la compréhension des mécanismes obstructifs et le suivi de l'évolution et de ces maladies. Les méthodes d'évaluation visuelles qualitatives sont sujettes à une subjectivité d'analyse et à une variabilité inter observateurs qui altèrent leur fiabilité. Le développement de nouvelles méthodes quantitatives fiables et reproductibles est donc une nécessité. La TDM et l'IRM sont les deux méthodes d'imagerie complètes à la fois des différents compartiments structuraux et fonctionnels du poumon, la première ayant pour avantage son excellente résolution spatiale et la seconde son innocuité. Les travaux ont porté sur la mise au point et la validation de méthodes d'imagerie quantitatives TDM et IRM.

Avec la TDM quantitative, nous avons montré que les mesures du remodelage bronchique et vasculaire chez les patients atteints d'une hypertension pulmonaire (HTP) sévère, phénotype particulier à la bronchopneumopathie chronique obstructive (BPCO), permettaient d'appréhender les interactions entre les systèmes cardiovasculaire et respiratoire. D'autre part nous avons mis au point et évalué une méthode de quantification de l'atteinte des voies aériennes distales dans une population de pneumonie chronique d'hypersensibilité. Cette méthode pourrait apporter une contribution à l'étude et au suivi des maladies bronchiques obstructives chroniques.

Avec l'IRM quantitative, les solutions que nous avons proposées dans la quantification de l'emphysème à l'IRM protonique permettent une analyse automatisée de la sévérité de l'extension de l'emphysème chez des patients atteints de BPCO. En outre, la transposition des méthodes de mesure des paramètres bronchiques de la TDM à l'IRM est devenue possible grâce aux nouvelles séquences à temps d'écho ultra court (UTE). Ainsi, la quantification du remodelage bronchique à l'IRM 3DUTE chez des patients atteints de mucoviscidose, chez lesquels il est nécessaire de réduire l'exposition aux rayons ionisants, permet d'obtenir des informations morphologiques similaires à celles de la TDM. Nous avons aussi montré que la quantification automatique des phénomènes destructifs et inflammatoires par l'IRM 3DUTE dans l'atteinte pulmonaire de la mucoviscidose était une méthode fiable et reproductible pour évaluer la sévérité de l'atteinte structurale. Par ailleurs, la faisabilité d'une quantification automatique des hypersignaux T2 à l'IRM a été démontrée et sa pertinence comme biomarqueur spécifique de l'atteinte inflammatoire des voies aériennes évaluée.

Ainsi, l'étude quantitative, en TDM comme en IRM, de diverses modifications structurales et fonctionnelles des maladies bronchiques obstructives chroniques ouvre le champ d'une analyse objective et fiable par l'imagerie aux

évaluations du suivi et de la réponse au traitement.

**Mots clés :** *TDM, IRM, quantification automatique, poumon, bronche, remodelage, BPCO, asthme, mucoviscidose*

---

## **Contribution of quantitative CT and MRI to the study of structural and functional respiratory changes in chronic obstructive airway diseases in humans**

**Abstract:** Chronic obstructive airway diseases are a major public health problem, characterized by chronic inflammation and airways remodeling. Imaging of the structural elements of the lungs (bronchi, bronchioles, vessels...) is essential for defining, phenotyping and following-up these diseases. Visual assessment is prone to inter-observer variability that affects its reliability. Therefore, the development of reliable and reproducible new quantitative methods is necessary. CT and MRI are the two complete imaging methods of the various structural and functional compartments of the lung. This work focused on the development and the validation of quantitative methods using CT and MRI of the lung.

Using quantitative CT, we have shown that measurements of bronchial and vascular remodeling in patients with severe pulmonary hypertension (PH), a particular phenotype in COPD patients, contributed to highlight interactions between the cardiovascular and respiratory systems. We have developed a method for small airway disease quantification, tested in a chronic hypersensitivity pneumonitis cohort, that may contribute to evaluate and monitor chronic obstructive airway diseases.

Using quantitative MRI, we have developed a fully automated quantification technique to assess the severity of emphysema extent in COPD patients. In addition, transposing bronchial measurement methods from CT to MRI has become possible thanks to the new ultra short echo time (UTE) sequences. Thus, the quantification of bronchial remodeling at 3DUTE MRI in patients with cystic fibrosis, for whom it is necessary to reduce exposure to ionizing radiation, has shown morphological information similar to that of CT. We have also shown that automatic quantification of destructive and inflammatory phenomena by 3DUTE MRI in cystic fibrosis is a reliable and reproducible method for assessing the severity of structural alterations. Furthermore, the feasibility of an automatic quantification of T2 high signal intensity on MRI has been demonstrated and its relevance as a specific biomarker for inflammatory airway disease has been assessed.

Thus, the quantitative analysis, in both CT and MRI, of various structural and functional modifications in chronic obstructive airway diseases could be a reliable method in the follow-up and the evaluation of the response to treatment in these diseases.

**Keywords:** *CT, MRI, automatic quantification, lung, bronchus, remodeling, COPD, asthma, cystic fibrosis*

---

### **Unité de recherche**

## **Remerciements**

### **À mes rapporteurs de thèse**

#### **Monsieur le Professeur Gilbert Ferretti**

Professeur des Universités

Praticien Hospitalier

Vous me faites l'honneur de présider le jury de cette thèse. Vos qualités professionnelles sont reconnues. Soyez assuré de mon profond respect et de mes remerciements les plus sincères.

#### **Monsieur le Professeur Arnaud Bourdin**

Professeur des Universités

Praticien Hospitalier

Je vous remercie d'avoir accepté d'être le rapporteur de cette thèse et d'être membre du jury. C'est un honneur de pouvoir vous compter parmi les membres de ce jury.

### **À mes juges**

#### **Monsieur le Professeur Bernard Padovani**

Professeur des Universités

Praticien Hospitalier

Je vous remercie d'avoir accepté de faire partie de mon jury. Je suis honoré de l'intérêt que vous portez à mon travail. Soyez assuré de mon profond respect et de ma sincère gratitude.

#### **Madame le Professeur Laurence Bordenave**

Professeur des Universités

Praticien Hospitalier

Je vous remercie de l'honneur que vous me faites en acceptant de juger cette thèse, ainsi que de votre intérêt pour mon travail. Soyez assurée de mon profond respect et de mes remerciements les plus sincères.

**Monsieur le Professeur Patrick Berger**

Professeur des Universités

Praticien Hospitalier

Je vous remercie sincèrement de m’ avoir accepté dans votre équipe. Vos indications et vos conseils judicieux ont contribué à alimenter mes réflexions. C’est un honneur de pouvoir travailler avec vous et de pouvoir vous compter parmi les membres de ce jury.

**À mes directeurs de thèse**

**Monsieur le Professeur François Laurent**

Professeur des Universités

Praticien Hospitalier

Je ne vous remercierai jamais assez de m’ avoir accompagné tout au long de mon cursus de recherche. Vous m’ avez proposé un sujet de stage pour mon Master qui m’ a mis le pied à l’ étrier et vous me faites l’ honneur de m’ encadrer dans ces travaux de thèse. Vous m’ avez dirigé avec un parfait équilibre entre confiance et encadrement attentif. Grace à vos idées pertinentes et vos brillantes intuitions, j’ ai pu me focaliser et prioriser nos travaux de recherche quand je m’ éparpillais dans tous les sens. Je vous remercie pour votre gentillesse, votre disponibilité permanente et vos nombreux encouragements.

**Monsieur le Docteur Gaël Dournes**

Maître de conférences des Universités

Praticien Hospitalier

Tu m’ as encadré lors de mon Master et tu codiriges cette thèse avec toujours autant d’ implication. C’est un plaisir de travailler avec toi. Ton intelligence et tes capacités de travail sont admirables (Je me souviens des quatre versions différentes du papier en une nuit). Nos longues conversations téléphoniques (qui ne risquent pas de s’ écourter maintenant que tu es aux États-Unis) ont permis d’ enrichir nos discussions scientifiques et de surmonter tant de problèmes techniques. Je te remercie pour tes conseils judicieux, ta disponibilité et tes encouragements.

À tous ceux qui ont apporté leur concours à la réalisation de ces travaux : Florence Coste, Fabien Baldacci, John Refait, Adrien Rispal, François Hocke, Cedric Leung, Shafey Elahee, Julie Macey.

À mes parents, à mon frère et à ma sœur, merci de votre attention et de votre soutien, vous m'avez permis de mener à bien ces longues études.

À ma femme Narimane, merci de ta présence au quotidien, de tes soins et de tes encouragements. À tes côtés tout devient plus facile.

# Table des matières

Liste des abréviations.....	5
Liste des publications et communications .....	6
INTRODUCTION.....	8
1. Etat de l'art.....	12
1.1 TDM quantitative dans les maladies obstructives chroniques des voies aériennes.....	13
1.2 IRM protonique quantitative dans les maladies obstructives chroniques des voies aériennes .....	31
2. Contribution à la TDM quantitative des maladies obstructives chroniques des voies aériennes.....	36
2.1 Publication n°1 : Evaluation quantitative du remodelage bronchique et vasculaire chez les patients atteints d'hypertension pulmonaire sévère secondaire à la BPCO.....	37
2.2 Publication n°2 : Développement d'une méthode semi-automatique pour la quantification de l'atteinte des voies aériennes distales.....	65
3. Contribution à l'IRM quantitative des maladies obstructives chroniques des voies aériennes.....	86
3.1 Publication n°3 : Comparaison d'un motif spiralé et d'un motif sphérique d'acquisition de l'espace de Fourier en IRM 3D à temps d'écho ultracourt.....	87
3.2 Publication n°4 : Quantification volumétrique automatique de la sévérité de l'emphysème à l'IRM à temps d'écho ultra court chez des patients atteints de BPCO.....	109
3.3 Publication n°5 : Quantification du remodelage bronchique à l'IRM 3D UTE chez des patients atteint de mucoviscidose.....	129
3.4 Publication n°6 : Evaluation de la quantification des hyper et hypo signaux en IRM 3DUTE comme marqueurs de la sévérité de l'atteinte pulmonaire dans la mucoviscidose ...	151
3.5 Publication n°7 : Quantification de l'atteinte inflammatoire des voies aériennes dans la mucoviscidose à l'aide de séquence IRM T2 Mapping .....	184
DISCUSSION ET PERSPECTIVES .....	207
CONCLUSION.....	215
REFERENCES .....	217

## Liste des abréviations

BPCO : Broncho-pneumopathie chronique obstructive

EFR : Explorations fonctionnelles respiratoires

GOLD : Global initiative for obstructive lung disease

HTAP : Hypertension artérielle pulmonaire

HTP : Hypertension pulmonaire

IRM : Imagerie par résonance magnétique

PETRA : Pointwise encoding time reduction with radial acquisition

PHS : Pneumopathie d'hypersensibilité

PIC : Pneumopathie interstitielle commune

PINS : Pneumopathie interstitielle non spécifique

TDM : Tomodensitométrie

UH : Unité Hounsfield

UTE : Ultra short echo time

VEMS : Volume expiratoire maximale en une seconde

## Liste des publications et communications

### Publications acceptées :

Benlala I, Hocke F, Macey J, Bui S, Berger P, Laurent F, Dournes G. Quantification of MRI T2 High Signal Volume in Cystic Fibrosis: a pilot study. Radiology 2019

Coste F\*, Benlala I\*, Dournes G, Berger P, Laurent F. Assessing pulmonary hypertension in COPD. Is there a role for computed tomography? Int J Chron Obstruct Pulmon Dis. 2019. \*co-premier auteur

Benlala I, Berger P, Girodet P.O, Dromer C, Macey J, Laurent F, Dournes G. Automated Volumetric Quantification of Emphysema Severity by Using Ultrashort Echo Time MRI: Validation in Participants with Chronic Obstructive Pulmonary Disease. Radiology 2019

Coste F\*, Benlala I\*, Dournes G, Baldacci F, Berger P, Laurent F. Quantitative CT assessment of bronchial and vascular alterations in severe precapillary pulmonary hypertension. Int J Chron Obstruct Pulmon Dis. 2019. \*co-premier auteur

Benlala I, Laurent F, Dournes G. T2 Weighted PROPELLER MRI is not suitable for pulmonary emphysema quantification. Rofo. 2018

Dournes G, Yazbek J, Benhassen W, Benlala I, Blanchard E, Macey J, Berger P, Laurent F. 3D ultrashort echo time MRI of the lung using stack-of-spirals and spherical k-Space coverages: Evaluation in healthy volunteers and parenchymal diseases. J Magn Reson Imaging 2018

### Article soumis :

Benlala I, Leung C, Point S, Raheison C, Berger P, Laurent F, Macey J, Dournes G. Automated quantification of high and low signal-intensity volumes using MRI with ultrashort echo times in cystic fibrosis: a cross-sectional and longitudinal study. Soumis à Eur Radiol

### Articles en cours de préparation :

Benlala I, Rispal A, Refait J, Begueret H, Berger P, Dournes G, Laurent F. Semi-Automated Quantification of Lobular Decreased Attenuation Areas Extent in patients with Chronic Hypersensitivity Pneumonitis. Soumission prévue à PLoS One

Elahee S, Baldacci F, Benlala I, Macey J, Bui S, Berger P, Laurent F, Dournes G. Quantitative measurements of bronchial dimensions using 3D-MRI with ultrashort echo times: a pilot study in cystic fibrosis. Soumission prévue à J Thorac Imaging

## **Communications :**

Benlala I, Dournes G, Laurent F. IRM pulmonaire : développement pour l'imagerie morphologique et fonctionnelle. JFR, Paris 2019

Benlala I, Leung C, Point S, Raheison C, Berger P, Laurent F, Macey J, Dournes G. Fully automated 3D quantification of "minus" and "plus" pathology in Cystic Fibrosis using 3D-UTE MRI: A validation study. JFR, Paris 2019

Benlala I, Berger P, Girodet PO, Dromer C, Macey J, Laurent F, Dournes G. Fully automated 3D quantification of the lung emphysema in COPD using 3D-UTE MRI. JFR, Paris 2019

Benlala I, Leung C, Point S, Raheison C, Berger P, Laurent F, Macey J, Dournes G. Fully automated 3D quantification of "minus" and "plus" pathology in Cystic Fibrosis using 3D-UTE MRI: A validation study. ESTI/Fleischner, Paris 2019

Benlala I, Berger P, Girodet PO, Dromer C, Macey J, Laurent F, Dournes G. Fully automated 3D quantification of the lung emphysema in COPD using 3D-UTE MRI. ECR, Vienne 2019

Benlala I, Dournes G, Laurent F. Imagerie des voies aériennes : principes d'interprétation et principales pathologies. JFR, Paris 2018

Benlala I, Coste F, Dournes G, Baldacci F, Berger P, Laurent F. Bronchial and vascular alterations in patients with severe pulmonary hypertension: Role of quantitative computed tomography. ESTI/ESCR, Genève 2018

## **Posters :**

Benlala I, Coste F, Dournes G, Baldacci F, Berger P, Laurent F. Quantitative CT assessment of bronchial and vascular alterations in severe precapillary pulmonary hypertension. Journée de l'école doctorale Sciences de la Vie et de la Santé, Talence 2019

Benlala I, Berger P, Girodet P.O, Dromer C, Macey J, Laurent F, Dournes G. Quantification automatique de l'emphysème chez les patients BPCO à l'aide d'IRM 3D-UTE. JFR, Paris 2019

## **Bourses et prix :**

Bourse de Recherche Alain Rahmouni SFR-CERF 2018. Phénotypage des patients atteints de BPCO par l'étude des modifications structurales et fonctionnelles quantifiées par l'imagerie TDM et IRM pulmonaire.

Bourse de Recherche Le nouveau Souffle 2019. Tomodensitométrie quantitative en double énergie dans l'hypertension pulmonaire.

Prix du Poster scientifique aux JFR 2019. Quantification automatique de l'emphysème chez les patients BPCO à l'aide d'IRM 3D-UTE.

# **INTRODUCTION**

L'inflammation et le remodelage des voies aériennes représentent des phénomènes importants dans la pathogénie des maladies bronchiques obstructives chroniques telles que la broncho-pneumopathie chronique obstructive (BPCO), l'asthme et la mucoviscidose. L'asthme et la BPCO sont des problèmes majeurs de santé publique dans la plupart des pays développés (1,2). La prévalence de la BPCO dans le monde est autour de 11% (3) et atteint même 20% de la population européennes adulte de plus de 40 ans (4). Elle est considérée comme la troisième cause de mortalité à travers le monde (5). La BPCO est caractérisée par une obstruction bronchique chronique incomplètement réversible, une inflammation chronique et un remodelage des voies aériennes. Il existe souvent une atteinte parenchymateuse avec perte des structures élastiques pouvant aller jusqu'à l'emphysème. L'asthme est une maladie fréquente qui toucherait 300 millions de personnes dans le monde (6). Sur le plan physiopathologique, l'asthme partage avec la BPCO deux des trois caractéristiques fondamentales de la maladie qui sont l'inflammation bronchique et le remodelage des voies aériennes en plus d'une hyperréactivité bronchique (7). Cliniquement, une coexistence de signes d'asthme et de BPCO chez le même patient est possible. Cette entité clinico-fonctionnelle appelée chevauchement asthme-BPCO ou ACO est définie comme une obstruction respiratoire non réversible avec des caractéristiques généralement associées à l'asthme et d'autres généralement associées à la BPCO (8). La mucoviscidose est la maladie génétique la plus fréquente dans les populations caucasiennes (9) mais reste tout de même une affection rare qui touche environ 60 000 patients dans le monde (10). C'est une maladie multi organe dont l'atteinte pulmonaire est responsable de complications pouvant provoquer la mort prématurément (11). Cependant, l'avènement de nouvelles thérapeutiques a amélioré la prise en charge des patients et l'espérance de vie est en constante augmentation (12). Tout comme l'asthme et la BPCO, le remodelage bronchique et l'inflammation chronique et répétée des voies aériennes caractérisent la pathogénie de l'atteinte pulmonaire de la mucoviscidose (13).

Le diagnostic et le suivi de ces maladies bronchiques obstructives chroniques s'appuient sur des examens clinico-biologiques et des explorations fonctionnelles respiratoires (EFR) qui sont peu sensibles à la détection des altérations précoces et aux modifications subtiles sous traitements (14). De plus, ces explorations ne permettent pas l'étude des modifications structurales inhérentes aux pathologies bronchiques obstructives chroniques qui ne sont accessibles de façon non invasive que par l'imagerie.

Actuellement, la tomodensitométrie (TDM) thoracique est le meilleur examen pour analyser le poumon et les voies aériennes (15). Dans la BPCO, la TDM thoracique rend accessible l'analyse des altérations structurales et permet de mieux caractériser les différents phénotypes ainsi qu'une meilleure compréhension de la variabilité de la maladie (16,17). Le scanner thoracique joue également un rôle important dans le diagnostic de l'asthme sévère (18). Il permet de visualiser les atteintes des voies aériennes proximales et distales ainsi que l'atteinte parenchymateuse (15,19,20). Dans la mucoviscidose, la TDM thoracique est devenue la méthode la plus utilisée pour évaluer les modifications morphologiques avec une sensibilité supérieure à celle de la spirométrie (21,22).

L'imagerie pulmonaire par résonance magnétique protonique est un défi en raison de la faible densité de protons des poumons et de la susceptibilité magnétique due aux nombreuses interfaces air-tissu (23). Dans la pratique clinique, les indications de l'IRM pulmonaire s'intéressent plus particulièrement aux anomalies dont le signal est d'intensité plus élevé comparativement au poumon environnant à faible signal (24). Néanmoins, avec le développement ces dernières années de séquences IRM à haute résolution (séquence à temps d'écho ultra court (UTE)) (25,26), il est possible d'identifier les structures à faible densité protonique. Ainsi, les anomalies pulmonaires morphologiques peuvent être visualisées à l'IRM UTE de façon semblable qu'avec le scanner (26,27). Par ailleurs, du fait du caractère non irradiant de l'IRM, son utilisation en clinique dans le suivi de patients atteints de mucoviscidose est considérée comme une alternative au scanner surtout dans les populations pédiatriques et le suivi à court terme (28–30). En outre, grâce à la possibilité d'une acquisition continue pendant le cycle respiratoire, l'IRM permet de façon totalement non invasive et sans contraste l'étude de la fonction ventilatoire et perfusionnelle du poumon (31–33). Également, l'excellente résolution en contraste de l'IRM permet d'identifier et de caractériser les lésions inflammatoire/fibrotique (34,35).

Malgré les avancées considérables dans la compréhension, le suivi de l'évolution et le phénotypage de ces maladies grâce à l'imagerie, l'évaluation qualitative basée sur des scores visuels a montré ses limites, notamment dans la reproductibilité inter observateurs et la détection de modifications subtiles dans le temps ou le suivi après traitement (36–40). Ainsi, le développement de nouvelles méthodes quantitatives fiables et reproductibles, mais aussi plus exhaustives que les évaluations visuelles catégorielles, est nécessaire. En effet, l'évaluation plus ou moins automatique et objective des lésions est indispensable dans un contexte où les

nouvelles thérapies proposées et/ou en développement nécessitent un suivi de la réponse au traitement et une détection plus sensible et plus spécifique des améliorations mais aussi des aggravations de ces lésions. Cette évaluation quantitative dénuée de toute subjectivité permettrait de mieux discriminer les différents phénotypes de ces maladies bronchiques chroniques pour une meilleure compréhension des phénomènes physiopathologiques sous-jacents et un meilleur suivi des malades.

Ce document se compose de trois parties. **La première partie** est consacrée à l'état de l'art de l'imagerie quantitative dans les maladies obstructives chroniques des voies aériennes. Nous exposons les méthodes de quantifications par TDM des différents compartiments impliqués dans la pathogénie de ces maladies (i.e. emphysème, remodelage bronchique et vasculaire et atteinte des voies aériennes distales). Nous rapportons les quelques tentatives de quantification par IRM protonique dans les maladies bronchiques obstructives chroniques.

**La deuxième partie** détaille spécifiquement les travaux de nos recherches dans la TDM quantitative des maladies obstructives chroniques des voies aériennes menées dans le cadre de cette thèse. Les travaux ayant fait l'objet de publications ou soumis sont intégralement présentés et commentés. Successivement sont présentés : l'apport de la quantification du remodelage bronchique et vasculaire dans la compréhension des maladies respiratoires chroniques, puis un travail qui propose et valide une technique de quantification de l'atteinte des voies aérienne distales.

**La troisième partie** est dédiée aux travaux liés à l'IRM protonique quantitative dans les maladies obstructives chroniques des voies aériennes : tout d'abord la faisabilité de l'IRM à haute résolution dans les maladie bronchique chroniques, puis la validation d'une nouvelle méthode de quantification de l'emphysème chez des patients BPCO, et l'étude de validation de la quantification du remodelage bronchique par IRM chez des patients atteints de mucoviscidose. Enfin, les deux dernières études sont consacrées au développement de méthodes de quantification des phénomènes destructifs et productifs/inflammatoire en T1 et en T2 chez des patients atteints de mucoviscidose.

Les résultats de ces travaux sont enfin discutés et les perspectives à venir sont exposées.

# **1. Etat de l'art**

## 1.1 TDM quantitative dans les maladies obstructives chroniques des voies aériennes

L'analyse de la littérature montre un intérêt croissant dans l'utilisation des techniques de quantification TDM afin d'évaluer de façon plus précise la sévérité et la distribution de l'atteinte des différents compartiments impliqués dans les maladies bronchiques obstructives chroniques. La quantification est en effet presque devenue constante lorsque les méthodes d'imagerie sont utilisées comme moyen objectif d'analyse d'effets thérapeutiques ou de suivi longitudinaux. L'engouement pour ces méthodes d'analyse est très largement dû aux insuffisances de l'analyse visuelle traditionnelle trop subjective qui en revanche reste la méthode essentielle dans la pratique clinique.

Pourtant l'analyse quantitative des images scanners du poumon ne date pas d'hier. L'utilisation de la méthode des masques de densité pour mesurer l'extension de l'emphysème sur des images TDM remonte à la fin des années 1980 (41). Elle est basée sur un seuil prédéfini de valeur d'atténuation du parenchyme pulmonaire afin de distinguer les zones d'atténuation normale mesurée en unité Hounsfield (UH) et les zones d'atténuation basses inférieure à -950UH considérées comme emphysemateuses. Ainsi, le pourcentage du volume pulmonaire emphysemateux est estimé sur des images de TDM thoracique en inspiration sans injection de produit de contraste et avec une épaisseur d'environ 1mm (42–44). Cette évaluation automatique quantitative de la sévérité de l'emphysème a été validé par les données histologiques macro et microscopiques (42,45–47). Bien que les seuils d'atténuation à -960 UH ou -970 UH aient montré de meilleures corrélations avec les données histologiques de l'emphysème (42,48), la valeur seuil à -950UH est presque toujours retenue car très employée dans les études et considérée comme un juste milieu pour une estimation plus sensible et plus spécifique de la sévérité de l'emphysème (49–53). Une approche alternative pour quantifier l'emphysème est basée sur les percentiles de l'histogramme cumulatif des densités (51). Cette approche serait plus robuste dans l'évaluation longitudinale de l'emphysème grâce à une sensibilité moindre aux changements du volume pulmonaire (54–56). Les études comparatives avec les données histologiques ont mis en évidence les meilleures corrélations en utilisant les valeurs du premier percentile (42). Cependant, afin de s'affranchir des artéfacts et du bruit dans les images TDM, la plupart des études utilisent le 15<sup>e</sup> percentile comme marqueur d'emphysème (51,55). Dans un souci de réduction de la dose délivrée, les acquisitions de TDM thoracique se font de plus en plus à faible dose, ce qui peut induire des erreurs de quantification

et une surestimation de l'emphysème (57). Cependant, avec les nouvelles techniques de reconstruction itératives, le bruit dans l'image TDM engendré par la réduction de dose se trouve minimisé ce qui rend la quantification acceptable (58,59).

La mesure des parois bronchiques en scanner constitue une méthode non invasive de quantification du remodelage bronchique. En effet, plusieurs études rapportent des corrélations significatives avec les données histologiques (60–62). Initialement, ces mesures ont été effectuées de façon manuelle et étaient limitées aux bronches dont la géométrie était quasi-orthogonale au plan de coupe TDM (48). Le caractère très fastidieux et la large variabilité inter et intra observateur de ces mesures ont conduit les développeurs à concevoir des méthodes plus ou moins automatisées permettant de mesurer la surface de la paroi et de la lumière bronchique de façon fiable et reproductible. Différents algorithmes plus ou moins complexes ont été publiés : seuillage binaire (63), érosion dilatation (64), largeur à mi-hauteur (48), modèle mesh déformable (65) ou laplacien d'une gaussienne (60). Ce dernier développé dans notre laboratoire a été validé versus les données histologiques (66) et utilisé dans les études dans l'asthme (67), la BPCO (68,69) et la mucoviscidose (70). Tous les algorithmes de segmentation publiés ont des avantages et des inconvénients et aucun n'est parfait. Par ailleurs, il n'existe pas de consensus sur un algorithme universel. La plupart des études qui utilisent la mesure des paramètres bronchiques sont des études de suivi dans lequel le patient est son propre témoin. L'absence de consensus sur l'algorithme à utiliser n'est donc pas un obstacle majeur à la réalisation de ces études, même multicentriques, si la méthode utilisée pour toutes les cohortes est la même. L'évolution des méthodes de reconstruction de l'image en scanner et des méthodes de réduction de la dose d'irradiation peuvent en revanche générer des difficultés d'analyse pour le suivi à long terme de cohortes.

L'atteinte obstructive des voies aérienne distales peut être quantifier sur les scanners en expiration en utilisant la méthode des masques de densité avec un seuil prédéfini à -856 UH ou -850UH. Cette mesure du piégeage expiratoire a montré de très bonnes corrélations avec les paramètres fonctionnels respiratoires chez les patients atteints de BPCO mais également chez les fumeurs (71,72). D'autres méthodes de quantification de piégeage d'air ont été évaluées, utilisant des acquisitions TDM en inspiration et en expiration. Des corrélations significatives ont été retrouvées entre les paramètres de piégeage aux EFR et la mesure du changement du volume entre inspiration et expiration des voxels dont la valeur d'atténuation est comprise entre -860UH et -950UH (73) ou le ratio de la moyenne de densité du poumon en expiration sur celle

en inspiration (E/I ratio) (74,75). De plus, ce ratio E/I de la densité moyenne du poumon à la TDM a montré une corrélation significative avec l'atteinte légère des voies aériennes distales évaluée par le test de rinçage à l'azote (76). Une approche plus régionale du piégeage d'air expiratoire ou de l'atteinte fonctionnelle des voies aériennes distales est basée sur le recalage élastique des images TDM acquises en inspiration et en expiration (77,78). Une carte de réponse paramétrique ainsi générée permet de distinguer les voxels emphysémateux (voxels  $<-950\text{UH}$  en inspiration) de l'atteinte fonctionnelles des voies aériennes distales (voxels  $>-950\text{UH}$  en inspiration mais  $<-856\text{UH}$  en expiration). Bien que ces mesures n'ont pas encore été validé histologiquement, il existe cependant des corrélations avec les EFR (73,79) et également avec la diminution du volume expiratoire maximale en une seconde (VEMS) dans le suivi longitudinal (80).

Le remodelage vasculaire pulmonaire fait partie de la pathogénie des maladies obstructives chroniques des voies aériennes (81–85). Des méthodes de quantification 2D et 3D des petits vaisseaux intra-pulmonaires existent (86–91). En effet, une réduction du volume/surface des petits vaisseaux intra pulmonaires est associée à un asthme sévère (92) ou à une morbi-mortalité élevée chez les patients atteints de BPCO (91,93). Le remodelage vasculaire intra-pulmonaire est également étudié dans l'hypertension pulmonaire (HTP) secondaire à la BPCO qui représente une complication fréquente de la maladie (82,94,95). Ainsi, la quantification des petits vaisseaux intra pulmonaires a montré des corrélations significatives avec la mesure de la pression artérielle pulmonaire moyenne (88–90,96). Egalement, pour les gros vaisseaux thoraciques, un rapport du diamètre de l'artère pulmonaire / diamètre de l'aorte  $>1$  est indicatif d'une hypertension pulmonaire (97,98).

Dans la revue de la littérature qui suit (99)(pages 16-30) nous nous sommes interrogés sur le rôle de la TDM quantitative dans l'évaluation de l'hypertension pulmonaire secondaire à la BPCO et avons présenté les récents progrès en matière de quantification automatique des différents compartiments pulmonaires atteints dans la BPCO associée à une hypertension pulmonaire de sévérité variable.

# Assessing pulmonary hypertension in COPD. Is there a role for computed tomography?

This article was published in the following Dove Press journal:  
*International Journal of Chronic Obstructive Pulmonary Disease*

Florence Coste<sup>1,2,\*</sup>  
Ilyes Benlala<sup>1-3,\*</sup>  
Gaël Dournes<sup>1-3</sup>  
Pierre-Olivier Girodet<sup>1-3</sup>  
François Laurent<sup>1-3,\*</sup>  
Patrick Berger<sup>1-3,\*</sup>

<sup>1</sup>University Bordeaux, Centre de Recherche Cardio-Thoracique de Bordeaux, U1045, Bordeaux, F-33000 France; <sup>2</sup>Inserm, Centre de Recherche Cardio-Thoracique de Bordeaux, U1045, CICI401, Bordeaux, F-33000 France; <sup>3</sup>CHU de Bordeaux, Service d'Imagerie Thoracique et Cardiovasculaire, Service des Maladies Respiratoires, CICI401, Service d'Explorations Fonctionnelles Respiratoires, Pessac, F-33600 France

\*These authors contributed equally to this work

**Abstract:** Pulmonary hypertension (PH) is a common complication of chronic obstructive pulmonary disease (COPD) and is associated with increased morbidity and mortality. Reference standard method to diagnose PH is right heart catheterization. Several non-invasive imaging techniques have been employed in the detection of PH. Among them, computed tomography (CT) is the most commonly used for phenotyping and detecting complications of COPD. Several CT findings have also been described in patients with severe PH. Nevertheless, CT analysis is currently based on visual findings which can lead to reproducibility failure. Therefore, there is a need for quantification in order to assess objective criteria. In this review, progresses in automated analyses of CT parameters and their values in predicting PH and COPD outcomes are presented.

**Keywords:** computed tomography, pulmonary hypertension, COPD, prediction

## Introduction

Chronic obstructive pulmonary disease (COPD) is a common, preventable and treatable disease that is characterized by persistent respiratory symptoms (ie, dyspnea, cough and/or sputum production) and airflow limitation that is due to airway and/or alveolar abnormalities usually caused by significant exposure to noxious particles or gases.<sup>1</sup> COPD has an increasing prevalence worldwide and is mainly caused by tobacco smoke exposure. Diagnosis is based on spirometry with a post-bronchodilator FEV<sub>1</sub>/FVC ratio lower than 0.70.<sup>2</sup> The level of COPD severity is now assessed using both functional (ie, FEV<sub>1</sub> in percentage of predicted values) and clinical data (ie, symptoms scores (CAT and/or mMRC) and the number of exacerbations within the previous 12 months).<sup>2</sup>

COPD is frequently associated with comorbidities. Among them, pulmonary hypertension (PH) is causally related to COPD. PH is defined by a mean pulmonary arterial pressure (mPAP) equal or higher than 25 mmHg at rest, measured using the reference method right heart catheterization (RHC).<sup>3-6</sup> The prevalence of PH and the underlying pathophysiologic processes in patients suffering from COPD remain unclear. Indeed, prevalence increases with COPD severity, and its rate has been reported varying from 20% to 90%.<sup>7-11</sup> An increase of mPAP is associated with an increased number of hospitalizations, morbidity and mortality in COPD.<sup>12-15</sup> The few patients with severe PH secondary to COPD, defined at RHC as a mPAP  $\geq$ 35 mmHg or mPAP  $\geq$ 25 with cardiac index (CI)  $<$ 2 l/min/m<sup>2</sup>, are considered as a subgroup with potentially serious and high complication rate.<sup>5</sup> So far, only a few studies have evaluated the effects of vasodilator in patients with severe PH

Correspondence: Florence Coste  
Centre de Recherche Cardio-thoracique de Bordeaux, INSERM U1045, Université Bordeaux, 146 rue Léo Saignat, Bordeaux Cedex 33076, France  
Tel +33 55 757 4602  
Fax +33 55 757 1695  
Email [florence-coste@hotmail.fr](mailto:florence-coste@hotmail.fr)

submit your manuscript | [www.dovepress.com](http://www.dovepress.com)

DovePress      
<http://doi.org/10.2147/COPD.S207363>

International Journal of Chronic Obstructive Pulmonary Disease 2019:14 2065–2079



© 2019 Coste et al. This work is published and licensed by Dove Medical Press Limited. The full terms of this license are available at <https://www.dovepress.com/terms.php> and incorporate the Creative Commons Attribution – Non Commercial (unported, v3.0) License (<http://creativecommons.org/licenses/by-nc/3.0/>). By accessing the work you hereby accept the Terms. Non-commercial uses of the work are permitted without any further permission from Dove Medical Press Limited, provided the work is properly attributed. For permission for commercial use of this work, please see paragraphs 4.2 and 5 of our Terms (<https://www.dovepress.com/terms.php>).

secondary to COPD, meaning that this subpopulation might benefit from a specific care.<sup>16–18</sup>

There are no specific clinical symptoms of PH, and this complication starts insidiously, the most common symptom being dyspnea.<sup>8</sup> PH in COPD patients has been shown to be associated with an increased exacerbation rate,<sup>8</sup> worsen exercise capacity<sup>8</sup> and a poorer prognosis.<sup>8,13,15</sup> For instance in a study from Andersen et al,<sup>19</sup> the survival rate was 63% for COPD patients without PH vs 37% in those with PH. The most reliable index of PH is the mPAP, a parameter so far measured only by RHC, an invasive technique which remains the reference method for the diagnosis of PH.<sup>3,4</sup> This unique test enables a direct assessment of various pulmonary arterial pressure indices, systolic, diastolic, mean and capillary pressures, as well as resistance, cardiac output and therefore enables to differentiate pre- and post-capillary PH,<sup>20,21</sup> a major way for assessing PH etiology. However, RHC can be responsible for the occurrence of adverse events, related to complication to venous access (such as hematoma, pneumothorax), but also those due to arrhythmias, hypotensive episodes due to vagal reaction or pulmonary vasoreactivity testing. Whereas RHC serious adverse events remain rare in experienced centers (ie, 1.1% and mortality is extremely rare),<sup>22</sup> RHC is not totally safe, especially in unstable patients. Thus, noninvasive diagnosis techniques able to reduce the delay in diagnosing PH and to avoid side effects of RHC are suitable. Echocardiography has been proposed to evaluate systolic pulmonary arterial pressure (sPAP), which is correlated with mPAP, but its specificity is low.<sup>23</sup> However, echocardiography remains the primary tool for patients screening, especially in others PH's etiologies.<sup>4</sup> Nevertheless, echocardiography may be technically difficult to perform, especially in patients with an inflated thorax and/or emphysema. Computed tomography (CT) is a common tool to investigate COPD and its role is crucial in the diagnosis and characterization of emphysema, airway disease, and advocated in various clinical situations such as follow-up, exacerbations, pre-operative surgery and lung transplantation.<sup>2,24–27</sup> CT is a useful tool to assess in vivo observation; nevertheless, radiation exposure risk is not null;<sup>28</sup> in addition, large inappropriate indications of this examination might lead to overrun radiology departments. Moreover, iodine contrast injection and repetitive CT acquisitions are needed to assess hemodynamic alterations related to PH which could increase risk of radiation and adverse reactions to contrast injection. Other interesting technics could be used to study PH,

such as Dual energy CT,<sup>29</sup> or magnetic resonance imaging (MRI). MRI is much less employed in lung diseases due to the low signal intensity of the lung but recent improvements have been published<sup>30–34</sup> and MRI is currently the best tool for evaluating heart morphology and function,<sup>35</sup> or estimating pulmonary arterial pressure using phase contrast MRI.<sup>36</sup>

CT is currently performed for screening PH etiology, notably in the assessment of chronic thromboembolic PH, lung disease, pulmonary arterial hypertension and pulmonary veno-occlusive disease.<sup>37–40</sup> CT is also used as a prognostic marker in patients with PH.<sup>41</sup>

This review is focused on the role of CT in detecting PH in COPD patients. We will first describe the technical characteristics of CT and then we will discuss the morphological assessment of the parenchymal, bronchial and vascular compartments in COPD and their relationships with PH with a special interest in quantitative characterization.

## COPD a multi-compartment disease

COPD is defined by functional irreversible airflow limitation but characteristic morphological changes are present in lung parenchyma, airways and pulmonary vasculature.<sup>1,42</sup> Airflow limitation can be, at least partially, explained by parenchymal destruction due to emphysema.<sup>1</sup> Emphysema is defined histologically by alveolar wall destruction and can be assessed visually using CT.<sup>43–45</sup> The severity of emphysema can also be measured by quantitative CT indices reflecting the low attenuation area due to lung destruction. These quantitative indices have been shown to correlate with macroscopic and microscopic changes histologically.<sup>46,47</sup>

Proximal bronchial wall thickening is a common feature in COPD.<sup>48,49</sup> Histological characteristics of proximal airways include increased infiltration of CD8(+) T lymphocytes, CD3+ T lymphocytes, macrophages.<sup>48–50</sup> This thickening appeared to be more important in a particular COPD-phenotype characterized by less severe respiratory disease, older subjects and higher rates of obesity and cardiovascular comorbidities.<sup>51</sup> Such a proximal thickening can be directly assessed by CT using 2D<sup>52,53</sup> and 3D reconstruction.<sup>54–60</sup>

Bronchial wall thickening is however predominant in distal airways.<sup>61–65</sup> At histological level, it associates luminal exudates, inflammatory cell infiltration and airway remodeling including peribronchial fibrosis, epithelial

metaplasia, mucous gland hypertrophy and increased bronchial smooth muscle mass of the small airways.<sup>62,66</sup> The higher the severity of COPD based on decreased FEV<sub>1</sub>, the higher the histological abnormalities.<sup>66</sup> Moreover, inflammatory cell infiltration is related with tobacco smoking.<sup>67</sup> A loss of small airways has been observed using microCT, a high-resolution imaging technique dedicated to small samples or animal models, contributing to airflow limitation.<sup>62</sup> In humans, the small airway disease can be assessed two-folds morphologically: directly by showing centrilobular opacities and indirectly by using air trapping.<sup>67–69</sup> Such an air trapping has been shown to correlate with the number of inflammatory cells (*ie*, neutrophils and mast cells) infiltrating the bronchial smooth muscle layer.<sup>67</sup>

It has been shown that the toxicity of tobacco smoke affects bronchi and parenchyma, but can also directly alter pulmonary vessels both in animals<sup>70</sup> and humans.<sup>6,71</sup> At histological level, pulmonary arterial remodeling appeared to be more important in COPD than in control subjects, and is particularly important in upper lobe and in small muscular pulmonary arteries.<sup>72</sup> Those vessel alterations are multiples and can happen at initial stage of COPD<sup>71</sup> with endothelial dysfunction, inflammation, suggesting that the history of PH in COPD might be related with cigarette-smoke-induced endothelial alterations.<sup>73,74</sup> The quantitative amount of emphysema in COPD was often negatively correlated to pulmonary microvasculature abnormalities measured using CT,<sup>75–79</sup> except for Wrobel et al,<sup>72</sup> which did not find any significant correlation.

## CT technical considerations

CT scan is the most reliable imaging modality for imaging pulmonary diseases, and it is available and commonly used in routine practice. The new generation of multidetector CT scanners allows acquisition of the whole lung in one breath hold with a submillimetric slice thickness and isotropic voxels using adequate matrix.

The COPD Gene study provides recommendations to standardize CT acquisition parameters in order to obtain high signal-to-noise ratio and accordingly accurate assessment of the images.<sup>80</sup> Thin sections with non-contrast-enhanced volumetric acquisition is a standard technique for COPD imaging.<sup>81</sup> However, intravenous iodinated contrast material is necessary in case of exacerbations or suspected pulmonary embolism. Standard reconstruction algorithm (smooth filter) is required for quantitative automatic analysis.<sup>82</sup> Spirometric gated acquisition have been

proposed to improve quantitative assessment, but is only used in dedicated research programs due to its complexity and low availability.<sup>83</sup> Although COPD patients are older and radiation risks are thus minimized, balance between radiation dose and image quality should be considered. Miscalculation of quantitative parameters because of noisy images leads to standard tube parameters (kVp and mAs).<sup>84</sup> However, low-dose CT acquisition with new iterative reconstruction algorithms allows noise reduction with acceptable quantitative measurements.<sup>83,85</sup>

## Lung parenchyma

Historically, parenchymal alteration, and more precisely, emphysema, has been the first lung component investigated in order to explain PH in COPD. Indeed, emphysema is a major characteristic of COPD that could be quantified in patients when CT is performed. At CT, emphysema can be quantitatively evaluated, using low attenuation area percent (LAA%) derived from the voxel frequency distribution histogram. Several thresholds have been proposed but the most commonly employed is the value of  $-950$  Hounsfield units (HU)<sup>45,46,86–89</sup> (see Figure 1). It has been initially hypothesized that emphysema was correlated with mPAP. However, surprisingly, no relationship between PH and emphysema has been demonstrated neither in human nor in animal models.<sup>7,44,45,90,91</sup> In addition, no significant difference in LAA% between COPD patients with or without PH was observed.<sup>45,92,93</sup> Nonetheless, one single study observed that among COPD patients with PH, the LAA% measured using automated CT was correlated with right ventricular (RV) dysfunction.<sup>94</sup> Emphysema can also be reflected using CT scan with the threshold of  $-960$  HU, the evaluation of the first percentile,<sup>95</sup> or in longitudinal studies, the 15<sup>th</sup> percentile is preferred to follow-up emphysema changes.<sup>96</sup>

## Proximal bronchi

Bronchi can be studied using CT with 2D<sup>52,53</sup> or 3D<sup>54–60</sup> acquisitions. Various methods of bronchial segmentation and various parameters have been proposed, with so far no consensus (see Figure 2). Lumen area, wall area, wall area %, wall thickness and  $-Pi10$ , that reflects the normalized wall area of a theoretical 10-mm bronchi section area, have been proposed as indices for quantitating the severity of bronchial wall changes.<sup>45,52,86,89,97–101</sup> We have demonstrated that bronchial thickness assessed by CT was increased in COPD patients with PH as compared to that of COPD patients without PH, whereas demographic, clinical and functional data (except PaO<sub>2</sub> and 6 mins walk test

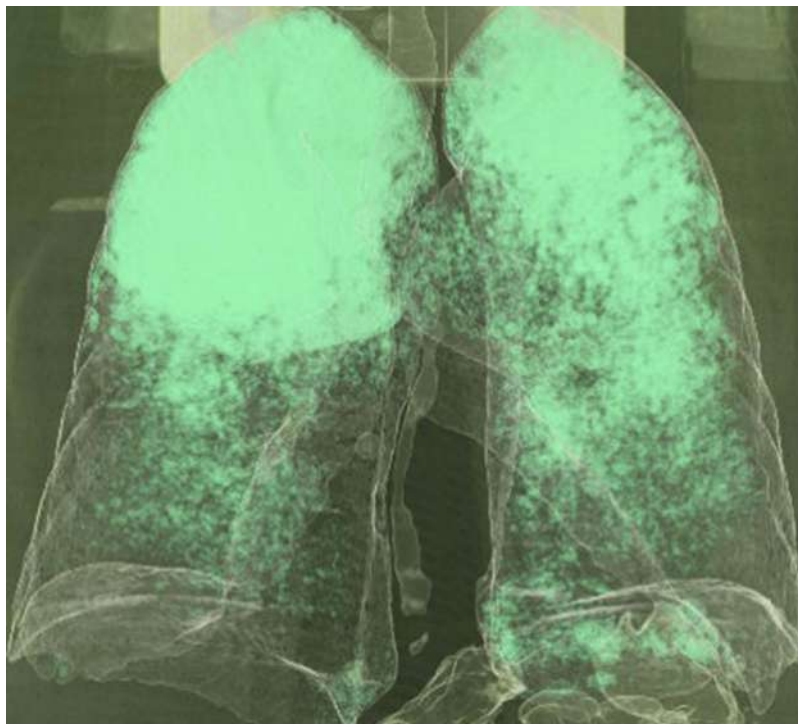


**Figure 1** Reconstructed chest CT scan in COPD patient. This image was acquired with high-spatial-frequency algorithm reconstruction using fully automated Pulmo3D software (Siemens, Munich, Germany). Low attenuation area (LAA%) was derived from the voxel frequency distribution histogram and represented the percentage of lung voxels less than  $-950$  HU. In this COPD patient, LAA value was 23%.

**Abbreviations:** COPD, chronic obstructive pulmonary disease; CT, computed tomography.

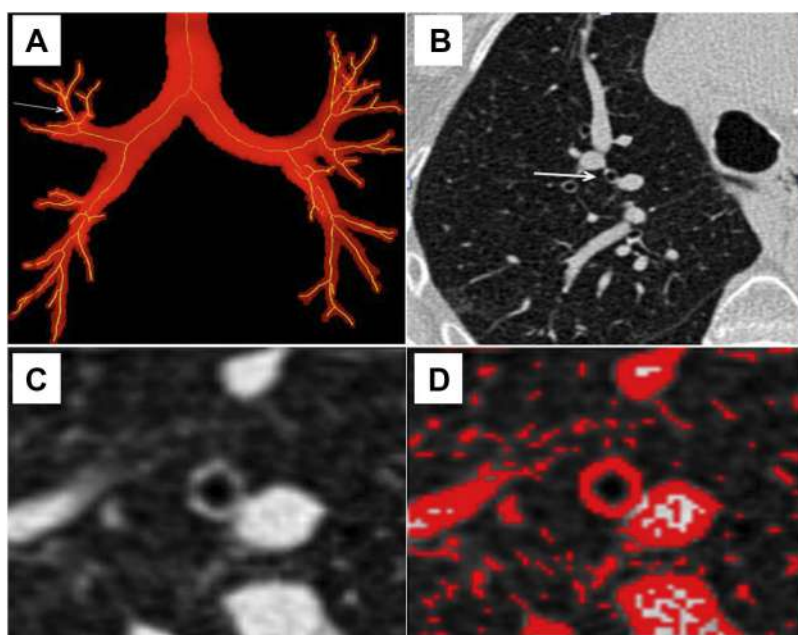


**Figure 2** Bronchi segmentation. (A) Frontal view of a propagation algorithm to obtain a skeleton binary volume based on bi-thresholding. Arrow shows bronchi in which measurements were assessed. (B) Peripheral bronchus is designated (arrow) on a native transverse thin-section CT. (C) Thin-section CT scan used to obtain measurements. (D) A Laplacian of Gaussian algorithm was assessed to segment the designed airway and measure bronchial thickness.

**Abbreviation:** CT, computed tomography.

distance, not surprisingly) remain unchanged.<sup>45</sup> Moreover, a correlation between bronchial wall thickness and mPAP has been reported both in PH<sup>45</sup> and in severe PH secondary to COPD.<sup>86,102</sup> In addition, bronchial wall thickness measured using CT was correlated to histological measurements of airway remodeling,<sup>52</sup> to exacerbation frequency,<sup>103</sup> respiratory symptoms<sup>89</sup> and to FEV1%.<sup>104</sup>

### Small airways

Since obstruction of small airways, defined as airways with a diameter under 2 mm, has been shown to be the main determinant of obstruction in COPD,<sup>62–65</sup> some imaging technics have intended to characterize small airway disease in COPD. Mosaic attenuation at inspiratory and air trapping at expiratory CT reflect small airway disease. Both are related to a decreased lung attenuation and therefore cannot be easily distinguished from emphysema.<sup>105</sup> However, we have found that air trapping was correlated with inflammatory cell infiltration and might reflect peripheral airway obstruction in patients exposed to cigarette smoking.<sup>67</sup> Galbán et al have assessed both expiratory and inspiratory CT using parametric response map in order to estimate functional small airway disease in COPD patients.<sup>106</sup> Parametric response map was able to differentiate COPD phenotypes. In addition, Matsuoka et al calculated relative volume change (expiratory minus inspiratory relative volume) using CT with the threshold of  $-860$  HU that was correlated with airway dysfunction (ie, assessed at PFTs) in COPD regardless of the degree of emphysema.<sup>68</sup> To the best of our knowledge, there is no

study dedicated to the small airways of COPD patients with PH using CT.

### Central vessels

In COPD, a correlation has been shown between mPAP and enlargement of the main pulmonary artery truncus (MAP) diameter, and this increase is observed when MAP is normalized by ascending aorta diameter (MAP/AO).<sup>86,107–110</sup> Usually, normalization is made on ascending aorta<sup>107,108,111,112</sup> (see Figure 3) but it has also been done on descending aorta.<sup>21</sup> Usually, MAP widest dimension is measured on axial CT images, on inspiratory acquisition, at bifurcation level, and, AO is measured on the same image.<sup>107,108,111,112</sup> Descending aorta is also measured at the same level.<sup>112</sup> Thresholds values to detect PH in COPD patients are: MAP  $\geq 29$  mm<sup>21,113,114</sup> and MAP/AO  $> 1$ .<sup>107,110,111,115,116</sup>

Increased MAP/AO ratio, a very simple index measured on a routine CT acquisition, has been shown linked to an increased risk of exacerbation in COPD<sup>108,111,117</sup> and a lower 6-mins walk distance.<sup>118</sup> Mortality in COPD population was also correlated to MAP/AO ratio in some reports<sup>115,119</sup> but not in others.<sup>108,110</sup> Interestingly, this ratio was not correlated to mortality in the general population.<sup>119</sup> However, in healthy children, the ratio MAP/AO is higher than one, so the threshold of 1 cannot be applied in children.<sup>112</sup>

Pulmonary artery distensibility, that reflects elasticity using volume variations of the MAP between diastole and systole, is decreased in PH.<sup>3,4,120</sup> The increase of stiffness is



**Figure 3** Pulmonary artery and aorta measurements. Ratio measurement obtained in a COPD patient in a transverse CT section.

**Abbreviations:** COPD, chronic obstructive pulmonary disease; CT, computed tomography.

also observed in group 3 of PH<sup>121</sup> and in PH related to COPD.<sup>122</sup> Cardiac magnetic resonance (CMR) or ECG-gated CT can be also used to evaluate PA stiffness.<sup>3,4,120,121</sup>

In addition, dynamic-contrast-enhanced CT can be used to discriminate patients with or without PH from different etiology.<sup>123</sup> A delayed flow of contrast and a reduced bolus propagation speed were observed in PH in comparison to control patients. Regions of interests were placed in the MAP and in the left and right pulmonary arteries. However, this study presented some limitations since bolus propagation also reflects the left heart function, the respiratory function and the speed of injection.<sup>123</sup>

## Small vessels

The segmental pulmonary artery-to-bronchus ratio, semi-quantitatively evaluated for apical and posterior segments that run perpendicularly to the axial CT-scan, is positively correlated with mPAP.<sup>124</sup> Ratio >1 in three or more lobes is specific of the presence of PH<sup>113,124</sup> in group 3 of PH classification that also comprise COPD.<sup>125</sup> In the same way, the size of the segmental arterial diameters is also positively correlated with mPAP<sup>124</sup> in group 3 of PH.<sup>125</sup>

Regarding small pulmonary arteries, several of their characteristics have been studied, notably, number, volumes and areas. CT is an efficient tool in order to evaluate in vivo alterations of vessels, follow-up of illness or evaluating drug effects.

Some tools have been developed using 2D<sup>35,79,86,102</sup> (see Figure 4) or 3D<sup>78,118,126</sup> reconstructions.

Using 2D reconstruction on CT images, an automated measurement has been assessed using a free software Image J. These automated measurements allowed the visualization of small vessels alterations first on 3 CT slices<sup>44,127,128</sup> and then on the whole lung.<sup>86,102</sup> Software enables calculation of the percentage of cross-sectional areas (CSA%) of small pulmonary vessels under 5 mm<sup>2</sup> (%CSA<sub><5</sub>) and between 5 and 10 mm<sup>2</sup> (CSA<sub>5-10</sub>),

normalized by lung area, measuring subsegmental and subsegmental levels, respectively. Thus, in COPD patients without severe PH, the correlation between %CSA<sub><5</sub> and mPAP was negative<sup>44,86</sup> whereas in COPD with severe PH correlation was positive.<sup>86,102</sup>

The 3D reconstruction technique allowed to measure volumes of small vessels.<sup>78,118,129</sup> In both studies,<sup>78,118</sup> index using 3D for assessment of pulmonary vessels was negatively correlated with MAP. For Ma et al,<sup>78</sup> 3D and 2D techniques were correlated. Studies using 2D and 3D are in the same line and showed a negative correlation between small pulmonary vessels and mPAP in COPD patients with most of the time moderate PH. As mentioned by others, all those vascular impairments support a vascular etiology of smoking-induced lung disease.<sup>6,130</sup> CT metrics, such as %CSA<sub><5</sub>, also allowed evaluation of the effect of pulmonary vasodilators in patients with PH related to COPD.<sup>79</sup>

In the automated measurements previously reported, pulmonary arteries were never separated from veins and this may affect the sensitivity of the technique. Tools have been developed in 3D in order to circumvent this limitation but not employed, to the best of our knowledge, for evaluating PH in COPD patients.<sup>126,129,131,132</sup> A summary of vessels analyses is presented in Table 1.

## Scores

As mentioned above, several parameters reflecting various components in COPD are modified in COPD patients with PH. Building a score involving these parameters can be a strategy to improve the detection and the severity assessment of PH in COPD.

Tan et al have associated MAP ≥29 mm with artery-to-bronchus ratio >1 in 3 or 4 lobes and have reached a specificity of 100% for detecting PH in patients suffering from parenchymal lung diseases.<sup>113</sup>

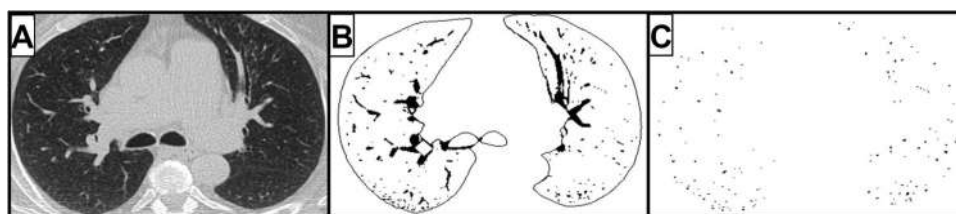


**Figure 4** Measurement of cross-sectional areas (CSA) of small pulmonary vessels using Image J free-software. (A) CT image segmented within the threshold values from -500 to -1024 HU of lung field. (B) Segmented image segmented into binary images. (C) Mask image for the particle analysis after setting circularity within [0.9-1.0] and vessel size within [0-5] mm<sup>2</sup>.

**Abbreviation:** CT, computed tomography.

Table 1 Summary of vessels analyzes in COPD with PH

Publication year	First author	Journal	CT findings	Qualitative /quantitative /Automated /manual	No. of patients	Screened population	Search for
2014	Iyer et al <sup>107</sup>	Chest	MAP/AO>1 better than echocardiography to evaluate PH in COPD patients	Quantitative manual	60	Severe COPD	mPAP ≥ 25 mmHg
2017	Iliaz S et al <sup>108</sup>	Clin Respir J	MAP/AO correlated with PH, number of exacerbation, not with mortality	Quantitative manual	156	COPD exacerbation	Number of COPD exacerbation 1 year after the first one
2017	Curtica MJ et al <sup>109</sup>	Int J Chron Obstruct Pulmon Dis	MAP/AO associated with pulmonary hemodynamics and right heart structure and function changes	Semi-quantitative manual	88	Mil-to-moderately severe COPD	mPAP ≥ 25 mmHg
2016	Ortaç Ersoy E et al <sup>110</sup>	J Crit Care	MAP/AO≥1 associated with pulmonary hypertension, but not with mortality	Quantitative manual	106	COPD	mPAP ≥ 25 mmHg
2016	Coste F et al <sup>86</sup>	Thorax	% cross-sectional area of small pulmonary vessels <5 mm <sup>2</sup> (%CSA<5) is negatively correlated to mPAP for moderated PH (25–35 mmHg), and positively correlated to mPAP for severe PH (>35 mmHg)	Quantitative automated	105	COPD	mPAP ≥ 25 mmHg 35 mmHg
2012	Wells JM et al <sup>111</sup>	NEJM	MAP/AO>1 associated with severe COPD exacerbation	Quantitative manual	3464	Smokers with COPD	COPD exacerbation
2015	Compton GL et al <sup>112</sup>	AJR	Description of technical measurements of MAP/AO in children, threshold is greater than 1, closer to 1.09	Quantitative manual	400	General children population	Threshold of MAP/AO in children
2011	Chan AL et al <sup>21</sup>	BMC Med Imaging	Significant predictors of PH: MAP≥ 29 mm, MAP/AO≥ 0.84, MAP/descending aorta≥ 1.29 mm	Quantitative manual	101	Heterogenous diagnoses	mPAP ≥ 25 mmHg
1998	Tan RT et al <sup>113</sup>	Chest	MAP≥ 29 mm. Artery to bronchus ratio ≥1 in 3 or 4 lobes	Quantitative manual	28	Parenchymal lung disease	mPAP ≥ 20 mmHg
2012	Truong QA et al <sup>114</sup>	Circ Cardiovasc Imaging	MAP≥ 29 mm in men, MAP≥ 27 mm in women, MAP/AO≥ 0.9	Quantitative manual	3171	Asymptomatic community-based population	90 <sup>th</sup> percentile
2014	Shin S et al <sup>115</sup>	Repir Med	MAP/AO>1 associated with PH in patients with COPD, independent predictor of mortality	Quantitative manual	65	Advanced COPD	mPAP ≥ 25 mmHg survival

(Continued)

Table 1 (Continued).

Publication year	First author	Journal	CT findings	Qualitative /quantitative /Automated /manual	No. of patients	Screened population	Search for
2016	Mohamed Hoessein FA et al <sup>116</sup>	Lung	MAP ≥ 30 mm and MAP/AO > I associated with PH	Quantitative manual	92	COPD	mPAP ≥ 25 mmHg
2016	Wells JM et al <sup>117</sup>	Chest	MAP/AO > I predict exacerbation of COPD	Quantitative manual	134	Patient with acute exacerbation of COPD	Predict clinical outcome with MAP/AO
2015	Wells JM et al <sup>118</sup>	Circ Cardiovasc Imaging	Intraparenchymal pulmonary blood vessel volume and the volume of distal vessels with cross-sectional area (CSA) of <5 mm <sup>2</sup> negatively correlated with MAP/AO, MAP/AO, MAP negatively correlated with 6MWT	Quantitative automated	24	Non severe COPD	MAP/AO > I
2017	Terzikhan N et al <sup>119</sup>	Eur Respir J	In general population, MAP/AO > I not associated with mortality. In COPD population, MAP/AO > I associated with mortality	Quantitative manual	2197	General and COPD populations	Prostic information of MAP/AO
2009	Revel MP et al <sup>120</sup>	Radiology	Decreased pulmonary arterial distensibility in PH, ECG-gated CT	Quantitative manual	45	Different group 1, 2 etiology of PH	mPAP ≥ 25 mmHg
2014	Pienn M et al <sup>123</sup>	Eur Radiol	Reduced bolus propagation speed and time differences between contrast material peaks in PH patients, using dynamic-contrast-enhanced CT	Quantitative semi-automated	33	Different potential etiology of PH, notably lung disease, and control patients	mPAP ≥ 25 mmHg
2010	Devaraj A et al <sup>124</sup>	Radiology	MAP/AO and Artery to bronchus ratio correlated with mPAP Size of segmental arterial diameter correlated positively with mPAP	Quantitative manual	77	Spectrum of disease associated with PH (Groups 1, 3, 4,5)	mPAP ≥ 25 mmHg 34 mmHg
2010	Matsuoka S et al <sup>144</sup>	Am J Respir Crit Care Med	% cross-sectional area of small pulmonary vessels <5 mm <sup>2</sup> (%CSA<5) is negatively correlated to mPAP for moderated PH, in severe emphysema population	Quantitative automated	79	COPD	Correlation with mPAP
2015	Ando K et al <sup>79</sup>	Lung	%CSA<5 used to assess pulmonary vasodilators longitudinal evaluation	Quantitative automated	42	COPD	Effect of pulmonary vasodilators in COPD-PH patients

(Continued)

Table 1 (Continued).

Publication year	First author	Journal	CT findings	Quantitative /quantitative /Automated /manual	No. of patients	Screened population	Search for
2017	Ma J et al <sup>78</sup>	J Xray Sci Technol	3D tool able to detect the mean lumen area that was negatively correlated with MAP, and mean number of vessels negatively correlated with emphysema (LAA%, -950 HU)	Quantitative automated	102	Heavy smokers	Computerized scheme to detect pulmonary vessels
2011	Matsuoka S et al <sup>76</sup>	Acad. Radiol.	Negative correlation between %CSA <sub>-5</sub> and LAA%	Quantitative automated	191	Smoking history	Evaluate correlation small vessels-emphysema
2011	Uejima I et al <sup>28</sup>	Jpn J Radiol	Positive correlation between %CSA <sub>-5</sub> and FEV <sub>1</sub> /FVC	Quantitative automated	30	Non smokers	Evaluate correlation small vessels- PFTs
2013	Park S et al <sup>29</sup>	Med Phys	Assessing volumetric technic allowing pulmonary artery/vein separation	Quantitative automated	10	COPD	Evaluate volumetric technic allowing pulmonary artery/vein separation
2016	Iyer S et al <sup>30</sup>	Am J Respir Crit Care Med	After sildenafil arterial CSA and perfused blood volume decreased only in centriacinar emphysema patients, using dual-energy CT perfused blood volume	Quantitative automated	17	Current smokers	Effect of sildenafil on vascular perfusion
2016	Payer C et al <sup>31</sup>	Med Image Anal	Assessing 3D technic allowing pulmonary artery/vein separation	Quantitative automated	25	Lung vascular disease	Evaluate 3D technic allowing pulmonary artery/vein separation
2016	Charbonnier JP et al <sup>32</sup>	IEEE Trans Med Imaging	Automatic separation and classification of pulmonary arteries and veins using CT with an accuracy of 0.89	Quantitative automated	55	Lung cancer	Evaluate separation and classification of pulmonary arteries/veins
2019	Coste F et al <sup>102</sup>	Int J Chron Obstruct Pulmon Dis	% cross-sectional area of small pulmonary vessels <5 mm <sup>2</sup> (% CSA <sub>-5</sub> ) is positively correlated to mPAP for severe PH (>35 mmHg)	Quantitative automated	24	COPD	mPAP ≥35 mmHg

Abbreviations: COPD, chronic obstructive pulmonary disease; CT, computed tomography; PH, pulmonary hypertension.

**Table 2** Summary of scores built in order to diagnose PH or severe PH in lung disease or COPD

Publication year	First author	Journal	Score	CT metrics	No. of patients	Screened population	Search for	Sens. Spe.	PPV NPV
1998	Tan RT et al <sup>113</sup>	Chest	MAP $\geq$ 29 mm + artery to bronchus ratio $\geq$ 1 in 3 or 4 lobes	MAP+A/B	28	Parenchymal lung disease	mPAP $\geq$ 20 mmHg	NA 1.00	NA NA
2010	Devaraj A et al <sup>124</sup>	Radiology	MAP/AO + Right ventricular systolic pressure (echocardiography)	MAP/AO	77	Spectrum of disease associated with PH (Groups 1, 3, 4, 5)	mPAP $\geq$ 25 mmHg 34 mmHg	0.96 0.59	NA
2016	Coste F et al <sup>86</sup>	Thorax	"Paw score": %cross-sectional area of small pulmonary vessels $<$ 5 mm <sup>2</sup> + bronchial wall thickening + PaO <sub>2</sub>	%CSA <sub>&lt;5</sub> + WT	105	COPD	mPAP $\geq$ 35 mmHg	0.75 0.80	0.36 0.96
2019	Coste F et al <sup>102</sup>	Int J Chron Obstruct Pulmon Dis	"Paw score": %cross-sectional area of small pulmonary vessels $<$ 5 mm <sup>2</sup> + bronchial wall thickening + PaO <sub>2</sub>	%CSA <sub>&lt;5</sub> + WT	24	COPD	mPAP $\geq$ 35 mmHg	0.88 NA	NA NA
2018	Johns CS et al <sup>133</sup>	Eur. Radio.	"CMR-RV": RV mass + septal angle		102	COPD	mPAP $\geq$ 25 mmHg	0.90 0.79	0.96 0.58
			"CMR-PA/RV": RV mass + septal angle + MAP measurement	MAP measurement					0.92 0.80
			" $\alpha$ -index": RV ejection fraction + minimal MAP size	Minimal MAP size				1.00 0.13	0.87 1.00

**Abbreviations:** COPD, chronic obstructive pulmonary disease; CT, computed tomography; NA, not attributed; NPV, negative predictive value; PPV, predictive positive value; PH, pulmonary hypertension.

Another index was composed of MAP/AO and right ventricular systolic pressure (RVSP) derived from echocardiography and was correlated with mPAP ( $R^2=0.55$ )<sup>124</sup> for group 1, 3, 4 and 5 of PH.<sup>3,4</sup>

Johns et al mentioned many RV parameters manually measured that are correlated with PH evolution in COPD patients.<sup>133</sup> They tried to identify the best combination able to predict PH. First combination “cardiac magnetic resonance-RV” (“CMR-RV”) included RV mass and septal angle,<sup>134</sup> second “CMR PA/RV” combined RV mass, septal angle and MAP measurements, and the third “ $\alpha$ -index” encompass RV ejection fraction (RVEF) and minimal MAP size.<sup>135</sup> The second model was the best model able to predict mPAP  $\geq 25$  mmHg. The same team also confirmed the interest of those results in another recent study using a validation cohort.<sup>136</sup>

We have built a “paw score” in order to predict severe PH in COPD patients combining CT automated measurements of bronchial wall thickness and pulmonary small vessels areas (%CSA<sub><5</sub>) with PaO<sub>2</sub><sup>86,102</sup>

The various scores and their sensitivity are reported in Table 2.

## Conclusion

PH secondary to COPD is a serious complication that is important to predict with non-invasive tools. Integration of imaging into standard clinical practice is an asset for patient's care. Automated measurements of markers reflecting pulmonary small vessels, bronchial wall and emphysema changes are emerging and might be used routinely in the future for predicting PH or severe PH. All these CT markers could be used in morpho-phenotyping studies. Further studies are required to assess their prognostic impact and follow-up under treatment.

## Abbreviations

AO, aorta; COPD, chronic obstructive pulmonary disease; CMR, cardiac magnetic resonance; CT, computed tomography; FEV<sub>1</sub>, forced expiratory volume in 1 second; FVC, forced volume capacity; HU, Hounsfield units; LAA%, low-attenuation area percentage; m, s, dPAP, mean, systolic, diastolic pulmonary arterial pressure; MAP, Main Pulmonary Artery truncus; MRI, magnetic resonance imaging; NA, not attributed; NPV, negative predictive value; PA, pulmonary artery; PaO<sub>2</sub>, arterial partial pressure of oxygen (mmHg); PFT: pulmonary Function test; PH, pulmonary hypertension; PPV, positive predictive value; RHC, right heart catheterization; RV, right ventricle; WA, bronchial Wall Area (mm); WT, mean bronchial Wall Thickness (mm); 6MWT, 6 mins walk

tests; %CSA<sub><5</sub>, percentage of total cross-sectional area of vessels less than 5 mm<sup>2</sup> normalized by lung area.

## Acknowledgment

This study has received funding from the Laboratory of Excellence TRAIL, ANR-10-LABX-57.

## Author contributions

All authors contributed to data analysis, drafting or revising the article, gave final approval of the version to be published, and agree to be accountable for all aspects of the work.

## Disclosure

Professor Laurent reports personal fees from Boehringer-Ingelheim, Roche, and Chiesi, outside the submitted work. Professor Pierre-Olivier Girodet reports personal fees, non-financial support from Novartis, personal fees, non-financial support from Chiesi, personal fees, non-financial support from Boehringer-Ingelheim, personal fees, non-financial support from AstraZeneca, personal fees, non-financial support from ALK, outside the submitted work. Professor Patrick Berger reports grants from Novartis, personal fees, non-financial support from AstraZeneca, personal fees, non-financial support from Menarini, personal fees, non-financial support from Circassia, personal fees, non-financial support from Sanofi, personal fees from Teva, outside the submitted work; in addition, Prof Berger has a patent Geometric characterization of airways using MRI. 22605-FR pending. The authors report no other conflicts of interest in this work.

## References

1. From the Global Strategy for the Diagnosis, Management and Prevention of COPD, Global Initiative for Chronic Obstructive Lung Disease (GOLD); 2018. Available from: <http://www.goldcopd.org/>. Accessed July 31, 2009.
2. From the Global Strategy for the Diagnosis, Management and Prevention of COPD, Global Initiative for Chronic Obstructive Lung Disease (GOLD); 2017. Available from: <https://goldcopd.org>. Accessed July 31, 2009.
3. Galie N, Humbert M, Vachiery JL, et al. 2015 ESC/ERS guidelines for the diagnosis and treatment of pulmonary hypertension. *Rev Esp Cardiol*. 2016;69(2):177. doi:10.1016/j.recresp.2016.01.002
4. Galie N, Humbert M, Vachiery JL, et al. 2015 ESC/ERS guidelines for the diagnosis and treatment of pulmonary hypertension: the joint task force for the diagnosis and treatment of pulmonary hypertension of the European Society of Cardiology (ESC) and the European Respiratory Society (ERS): endorsed by: association for European Paediatric and Congenital Cardiology (AEPC), International Society for Heart and Lung Transplantation (ISHLT). *Eur Heart J*. 2016;37(1):67–119. doi:10.1093/eurheartj/ehv317
5. Seeger W, Adir Y, Barbera JA, et al. Pulmonary hypertension in chronic lung diseases. *J Am Coll Cardiol*. 2013;62(25 Suppl):D109–D116. doi:10.1016/j.jacc.2013.10.036
6. Barbera JA, Peinado VI, Santos S. Pulmonary hypertension in chronic obstructive pulmonary disease. *Eur Respir J*. 2003;21(5):892–905.

7. Scharf SM, Iqbal M, Keller C, et al. Hemodynamic characterization of patients with severe emphysema. *Am J Respir Crit Care Med*. 2002;166(3):314–322. doi:10.1164/rccm.2107027
8. Chaouat A, Naeije R, Weitzenblum E. Pulmonary hypertension in COPD. *Eur Respir J*. 2008;32(5):1371–1385. doi:10.1183/09031936.00015608
9. Blanco I, Piccari L, Barbera JA. Pulmonary vasculature in COPD: the silent component. *Respirology*. 2016;21(6):984–994. doi:10.1111/resp.12772
10. Thabut G, Dauriat G, Stern JB, et al. Pulmonary hemodynamics in advanced COPD candidates for lung volume reduction surgery or lung transplantation. *Chest*. 2005;127(5):1531–1536. doi:10.1378/chest.127.5.1531
11. Hoepfer MM, Humbert M, Souza R, et al. A global view of pulmonary hypertension. *Lancet Respir Med*. 2016;4(4):306–322. doi:10.1016/S2213-2600(15)00543-3
12. Kessler R, Faller M, Fourgaut G, Mennecier B, Weitzenblum E. Predictive factors of hospitalization for acute exacerbation in a series of 64 patients with chronic obstructive pulmonary disease. *Am J Respir Crit Care Med*. 1999;159(1):158–164. doi:10.1164/ajrccm.159.1.9803117
13. Weitzenblum E, Hirth C, Ducolone A, Mirhom R, Rasaholijnahary J, Ehrhart M. Prognostic value of pulmonary artery pressure in chronic obstructive pulmonary disease. *Thorax*. 1981;36(10):752–758. doi:10.1136/thx.36.10.752
14. Cooper R, Ghali J, Simmons BE, Castaner A. Elevated pulmonary artery pressure. An independent predictor of mortality. *Chest*. 1991;99(1):112–120. doi:10.1378/chest.99.1.112
15. Oswald-Mammosser M, Weitzenblum E, Quoix E, et al. Prognostic factors in COPD patients receiving long-term oxygen therapy. Importance of pulmonary artery pressure. *Chest*. 1995;107(5):1193–1198. doi:10.1378/chest.107.5.1193
16. Barbera JA, Blanco I. Management of pulmonary hypertension in patients with chronic lung disease. *Curr Hypertens Rep*. 2015;17(8):62. doi:10.1007/s11906-015-0574-9
17. Tanabe N, Taniguchi H, Tsujino I, et al. Multi-institutional retrospective cohort study of patients with severe pulmonary hypertension associated with respiratory diseases. *Respirology*. 2015;20(5):805–812. doi:10.1111/resp.12530
18. Vitulo P, Stanzola A, Confalonieri M, et al. Sildenafil in severe pulmonary hypertension associated with chronic obstructive pulmonary disease: a randomized controlled multicenter clinical trial. *J Heart Lung Transplant*. 2017;36(2):166–174. doi:10.1016/j.healun.2016.04.010
19. Andersen KH, Iversen M, Kjaergaard J, et al. Prevalence, predictors, and survival in pulmonary hypertension related to end-stage chronic obstructive pulmonary disease. *J Heart Lung Transplant*. 2012;31(4):373–380. doi:10.1016/j.healun.2011.11.020
20. Tudor RM, Archer SL, Dorfmueller P, et al. Relevant issues in the pathology and pathobiology of pulmonary hypertension. *J Am Coll Cardiol*. 2013;62(25 Suppl):D4–D12. doi:10.1016/j.jacc.2013.10.025
21. Chan AL, Juarez MM, Shelton DK, et al. Novel computed tomographic chest metrics to detect pulmonary hypertension. *BMC Med Imaging*. 2011;11:7. doi:10.1186/1471-2342-11-7
22. Hoepfer MM, Lee SH, Voswinckel R, et al. Complications of right heart catheterization procedures in patients with pulmonary hypertension in experienced centers. *J Am Coll Cardiol*. 2006;48(12):2546–2552. doi:10.1016/j.jacc.2006.07.061
23. Arcasoy SM, Christie JD, Ferrari VA, et al. Echocardiographic assessment of pulmonary hypertension in patients with advanced lung disease. *Am J Respir Crit Care Med*. 2003;167(5):735–740. doi:10.1164/rccm.200210-1130OC
24. O'Brien C, Guest PJ, Hill SL, Stockley RA. Physiological and radiological characterisation of patients diagnosed with chronic obstructive pulmonary disease in primary care. *Thorax*. 2000;55(8):635–642. doi:10.1136/thorax.55.8.635
25. Fishman A, Martinez F, Naunheim K, et al. A randomized trial comparing lung-volume-reduction surgery with medical therapy for severe emphysema. *N Engl J Med*. 2003;348(21):2059–2073. doi:10.1056/NEJMoa030287
26. Klooster K, ten Hacken NH, Hartman JE, Kerstjens HA, van Rikxoort EM, Slebos DJ. Endobronchial valves for emphysema without interlobar collateral ventilation. *N Engl J Med*. 2015;373(24):2325–2335. doi:10.1056/NEJMoa1507807
27. Reilly J. Using computed tomographic scanning to advance understanding of chronic obstructive pulmonary disease. *Proc Am Thorac Soc*. 2006;3(5):450–455. doi:10.1513/pats.200604-101AW
28. Leuraud K, Richardson DB, Cardis E, et al. Ionising radiation and risk of death from leukaemia and lymphoma in radiation-monitored workers (INWORKS): an international cohort study. *Lancet Haematol*. 2015;2(7):e276–e281. doi:10.1016/S2352-3026(15)00094-0
29. Dournes G, Verdier D, Montaudon M, et al. Dual-energy CT perfusion and angiography in chronic thromboembolic pulmonary hypertension: diagnostic accuracy and concordance with radionuclide scintigraphy. *Eur Radiol*. 2014;24(1):42–51. doi:10.1007/s00330-013-2975-y
30. Dournes G, Grodzki D, Macey J, et al. Quiet submillimeter MR imaging of the lung is feasible with a PETRA Sequence at 1.5 T. *Radiology*. 2015;276(1):258–265. doi:10.1148/radiol.15141655
31. Dournes G, Menut F, Macey J, et al. Lung morphology assessment of cystic fibrosis using MRI with ultra-short echo time at submillimeter spatial resolution. *Eur Radiol*. 2016;26(11):3811–3820. doi:10.1007/s00330-016-4218-5
32. Dournes G, Berger P, Refait J, et al. Allergic bronchopulmonary aspergillosis in cystic fibrosis: MR imaging of airway mucus contrasts as a tool for diagnosis. *Radiology*. 2017;285(1):261–269. doi:10.1148/radiol.2017162350
33. Dournes G, Yazbek J, Benhassen W, et al. 3D ultrashort echo time MRI of the lung using stack-of-spirals and spherical k-space coverages: evaluation in healthy volunteers and parenchymal diseases. *J Magn Reson Imaging*. 2018;48(6):1489–1497. doi:10.1002/jmri.26212
34. Benlala I, Berger P, Girodet PO, Dromer C, Macey J, Laurent F. Automated Volumetric Quantification of Emphysema Severity by Using Ultrashort Echo Time MRI: Validation in Participants with Chronic Obstructive Pulmonary Disease. *Radiology*. 2019. Jul;292(1):216–225. doi:10.1148/radiol.2019190052 (in press).
35. Vonk-Noordegraaf A, Haddad F, Chin KM, et al. Right heart adaptation to pulmonary arterial hypertension: physiology and pathobiology. *J Am Coll Cardiol*. 2013;62(25 Suppl):D22–D33. doi:10.1016/j.jacc.2013.10.027
36. Reiter U, Reiter G, Fuchsjäger M. MR phase-contrast imaging in pulmonary hypertension. *Br J Radiol*. 2016;89(1063):20150995. doi:10.1259/bjr.20150995
37. Reichelt A, Hoepfer MM, Galanski M, Keberle M. Chronic thromboembolic pulmonary hypertension: evaluation with 64-detector row CT versus digital subtraction angiography. *Eur J Radiol*. 2009;71(1):49–54. doi:10.1016/j.ejrad.2008.03.016
38. Tamura M, Yamada Y, Kawakami T, et al. Diagnostic accuracy of lung subtraction iodine mapping CT for the evaluation of pulmonary perfusion in patients with chronic thromboembolic pulmonary hypertension: correlation with perfusion SPECT/CT. *Int J Cardiol*. 2017;243:538–543. doi:10.1016/j.ijcard.2017.05.006
39. Resten A, Maitre S, Capron F, Simonneau G, Musset D. [Pulmonary hypertension: CT findings in pulmonary veno-occlusive disease]. *J Radiol*. 2003;84(11 Pt 1):1739–1745.
40. Mineo G, Attina D, Mughetti M, et al. Pulmonary veno-occlusive disease: the role of CT. *Radiol Med*. 2014;119(9):667–673. doi:10.1007/s11547-013-0363-y
41. Rajaram S, Swift AJ, Condliffe R, et al. CT features of pulmonary arterial hypertension and its major subtypes: a systematic CT evaluation of 292 patients from the ASPIRE registry. *Thorax*. 2015;70(4):382–387. doi:10.1136/thoraxjnl-2014-206088

42. Hogg JC, Timens W. The pathology of chronic obstructive pulmonary disease. *Annu Rev Pathol.* 2009;4:435–459. doi:10.1146/annurev.pathol.4.110807.092145
43. Coxson HO, Dirksen A, Edwards LD, et al. The presence and progression of emphysema in COPD as determined by CT scanning and biomarker expression: a prospective analysis from the ECLIPSE study. *Lancet Respir Med.* 2013;1(2):129–136. doi:10.1016/S2213-2600(13)70006-7
44. Matsuoka S, Washko GR, Yamashiro T, et al. Pulmonary hypertension and computed tomography measurement of small pulmonary vessels in severe emphysema. *Am J Respir Crit Care Med.* 2010;181(3):218–225. doi:10.1164/rccm.200908-1189OC
45. Dournes G, Laurent F, Coste F, et al. Computed tomographic measurement of airway remodeling and emphysema in advanced chronic obstructive pulmonary disease. Correlation with pulmonary hypertension. *Am J Respir Crit Care Med.* 2015;191(1):63–70. doi:10.1164/rccm.201408-1423OC
46. Bankier AA, De Maertelaer V, Keyzer C, Gevenois PA. Pulmonary emphysema: subjective visual grading versus objective quantification with macroscopic morphometry and thin-section CT densitometry. *Radiology.* 1999;211(3):851–858. doi:10.1148/radiology.211.3.r99jn05851
47. Madani A, Zanen J, de Maertelaer V, Gevenois PA. Pulmonary emphysema: objective quantification at multi-detector row CT—comparison with macroscopic and microscopic morphometry. *Radiology.* 2006;238(3):1036–1043. doi:10.1148/radiol.2382042196
48. Di Stefano A, Turato G, Maestrelli P, et al. Airflow limitation in chronic bronchitis is associated with T-lymphocyte and macrophage infiltration of the bronchial mucosa. *Am J Respir Crit Care Med.* 1996;153(2):629–632. doi:10.1164/ajrccm.153.2.8564109
49. O'Shaughnessy TC, Ansari TW, Barnes NC, Jeffery PK. Inflammation in bronchial biopsies of subjects with chronic bronchitis: inverse relationship of CD8+ T lymphocytes with FEV1. *Am J Respir Crit Care Med.* 1997;155(3):852–857. doi:10.1164/ajrccm.155.3.9117016
50. Saetta M. Airway inflammation in chronic obstructive pulmonary disease. *Am J Respir Crit Care Med.* 1999;160(5 Pt 2):S17–S20. doi:10.1164/ajrccm.160.supplement\_1.6
51. Burgel PR, Paillasseur JL, Peene B, et al. Two distinct chronic obstructive pulmonary disease (COPD) phenotypes are associated with high risk of mortality. *PLoS One.* 2012;7(12):e51048. doi:10.1371/journal.pone.0051048
52. Nakano Y, Wong JC, de Jong PA, et al. The prediction of small airway dimensions using computed tomography. *Am J Respir Crit Care Med.* 2005;171(2):142–146. doi:10.1164/rccm.200407-874OC
53. Berger P, Perot V, Desbarats P, Tunon-de-Lara JM, Marthan R, Laurent F. Airway wall thickness in cigarette smokers: quantitative thin-section CT assessment. *Radiology.* 2005;235(3):1055–1064. doi:10.1148/radiol.2353040121
54. Montaudon M, Berger P, de Dietrich G, et al. Assessment of airways with three-dimensional quantitative thin-section CT: in vitro and in vivo validation. *Radiology.* 2007;242(2):563–572. doi:10.1148/radiol.2422060029
55. Meng Q, Kitasaka T, Nimura Y, Oda M, Ueno J, Mori K. Automatic segmentation of airway tree based on local intensity filter and machine learning technique in 3D chest CT volume. *Int J Comput Assist Radiol Surg.* 2017;12(2):245–261. doi:10.1007/s11548-016-1492-2
56. Lo P, van Ginneken B, Reinhardt JM, et al. Extraction of airways from CT (EXACT'09). *IEEE Trans Med Imaging.* 2012;31(11):2093–2107. doi:10.1109/TMI.2012.2209674
57. Aykac D, Hoffman EA, McLennan G, Reinhardt JM. Segmentation and analysis of the human airway tree from three-dimensional X-ray CT images. *IEEE Trans Med Imaging.* 2003;22(8):940–950. doi:10.1109/TMI.2003.815905
58. Tschirren J, Hoffman EA, McLennan G, Sonka M. Intrathoracic airway trees: segmentation and airway morphology analysis from low-dose CT scans. *IEEE Trans Med Imaging.* 2005;24(12):1529–1539. doi:10.1109/TMI.2005.857654
59. Lo P, Sparring J, Ashraf H, Pedersen JJ, de Bruijne M. Vessel-guided airway tree segmentation: a voxel classification approach. *Med Image Anal.* 2010;14(4):527–538. doi:10.1016/j.media.2010.03.004
60. Patyk M, Obojski A, Gojny L, Panaszek B, Zaleska-Dorobisz U. Airway evaluation with multidetector computed tomography post-processing methods in asthmatic patients. *Adv Exp Med Biol.* 2016;934:41–47. doi:10.1007/5584\_2016\_23
61. Monzon J, Liu L, Brill H, et al. CDKN2A mutations in multiple primary melanomas. *N Engl J Med.* 1998;338(13):879–887. doi:10.1056/NEJM199803263381305
62. McDonough JE, Yuan R, Suzuki M, et al. Small-airway obstruction and emphysema in chronic obstructive pulmonary disease. *N Engl J Med.* 2011;365(17):1567–1575. doi:10.1056/NEJMoa1106955
63. Hogg JC, Macklem PT, Thurlbeck WM. Site and nature of airway obstruction in chronic obstructive lung disease. *N Engl J Med.* 1968;278(25):1355–1360. doi:10.1056/NEJM196806202782501
64. Van Brabant H, Cauberghe M, Verbeken E, Moerman P, Lauweryns JM, Van de Woestijne KP. Partitioning of pulmonary impedance in excised human and canine lungs. *J Appl Physiol.* 1983;55(6):1733–1742. doi:10.1152/jappl.1983.55.6.1733
65. Yanai M, Sekizawa K, Ohru T, Sasaki H, Takishima T. Site of airway obstruction in pulmonary disease: direct measurement of intrabronchial pressure. *J Appl Physiol.* 1992;72(3):1016–1023. doi:10.1152/jappl.1992.72.3.1016
66. Hogg JC, Chu F, Utokaparch S, et al. The nature of small-airway obstruction in chronic obstructive pulmonary disease. *N Engl J Med.* 2004;350(26):2645–2653. doi:10.1056/NEJMoa032158
67. Berger P, Laurent F, Begueret H, et al. Structure and function of small airways in smokers: relationship between air trapping at CT and airway inflammation. *Radiology.* 2003;228(1):85–94. doi:10.1148/radiol.2281020187
68. Matsuoka S, Kurihara Y, Yagihashi K, Hoshino M, Watanabe N, Nakajima Y. Quantitative assessment of air trapping in chronic obstructive pulmonary disease using inspiratory and expiratory volumetric MDCT. *AJR Am J Roentgenol.* 2008;190(3):762–769. doi:10.2214/AJR.07.2820
69. Gruden JF, Webb WR, Warnock M. Centrilobular opacities in the lung on high-resolution CT: diagnostic considerations and pathologic correlation. *AJR Am J Roentgenol.* 1994;162(3):569–574. doi:10.2214/ajr.162.3.8109498
70. Xing AP, Hu XY, Shi YW, Du YC. Implication of PDGF signaling in cigarette smoke-induced pulmonary arterial hypertension in rat. *Inhal Toxicol.* 2012;24(8):468–475. doi:10.3109/08958378.2012.688885
71. Peinado VI, Barbera JA, Ramirez J, et al. Endothelial dysfunction in pulmonary arteries of patients with mild COPD. *Am J Physiol.* 1998;274(6 Pt 1):L908–L913. doi:10.1152/ajplung.1998.274.6.L908
72. Wrobel JP, McLean CA, Thompson BR, et al. Pulmonary arterial remodeling in chronic obstructive pulmonary disease is lobe dependent. *Pulm Circ.* 2013;3(3):665–674. doi:10.1086/674339
73. Barbera JA, Peinado VI, Santos S, Ramirez J, Roca J, Rodriguez-Roisin R. Reduced expression of endothelial nitric oxide synthase in pulmonary arteries of smokers. *Am J Respir Crit Care Med.* 2001;164(4):709–713. doi:10.1164/ajrccm.164.4.2101023
74. Peinado VI, Barbera JA, Abate P, et al. Inflammatory reaction in pulmonary muscular arteries of patients with mild chronic obstructive pulmonary disease. *Am J Respir Crit Care Med.* 1999;159(5 Pt 1):1605–1611. doi:10.1164/ajrccm.159.5.9807059
75. Yoshimura K, Suzuki Y, Uto T, Sato J, Imokawa S, Suda T. Morphological changes in small pulmonary vessels are associated with severe acute exacerbation in chronic obstructive pulmonary disease. *Int J Chron Obstruct Pulmon Dis.* 2016;11:1435–1445. doi:10.2147/COPD.S107424

76. Matsuoka S, Yamashiro T, Diaz A, et al. The relationship between small pulmonary vascular alteration and aortic atherosclerosis in chronic obstructive pulmonary disease: quantitative CT analysis. *Acad Radiol.* 2011;18(1):40–46. doi:10.1016/j.acra.2010.08.013
77. Estepar RS, Kinney GL, Black-Shinn JL, et al. Computed tomographic measures of pulmonary vascular morphology in smokers and their clinical implications. *Am J Respir Crit Care Med.* 2013;188(2):231–239. doi:10.1164/rccm.201301-0162OC
78. Ma J, Yu N, Shen C, Wang Z, He T, Guo YM. A three-dimensional approach for identifying small pulmonary vessels in smokers. *J Xray Sci Technol.* 2017;25(3):391–402. doi:10.3233/XST-16216
79. Ando K, Kuraishi H, Nagaoka T, et al. Potential role of CT metrics in chronic obstructive pulmonary disease with pulmonary hypertension. *Lung.* 2015;193(6):911–918. doi:10.1007/s00408-015-9813-8
80. Regan EA, Hokanson JE, Murphy JR, et al. Genetic epidemiology of COPD (COPDGene) study design. *Copd.* 2010;7(1):32–43. doi:10.3109/15412550903499522
81. Mayo JR. CT evaluation of diffuse infiltrative lung disease: dose considerations and optimal technique. *J Thorac Imaging.* 2009;24(4):252–259. doi:10.1097/RTI.0b013e3181c227b2
82. Hackx M, Bankier AA, Gevenois PA. Chronic obstructive pulmonary disease: CT quantification of airways disease. *Radiology.* 2012;265(1):34–48. doi:10.1148/radiol.12111270
83. Madani A, Van Muylem A, Gevenois PA. Pulmonary emphysema: effect of lung volume on objective quantification at thin-section CT. *Radiology.* 2010;257(1):260–268. doi:10.1148/radiol.10091446
84. Madani A, De Maertelaer V, Zanen J, Gevenois PA. Pulmonary emphysema: radiation dose and section thickness at multidetector CT quantification—comparison with macroscopic and microscopic morphometry. *Radiology.* 2007;243(1):250–257. doi:10.1148/radiol.2431060194
85. Mets OM, Willeminck MJ, de Kort FP, et al. The effect of iterative reconstruction on computed tomography assessment of emphysema, air trapping and airway dimensions. *Eur Radiol.* 2012;22(10):2103–2109. doi:10.1007/s00330-012-2489-z
86. Coste F, Dournes G, Dromer C, et al. CT evaluation of small pulmonary vessels area in patients with COPD with severe pulmonary hypertension. *Thorax.* 2016;71(9):830–837. doi:10.1136/thoraxjnl-2015-207696
87. Matsuoka S, Yamashiro T, Washko GR, Kurihara Y, Nakajima Y, Hatabu H. Quantitative CT assessment of chronic obstructive pulmonary disease. *Radiographics.* 2010;30(1):55–66. doi:10.1148/rg.301095110
88. Gevenois PA, De Vuyst P, de Maertelaer V, et al. Comparison of computed density and microscopic morphometry in pulmonary emphysema. *Am J Respir Crit Care Med.* 1996;154(1):187–192. doi:10.1164/ajrccm.154.1.8680679
89. Grydeland TB, Dirksen A, Coxson HO, et al. Quantitative computed tomography measures of emphysema and airway wall thickness are related to respiratory symptoms. *Am J Respir Crit Care Med.* 2010;181(4):353–359. doi:10.1164/rccm.200907-1008OC
90. Biernacki W, Gould GA, Whyte KF, Flenley DC. Pulmonary hemodynamics, gas exchange, and the severity of emphysema as assessed by quantitative CT scan in chronic bronchitis and emphysema. *Am Rev Respir Dis.* 1989;139(6):1509–1515. doi:10.1164/ajrccm/139.6.1509
91. Criner GJ, Scharf SM, Falk JA, et al. Effect of lung volume reduction surgery on resting pulmonary hemodynamics in severe emphysema. *Am J Respir Crit Care Med.* 2007;176(3):253–260. doi:10.1164/rccm.200608-1114OC
92. Chaouat A, Savale L, Chouaid C, et al. Role for interleukin-6 in COPD-related pulmonary hypertension. *Chest.* 2009;136(3):678–687. doi:10.1378/chest.08-2420
93. Hurdman J, Condliffe R, Elliot CA, et al. Pulmonary hypertension in COPD: results from the ASPIRE registry. *Eur Respir J.* 2013;41(6):1292–1301. doi:10.1183/09031936.00079512
94. Huang YS, Hsu HH, Chen JY, Tai MH, Jaw FS, Chang YC. Quantitative computed tomography of pulmonary emphysema and ventricular function in chronic obstructive pulmonary disease patients with pulmonary hypertension. *Korean J Radiol.* 2014;15(6):871–877. doi:10.3348/kjr.2014.15.6.871
95. Madani A, Van Muylem A, de Maertelaer V, Zanen J, Gevenois PA. Pulmonary emphysema: size distribution of emphysematous spaces on multidetector CT images – comparison with macroscopic and microscopic morphometry. *Radiology.* 2008;248(3):1036–1041. doi:10.1148/radiol.2483071434
96. Diaz AA, Strand M, Coxson HO, et al. Disease severity dependence of the longitudinal association between CT lung density and lung function in smokers. *Chest.* 2018;153(3):638–645. doi:10.1016/j.chest.2017.10.012
97. Johannessen A, Skorge TD, Bottai M, et al. Mortality by level of emphysema and airway wall thickness. *Am J Respir Crit Care Med.* 2013;187(6):602–608. doi:10.1164/rccm.201209-1722OC
98. Ostridge K, Williams NP, Kim V, et al. Relationship of CT-quantified emphysema, small airways disease and bronchial wall dimensions with physiological, inflammatory and infective measures in COPD. *Respir Res.* 2018;19(1):31. doi:10.1186/s12931-018-0734-y
99. Grydeland TB, Thorsen E, Dirksen A, et al. Quantitative CT measures of emphysema and airway wall thickness are related to D(L)CO. *Respir Med.* 2011;105(3):343–351. doi:10.1016/j.rmed.2010.10.018
100. Nakano Y, Muro S, Sakai H, et al. Computed tomographic measurements of airway dimensions and emphysema in smokers. Correlation with lung function. *Am J Respir Crit Care Med.* 2000;162(3 Pt 1):1102–1108. doi:10.1164/ajrccm.162.3.9907120
101. Lee YK, Oh YM, Lee JH, et al. Quantitative assessment of emphysema, air trapping, and airway thickening on computed tomography. *Lung.* 2008;186(3):157–165. doi:10.1007/s00408-008-9071-0
102. Coste F, Benlala I, Dournes G, et al. Quantitative CT assessment of bronchial and vascular alterations in severe precapillary pulmonary hypertension. *Int J Chron Obstruct Pulmon Dis.* 2019;14:381–389. doi:10.2147/COPD.S177638
103. Han MK, Kazerooni EA, Lynch DA, et al. Chronic obstructive pulmonary disease exacerbations in the COPDGene study: associated radiologic phenotypes. *Radiology.* 2011;261(1):274–282. doi:10.1148/radiol.11110173
104. Washko GR, Dransfield MT, Estepar RS, et al. Airway wall attenuation: a biomarker of airway disease in subjects with COPD. *J Appl Physiol.* 2009;107(1):185–191. doi:10.1152/jappphysiol.00216.2009
105. Burgel PR, Bourdin A, Chanez P, et al. Update on the roles of distal airways in COPD. *Eur Respir Rev.* 2011;20(119):7–22. doi:10.1183/09059180.10010610
106. Galban CJ, Han MK, Boes JL, et al. Computed tomography-based biomarker provides unique signature for diagnosis of COPD phenotypes and disease progression. *Nat Med.* 2012;18(11):1711–1715. doi:10.1038/nm.2971
107. Iyer AS, Wells JM, Vishin S, Bhatt SP, Wille KM, Dransfield MT. CT scan-measured pulmonary artery to aorta ratio and echocardiography for detecting pulmonary hypertension in severe COPD. *Chest.* 2014;145(4):824–832. doi:10.1378/chest.13-1422
108. Iliasz S, Tanriverdio E, Chousein EGU, et al. Importance of pulmonary artery to ascending aorta ratio in chronic obstructive pulmonary disease. *Clin Respir J.* 2018;12(3):961–965. doi:10.1111/crj.12612
109. Cuttica MJ, Bhatt SP, Rosenberg SR, et al. Pulmonary artery to aorta ratio is associated with cardiac structure and functional changes in mild-to-moderate COPD. *Int J Chron Obstruct Pulmon Dis.* 2017;12:1439–1446. doi:10.2147/COPD.S131413

110. Ortac Ersoy E, Durusu Tanriover M, Ocal S, Gulsun Akpınar M, Topeli A. Measurement of pulmonary artery to aorta ratio in computed tomography is correlated with pulmonary artery pressure in critically ill chronic obstructive pulmonary disease patients. *J Crit Care*. 2016;33:42–46. doi:10.1016/j.jcrc.2016.01.020
111. Wells JM, Washko GR, Han MK, et al. Pulmonary arterial enlargement and acute exacerbations of COPD. *N Engl J Med*. 2012;367(10):913–921. doi:10.1056/NEJMoa1203830
112. Compton GL, Florence J, MacDonald C, Yoo SJ, Humpl T, Manson D. Main pulmonary artery-to-ascending aorta diameter ratio in healthy children on MDCT. *AJR Am J Roentgenol*. 2015;205(6):1322–1325. doi:10.2214/AJR.15.14301
113. Tan RT, Kuzo R, Goodman LR, Siegel R, Haasler GB, Presberg KW. Utility of CT scan evaluation for predicting pulmonary hypertension in patients with parenchymal lung disease. Medical college of wisconsin lung transplant group. *Chest*. 1998;113(5):1250–1256. doi:10.1378/chest.113.5.1250
114. Truong QA, Massaro JM, Rogers IS, et al. Reference values for normal pulmonary artery dimensions by noncontrast cardiac computed tomography: the Framingham Heart Study. *Circ Cardiovasc Imaging*. 2012;5(1):147–154. doi:10.1161/CIRCIMAGING.111.968610
115. Shin S, King CS, Brown AW, et al. Pulmonary artery size as a predictor of pulmonary hypertension and outcomes in patients with chronic obstructive pulmonary disease. *Respir Med*. 2014;108(11):1626–1632. doi:10.1016/j.rmed.2014.08.009
116. Mohamed Hoessein FA, Besselinck T, Pompe E, et al. Accuracy of CT pulmonary artery diameter for pulmonary hypertension in end-stage COPD. *Lung*. 2016;194(5):813–819. doi:10.1007/s00408-016-9926-8
117. Wells JM, Morrison JB, Bhatt SP, Nath H, Dransfield MT. Pulmonary artery enlargement is associated with cardiac injury during severe exacerbations of COPD. *Chest*. 2016;149(5):1197–1204. doi:10.1378/chest.15-1504
118. Wells JM, Iyer AS, Rahaghi FN, et al. Pulmonary artery enlargement is associated with right ventricular dysfunction and loss of blood volume in small pulmonary vessels in chronic obstructive pulmonary disease. *Circ Cardiovasc Imaging*. 2015;8(4):e002546. doi:10.1161/CIRCIMAGING.114.002546
119. Terzikhan N, Bos D, Lahousse L, et al. Pulmonary artery to aorta ratio and risk of all-cause mortality in the general population: the Rotterdam Study. *Eur Respir J*. 2017;49(6):1602168. doi:10.1183/13993003.02168-2016
120. Revel MP, Faivre JB, Remy-Jardin M, Delannoy-Deken V, Duhamel A, Remy J. Pulmonary hypertension: ECG-gated 64-section CT angiographic evaluation of new functional parameters as diagnostic criteria. *Radiology*. 2009;250(2):558–566. doi:10.1148/radiol.2502080315
121. Sanz J, Kariisa M, Dellegrottaglie S, et al. Evaluation of pulmonary artery stiffness in pulmonary hypertension with cardiac magnetic resonance. *JACC Cardiovasc Imaging*. 2009;2(3):286–295. doi:10.1016/j.jcmg.2008.08.007
122. Ertan C, Tarakci N, Ozeke O, Demir AD. Pulmonary artery distensibility in chronic obstructive pulmonary disease. *Echocardiography*. 2013;30(8):940–944. doi:10.1111/echo.12170
123. Pienn M, Kovacs G, Tscherner M, et al. Non-invasive determination of pulmonary hypertension with dynamic contrast-enhanced computed tomography: a pilot study. *Eur Radiol*. 2014;24(3):668–676. doi:10.1007/s00330-013-3067-8
124. Devaraj A, Wells AU, Meister MG, Corte TJ, Wort SJ, Hansell DM. Detection of pulmonary hypertension with multidetector CT and echocardiography alone and in combination. *Radiology*. 2010;254(2):609–616. doi:10.1148/radiol.09090548
125. Simonneau G, Gatzoulis MA, Adatia I, et al. Updated clinical classification of pulmonary hypertension. *J Am Coll Cardiol*. 2013;62(25 Suppl):D34–D41. doi:10.1016/j.jacc.2013.10.029
126. Washko GR, Nardelli P, Ash SY, et al. Arterial vascular pruning, right ventricular size and clinical outcomes in COPD. *Am J Respir Crit Care Med*. 2019. doi:10.1164/rccm.201811-2063OC
127. Matsuoka S, Washko GR, Dransfield MT, et al. Quantitative CT measurement of cross-sectional area of small pulmonary vessel in COPD: correlations with emphysema and airflow limitation. *Acad Radiol*. 2010;17(1):93–99. doi:10.1016/j.acra.2009.07.022
128. Uejima I, Matsuoka S, Yamashiro T, Yagihashi K, Kurihara Y, Nakajima Y. Quantitative computed tomographic measurement of a cross-sectional area of a small pulmonary vessel in nonsmokers without airflow limitation. *Jpn J Radiol*. 2011;29(4):251–255. doi:10.1007/s11604-010-0551-9
129. Park S, Lee SM, Kim N, Seo JB, Shin H. Automatic reconstruction of the arterial and venous trees on volumetric chest CT. *Med Phys*. 2013;40(7):071906. doi:10.1118/1.4771960
130. Iyer KS, Newell JD Jr, Jin D, et al. Quantitative dual-energy computed tomography supports a vascular etiology of smoking-induced inflammatory lung disease. *Am J Respir Crit Care Med*. 2016;193(6):652–661. doi:10.1164/rccm.201506-1196OC
131. Payer C, Pienn M, Balint Z, et al. Automated integer programming based separation of arteries and veins from thoracic CT images. *Med Image Anal*. 2016;34:109–122. doi:10.1016/j.media.2016.05.002
132. Charbonnier JP, Brink M, Ciompi F, Scholten ET, Schaefer-Prokop CM, van Rikxoort EM. Automatic pulmonary artery-vein separation and classification in computed tomography using tree partitioning and peripheral vessel matching. *IEEE Trans Med Imaging*. 2016;35(3):882–892. doi:10.1109/TMI.2015.2500279
133. Johns CS, Rajaram S, Capener DA, et al. Non-invasive methods for estimating mPAP in COPD using cardiovascular magnetic resonance imaging. *Eur Radiol*. 2018;28(4):1438–1448. doi:10.1007/s00330-017-5143-y
134. Swift AJ, Rajaram S, Hurdman J, et al. Noninvasive estimation of PA pressure, flow, and resistance with CMR imaging: derivation and prospective validation study from the ASPIRE registry. *JACC Cardiovasc Imaging*. 2013;6(10):1036–1047. doi:10.1016/j.jcmg.2013.01.013
135. Moral S, Fernandez-Friera L, Stevens G, et al. New index alpha improves detection of pulmonary hypertension in comparison with other cardiac magnetic resonance indices. *Int J Cardiol*. 2012;161(1):25–30. doi:10.1016/j.ijcard.2011.04.024
136. Johns CS, Kiely DG, Rajaram S, et al. Diagnosis of pulmonary hypertension with cardiac MRI: derivation and validation of regression models. *Radiology*. 2019;290(1):61–68. doi:10.1148/radiol.2018180603

## International Journal of Chronic Obstructive Pulmonary Disease

Dovepress

### Publish your work in this journal

The International Journal of COPD is an international, peer-reviewed journal of therapeutics and pharmacology focusing on concise rapid reporting of clinical studies and reviews in COPD. Special focus is given to the pathophysiological processes underlying the disease, intervention programs, patient focused education, and self management

protocols. This journal is indexed on PubMed Central, MedLine and CAS. The manuscript management system is completely online and includes a very quick and fair peer-review system, which is all easy to use. Visit <http://www.dovepress.com/testimonials.php> to read real quotes from published authors.

Submit your manuscript here: <https://www.dovepress.com/international-journal-of-chronic-obstructive-pulmonary-disease-journal>

## 1.2 IRM protonique quantitative dans les maladies obstructives chroniques des voies aériennes

L'IRM protonique quantitative n'en est qu'à ses prémices et cela est dû aux limitations inhérentes de l'imagerie IRM pulmonaire. La faible densité en proton du parenchyme pulmonaire aéré ainsi que les nombreuses interfaces entre l'air et les parois alvéolaires rendent le signal du parenchyme pulmonaire extrêmement faible. De surcroît, les artefacts des mouvements cardiaques et respiratoires compliquent l'utilisation de l'IRM dans les maladies bronchiques chroniques. Cependant, l'avènement des séquences UTE a permis d'améliorer la résolution spatiale de l'IRM pulmonaire atteignant des niveaux sous millimétrique en 3D (26). Elles permettent d'accélérer la vitesse d'encodage pour acquérir le signal du parenchyme pulmonaire avant sa décroissance et s'affranchir ainsi des artefacts habituels de l'IRM pulmonaire. Ainsi, l'imagerie morphologique des voies aériennes et la détection du signal du parenchyme pulmonaire deviennent possibles. Dans la littérature, il existe quelques études précurseurs de la quantification de l'emphysème chez des patients atteints de BPCO (Figure1) (100–102). Néanmoins, les problématiques posées par l'imagerie IRM pulmonaire (i.e. normalisation/calibration du signal, sélection du seuil de segmentation pulmonaire) n'ont pas été toutes solutionnées. De plus, l'utilisation de séquences classique en pondération T2 pour quantifier l'emphysème est critiquable (103). Ainsi, à travers une lettre à l'éditeur (104)(pages 34-35) nous discutons les résultats controversés de la quantification de l'emphysème en utilisant des séquences dont le temps d'écho est bien supérieur au T2\* du poumon, engendrant des images où les champs pulmonaires seraient normalement vides de signal.

La quantification en IRM protonique pulmonaire sans contraste du remodelage bronchique et vasculaire ainsi que l'atteinte des voies aériennes distales est inexistante dans la littérature. En revanche, la fonction ventilatoire respiratoire a été évaluée par IRM quantitative fonctionnelle dans les maladies bronchiques obstructives chroniques soit en utilisant des séquences classiques pondérées en T1 avec acquisition en inspiration et en expiration (105,106) soit par l'utilisation de nouvelles techniques comme la décomposition de Fourier (107), l'inhalation de gaz hyperpolarisés (Figure2) (105,108–112) ou l'inhalation d'oxygène (113). Enfin, la composante vasculaire de ces maladies bronchiques chroniques a été étudiée par des séquences de perfusion après injection de produit de contraste (114–116) ou par des séquences ciné d'IRM cardiaque couplé à de l'imagerie de phase pour évaluer la pression artérielle pulmonaire moyenne dans l'HTP secondaire aux maladies bronchiques obstructives (117).

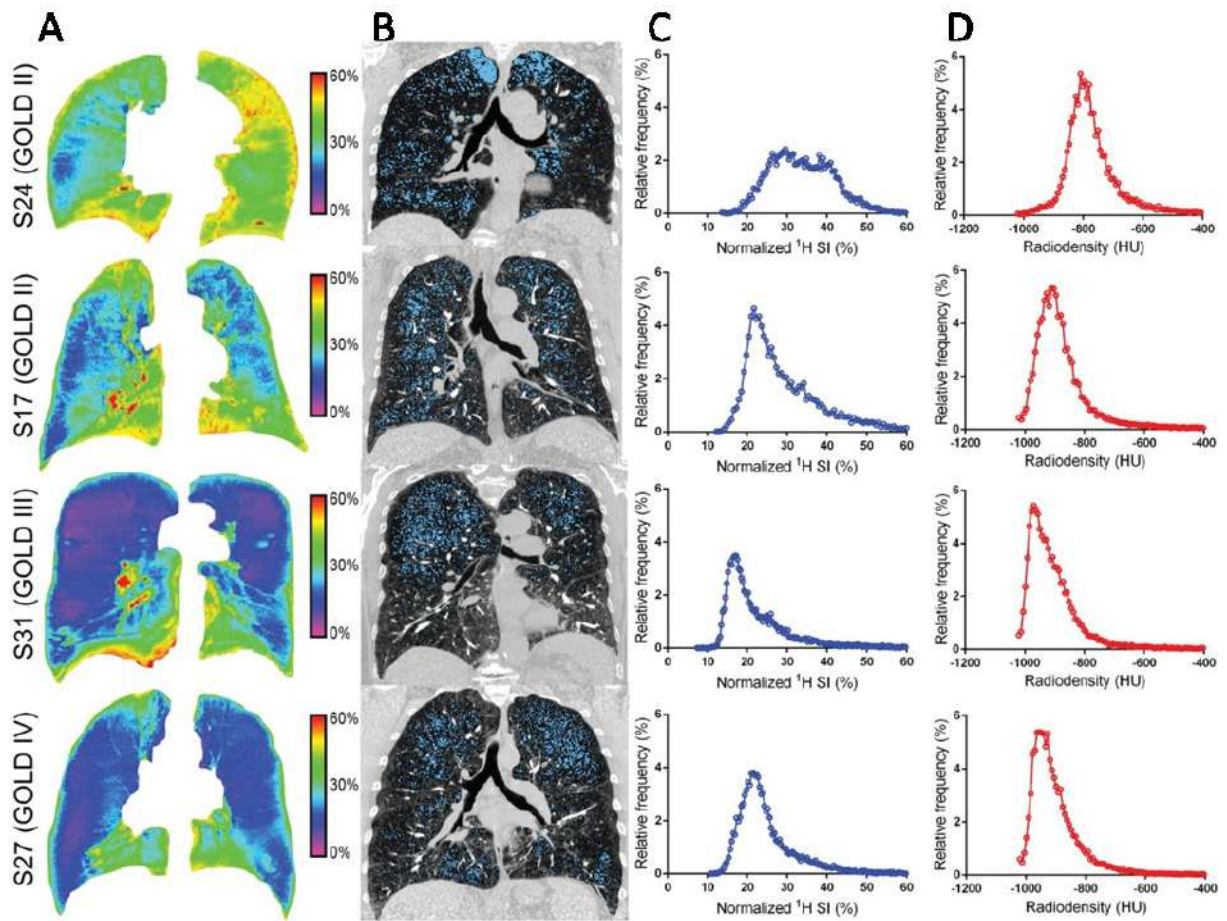


**Figure 1. Quantification de l'emphysème à l'IRM UTE.** (A) Cartographie du signal IRM UTE normalisé de patients BPCO. (B) Images TDM avec le masque en bleu du 15<sup>e</sup> percentile de l'histogramme cumulatif des densités. (C) Histogramme du signal IRM UTE. (D) Histogramme des densités à la TDM. (D'après (100))

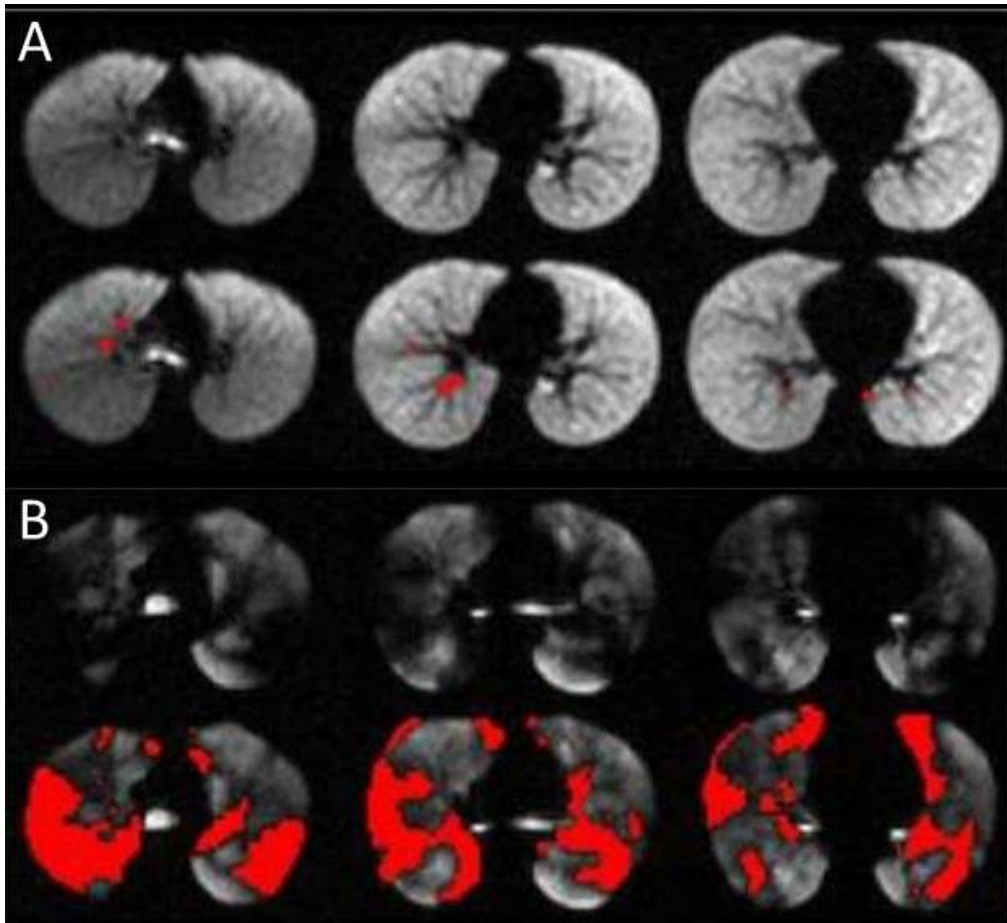


**Figure 2. Quantification de l'atteinte des voies aériennes distales chez des patients atteints de mucoviscidose à l'IRM après inhalation de gaz hyperpolarisé ( $^{129}\text{Xe}$ ). (A) Volontaire sain (VEMS = 95%). (B) Patient atteint de mucoviscidose (VEMS = 102%). Déficits ventilatoires en rouge. (D'après (108))**

## T2-weighted PROPELLER MRI is not suitable for pulmonary emphysema quantification

To the Editor:

We read with interest the recent publication by Meier-Schroers M et al. [1] related to the Quantitative and Qualitative Assessment of Pulmonary Emphysema with T2-Weighted PROPELLER MRI in a High-Risk Population Compared to Low-Dose CT. Quantifying emphysema is a crucial issue for the phenotype and the follow-up of chronic obstructive pulmonary disease (COPD) patients who will need to undergo chest computed tomography (CT) scans periodically. Thus, lung magnetic resonance imaging (MRI) could be a non-ionizing noninvasive imaging alternative. However, due to low intrinsic proton density of the lung, cardio respiratory motion effects and a very short T2\* caused by air-tissue interfaces, the parenchymal MR signal acquired using standard sequences is very low. In addition, emphysema characterized by tissue destruction, decreased perfusion and hyperinflation further reduces the parenchymal MRI signal.

In the study by Meier-Schroers M et al. [1], qualitative assessment of emphysema using a standard MRI sequence had good correlation with CT assessment and the authors must be congratulated for this result. Also, morphological patterns of emphysema correlated well between MRI and CT. However, qualitative assessment of emphysema is known to have poor to moderate agreement [2]. However, for quantitative evaluation, the authors have chosen an arbitrary threshold and have referred to the percentage of pixels with an attenuation value below of -930 HU as an emphysema index (EI). This choice is surprising since a threshold of -950 HU is more commonly used [3]. Madani et al. [4] have showed that a relative area of lung with an attenuation coefficient lower than -960 HU or -970 HU (RA-960, RA-970) has the best correlation coefficient with macroscopic and microscopic measurements of emphysema. Moreover, in another study [5], they showed that a dose reduction to 20 mAs does not substantially change correlations between histological measurements and quantitative CT indexes. However, low dose acquisition leads to an overestimation of RA-960 and RA-970. In a study to evaluate emphysema

quantification agreement between standard-dose CT (SDCT) and ultra-low-dose CT (ULDCT), Nishio et al. [6] found a concordance correlation coefficient (CCC) of 0.956 [0.933–0.971] with respect to a threshold of -950 HU when iterative reconstruction (IR) was performed in ULDCT and poor agreement (CCC = 0.441 [0.315–0.552]) with an overestimation of low attenuation volume at -950 HU in ULDCT without IR. In this case, it is highly relevant to question the choice of -930 HU and an overestimation of what the authors have called EI can be expected, especially knowing that LDCT increases noise and can mimic emphysema lucencies. In order to explain their choice, the authors argued that the optimal threshold with dose levels below 30 mAs has to be determined since LDCT can simulate emphysema, particularly in quantitative analysis. However, based on these arguments, a lower threshold than -930 HU should have been chosen. In addition, regardless of their arguments, they considered lucencies that could be due to noise in LDCT as centrilobular emphysema.

Correlations between LDCT EI with a common or validated threshold (-950 HU or -970 HU) and MRI EI using different MRI thresholds would have been suitable for better assessing the degree of correlation between the 2 techniques. Furthermore, another major limitation of this study was the exclusion of patients for whom quantitative analysis has shown an excessive EI.

Last but not least, there are some technical considerations regarding MRI that must be taken into account. First, the authors performed T2-weighted PROPELLER MRI with a TE of 60 ms, which is longer than the T2\* of the lung  $\approx$  1 ms. Thus, the signal recorded from the parenchyma is most likely due to pulmonary vessels and partial volume artifacts. Second, the difference in slice thickness between CT and MRI (2 mm and 6 mm, respectively) could have led to incorrect measurements of EI. Third, large arterial vessels show dark signal intensity on T2-weighted PROPELLER sequences, which makes automated lung segmentation more difficult requiring arduous manual corrections.

In conclusion, qualitative assessment of emphysema using T2 PROPELLER could be valuable but limited in the case of advanced destructive emphysema where no signal can be recorded from neighboring vessels.

### Conflict of Interest

The authors declare that they have no conflict of interest.

### Authors

Ilyes Benlala, François Laurent, Gael Dournes

Université de Bordeaux Collège Sciences de la Santé, Centre Hospitalier Universitaire de Bordeaux

### Correspondence

Dr. Ilyes Benlala

Université de Bordeaux Collège Sciences de la Santé, Centre Hospitalier Universitaire de Bordeaux  
Avenue de Magellan  
33604 Pessac  
France  
Tel.: ++ 33/557/65 65 42  
ilyes.ben-lala@chu-bordeaux.fr

### References

- [1] Meier-Schroers M, Sprinkart AM, Becker M et al. Quantitative and Qualitative Assessment of Pulmonary Emphysema with T2-Weighted PROPELLER MRI in a High-Risk Population Compared to Low-Dose CT. *ROFO Fortschr Geb Röntgenstr Nuklearmed* 2018; 190: 733–739
- [2] Smith BM, Austin JHM, Newell JD et al. Pulmonary Emphysema Subtypes on Computed Tomography in Smokers. *Am J Med [Internet]*. 2014; 127: 94.e7–94.e23
- [3] Lynch DA, Al-Qaisi MA. Quantitative computed tomography in chronic obstructive pulmonary disease. *J Thorac Imaging* 2013; 28: 284–290
- [4] Madani A, Zanen J, de Maertelaer V et al. Pulmonary emphysema: objective quantification at multi-detector row CT—comparison with macroscopic and microscopic morphometry. *Radiology* 2006; 238: 1036–1043
- [5] Madani A, De Maertelaer V, Zanen J et al. Pulmonary emphysema: radiation dose and section thickness at multidetector CT quantification—comparison with macroscopic and microscopic morphometry. *Radiology* 2007; 243: 250–257

- [6] Nishio M, Koyama H, Ohno Y et al. Emphysema Quantification Using Ultralow-Dose CT With Iterative Reconstruction and Filtered Back Projection. *Am J Roentgenol* 2016; 206: 1184 – 1192

## Bibliography

---

**DOI** <https://doi.org/10.1055/a-0757-0094>

Published online: 2018

Fortschr Röntgenstr

© Georg Thieme Verlag KG, Stuttgart · New York

ISSN 1438-9029

## **2. Contribution à la TDM quantitative des maladies obstructives chroniques des voies aériennes**

## **2.1 Publication n°1 : Evaluation quantitative du remodelage bronchique et vasculaire chez les patients atteints d'hypertension pulmonaire sévère secondaire à la BPCO**

L'hypertension pulmonaire (HTP) est une complication établie de la BPCO responsable d'une morbi-mortalité élevée. Le plus souvent cette HTP est modérée mais parfois elle peut être sévère sans lien évident avec le degré d'obstruction respiratoire. Les mécanismes pouvant expliquer la survenue d'une HTP sévère sont mal connus. Deux études antérieures de notre équipe ont mis en évidence une association entre la sévérité de l'HTP et le remodelage bronchique et vasculaire. Cependant une question reste en suspens : s'agit-il d'une maladie vasculaire pure ou bien est-elle la résultante d'une interaction entre les voies aériennes et les vaisseaux pulmonaires ? De plus, il n'est pas rare de mettre en évidence un syndrome obstructif chez les patients atteints d'une hypertension artérielle pulmonaire idiopathique (HTAP) dont la sévérité est souvent importante. Dans cette étude rétrospective, les données cliniques et hémodynamiques de patients atteints d'HTP sévère secondaire à la BPCO et de patients atteints d'HTAP sévère ont été collectées. Les mesures quantitatives du remodelage bronchique et vasculaire ont été comparées. Les résultats ont montré un épaississement des parois bronchique plus important chez les BPCO porteurs d'HTP sévère que chez les patients atteints d'HTAP. La mesure des petits vaisseaux intra-pulmonaire était significativement moins élevée chez les BPCO avec HTP sévère. L'atteinte des petits vaisseaux pulmonaire et le degré de sévérité de l'HTP ont montré des corrélations opposées dans les deux groupes avec une corrélation positive chez les BPCO et une corrélation négative chez les patients atteints d'HTAP. Un score prédictif construit en incluant les données quantitatives du remodelage bronchique et vasculaire avait une bonne sensibilité dans le groupe des BPCO contrairement au groupe d'HTAP. Ces résultats apportent des arguments au fait que la TDM quantitative du remodelage bronchique et vasculaire est capable de démasquer des atteintes morphologiques et des interactions différentes qui pourraient être propres aux patients atteints d'une HTP sévère secondaire à la BPCO.

# Quantitative CT assessment of bronchial and vascular alterations in severe precapillary pulmonary hypertension

This article was published in the following Dove Medical Press journal:  
*International Journal of COPD*

Florence Coste<sup>1,2,\*</sup>  
Ilyes Benlala<sup>1,2,\*</sup>  
Gaël Dournes<sup>1-3</sup>  
Claire Dromer<sup>3</sup>  
Elodie Blanchard<sup>3</sup>  
Pierre-Olivier Girodet<sup>1-3</sup>  
Michel Montaudon<sup>1-3</sup>  
Fabien Baldacci<sup>4</sup>  
François Picard<sup>3</sup>  
Roger Marthan<sup>1-3</sup>  
François Laurent<sup>1-3,\*</sup>  
Patrick Berger<sup>1-3,\*</sup>

<sup>1</sup>Université de Bordeaux, Centre de Recherche Cardio-Thoracique de Bordeaux, U1045, F-33000 Bordeaux, France; <sup>2</sup>Centre de Recherche Cardio-Thoracique de Bordeaux, INSERM, U1045, Université de Bordeaux, CIC1401, F-33000 Bordeaux, France; <sup>3</sup>CHU de Bordeaux, Service d'Imagerie Thoracique et Cardiovasculaire, Service des Maladies Respiratoires, Service de Cardiologie, CIC1401, Service d'Explorations Fonctionnelles Respiratoires, F-33600 Pessac, France; <sup>4</sup>Université de Bordeaux, LaBRI, F-33405 Talence Cedex, France

\*These authors contributed equally to this work

Correspondence: Florence Coste  
Centre de Recherche Cardio-Thoracique de Bordeaux, INSERM, U1045, Université de Bordeaux, 146 Rue Léo Saignat, 33076 Bordeaux Cedex, France  
Tel +33 547 30 27 51  
Fax +33 55 757 1695  
Email [florence-coste@hotmail.fr](mailto:florence-coste@hotmail.fr)

**Background:** Little is known about in vivo alterations at bronchial and vascular levels in severe pulmonary hypertension (PH) of different etiologies. We aimed to compare quantitative computed tomography (CT) data from the following three groups of severe precapillary PH patients: COPD, idiopathic pulmonary arterial hypertension (iPAH), and chronic thromboembolic PH (CTEPH).

**Patients and methods:** This study was approved by the institutional review board. Severe PH patients (mean pulmonary arterial pressure [mPAP]  $\geq 35$  mmHg) with COPD, iPAH, or CTEPH (n=24, 16, or 16, respectively) were included retrospectively between January 2008 and January 2017. Univariate analysis of mPAP was performed in each severe PH group. Bronchial wall thickness (WT) and percentage of cross sectional area of pulmonary vessels less than 5 mm<sup>2</sup> normalized by lung area (%CSA<sub><5</sub>) were measured and compared using CT, and then combined to arterial partial pressure of oxygen (PaO<sub>2</sub>) to generate a “paw score” compared within the three groups using Kruskal–Wallis and its sensitivity using Fisher’s exact test.

**Results:** WT was higher and %CSA<sub><5</sub> was lower in the COPD group compared to iPAH and CTEPH groups. Mosaic pattern was higher in CTEPH group than in others. In severe PH patients secondary to COPD, mPAP was positively correlated to %CSA<sub><5</sub>. By contrast, in severe iPAH, this correlation was negative, or not correlated in severe CTEPH groups. In the COPD group, “paw score” showed higher sensitivity than in the other two groups.

**Conclusion:** Unlike in severe iPAH and CTEPH, severe PH with COPD can be predicted by “paw score” reflecting bronchial and vascular morphological differential alterations.

**Keywords:** computed tomography, pulmonary hypertension, COPD, prediction, quantitative

## Plain language summary

Mortality of pulmonary hypertension (PH) increases with severity of the disease. It is thus crucial to identify severe forms of PH, characterized by a higher elevation of mPAP. In addition, little is known about bronchial and vascular alterations in severe PH of different etiologies.

Our purpose was to compare the following three groups of severe precapillary PH patients using quantitative computed tomography (CT): COPD, idiopathic pulmonary arterial hypertension (iPAH) and chronic thromboembolic PH (CTEPH).

Bronchial wall thickness (WT) was higher and small pulmonary vessels area was lower in the COPD group compared to iPAH and CTEPH groups. The mPAP was positively correlated to small pulmonary vessels area in the COPD group and negatively or not correlated in iPAH or CTEPH groups.

Unlike severe iPAH or CTEPH, severe PH secondary to COPD is characterized by vascular and bronchial morphological alterations assessed by quantitative CT. These values combined with that of PaO<sub>2</sub> in a “paw score” can predict the presence of severe PH, only in COPD patients.

submit your manuscript | [www.dovepress.com](http://www.dovepress.com)

Dovepress      
<http://dx.doi.org/10.2147/COPD.S177638>

International Journal of COPD 2019:14 381–389



© 2019 Coste et al. This work is published and licensed by Dove Medical Press Limited. The full terms of this license are available at <https://www.dovepress.com/terms.php> and incorporate the Creative Commons Attribution – Non Commercial (unported, v3.0) License (<http://creativecommons.org/licenses/by-nc/3.0/>). By accessing the work you hereby accept the Terms. Non-commercial uses of the work are permitted without any further permission from Dove Medical Press Limited, provided the work is properly attributed. For permission for commercial use of this work, please see paragraphs 4.2 and 5 of our Terms (<https://www.dovepress.com/terms.php>).

Such a paw score could be thus used to select COPD patients for right heart catheterization.

## Introduction

Pulmonary hypertension (PH) is defined by a mean pulmonary arterial pressure (mPAP)  $\geq 25$  mmHg, at rest, subsequently inducing right heart failure, and ultimately patient's death.<sup>1,2</sup> Among the five groups of PH, defined in the last international classification,<sup>1</sup> three of them correspond to a precapillary PH (ie, PH due to lung diseases and/or hypoxemia [group 3], pulmonary arterial hypertension [(PAH), group 1] notably idiopathic PAH (iPAH), and chronic thromboembolic PH [(CTEPH), group 4]). Despite comparable hemodynamic alterations assessed invasively by right heart catheterization (RHC), these three groups have different underlying mechanisms, treatment, and prognosis.<sup>1</sup>

The mortality of PH increases by more than fourfold when the mPAP increases by 10 mmHg.<sup>3</sup> It is thus crucial to identify severe forms of PH, characterized by a higher elevation of mPAP.<sup>4</sup> In patients with COPD (group 3), severe PH is defined as mPAP  $\geq 35$  mmHg at rest.<sup>5</sup> However, RHC cannot be performed in all COPD patients. To circumvent this limitation, a "paw score" was proposed, combining arterial partial pressure of oxygen (PaO<sub>2</sub>) and quantitative computed tomography (CT) measurements of both bronchial wall thickness (WT) and small pulmonary vessels. This "paw score" was able to predict the presence of severe PH in a COPD population with 75% sensitivity and 80% specificity.<sup>6</sup> Interestingly, its negative predictive value was more than 95%, allowing to predict the absence of severe PH when the "paw score" was  $< 5$  with  $< 5\%$  error.<sup>6</sup> Although the "paw score" appeared accurate in a COPD population, it remains unclear whether this score may be relevant to other forms of severe PH. Moreover, relationships between mPAP and quantitative CT measurements of both bronchi and small pulmonary vessels have not been described so far in the various groups of patients with severe precapillary PH.

Thus, we aimed at comparing quantitative CT measurements of bronchial wall, lung parenchyma, and small pulmonary vessels in patients with severe precapillary PH related to COPD, iPAH, or CTEPH. We also assessed correlations between mPAP, CT, clinical, and functional parameters in order to find predictors of mPAP variability. Finally, we compared the sensitivity of the "paw score" to diagnose severe PH in each of these three groups.

## Patients and methods

### Study population

This study was observational, retrospective, and conducted according to the principles of the Declaration of Helsinki

and approved by our institutional review board. One hundred eighty-nine patients were consecutively referred for complete examination of severe PH to our institution, a tertiary medical center, between January 2008 and January 2017. From a prior study,<sup>6</sup> 20 COPD patients were also included in the current study (out of 24 patients) and none in the two other groups. However, these 20 patients were completely reanalyzed by another radiologist and they were implemented with four new subjects. Before initiation of any treatment, within 1 week, all patients had physical examination, medical questioning, 6-minute walk tests (6-MWT), blood tests (C-reactive protein [CRP], brain natriuretic peptide, and HIV serology), transthoracic-echocardiography, ventilation/perfusion scintigraphy, pulmonary function test (PFT), RHC, and unenhanced CT within a minimal period of 1 month of disease stability. PFT involved body plethysmography, transfer lung capacity of carbon monoxide ([TLCO]; Medisoft, Sorinnes, Belgium), and arterial blood gases. Reference values were chosen from the European Respiratory Society and the American Thoracic Society guidelines.<sup>7,8</sup> From the 189 screened patients, 103 patients had both mPAP value  $\geq 35$  mmHg at RHC<sup>5</sup> and a diagnosis of either COPD, iPAH, or CTEPH. However, 16 patients were not fully screened and 19 patients could not be included because of associated diseases (Figure 1). Thus, from the 68 remaining patients, we focused the study on the 56 adult patients with only severe precapillary PH with either COPD, iPAH, or CTEPH, without any other condition to explain PH, and with an adequate CT examination without any abnormality possibly altering CT measurements (Figure 1). Chest CT scans were acquired at full inspiration on a Somatom Definition 64 (Siemens, Munich, Germany). Dedicated and validated software were used to quantitatively analyze scans.<sup>9,10</sup> Emphysema was automatically quantified with Myrian software (Intrasense, Montpellier, France) using the low-attenuation area percent (LAA%).<sup>6,11</sup> Mosaic attenuation was assessed using a semiquantitative score derived from evaluation of each lobe.<sup>12</sup> Bronchial wall area (WA), lumen area, and WT were automatically quantified on orthogonal bronchial cross sections using previously validated homemade software (ie, Neko).<sup>10,13</sup> Small vessel areas from CT images were automatically measured, as previously described.<sup>6,14–18</sup> Percentage of cross sectional area of pulmonary vessels less than 5 mm<sup>2</sup> normalized by lung area (%CSA<sub><5</sub>) at each CT slice were acquired using ImageJ software. Large vessel diameters were manually measured, at the level of pulmonary artery bifurcation, for both pulmonary arterial truncus (AP) and ascending aorta (AO) using the same axial image.<sup>6,11</sup>

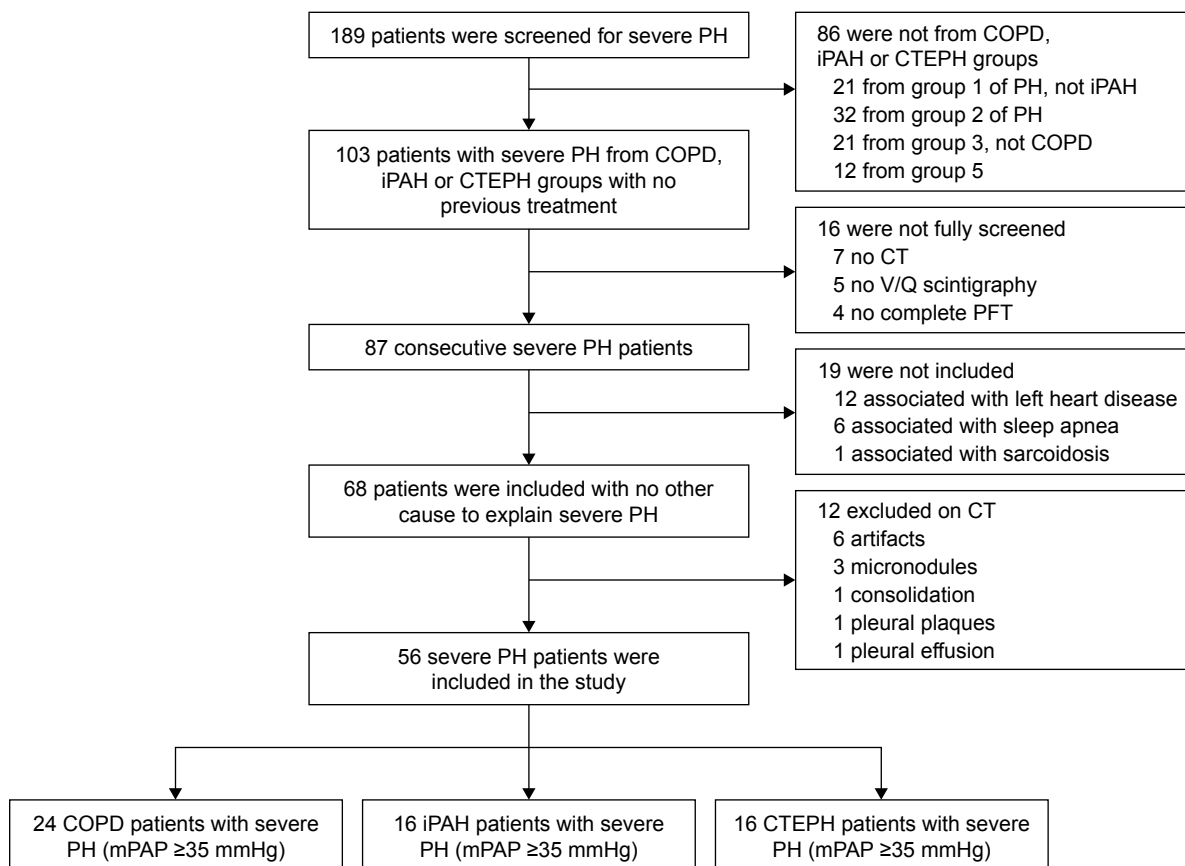


**Figure 1** Flowchart of study design.

**Note:** Number of patients who were screened, enrolled, and assigned to a study group.

**Abbreviations:** CT, computed tomography; CTEPH, chronic thromboembolic PH; iPAH, idiopathic pulmonary arterial hypertension; mPAP, mean pulmonary arterial pressure; PFT, pulmonary function tests; PH, pulmonary hypertension; V/Q, ventilation/perfusion scintigraphy.

## Statistical analyses

Statistical analyses were performed using NCSS software (v. 2001; NCSS, Kaysville, UT, USA). Results are expressed as mean with SD and analyzed using one-way ANOVA and Tukey post hoc tests. Parameters that were not normally distributed are expressed as median with interquartile ranges and tested by Kruskal–Wallis and multiple comparisons z-value post hoc tests. Categorical variables were analyzed with Fisher’s exact tests. Univariate correlations were assessed using Pearson’s correlation coefficient test. In order to predict severe PH, “paw scores” were built, combining three variables, ie, PaO<sub>2</sub>, WT, and %CSA<sub>-5</sub>, as described elsewhere ([Table S1](#)).<sup>6</sup> *P*-value <0.05 was considered significant.

Details about PFT, RHC, CT protocols, echocardiography, “paw score”, and statistical analysis, are available in the electronic [supplementary material](#).

## Ethics approval and informed consent

This study was observational, retrospective, and conducted according to the principles of the Declaration of Helsinki and approved by our institutional review board “the Ethics

Committee of the University Hospital of Bordeaux” reference: GP-CE 2018/20. Every patient was informed and agreed that their data can be used for further research studies anonymously. Data were anonymized and they complied with the requirements of the “Commission nationale informatique et libertés” (CNIL) that approved the methods this organization was being responsible for ensuring the ethical use of data collected for scientific purposes in France (approval number: 1909530 v 0).

## Results

### Patients characteristics

Among the 56 included patients with severe PH, 24 patients suffered from COPD, 16 from iPAH, and 16 from CTEPH (Figure 1). Demographic, plethysmographic, clinical, biological, and hemodynamic characteristics of the three groups are detailed in Table 1. Significant lower FEV<sub>1</sub>, FEV<sub>1</sub>/FVC ratio, and TLCO, and a higher residual volume were found in COPD subjects compared to the other two groups. Moreover, both a lower PaO<sub>2</sub> and a higher left ventricular ejection fraction were measured in COPD patients compared

**Table 1** Characteristics of severe PH patients

	COPD with severe PH	Severe iPAH	Severe CTEPH	P-value
N	24	16	16	
Age				
Years	70 (64–73)	71 (62–76)	66 (56–75)	0.59
Sex ratio				
Male/female	20/4 <sup>a,b</sup>	9/7 <sup>c</sup>	5/11 <sup>c</sup>	<0.01
BMI				
kg.m <sup>-2</sup>	26±5	25±4	25±7	0.67
PFT				
FEV <sub>1</sub> (% pred)	55±21 <sup>a,b</sup>	91±14 <sup>c</sup>	92±14 <sup>c</sup>	<0.01
FEV <sub>1</sub> /FVC (%)	57 (49–63) <sup>a,b</sup>	73 (72–78) <sup>c</sup>	76 (74–78) <sup>c</sup>	<0.01
FVC (%)	80±22 <sup>a,b</sup>	98±17 <sup>c</sup>	97±14 <sup>c</sup>	<0.01
TLC (%)	95 (87–104)	93 (83–101)	99 (93–101)	0.26
RV (%)	115 (101–141) <sup>a</sup>	92 (83–105) <sup>c</sup>	109 (87–115)	<0.01
TLCO (%)	23 (16–32) <sup>a,b</sup>	40 (35–80) <sup>c</sup>	66 (57–87) <sup>c</sup>	<0.01
6-MWT				
Distance (m)	275 (180–300)	317 (270–390)	325 (228–510)	0.14
Arterial blood gases				
PaO <sub>2</sub> (mmHg)	49 (46–53) <sup>b</sup>	67 (53–75) <sup>c</sup>	60 (52–68)	<0.01
PaCO <sub>2</sub> (mmHg)	34 (29–37)	32 (30–36)	33 (31–36)	0.60
RHC				
mPAP (mmHg)	45±7	42±4	47±9	0.11
sPAP (mmHg)	72±14 <sup>b</sup>	69±11 <sup>b</sup>	83±16 <sup>a,c</sup>	0.01
dPAP (mmHg)	29±6	27±5	27±8	0.54
PCWP (mmHg)	9±3	8±3	8±3	0.55
Gradient (mmHg)	20±5	20±6	18±8	0.85
PVR (Wood unit)	8±3	9±4	10±4	0.19
PVRi (Wood unit.m <sup>-2</sup> )	15±6	17±4	16±6	0.51
CO (L.min <sup>-1</sup> )	5±1.2	4±1.4	4±1.1	0.09
CI (L.min <sup>-1</sup> .m <sup>-2</sup> )	3±0.7	2±0.7	2±0.5	0.14
Echocardiography				
sPAP (mmHg)	69±24	72±18	82±24	0.28
ITVmax (m/s)	3.8±0.7	3.8±0.4	4.1±0.6	0.26
ITGdmax (mmHg)	59±22	59±13	69±21	0.28
LVEF (%)	68±9 <sup>a</sup>	57±10 <sup>c</sup>	64±11	0.02
Biology				
CRP (pg/mL)	4 (2–7)	6 (4–16)	5 (1–6)	0.27
BNP (mg/mL)	375 (35–610)	467 (66–936)	186 (73–376)	0.29

**Notes:** Data are mean ± SD for continuous normal variables, or median with IQR if their distribution was not normal. Comparisons of parametric and nonparametric variables were performed using ANOVA and with Kruskal–Wallis tests, respectively. <sup>a</sup>Different from iPAH group, <sup>b</sup>different from CTEPH group, and <sup>c</sup>different from COPD group.

**Abbreviations:** BMI, body mass index; BNP, brain natriuretic peptide; CI, cardiac index; CO, cardiac output; CRP, C-reactive protein; CTEPH, chronic thromboembolic PH; FVC, forced volume capacity; Gradient, dPAP-PCWP; iPAH, idiopathic pulmonary arterial hypertension; ITGdmax, maximal transtricuspid pressure gradient; ITVmax, maximal tricuspid regurgitation velocity; IQR, interquartile range; LVEF, left ventricular ejection fraction; 6-MWT, 6-minute walk test; m, s, dPAP, mean, systolic, diastolic pulmonary arterial pressure; PCWP, pulmonary capillary wedge pressure; PFT, pulmonary function test; PH, pulmonary hypertension; PVR, pulmonary vascular resistance; PVRi, indexed PVR; PaCO<sub>2</sub>, arterial partial pressure of carbon dioxide; PaO<sub>2</sub>, arterial partial pressure of oxygen; pred, predicted; RHC, right heart catheterization; RV, residual volume; TLC, total lung capacity; TLCO, transfer lung capacity of carbon monoxide.

to iPAH patients (Table 1). The mPAP was similar in the three groups, as well as most of the RHC parameters except the systolic PAP (sPAP), which was higher in severe CTEPH patients (Table 1).

### Comparison of CT measurements of bronchi, parenchyma, and vessels

Morphological CT parameters were compared in the three groups (Table 2). Bronchial morphological parameters were greater in COPD patients with severe PH (Figure S1) than in iPAH (ie, WT and WA; Figure S2) and CTEPH (ie, WT; Figure S3). Moreover, emphysema extent, assessed by the LAA%, was higher in patients with COPD than in those with iPAH or CTEPH. In addition, mosaic attenuation score was higher in patients with severe CTEPH than in those with iPAH or COPD. Whereas large vessels ratio was not different within the three groups, the %CSA<sub><5</sub> was smaller in patients with COPD than in those with iPAH.

### Univariate analysis of mPAP

In COPD patients with severe PH, significant univariate correlations were found between mPAP and a variety of variables including: CRP, echocardiographic sPAP, %CSA<sub><5</sub>, and WT (Tables 3 and S2). In severe iPAH patients, mPAP was correlated only with maximal tricuspid regurgitation velocity (ITVmax) and %CSA<sub><5</sub>. Correlation between mPAP and %CSA<sub><5</sub> was positive in patients with COPD, whereas it was negative in those with iPAH (Figure S4). By contrast, mPAP of severe CTEPH patients

was not correlated to %CSA<sub><5</sub>, but with LAA%, TLCO, and 6-MWT.

### Validity of “paw scores” in each group and comparison to sPAP on echocardiography

As a consequence, the “paw score” combining three variables, ie, PaO<sub>2</sub>, WT, and %CSA<sub><5</sub>, was significantly higher in COPD patients with severe PH than in the two other groups, without any difference between severe iPAH and severe CTEPH (Figure 2A). Using a threshold of 5, as assessed previously,<sup>6</sup> the sensitivity of “paw score” for predicting the presence of severe PH was 87.5% (21/24), 43.8% (7/16), and 62.5% (10/16) in COPD, iPAH, and CTEPH groups, respectively. A significant difference in the number of true positives and false negatives between the three groups of severe PH was found (Figure 2B). We also assessed the sensitivity of ultrasound echocardiography to predict the presence of severe PH using various sPAP cutoff (ie, 50 mmHg,<sup>19</sup> 60 mmHg,<sup>20</sup> and 65 mmHg<sup>21</sup> in the three groups of patients (Table S3). In COPD patients, the sensitivity of the “paw score” was higher than that of echocardiography for each cutoff.

### Discussion

The present study demonstrates that, unlike severe iPAH or severe CTEPH, severe PH secondary to COPD is characterized by vascular and bronchial morphological alterations assessed by quantitative CT. Values derived from these measurements, combined with that of PaO<sub>2</sub> in

**Table 2** Comparison of CT parameters between groups

	COPD with severe PH	Severe iPAH	Severe CTEPH	P-value
n	24	16	16	
Bronchi				
WA	20.06±4.63 <sup>a</sup>	16.44±3.25 <sup>b</sup>	17.61±3.76	0.02
LA	9.03±2.73	8.20±2.49	9.28±2.84	0.50
WT	1.34±0.15 <sup>a,c</sup>	1.19±0.15 <sup>b</sup>	1.20±0.13 <sup>b</sup>	<0.01
Parenchyma				
LAA%	4.59 (2.70–10.50) <sup>a,c</sup>	1.26 (0.74–1.84) <sup>b</sup>	1.30 (0.84–2.80) <sup>b</sup>	<0.01
Mosaic attenuation	0 (0–0) <sup>c</sup>	0 (0–17) <sup>c</sup>	30 (4–52) <sup>a,b</sup>	<0.01
Vessels				
AP/AO	1.06 (0.98–1.16)	1.09 (0.99–1.16)	1.14 (1.08–1.21)	0.11
%CSA <sub>&lt;5</sub>	0.54±0.19 <sup>a</sup>	0.77±0.29 <sup>b</sup>	0.67±0.24	0.01

**Notes:** Data are mean ± SD for continuous normal variables, or median with IQR if their distribution is not normal. Comparisons of parametric and nonparametric variables were performed using ANOVA and with Kruskal–Wallis tests, respectively. <sup>a</sup>Different from iPAH group, <sup>b</sup>different from COPD group, and <sup>c</sup>different from CTEPH group.

**Abbreviations:** AO, aorta; AP, pulmonary arterial truncus; %CSA<sub><5</sub>, percentage of cross sectional area of pulmonary vessels less than 5 mm<sup>2</sup> normalized by lung area; CTEPH, chronic thromboembolic PH; iPAH, idiopathic pulmonary arterial hypertension; IQR, interquartile range; LA, mean lumen area (mm<sup>2</sup>); LAA%, low-attenuation area percentage; PH, pulmonary hypertension; WA, mean wall area (mm<sup>2</sup>); WT, mean wall thickness (mm).

**Table 3** Univariate correlations between mPAP and CT parameters

		COPD with severe PH			Severe iPAH			Severe CTEPH		
		n	Coef	P-value	N	Coef	P-value	n	Coef	P-value
Parenchyma emphysema	LAA%	24	-0.10	0.65	16	0.45	0.08	16	-0.58	<b>0.02</b>
Mosaic attenuation	MA%	24	0	1	16	0.08	0.77	16	0.44	0.08
Bronchi	WA	24	0.38	0.07	16	-0.04	0.88	16	0.06	0.81
	LA	24	0.15	0.49	16	0.13	0.63	16	-0.02	0.93
	WT	24	0.43	<b>0.04</b>	16	-0.15	0.59	16	0.13	0.62
Vessels										
Large vessels	AP/AO	24	0.01	0.95	16	0.45	0.08	16	0.38	0.15
Small vessels	%CSA <sub>&lt;5</sub>	24	0.41	<b>0.04</b>	16	-0.55	<b>0.03</b>	16	0.14	0.61

**Notes:** Data are Pearson correlation coefficients. Bold indicates statistical significance,  $P < 0.05$ .

**Abbreviations:** AO, aorta; AP, pulmonary arterial truncus diameter; %CSA<sub><5</sub>, percentage of cross sectional area of pulmonary vessels less than 5 mm<sup>2</sup> normalized by lung area; CTEPH, chronic thromboembolic PH; CT, computed tomography; Coef, coefficient; LA, mean lumen area (mm<sup>2</sup>); iPAH, idiopathic pulmonary arterial hypertension; LAA%, low-attenuation area percentage; MA, mosaic attenuation; mPAP, mean pulmonary arterial pressure; PH, pulmonary hypertension; WA, mean wall area (mm<sup>2</sup>); WT, mean wall thickness (mm).

a “paw score” can predict the presence of severe PH, in COPD patients.

To the best of our knowledge, this quantitative CT study is the first one including cohorts from three distinct groups of precapillary severe PH, and reporting in vivo data of small vessels alterations in severe PH. Whereas these three groups presented similar values of mPAP, all being  $\geq 35$  mmHg, several differences in quantitative CT parameters between groups and univariate relationships with mPAP within groups have been highlighted. These three groups of severe PH patients allows us to consider two groups as control for the third one. Regarding bronchial parameters, we showed that WT was higher in COPD patients with severe PH, as compared to the two other groups and was positively correlated to mPAP only in COPD, as previously described in the literature,<sup>6,11</sup> but not in the two other groups, a finding that has not been reported so far. Regarding vascular parameters, the %CSA<sub><5</sub> was lower in COPD patients with severe

PH compared to iPAH. This result could be related with the emphysema extent, which was higher in COPD patients. In addition, a strong negative correlation between %CSA<sub><5</sub> and emphysema has been demonstrated in this study confirming previous findings.<sup>15,17,18</sup> Moreover, we demonstrated a positive correlation between mPAP and %CSA<sub><5</sub> in COPD patients with severe PH, in line with recent published results.<sup>6</sup> By contrast, this correlation was negative in severe iPAH. Such a negative correlation between mPAP values and %CSA<sub><5</sub> may suggest that the decrease in the number of vascular structure may accompany iPAH. This observation could be explained by angiogenesis disturbance in iPAH.<sup>2,22</sup> Our finding may bring insights into this uncertainty, suggesting that severe PH in COPD may be secondary to complex pathophysiology interactions that might be different from iPAH. These opposite findings cannot, nevertheless, rule out the previously proposed hypothesis that the severity of PH in COPD might be related with coexistence of iPAH.<sup>5,23,24</sup> In the present study,

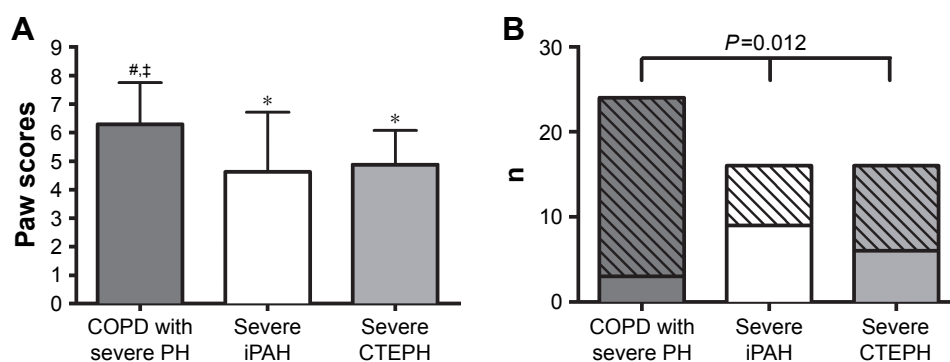


**Figure 2** Comparison of “paw score” and its sensitivity between severe PH groups.

**Notes:** (A) Comparison of “paw scores” in each severe PH groups: COPD, iPAH, and CTEPH. Comparison was performed using Kruskal–Wallis and multiple comparisons z-value post hoc tests. #Different from COPD group, \*Different from iPAH group, †Different from CTEPH group. (B) Comparison of “paw score” sensitivity in each severe PH group was assessed by a Fisher’s exact test. Hashed bars represent true positives and plain bars represent false negatives.

**Abbreviations:** CTEPH, chronic thromboembolic PH; iPAH, idiopathic pulmonary arterial hypertension; PH, pulmonary hypertension.

there was also no correlation between %CSA<sub><5</sub> and mPAP within the CTEPH population. This result is in agreement with that published by Rahaghi et al,<sup>25</sup> who reported that the volume of small vessels with cross-sectional area <5 mm<sup>2</sup>, assessed by a 3D reconstruction of the intraparenchymal pulmonary vasculature, was not correlated with mPAP, but with cardiac index.

With respect to PFT parameters, as expected, we found marked differences between COPD and the other groups. It should be noted that three severe iPAH patients presented a mild restrictive defect, assessed by a total lung capacity lower than 80% of predicted, as previously reported by others.<sup>26</sup> Indeed, it has been hypothesized that, in iPAH, the mechanical coupling of vessels and airways with changes in vascular rigidity could lead to a reduction in lung compliance.<sup>26,27</sup> Moreover, we did not observe any correlation between mPAP and PFT parameters in both COPD and iPAH groups, as already shown in previous studies.<sup>6,14,23,27</sup> Regarding the relationship between PFT and mPAP in CTEPH, to the best of our knowledge, the lack of correlations between these parameters has not been reported before. However, we found a significant correlation between mPAP and TLCO in patients with severe CTEPH. Although hypoxia was believed to be a factor causing PH,<sup>1,28</sup> in agreement with numerous studies, no significant correlation has been reported between PaO<sub>2</sub> and mPAP within COPD group of severe PH<sup>6,23</sup> and iPAH.<sup>29</sup> In the present study, the significant difference shown between COPD and iPAH groups is consistent with Chaouat et al's report, in which COPD patients with severe PH showed severe hypoxia whereas patients with severe iPAH had only mild hypoxia.<sup>6,23,29</sup>

Regarding quantitative CT parameters, there is a renewed interest in the identification and evaluation of COPD phenotypes, and pulmonary imaging biomarkers may contribute to determine these phenotypes. CT has several advantages in this field, being the most commonly used method for imaging the lung on one side, and, on the other side, being able to provide quantitative data related to alterations of components of the lung, ie, parenchyma, bronchi, and vascular compartments. In the particular setting of COPD, a close relationship between pulmonary arterial pressure and bronchial wall thickening has already been shown.<sup>11</sup> Quantitative CT data derived from small vessels analysis have also suggested that a vascular alteration is more likely to explain severe PH in COPD rather than an airway disease.<sup>6,23</sup> The role of both bronchial and small vessel alteration in the prediction of severe PH in COPD patients is supported by our univariate analysis. Using quantitative CT, a previous hypothesis that only

tissue destruction and emphysema extent could lead to the increase of mPAP in COPD patients has already been disproved by recent studies.<sup>6,11,14</sup> The present study confirms these results, since there was no correlation between mPAP and emphysema extent.

In this study, we found that a score combining PaO<sub>2</sub> and both bronchial and vascular quantitative CT parameters, ie, the so-called "paw score" had a greater sensitivity for detecting severe PH in COPD patients. Interestingly, although the specificity of the "paw score" cannot be calculated, since true negatives and false positives were not available, its sensitivity was significantly higher in COPD than in iPAH and CTEPH groups, further supporting the interest of calculating the "paw score" in COPD patients only. These differences might be related to different morphological and functional alterations of bronchial and vascular components in other groups.

Other non-interventional study, ie, echocardiography, is currently used to explore PH. Indeed, in the present study, we observed that the sensitivity to detect severe PH in COPD group was higher with "paw score" than that with sPAP. Conversely, we showed that the sensitivity to detect severe PH with "paw score" was lower than that of sPAP, in iPAH or CTEPH patients. Indeed, ultrasound echocardiography is a very useful tool to detect PH. However, it suffers some limitation such as, insufficient tricuspid regurgitation prevents sPAP estimation, explaining some missing values, and in COPD patients hyperinflated lung can increase the difficulty of measurement.<sup>30</sup> These observations might suggest that echocardiography should be preferred to detect severe PH in iPAH and CTEPH patients, whereas "paw score" should be preferred in COPD patients.

The present study suffers from some limitations. First, the study design was observational and retrospective. However, 1) all consecutive patients were characterized using the same processes during the whole inclusion period; 2) the definition of severe PH (ie, mPAP ≥35 mmHg) was the same for the three groups; and 3) CT scans have been acquired and analyzed consistently in the three groups. Second, since severe PH is uncommon, the number of patients in each group was limited. Third, considering small vessel measurements, veins cannot be distinguished from arteries using CT scan. The study, however, was limited to precapillary PH at RHC. Fourth, %CSA<sub><5</sub> is a global measurement area, irrespective of wall and lumen changes in the vessel, thus making impossible the distinction between lumen narrowing and vessel wall thickening. Finally, a multivariate analysis has not been performed since it would have been underpowered by the low number of patient in each group.

## Conclusion

We demonstrated that the “paw score” (ie, combination of quantitative CT measurements of both bronchial thickness and vascular alterations with PaO<sub>2</sub>) can predict the presence of severe PH, in COPD patients only. Thus, the “paw score” is not appropriate to predict PH severity in iPAH or in CTEPH patients. Therefore, quantitative CT may be used to select among patients with COPD, who should be prioritized for RHC.

## Data availability

The datasets used and/or analyzed during the current study are available from the corresponding author on reasonable request.

## Acknowledgments

Berger reports grants from Laboratory of Excellence (LabEx) Transitional Research International Laboratory (TRAIL, Université de Bordeaux, France) ANR-10-LABX-57, during the conduct of the study. Laurent reports grants from TRAIL ANR-10-LABX-57, during the conduct of the study. Coste reports funding for salary from LabEx TRAIL ANR-10-LABX-57, during the conduct of the study. This study has received funding from the LabEx TRAIL, ANR-10-LABX-57.

## Author contributions

Conception and design: FC, GD, FL, PB; analysis and interpretation: FC, IB, GD, FL, PB; drafting the manuscript for important intellectual content: FC, IB, GD, FL, PB; revising the manuscript for important intellectual content: FC, IB, GD, RM, FL, PB; and final approval of the manuscript: FC, IB, GD, CD, EB, POG, MM, FB, FP, RM, FL, PB. All authors contributed to data analysis, drafting and revising the article, gave final approval of the version to be published, and agree to be accountable for all aspects of the work.

## Disclosure

Berger reports personal fees, nonfinancial support from Novartis, Boehringer Ingelheim, AstraZeneca, and GSK outside the submitted work; in addition, he has a patent EP N°15152886.6, ie, new compositions and methods of treating and/or preventing COPD, which is pending. Laurent reports personal fees from Boehringer Ingelheim, Roche, Novartis, Bayer, Guerbet, and Chiesi outside the submitted work. Girodet reports personal fees and nonfinancial support from Novartis, Chiesi, Takeda, Boehringer Ingelheim, and AstraZeneca outside the submitted work. The other authors report no conflicts of interest in this work.

## References

- Galiè N, Humbert M, Vachiery JL, et al. 2015 ESC/ERS guidelines for the diagnosis and treatment of pulmonary hypertension: the joint Task Force for the diagnosis and treatment of pulmonary hypertension of the European Society of cardiology (ESC) and the European Respiratory Society (ERS): endorsed by: association for European paediatric and congenital cardiology (AEPC), International Society for Heart and lung transplantation (ISHLT). *Eur Respir J*. 2015;46(4):903–975.
- Guignabert C, Tu L, Le Hir M, et al. Pathogenesis of pulmonary arterial hypertension: lessons from cancer. *Eur Respir Rev*. 2013;22(130):543–551.
- Cooper R, Ghali J, Simmons BE, Castaner A. Elevated pulmonary artery pressure. An independent predictor of mortality. *Chest*. 1991;99(1):112–120.
- Barst RJ, Rubin LJ, Long WA, et al. A comparison of continuous intravenous epoprostenol (prostacyclin) with conventional therapy for primary pulmonary hypertension. *N Engl J Med*. 1996;334(5):296–301.
- Seeger W, Adir Y, Barberà JA, et al. Pulmonary hypertension in chronic lung diseases. *J Am Coll Cardiol*. 2013;62(25 Suppl):D109–D116.
- Coste F, Dournes G, Dromer C, et al. CT evaluation of small pulmonary vessels area in patients with COPD with severe pulmonary hypertension. *Thorax*. 2016;71(9):830–837.
- Miller MR, Hankinson J, Brusasco V, et al. Standardisation of spirometry. *Eur Respir J*. 2005;26(2):319–338.
- Wanger J, Clausen JL, Coates A, et al. Standardisation of the measurement of lung volumes. *Eur Respir J*. 2005;26(3):511–522.
- Montaudon M, Lederlin M, Reich S, et al. Bronchial measurements in patients with asthma: comparison of quantitative thin-section CT findings with those in healthy subjects and correlation with pathologic findings. *Radiology*. 2009;253(3):844–853.
- Berger P, Perot V, Desbarats P, Tunon-de-Lara JM, Marthan R, Laurent F. Airway wall thickness in cigarette smokers: quantitative thin-section CT assessment. *Radiology*. 2005;235(3):1055–1064.
- Dournes G, Laurent F, Coste F, et al. Computed tomographic measurement of airway remodeling and emphysema in advanced chronic obstructive pulmonary disease. Correlation with pulmonary hypertension. *Am J Respir Crit Care Med*. 2015;191(1):63–70.
- Hoey ET, Mirsadraee S, Pepke-Zaba J, Jenkins DP, Gopalan D, Screaton NJ. Dual-energy CT angiography for assessment of regional pulmonary perfusion in patients with chronic thromboembolic pulmonary hypertension: initial experience. *AJR Am J Roentgenol*. 2011;196(3):524–532.
- Montaudon M, Berger P, de Dietrich G, et al. Assessment of airways with three-dimensional quantitative thin-section CT: in vitro and in vivo validation. *Radiology*. 2007;242(2):563–572.
- Matsuoka S, Washko GR, Yamashiro T, et al. Pulmonary hypertension and computed tomography measurement of small pulmonary vessels in severe emphysema. *Am J Respir Crit Care Med*. 2010;181(3):218–225.
- Matsuoka S, Washko GR, Dransfield MT, et al. Quantitative CT measurement of cross-sectional area of small pulmonary vessel in COPD: correlations with emphysema and airflow limitation. *Acad Radiol*. 2010;17(1):93–99.
- Uejima I, Matsuoka S, Yamashiro T, Yagihashi K, Kurihara Y, Nakajima Y. Quantitative computed tomographic measurement of a cross-sectional area of a small pulmonary vessel in nonsmokers without airflow limitation. *Jpn J Radiol*. 2011;29(4):251–255.
- Wang Z, Chen X, Liu K, et al. Small pulmonary vascular alteration and acute exacerbations of COPD: quantitative computed tomography analysis. *Int J Chron Obstruct Pulmon Dis*. 2016;11:1965–1971.
- Yoshimura K, Suzuki Y, Uto T, Sato J, Imokawa S, Suda T. Morphological changes in small pulmonary vessels are associated with severe acute exacerbation in chronic obstructive pulmonary disease. *Int J Chron Obstruct Pulmon Dis*. 2016;11:1435–1445.
- Barst RJ, McGoon M, Torbicki A, et al. Diagnosis and differential assessment of pulmonary arterial hypertension. *J Am Coll Cardiol*. 2004;43(12 Suppl S):S40–S47.
- Strange G, Playford D, Stewart S, et al. Pulmonary hypertension: prevalence and mortality in the Armadale echocardiography cohort. *Heart*. 2012;98(24):1805–1811.

21. Fisher MR, Forfia PR, Chamera E, et al. Accuracy of Doppler echocardiography in the hemodynamic assessment of pulmonary hypertension. *Am J Respir Crit Care Med*. 2009;179(7):615–621.
22. Mooi W, Wagenvoort CA. Decreased numbers of pulmonary blood vessels: reality or artifact? *J Pathol*. 1983;141(4):441–447.
23. Chaouat A, Bugnet AS, Kadaoui N, et al. Severe pulmonary hypertension and chronic obstructive pulmonary disease. *Am J Respir Crit Care Med*. 2005;172(2):189–194.
24. Barberà JA, Peinado VI, Santos S. Pulmonary hypertension in chronic obstructive pulmonary disease. *Eur Respir J*. 2003;21(5):892–905.
25. Rahaghi FN, Ross JC, Agarwal M, et al. Pulmonary vascular morphology as an imaging biomarker in chronic thromboembolic pulmonary hypertension. *Pulm Circ*. 2016;6(1):70–81.
26. Burke CM, Glanville AR, Morris AJ, et al. Pulmonary function in advanced pulmonary hypertension. *Thorax*. 1987;42(2):131–135.
27. Meyer FJ, Ewert R, Hoeper MM, et al. Peripheral airway obstruction in primary pulmonary hypertension. *Thorax*. 2002;57(6):473–476.
28. Stenmark KR, Fagan KA, Frid MG. Hypoxia-induced pulmonary vascular remodeling: cellular and molecular mechanisms. *Circ Res*. 2006;99(7):675–691.
29. Kanemoto N, Sasamoto H. Pulmonary hemodynamics in primary pulmonary hypertension. *Jpn Heart J*. 1979;20(4):395–405.
30. Arcasoy SM, Christie JD, Ferrari VA, et al. Echocardiographic assessment of pulmonary hypertension in patients with advanced lung disease. *Am J Respir Crit Care Med*. 2003;167(5):735–740.

### International Journal of COPD

#### Publish your work in this journal

The International Journal of COPD is an international, peer-reviewed journal of therapeutics and pharmacology focusing on concise rapid reporting of clinical studies and reviews in COPD. Special focus is given to the pathophysiological processes underlying the disease, intervention programs, patient focused education, and self management protocols.

Submit your manuscript here: <http://www.dovepress.com/international-journal-of-chronic-obstructive-pulmonary-disease-journal>

Dovepress

This journal is indexed on PubMed Central, MedLine and CAS. The manuscript management system is completely online and includes a very quick and fair peer-review system, which is all easy to use. Visit <http://www.dovepress.com/testimonials.php> to read real quotes from published authors.

## **Quantitative CT assessment of bronchial and vascular alterations in severe precapillary pulmonary hypertension**

### **Supplemental methods**

#### *Study population*

This study was observational, retrospective and conducted according to the principles of the Declaration of Helsinki, French law and approved by our institutional review board. Every patient was informed and agreed that their data can be used for further research studies anonymously. From a prior study <sup>1</sup>, 20 COPD patients were also included in the current study (out of 24 patients) and none in the 2 other groups of severe PH. However, these 20 patients were completely re-analysed by another radiologist. Data were anonymized and they complied with the requirements of the “commission nationale informatique et libertés” (CNIL), that approved the methods, this organisation is responsible for ensuring the ethical use of data collected for scientific purposes in France (approval number: 1909530 v 0). Severe PH patients were consecutively referred between January 2008 and January 2017 to our institution, a tertiary medical center for complete examination of PH, before initiation of any treatment. Each patient underwent within 1 week: medical questioning, physical examination, arterial blood gases, 6-minutes walk tests (6-MWT), blood tests (C-reactive protein (CRP), brain natriuretic peptide (BNP), antinuclear antibodies and HIV serology), trans-thoracic echocardiography, ventilation/perfusion scintigraphy (V/Q scan), pulmonary function testing (PFT), right heart catheterisation (RHC), and unenhanced computed tomography (CT) within a minimal period of 1 month of disease stability. Final statement about disease aetiology, for every patient, was

made by agreement between experienced cardiologists, pneumologists and radiologists, after careful review of all information available.

Only patients with no treatment undertaken, fully screened and with mPAP value equal to or higher than 35 mmHg<sup>2</sup> were included in the study. In addition, we only evaluated pre-capillary PH from chronic obstructive pulmonary disease (COPD), idiopathic pulmonary arterial hypertension (iPAH) and chronic thromboembolic pulmonary hypertension (CTEPH), in adults with a pulmonary capillary wedge pressure (PCWP) values less than 15 mmHg and with no other condition to explain PH in each group.

From the 189 consecutive screened patients, 103 patients had both mPAP value equal or higher than 35 mmHg at RHC<sup>2</sup> and a diagnosis of COPD, iPAH and CTEPH. However, 16 patients were not fully screened and 19 patients could not be included because of related associated diseases. Thus, from the remaining 68 patients included, we focused on 56 adult patients with severe precapillary PH from either COPD, iPAH, or CTEPH, without any other condition to explain PH and with an adequate CT without any other abnormality possibly altering CT measurements. The 19 non-included patients presented concomitant: left heart disease as defined by history of coronaropathy and a left heart function on echocardiography less than 40% (n = 12), sleep apnea syndrome (n = 6), or sarcoidosis (n = 1). No patient appeared to have other concomitant cause of PH, all were precapillary only. Twelve patients were then excluded because of prominent motion artifacts on CT examination (n = 6), presence of lung micronodules (n = 3), pleural plaques (n = 1), pleural effusion (n = 1) and consolidation (n = 1). Among the 56 severe PH patients, 24 patients demonstrated severe PH associated to COPD, diagnosed on PFT (post-bronchodilator FEV<sub>1</sub>/FVC < 70%) and exposure to tobacco; 16 had with severe iPAH, and 16 had severe CTEPH.

### *Pulmonary function tests*

Body plethysmography (BodyBox, Medisoft, Belgium) were used to assess lung mechanics. Functional parameters were recorded in litres and expressed as percentages of predicted values: forced expiratory volume in 1 second (FEV<sub>1</sub>), forced vital capacity (FVC), total lung capacity (TLC), residual volume (RV). Transferrable lung capacity of carbon monoxide (TLCO) were recorded, using HypAir Compact (Medisoft), and expressed as percentage of predicted value. European Respiratory Society and American Thoracic Society (ATS) guidelines were chosen for reference values<sup>3,4</sup>. Arterial blood, at room air, was drawn in order to record arterial blood gases PaO<sub>2</sub>, PaCO<sub>2</sub> (mmHg). ATS recommendation were followed to perform 6-MWT and expressed in meters.

#### *CT protocol*

Chest CT scans were acquired with a 64-section multidetector CT scanner (Somatom Definition; Siemens, Erlangen, Germany) by using the following parameters: 110-kV tube voltage, 50-mAs tube current and 75-msec rotation time, 0.75-mm collimation, no contrast injection. Data were acquired in the supine position at full inspiration and reconstructed with both high-spatial-frequency and standard algorithm, with a 1-mm reconstruction section thickness, 1-mm reconstruction interval, 320x320-mm field-of-view, pixel size (0.625mm)<sup>2</sup>, and 512x512 matrix. CT scans were anonymized in a blinded fashion before automatic quantitative analysis.

#### *Quantitative CT analysis of bronchial wall thickness and emphysema*

High-spatial-frequency algorithm reconstructions of datasets of images were transferred into a workstation and displayed with a parenchymal window width (1800 Hounsfield units (HU)) and level (-600 HU). Dedicated and validated software were used to quantitatively analyse CT scans<sup>5,6</sup>. CT measurements of intrapulmonary airways were performed at subsegmental level.

Automatic quantification of bronchi wall area (WA), lumen area (LA) and wall thickness (WT) were obtained on orthogonal bronchial cross sections perpendicular to bronchial main axis by using the Laplacian-of-Gaussian algorithm, as previously described <sup>6,7</sup>.

Emphysema was automatically quantified and was assessed on CT images reconstructed with standard algorithm by using whole-lung densitometry with Myrian<sup>®</sup> software (Intrasens, Montpellier, France). CT attenuation values of -500 and -1024 HU were used to isolate lungs from the rest of thoracic structures on a threshold-based technique. Low attenuation area (LAA%) was derived from the voxel frequency distribution histogram and represented the percentage of lung voxels less than -950 HU, as previously described <sup>1,8,9</sup>.

#### *Mosaic attenuation evaluation*

CT set of images reconstructed with sharp algorithm (B70f) were seen at window settings appropriate for parenchymal assessment (width: 1,500 HU, level: -700 HU). Mosaic attenuation score was built and derived from a semi-quantitative evaluation of each lobe using a published method <sup>10</sup>. Mosaic attenuation was determined for each lobe as a percentage score ranging from 0 to 100% of reduced attenuation with 10% increments. Reduced attenuation has been subjectively defined as a decrease in parenchymal attenuation conforming to the borders of secondary pulmonary lobules that contain vessels with caliber smaller than expected <sup>11</sup>.

A weighting factor was applied for each lung's lobe score to calculate a total mosaic attenuation score. Weighting factors were 3/20, 2/20 and 5/20 for each upper, middle and lower lobes, respectively <sup>10</sup>.

#### *Measurement of small pulmonary vessels area*

Automated measurement of small vessels was obtained from CT images, as previously described<sup>1,12-16</sup>. CT set of images reconstructed with sharp algorithm (B70f) were transferred into a workstation for post-processing and analysed by using the ImageJ software version 1.40g (a public domain Java image program available at <http://rsb.info.nih.gov/ij/>). First, in order to eliminate image noise, all CT images were smoothed by applying a Gaussian filter. A threshold technique to select pixels between -500 and -1024 Hounsfield units (HU) was used to segment the lung fields. The segmented lung fields were then converted into binary images with a window level of -720 HU. The ImageJ software “Analyze particles” function was applied. This function is useful to count and measure objects on binary images, here it detected the cross sectional area and number of vessels. The ImageJ software “Circularity” function was used to select objects within range of circularity between 0.9 and 1, and allowed selection of vessels running orthogonal to the axial plane.

The cross-section area (CSA) of small pulmonary vessels were automatically quantified separately for each CT slice at the sub-subsegmental levels using ImageJ software. The sub-subsegmental level is defined by a vessel area less than 5 mm<sup>2</sup>. At the same time, lung area was measured for each CT slices. Finally, quantifications were obtained after normalisation by the corresponding lung section area at each CT slice: the cross sectional area of small pulmonary vessels less than 5 mm<sup>2</sup> (%CSA<sub><5</sub>). Then, a mean of %CSA<sub><5</sub> of all CT slices for each patient was calculated.

#### *Measurement of main pulmonary artery ratio diameter*

Large vessels diameters were manually measured, at the level of pulmonary artery bifurcation, for both pulmonary arterial truncus (AP) and ascending aorta (AO) using the same image<sup>1,8</sup>.

The largest diameters were measured by one observer. The ratio AP/AO was then calculated<sup>1,8</sup>.

#### *Right heart catheterisation*

After jugular insertion, a flow-directed balloon-tipped 7F Swan-Ganz catheter (131HF7; Baxter Healthcare Cop., Irvine, USA) was moved in order to assess a right heart catheterisation (RHC)<sup>17</sup>. At end expiration, systolic, mean and diastolic pulmonary artery pressure (s-,m-,dPAP), pulmonary capillary wedge pressure (PCWP) were determined. Gradient was calculated by difference between dPAP and PCWP. Cardiac output (CO) was determined using the Fick method.

#### *Echocardiography*

Standard techniques of two-dimensional Doppler Echocardiography were used at rest to assess right and left heart functions. Measurement of maximal tricuspid regurgitation velocity (ITVmax) and determination of transtricuspid pressure gradient (ITGdmax) with the estimation of the right atrial pressure, allowed to calculate the systolic pulmonary arterial pressure (SPAP). Measurements of end-systolic and end-diastolic left ventricular volumes lead to calculation of the left ventricular ejection fraction (LVEF%).

#### *Statistical analysis*

Statistical analyses were performed using NCSS software (NCSS 2001, Kaysville, UT, USA). Results were expressed as mean with standard deviation and analysed using one-way ANOVA and Tukey post-hoc test. Parameters that were not normally distributed were expressed as median with inter quartile ranges and tested by Kruskal-Wallis and multiple comparisons z-value post-hoc test. Categorical variables were tested with Fisher's exact tests. Univariate

correlations were assessed using r coefficient of Pearson, when data were not normally distributed a log-transformation was applied.

Paw score was calculated to predict severe PH, combining 3 variables (*ie*, PaO<sub>2</sub>, WT and %CSA<sub><5</sub>)<sup>1</sup>. Briefly, each patient received points, ranging from 0 (minimal value) to 3 (maximal value) for every variable, as previously published<sup>1</sup> (See supplemental Table 1). Thresholds were determined previously using interquartile ranges of each variables<sup>1</sup>. Then, the scores ranged from 0 to 9 points, the higher value indicating a higher risk of severe PH. Finally, scores and sensitivity were compared. *P* values less than 0.05 were considered significant.

## References

1. Coste F, Dournes G, Dromer C, et al. CT evaluation of small pulmonary vessels area in patients with COPD with severe pulmonary hypertension. *Thorax*. 2016;71(9):830-837.
2. Seeger W, Adir Y, Barbera JA, et al. Pulmonary hypertension in chronic lung diseases. *J Am Coll Cardiol*. 2013;62(25 Suppl):D109-116.
3. Miller MR, Hankinson J, Brusasco V, et al. Standardisation of spirometry. *Eur Respir J*. 2005;26(2):319-338.
4. Wanger J, Clausen JL, Coates A, et al. Standardisation of the measurement of lung volumes. *Eur Respir J*. 2005;26(3):511-522.
5. Montaudon M, Lederlin M, Reich S, et al. Bronchial measurements in patients with asthma: comparison of quantitative thin-section CT findings with those in healthy subjects and correlation with pathologic findings. *Radiology*. 2009;253(3):844-853.
6. Berger P, Perot V, Desbarats P, Tunon-de-Lara JM, Marthan R, Laurent F. Airway wall thickness in cigarette smokers: quantitative thin-section CT assessment. *Radiology*. 2005;235(3):1055-1064.
7. Montaudon M, Berger P, de Dietrich G, et al. Assessment of airways with three-dimensional quantitative thin-section CT: in vitro and in vivo validation. *Radiology*. 2007;242(2):563-572.
8. Dournes G, Laurent F, Coste F, et al. Computed tomographic measurement of airway remodeling and emphysema in advanced chronic obstructive pulmonary disease. Correlation with pulmonary hypertension. *Am J Respir Crit Care Med*. 2015;191(1):63-70.
9. Bankier AA, De Maertelaer V, Keyzer C, Gevenois PA. Pulmonary emphysema: subjective visual grading versus objective quantification with macroscopic morphometry and thin-section CT densitometry. *Radiology*. 1999;211(3):851-858.

10. Hoey ET, Mirsadraee S, Pepke-Zaba J, Jenkins DP, Gopalan D, Screaton NJ. Dual-energy CT angiography for assessment of regional pulmonary perfusion in patients with chronic thromboembolic pulmonary hypertension: initial experience. *AJR Am J Roentgenol.* 2011;196(3):524-532.
11. Castaner E, Gallardo X, Ballesteros E, et al. CT diagnosis of chronic pulmonary thromboembolism. *Radiographics.* 2009;29(1):31-50; discussion 50-33.
12. Matsuoka S, Washko GR, Yamashiro T, et al. Pulmonary hypertension and computed tomography measurement of small pulmonary vessels in severe emphysema. *Am J Respir Crit Care Med.* 2010;181(3):218-225.
13. Uejima I, Matsuoka S, Yamashiro T, Yagihashi K, Kurihara Y, Nakajima Y. Quantitative computed tomographic measurement of a cross-sectional area of a small pulmonary vessel in nonsmokers without airflow limitation. *Japanese journal of radiology.* 2011;29(4):251-255.
14. Matsuoka S, Washko GR, Dransfield MT, et al. Quantitative CT measurement of cross-sectional area of small pulmonary vessel in COPD: correlations with emphysema and airflow limitation. *Acad Radiol.* 2010;17(1):93-99.
15. Wang Z, Chen X, Liu K, et al. Small pulmonary vascular alteration and acute exacerbations of COPD: quantitative computed tomography analysis. *International journal of chronic obstructive pulmonary disease.* 2016;11:1965-1971.
16. Yoshimura K, Suzuki Y, Uto T, Sato J, Imokawa S, Suda T. Morphological changes in small pulmonary vessels are associated with severe acute exacerbation in chronic obstructive pulmonary disease. *International journal of chronic obstructive pulmonary disease.* 2016;11:1435-1445.

17. Dumas de La Roque E, Savineau JP, Metivier AC, et al. Dehydroepiandrosterone (DHEA) improves pulmonary hypertension in chronic obstructive pulmonary disease (COPD): a pilot study. *Annales d'endocrinologie*. 2012;73(1):20-25.

**Supplemental Table 1:** Paw score variables and range

Paw score points	Variables		
	PaO <sub>2</sub> (mmHg)	% CSA <sub>&lt;5</sub>	WT
0	≥ 64.5	< 0.313	< 1.095
1	[51.5-64.4]	[0.313-0.432]	[1.095-1.179]
2	[46.5-51.4]	[0.433-0.547]	[1.180-1.324]
3	< 46.5	≥ 0.548	≥ 1.325

Definition of abbreviations: PaO<sub>2</sub>: Arterial partial pressure in oxygen; %CSA<sub><5</sub>, percentage of total lung area taken up by the cross-sectional area of pulmonary vessels less than 5mm<sup>2</sup>; WT, mean Wall Thickness.

**Supplemental Table 2:** Univariate correlation between mPAP and different clinical, biological and functional parameters

	COPD with severe PH			Severe iPAH			Severe CTEPH		
	n	Coef	p-value	n	Coef	p-value	n	Coef	p-value
Age (years)	24	0.27	<b>0.04</b>	16	-0.24	0.37	16	-0.17	0.53
BMI (kg.m <sup>-2</sup> )	24	0.08	0.67	16	-0.24	0.38	16	0.41	0.12
PFT									
FEV <sub>1</sub> (% pred)	24	0.27	0.21	15	0.06	0.84	16	-0.31	0.25
FEV <sub>1</sub> /FVC (%)	24	0.25	0.24						
									<b>0.03</b>
		<b>0.05</b>							
		<b>0.04</b>							
		<b>0.02</b>							
					<b>0.01</b>		13		
					<b>0.01</b>				
									<b>0.03</b>

Data are Pearson correlation coefficients.

Definition of abbreviations: COPD, chronic obstructive pulmonary disease; iPAH, idiopathic pulmonary arterial hypertension; CTEPH, chronic thromboembolic pulmonary hypertension; Coef, Coefficient; BMI, body mass index; BNP, brain natriuretic peptide; CRP, C reactive protein; FEV<sub>1</sub>, forced expiratory volume in 1 second; FVC, forced volume capacity; ITVmax, maximal tricuspid regurgitation velocity; ITGdmax, maximal transtricuspid pressure gradient; LVEF, left ventricular ejection fraction; sPAP, systolic pulmonary arterial pressure; PFT, pulmonary function test; pred, predicted; PVR, pulmonary vascular resistance; PVR<sub>i</sub>, indexed PVR; RV, residual volume; TLC, total lung capacity; TLCO, transfer lung capacity of carbon monoxide.

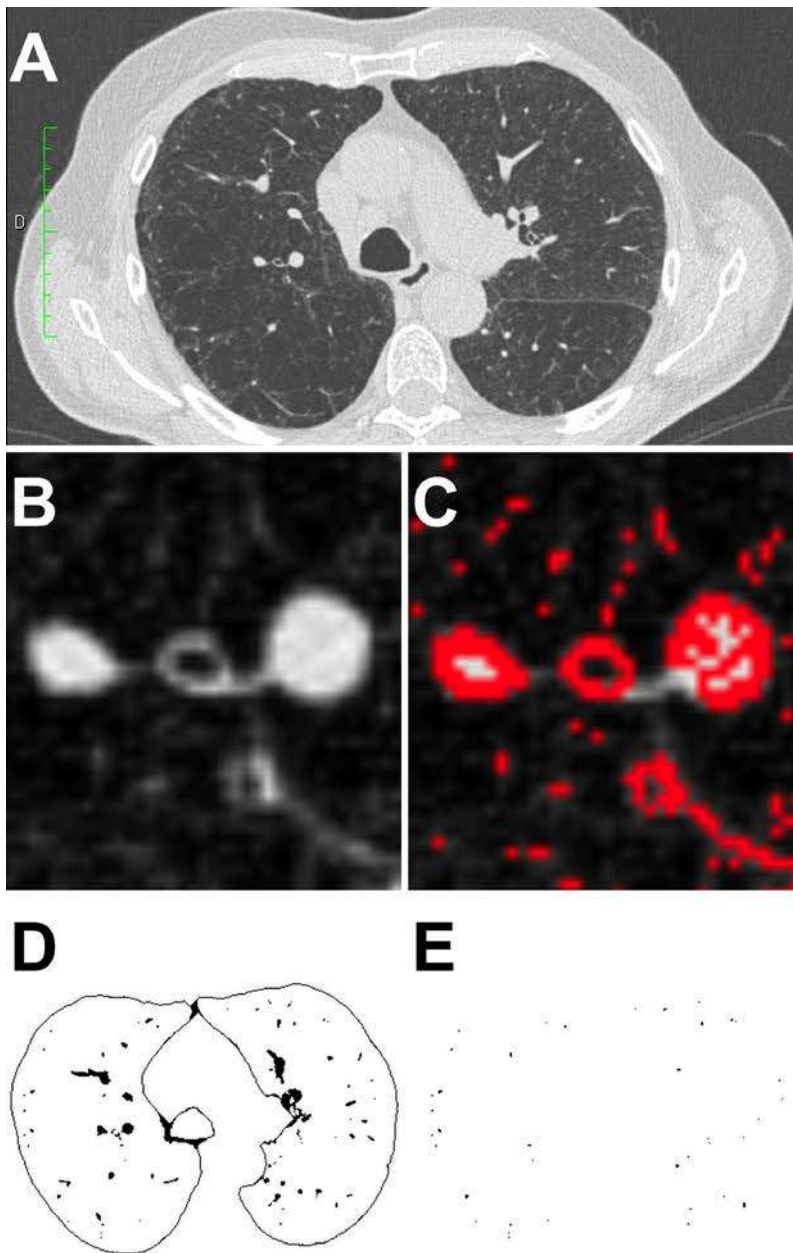
**Supplemental Table 3:** Sensitivity of ultrasound echocardiography and Paw score to detect severe PH

	COPD with severe PH	Severe iPAH	Severe CTEPH
SPAP> 50 mmHg	69.6%	87.5%	100%
SPAP> 60 mmHg	60.9%	75.0%	85.7%
SPAP> 65 mmHg	52.2%	68.8%	78.6%
Paw score≥ 5 points	87.5%	43.8%	62.5%

Values are sensitivity to detect severe PH based on RHC using either sPAP assessed by echocardiography or Paw score.

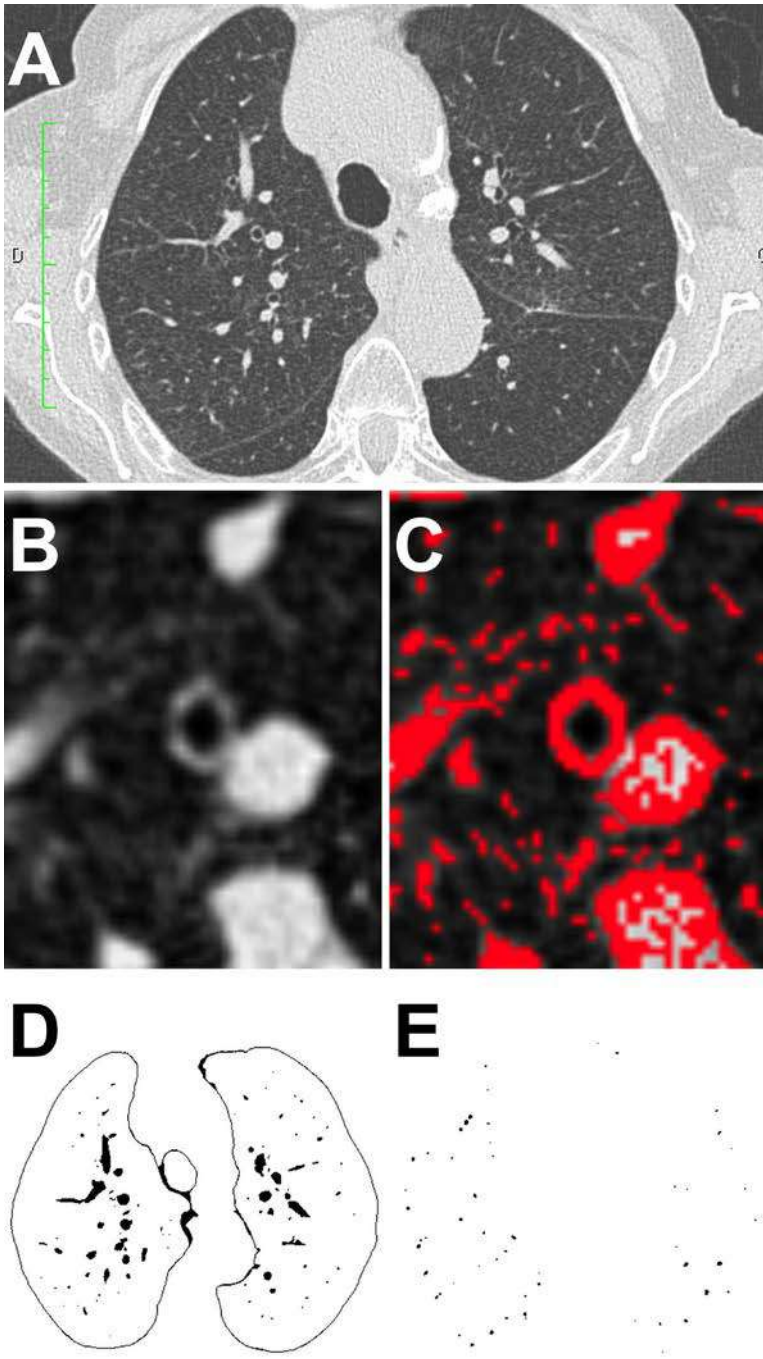
Definition of abbreviations: COPD, chronic obstructive pulmonary disease; iPAH, idiopathic pulmonary arterial hypertension; CTEPH, chronic thromboembolic pulmonary hypertension; SPAP, systolic pulmonary arterial pressure on echocardiography.

## Figures legends



**Supplemental Figure 1:** CT scans representative of a COPD patient with severe PH.

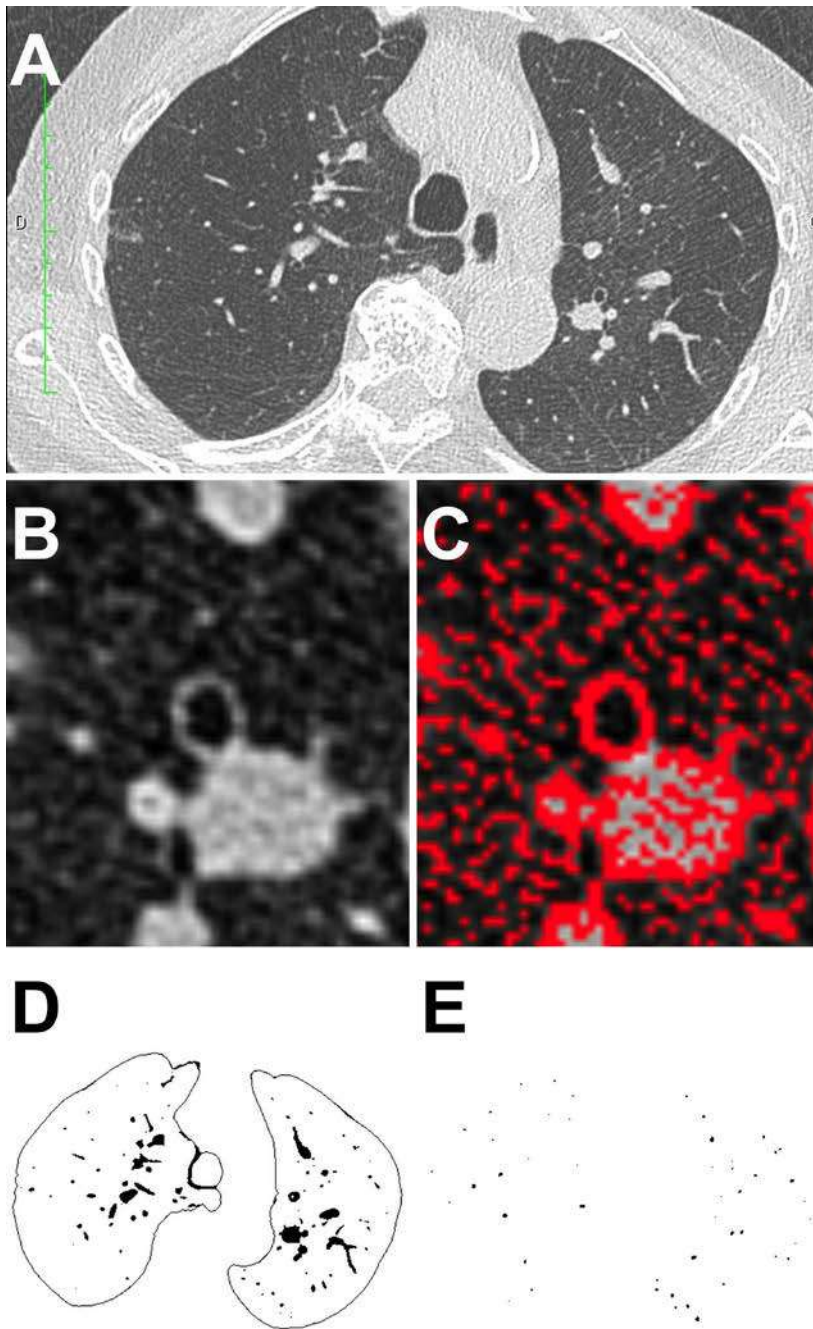
(A) Native transverse thin-section CT-image. (B) Reformatted section perpendicular to the main bronchial axis before and (C) after segmentation for bronchial wall measurement. (D) Converted binary image after bi-thresholding (E) Mask image analysis for small vessels ranging from 0 to 5 mm<sup>2</sup>.



**Supplemental Figure 2:** CT scans representative of a severe iPAH patient.

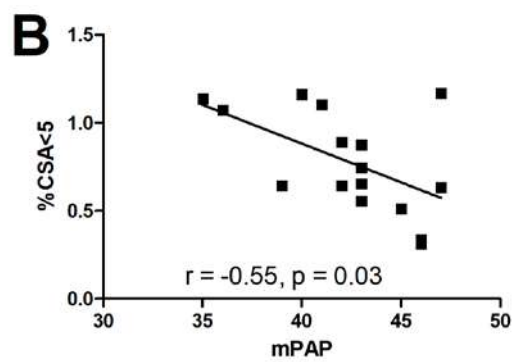
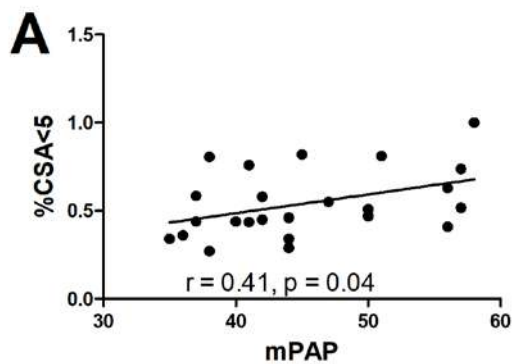
(A) Native transverse thin-section CT-image. (B) Reformatted section perpendicular to the main bronchial axis before and (C) after segmentation for bronchial wall measurement.

(D) Converted binary image after bi-thresholding (E) Mask image analysis for small vessels ranging from 0 to 5 mm<sup>2</sup>.



**Supplemental Figure 3:** CT scans representative of a severe CTEPH patient.

(A) Native transverse thin-section CT-image. (B) Reformatted section perpendicular to the main bronchial axis before and (C) after segmentation for bronchial wall measurement. (D) Converted binary image after bi-thresholding (E) Mask image analysis for small vessels ranging from 0 to 5 mm<sup>2</sup>.



**Supplemental Figure 4:** Correlations between mean pulmonary arterial pressure (mPAP) and percentage of total lung area taken up by the cross-sectional area of pulmonary vessels less than 5 mm<sup>2</sup> (%CSA<5)

(A) Correlations for COPD subjects and (B) Correlations for iPAH subjects with severe PH.

## **2.2 Publication n°2 : Développement d'une méthode semi-automatique pour la quantification de l'atteinte des voies aériennes distales**

Les méthodes des masques de densité, actuellement disponibles pour la quantification de l'atteinte obstructive des voies aériennes distales, ne fournissent qu'une évaluation globale de l'atteinte. De plus, les cartes de réponses paramétriques basées sur le recalage élastique des images comportent une incertitude de mesure liée à la déformation nécessaire au recalage des volumes expiratoire et inspiratoire. Dans cette étude nous avons développé une nouvelle méthode semi-automatique de quantification de l'atteinte des voies aériennes distales basée sur des algorithmes de classification (clustering) spectrale. Nous l'avons ensuite appliquée sur une cohorte de patients atteints de pneumopathie d'hypersensibilité (PHS) chronique. En effet, l'atteinte bronchiolaire dans la PHS est bien établie. En plus, la présence de zones pulmonaires lobulaires hypodenses au scanner thoracique est connue pour être une aide supplémentaire au diagnostic de PHS. Dans les formes fibrosantes de PHS, lorsqu'il existe des signes de distorsion, la présence de « lobules clairs » qui témoignent de cette atteinte bronchiolaire sous-jacente est un argument pour le diagnostic de PHS chronique. Les études ayant comparé les PHS chroniques et les maladies interstitielles fibrosantes primitives que sont la Fibrose Idiopathique et la pneumopathie interstitielle non spécifique (PINS) ont montré que si ces lobules clairs étaient possiblement présents dans toutes ces affections, leur nombre était beaucoup plus important dans les PHS fibrosantes. Il y a donc un intérêt à développer une méthode d'analyse automatique qui permette de quantifier ces lobules. Les méthodes quantitatives existantes peuvent difficilement être appliquées à cette problématique car les lobules clairs sont présents avec d'autres signes TDM en rapport avec la PHS ou les pneumopathies interstitielles diffuses (PID) fibrosantes et peuvent être des facteurs confondants dans une analyse quantitative qui ne reposerait que sur une méthode basée sur un histogramme des valeurs de pixels. Nous avons développé, à partir d'une analyse de clusters de pixels de faible densité, une méthode permettant d'identifier et de mesurer le volume des pixels de faible densité présents dans les lobules clairs et l'avons évaluée sur une population de patients porteurs d'une pneumonie interstitielle fibrosante. L'objectif de cette étude était de décrire la méthode et d'évaluer l'intérêt de la quantification de l'extension de ces zones lobulaires d'hypodensité dans le diagnostic différentiel avec les pneumopathies interstitielles communes (PIC) et les PINS. Les données histologiques et paramètres de la fonction pulmonaire de 15 patients atteints

de PHS chronique et 17 patients atteints de PIC/PINS ont été collectés. Les données quantitatives de l'extension des zones d'hypodensité lobulaire ont été comparées. Les résultats ont montré un pourcentage d'extension des zones d'hypodensité lobulaire plus élevé chez les patients PHS fibrosante. De plus, ces mesures ont présenté des corrélations significatives avec les paramètres obstructifs aux explorations fonctionnelles respiratoires renforçant ainsi la validité de notre méthode quantitative. Egalement, la reproductibilité de notre méthode semi-automatique était très bonne. Ainsi, la quantification des zones d'hypodensité lobulaire par notre nouvelle méthode est susceptible d'aider à discriminer les patients atteints de PHS fibrosante et ceux souffrants de PIC ou PINS.

**Title: Semi-Automated Quantification of Lobular Decreased Attenuation Areas Extent in patients with Chronic Hypersensitivity Pneumonitis**

**Article type: Original research**

**Authors**

Ilyes Benlala<sup>1,2,3</sup>, Adrien Rispal<sup>3</sup>, John Refait<sup>3</sup>, Hugues Begueret<sup>3</sup>, Patrick Berger<sup>1,2,3</sup>, Gael Dournes<sup>1,2,3</sup>, François Laurent<sup>1,2,3</sup>

**Affiliations**

<sup>1</sup> Univ. Bordeaux, Centre de Recherche Cardio-Thoracique de Bordeaux, U1045, CIC 1401, F-33000 Bordeaux, France

<sup>2</sup> Inserm, Centre de Recherche Cardio-Thoracique de Bordeaux, U1045, CIC 1401, F-33000 Bordeaux, France

<sup>3</sup> CHU de Bordeaux, Service d'Imagerie Thoracique et Cardiovasculaire, Service d'Anatomopathologie, CIC 1401, F-33600 Pessac, France

**Contact author :**

Dr Ilyes Benlala, Centre de Recherche Cardio-thoracique de Bordeaux, INSERM U1045, Université Bordeaux, 146 rue Léo Saignat, 33076 Bordeaux Cedex, France

E-mail: [ilyes.ben-lala@u-bordeaux.fr](mailto:ilyes.ben-lala@u-bordeaux.fr)

**Abbreviations:**

%LDAA=percentage of lobular decreased attenuation areas

AUC=area under the curve

CI = confidence interval

HP=Hypersensitivity pneumonitis

ICC = intraclass correlation coefficient

IPF=Idiopathic pulmonary fibrosis

NSIP=nonspecific interstitial pneumonia

PFT=pulmonary function testing

ROC=receiver operating characteristics

UIP=usual interstitial pneumonia

## **Abstract**

**Background:** The usefulness of the quantification of lobular decreased attenuation areas on chest CT scans to diagnose chronic hypersensitivity pneumonitis (HP) still remains to be determined.

**Purpose:** To assess whether the quantification of lobular decreased attenuation areas could distinguish between chronic HP and idiopathic pulmonary fibrosis / nonspecific interstitial pneumonia (IPF/NSIP) patients using a novel semi-automated method.

**Methods and Materials:** Fifteen chronic HP patients (8males; mean age 65±14) and 17 controls with 12 IPF patients and 5 NSIP (13males; mean age 65±8) were retrospectively included between 2004 and 2018. Patients had available pathological slides for expert reviewing, chest CT scans and pulmonary function testing (PFTs). Lobular decreased attenuation areas extent was visually evaluated by two readers. Semi-automated quantification of percentage of lobular decreased attenuation areas (%LDAA) was performed. Comparison of means was made using Student's t-test. Comparison of categorical variables and proportions was performed using the Fisher exact test. Correlation was determined using Pearson's test. Agreement was found using kappa index, and reproducibility was determined using intraclass correlation coefficient (ICC). Diagnostic performance was assessed by calculating the area under the receiver operating characteristics curve (AUC).

**Results:** Using visual analysis, lobular decreased attenuation areas were most likely to be found in chronic HP patients than in controls (p=0.20). Intra and interobserver agreement was very good ( $\kappa \geq 0.91$ ). Using semi-automated quantification, %LDAA was significantly higher in chronic HP patients in comparison to controls (p<0.001). Significant correlations were found with PFTs parameters and transfert lung capacity of carbon monoxyde. The diagnostic performance and reproducibility of %LDAA were very good (AUC, 0.84 [95%CI: 0.70, 0.99] and ICCs $\geq$ 0.89, respectively).

**Conclusion:** Semi-automated quantification of the extent of lobular decreased attenuation areas might be helpful to distinguish chronic HP from IPF/NSIP in patients with unusual/indeterminate CT patterns.

**Word count of Abstract:** 291

**Word count of main manuscript:** 2888

## INTRODUCTION

Hypersensitivity pneumonitis (HP) is a respiratory disease triggered by antigens inhalation in pre-sensitized subjects. The antigen inhalation is responsible for local immunologically induced inflammation of the lung parenchyma and distal airways (1). Clinically, HP may manifest as acute, subacute or chronic illness (2). Acute form is usually induced by intense antigen exposure and clinical improvement is often obtained after exposure removal. However, low-level persistent or recurrent exposure may lead to chronic HP with end-stage fibrosis (3,4). Besides clinical symptoms of HP (1), High-resolution computed tomography (HRCT) plays an important role to help clinicians in a confident diagnosis of HP (5–9). Acute/subacute HP CT patterns mostly appear as patchy or diffuse ground glass opacities with poorly defined centrilobular nodules associated with lobular areas of decreased attenuation (3). In chronic HP, radiologic findings are secondary to fibrotic damage with the presence of reticulation and traction bronchiectasis/bronchiolectasis overlapping subacute HP CT patterns with in some cases rare sub pleural honeycombing (3). However, CT features of chronic HP may mimic those of usual interstitial pneumonia (UIP) and nonspecific interstitial pneumonia (NSIP) (6,7,9). The most efficient factor in the management of HP is the antigen exposure removal. Therefore, it is crucial to differentiate chronic HP from other interstitial lung diseases (i.e. UIP and NSIP) (10). Several studies predating the recent American Thoracic Society and European Respiratory Society Japanese Respiratory Society, and Latin American Thoracic Society clinical practice guidelines (11) proposed the use of chest CT to differentiate HP from other chronic interstitial lung diseases (7,9,12,13).

In the study by Sliva et al. (9), the authors suggested that the best CT features to distinguish chronic HP from idiopathic pulmonary fibrosis (IPF) and NSIP are lobular areas with decreased attenuation and vascularity, centrilobular nodules and absence of lower-zone predominance of abnormalities. However, lobular areas of decreased attenuation were visually evaluated by counting the number of secondary lobules with decreased attenuation on inspiratory images (9). Furthermore, the reproducibility of this visual counting for extent evaluation was not assessed. The purpose of this study was to assess the accuracy of the quantification of lobular decreased attenuation areas on chest CT scans to distinguish chronic HP from IPF and NSIP using an innovative quantitative semi-automated method. Pathologic findings were used as reference standard. Secondary objectives were to assess correlation with lung function, to evaluate the diagnostic performance of lobular decreased attenuation areas quantification to identify chronic HP, and to determine the reproducibility of the evaluation.

## **MATERIALS AND METHODS**

### **Study patients**

This was a retrospective study approved by our institutional review board and the requirement for written informed consent was waived. Our institutional anatomic pathology database was reviewed between January 2004 and January 2018. All consecutive patients with diagnostic of chronic HP, IPF and NSIP were screened. Patients that had underwent chest CT scan within maximum interval of 30 days before surgical lung biopsy and that had pathologic slides for expert reviewing were included. After the second expert reading of the pathologic slides, diagnostic of chronic HP, IPF or NSIP was determined according to standard criteria (11,14,15).

### **Pulmonary function tests**

Body plethysmography (BodyBox, Medisoft, Belgium) were used to assess lung mechanics. Functional parameters were recorded in liters and expressed as percentages of predicted values: forced expiratory volume in 1 second (FEV1%), forced vital capacity (FVC), total lung capacity (TLC), functional residual capacity (FRC), residual volume (RV) and forced expiratory flow at 25-75% (FEF25-75%). Transferr lung capacity of carbon monoxide (TLCO) were recorded, using HypAir Compact (Medisoft), and expressed as percentage of predicted value. Arterial blood, at room air, was drawn in order to record partial arterial pressure of oxygen PaO<sub>2</sub> (mmHg).

### **CT protocol**

Chest CT scans were acquired with a 64-section multidetector CT scanner (Somatom Definition; Siemens, Erlangen, Germany) by using the following parameters: 110-kV tube voltage, 50-mAs tube current and 75-msec rotation time, 0.75-mm collimation, no contrast injection. Data were acquired in the supine position at full inspiration and reconstructed with both high-spatial-frequency and standard algorithm, with a 1-mm reconstruction section thickness, 1-mm reconstruction interval, 320x320-mm field-of-view, pixel size (0.625mm)<sup>2</sup>, and 512x512 matrix. CT scans were anonymized before image analysis.

### **Image evaluation**

#### *Visual analysis*

Images reconstructed using high-spatial-frequency algorithm were used for visual evaluation and multi-planar reconstruction was allowed. Image settings for the visual analysis of CT datasets were: window width 1500 Hounsfield Units (HU) and window level -700 HU. Two

chest radiologists (A.R and J.R), blinded to the clinical/pathologic diagnosis and after pre-training session on CT images not included in this study, they independently interpreted CT scans to evaluate the presence/extent and the distribution of the following findings: inter/intralobular reticulations, honeycombing, ground glass opacities/centrilobular micronodules and lobular decreased attenuation areas (Figure 1). Using a scale reported by Silva et al. (9), lobular decreased attenuation areas were scored from 0 (no areas of decreased attenuation) to 3 (at least 5 lobular decreased attenuation area in more than 4 lobes of the lung). Definitions of CT findings were based on the Nomenclature Committee of the Fleischner Society (16) . Any discrepancies in the evaluations were resolved through consensus.

### *Quantitative analysis*

We used an in-house software program written in Matlab (MathWorks, Natick, Mass) to quantify, in a semi-automated fashion, the extent of the lobular decreased attenuation areas. For this, Images reconstructed with smooth standard filter were used. First, automated volumetric segmentation of the lungs was obtained using a threshold-based method (17). To do so, an iterative algorithm to select the optimal threshold based on splitting image histogram into two classes (background/foreground) was performed. In order to exclude pixels with attenuation value equal or less than -950HU which may be considered as representative of emphysema (18), those pixels were assigned a value of -3024HU as the pixels of the background. Second, to minimize heterogeneity of pixel attenuation values within lobular decreased attenuation areas, 2D smooth median filter was applied to the segmented images after reconstruction in coronal plan. Finally, spectral clustering algorithm was performed using pixels of the total lung volume in order to regroup pixels in different clusters with close attenuation values (Figure E1) (19). briefly, similarity graph of the lung pixels was built using mutual weighted k-nearest neighbors algorithm with k=10. Then normalized Laplacian matrix was computed and k-means clustering algorithm applied with a number of clusters equal to 10. The number of 10 clusters was chosen and validated under visual control after investigating different numbers of clusters (i.e. between 5 and 15 clusters). Indeed, a low number of clusters leads to insufficient and incorrect identification of lobular decreased attenuation areas mixed with normal lung attenuation areas, and a high number of clusters results in over segmentation of lung pixels. The cluster of pixels with the lowest attenuation value that remain higher than -950HU was selected automatically. To validate the cluster which most likely refers to lobular decreased attenuation areas, coronal lung images representative of the 10 different clusters were displayed beside the coronal native images, allowing the radiologist to scroll through lung

volume and to select the accurate cluster if different from the automatic chosen one. The percentage of lobular decreased attenuation areas (%LDAA) was finally calculated as the number of pixels belonging to the selected cluster over the total number of lung pixels. In addition, regional analysis of upper and lower lung was performed. Along the cranio-caudal direction, the first and the last slice belonging to the lung mask were identified as the upper and the lower boundaries. Therefore, the upper lung was defined as the upper half between these two boundaries, and the lower lung as the lower half part between these two boundaries. The average time for post processing and spectral clustering did not exceed 2 minutes with about 30 seconds for radiologist validation.

### **Additional evaluation to validate quantitative analysis**

To further validate the semi-automated quantification of lobular decreased attenuation areas of the lung, correlations between %LDAA and pulmonary function tests parameters were determined. In addition, diagnostic performance of %LDAA measurements to differentiate chronic HP from IPF/NSIP was assessed with pathologic finding as standard reference.

### **Reproducibility Assessment**

Qualitative and quantitative independent measurements of the two radiologists (J.R and I.B) were analyzed to assess interobserver reproducibility. The second reader (I.B) evaluated all blinded images 2 months later, in random order, to prevent recall bias and assess intraobserver reproducibility.

### **Statistical Analysis**

Statistical analyses were performed by using software (NCSS 2001; NCSS, Kaysville, Utah). For independent variables, comparisons of parametric and nonparametric data were performed by using the Student t test and Mann-Whitney test, respectively. Comparison of categorical variables and proportions was performed by using the Fisher exact test. Univariate correlations were assessed by using the Pearson test for parametric variables and the Spearman test for nonparametric variables. A p value less than 0.05 was considered to indicate statistical significance. Agreement was assessed by using weighted kappa index. Reproducibility was assessed by using intraclass correlation coefficients with 95% confidence intervals and Bland-Altman analysis (20). Weighted k and intraclass correlation coefficient values were classified from null (ie, 0), slight ( $>0$  to  $\leq 0.20$ ), fair ( $>0.20$  to  $\leq 0.40$ ), moderate ( $>0.40$  to  $\leq 0.60$ ), good

(>0.60 to  $\leq$ 0.80), and very good (>0.80) according to Landis et al (21). Diagnostic performance was measured by calculating sensitivity, specificity, and area under the receiver operating characteristic curve.

## RESULTS

### *Study patients*

The review of our institutional pathologic database revealed 100 patients with diagnostic of chronic HP. Only 30 patients had undergone CT scans within 30 days before lung biopsy. Thirteen pathologic slides were missing for expert reviewing. Thus, 17 chronic HP patients were included in the study in addition to 17 UIP and NSIP consecutive patients with the same inclusion criteria (i.e. CT scan within 30 days before lung biopsy and available pathologic slides for expert reviewing).

Two patients with chronic HP were excluded after the second pathologist reviewing.

Final study population was composed of 15 chronic HP patients (8males/7females; mean age  $65\pm 14$ ) and 17 controls with 12 IPF patients and 5 NSIP (13males/4females; mean age  $65\pm 8$ ). Functional residual capacity was significantly lower in IPF/NSIP group in comparison to chronic HP patients ( $p=0.01$ ). Moreover, in chronic HP group, forced expiratory flow at 25-75% (FEF<sub>25-75</sub>) was found lower than in controls ( $p=0.03$ ). There were no statistically significant differences in the other PFTs parameters or gas exchange parameters between the two groups (Table 1).

### *CT Visual analysis*

Lobular decreased attenuation areas were more likely to be found in chronic HP patients than in controls (13/15 (87%) and 10/17 (59%), respectively;  $p=0.20$ ). The median score of the extent of lobular decreased attenuation areas was higher in chronic HP patients than in control group ( $p=0.044$ ). The extent of lobular decreased attenuation areas was predominantly scored 3 in chronic HP group (8/15 (53%)) in comparison to IPF/NSIP group where only 3/17 (18%) were scored 3 for the extent of decreased attenuation areas (Table2).

In addition, honey combing, ground glass opacities and reticulations were not significantly different between the two groups ( $p = 0.72$ ,  $p = 0.29$  and  $p = 0.48$ ; respectively). However, a

sub-pleural predominance of these parenchymal abnormalities was found in IPF/NSIP group 94% (16/17) versus 53% (8/15) in chronic HP group ( $p=0.01$ ) (Table2).

#### *CT quantitative analysis*

Using the semi-automated quantification method (Figure 2), %LDAA was higher in chronic HP patients in comparison to controls ( $p<0.001$ ) (Table1). In addition, regional analysis between upper and lower lung shows no significant difference in chronic HP and control group ( $p = 0.20$  and  $p = 0.58$ ; respectively) (Data not shown).

In chronic HP group, significant correlations were found between %LDAA and pulmonary function tests parameters (i.e. TLC, FVC, FEV1%) ( $r = -0.65$ ;  $p=0.02$ ,  $r = -0.70$ ;  $p<0.01$ ,  $r = -0.74$ ;  $p<0.01$ , respectively) and transfer lung carbon monoxide diffusing capacity ( $r = -0.79$ ;  $p<0.01$ ). In controls, only TLC and FVC showed significant correlations with %LDAA ( $r = -0.52$ ,  $p = 0.03$  and  $r = -0.56$ ,  $p = 0.02$ ; respectively).

#### *Diagnostic performance of lobular decreased attenuation areas to differentiate chronic HP from IPF and NSIP*

Using the semi-automated quantification of lobular decreased attenuation areas, a threshold of %LDAA greater than 10.4% would be able to distinguish chronic HP from IPF/NSIP with a sensitivity equal to 80% [52;96] (12/15), a specificity of 82% [57;96] (14/17) and AUC equal to 0.84 [0.70;0.99]. However, the visual evaluation of lobular decreased attenuation areas extent had greater sensitivity (87% (13/15)) but with poor specificity (41% (7/17)).

#### *Assessment of reproducibility*

Visual assessment of lobular decreasing attenuation areas extent had very good inter and intra observer agreement ( $k = 0.91$  [0.80; 1] and  $k = 0.98$  [0.95; 1]; respectively). Using semi-automated quantification of %LDAA, very good inter and intra observer reproducibility were obtained (ICC = 0.89 [0.77;0.95] and ICC = 0.98 [0.97;0.99] respectively). The mean difference at Bland-Altman analysis was equal to 0% (LoA [-0.07;0.07]) (Table3).

## Discussion

This retrospective study analyzed whether the quantification of lobular decreased attenuation areas could distinguish between chronic HP and IPF/NSIP patients using a novel semi-automated method. Thus, %LDAA was higher in chronic HP patients in comparison to IPF/NSIP group ( $p < 0.001$ ). Furthermore, strong correlations were found between %LDAA and PFT/gas exchange parameters ( $p < 0.01$ ). Moreover, %LDAA was found to help diagnose chronic HP with AUC equal to 0.84 [0.71;0.99]. Finally, the semi-automated quantification showed good to very good reproducibility ( $ICC \geq 0.89$ ).

In our study, chronic HP patients showed a restrictive pattern in PFTs with decreased TLCO which is consistent with previously reported data (4,22,23). Indeed, FVC and TLC predicted values were close to that of IPF/NSIP patients with only FRC that was significantly lower in the latter group(24). Moreover, small airways dysfunction is known to be part of chronic HP pathogeny due to cellular or constrictive bronchiolitis (4,25,26). Therefore, decreased FEF25-75 in chronic HP group could reflect HP physiopathology mechanisms. Indeed, lobular decreased attenuation areas which are believed to be secondary to small airway obstruction, were present in 87% of chronic HP patients in our study which is similar to that of already reported studies (4,9,25). In IPF/NSIP patients, the rate of CT examinations with lobular decreased attenuation areas was 59% which is slightly higher than in Silva et al. study (9). This could be due to peribronchiolar metaplasia found in 10 IPF/NSIP patients at pathology reviewing which could lead to small airway obstruction (27). In addition, visual misinterpretation of normal lung areas surrounded by fibrotic lesions may result in an overestimation of lobular decreased attenuation areas extent. Another point to discuss is that CT patterns of IPF/NSIP patients included in our study were not the usual radiological patterns of these diseases and the diagnosis could not be made with confidence without surgical lung biopsy. Hence, lobular decreased attenuation areas were seen extensively in IPF/NSIP group. Nevertheless, the visual score was significantly higher in chronic HP in comparison to IPF/NSIP group. Although fibrotic lesions were seen similarly in both groups, their distribution with sub pleural predominance was more likely to be found in IPF/NSIP patients ( $p = 0.01$ ) as already reported (9,28,29). However, sub pleural distribution was found in 8/15 (53%) of chronic HP patients.

Conversely, semi-automated quantification of the extent of lobular decreased attenuation areas was able to differentiate chronic HP from IPF/NSIP patients ( $p < 0.001$ ) with 0.84 AUC in ROC curve analysis. One can argue that the semi-automated method is still dependent on the visual

validation of the radiologist. However, to validate the chosen cluster no estimation of the extent of lobular decreased attenuation areas was needed. In addition, to gain reproducibility the categorical score of the visual analysis lacks accuracy and precision, which led to poor specificity to differentiate chronic HP from IPF/NSIP. Indeed, the large range of the semi-automated quantification in our study (0%-27%) allowed distinguishing chronic HP with good specificity (82%) in patients with close overlapping CT patterns. Moreover, quantification of lobular decreased attenuation areas showed significant correlations with PFTs parameters, which could further validate the clinical relevance of this biomarker. In a study by Hansell et al. (4), authors reported significant correlation between percentage of decreased attenuation and RV ( $r= 0.55$ ). The population evaluated in their study were patients with subacute and chronic HP but only 8/22 showed fibrotic lesions on CT images.

Our study had several limitations. This was a retrospective study with a small number of patients. Indeed, patient inclusion was dependent on available pathological slides for expert reviewing. Furthermore, surgical lung biopsy was performed only in patients with not confident clinical/biological and radiological diagnosis. Then study population was composed of patients with unusual/indeterminate CT patterns of ILD. The small number of patients prevented to perform multivariate analysis including other CT patterns (i.e. basal/sub-pleural predominance), which could increase the accuracy of visual analysis to distinguish between chronic HP and IPF/NSIP as previously reported (9). However, the aim of this study was to assess the value of the sole quantification of decreased attenuation areas in a semi-automated fashion to discriminate chronic HP. Expiratory CT examinations were not available to assess air trapping extent. Nonetheless, lobular decreased attenuation areas on inspiratory examinations can reflect small airways obstruction or vasoconstriction (16). A fully automated method is worth testing (30) however, it could be time and/or computational power consuming. In addition, in this particular context of fibrotic ILD, the visual validation of the radiologist remains a guarantee of reliable quantification. Moreover, the semi-automated method showed very good intra and interobserver reproducibility.

In conclusion, semi-automated quantification of the extent of lobular decreased attenuation areas might be helpful to distinguish chronic HP from IPF/NSIP in patients with unusual/indeterminate CT patterns.

**Table 1. Characteristics of the study patients**

	<b>Chronic HP</b> (n=15)	<b>IPF/NSIP</b> (n=17)	<b>p-value</b>
<b>Age</b>	65 ±14	65 ±8	0.92
<b>Sex</b>			0.26
M	8	13	
F	7	4	
<b>Tobacco use</b>			
Ever smoker			0.64
Yes	4	6	
No	11	11	
Current Smoker			0.64
Yes	1	2	
No	14	15	
<b>PFTs</b>			
TLC%*	73 ±26	66 ±13	0.35
FRC %**	85 ±27	65 ±10	0.01
FVC%***	66 ±25	66 ±18	0.97
FEV <sub>1</sub> %***	66 ±23	70 ±19	0.63
FEF <sub>25_75</sub> %****	58 (41-85)	94 (65-132)	0.03
RV%****	81 (58-103)	69 (54-85)	0.10
<b>Gas exchange</b>			
TLCO%**	45 ±20	49 ±17	0.58
PaO <sub>2</sub> (mmHg)***	73 (60-93)	69 (63-75)	0.50

Note: Data are means ± SD for continuous normal variables, or median with [95% confidence interval] if their distribution was not normal.

Legends: HP=hypersensitivity pneumonitis; IPF=idiopathic pulmonary fibrosis; NSIP=nonspecific interstitial pneumonitis; TLC=total lung capacity; FRC=functional residual capacity; FVC=forced vital capacity; FEV<sub>1</sub>=forced expiratory volume in 1 second; FEF<sub>25\_75</sub>=forced expiratory flow at 25-75%; RV=residual volume; TLCO=transfer lung capacity of carbon monoxide; PaO<sub>2</sub>=arterial partial pressure of oxygen. \* Measurements were missing in 3 patients with chronic HP and 1 patient with IPF/NSIP \*\* Measurements were missing in 3 patients with chronic HP and 3 patients with IPF/NSIP. \*\*\* Measurements were missing in 2 patients with chronic HP and 1 patient with IPF/NSIP. \*\*\*\* Measurements were missing in 3 patients with chronic HP and 2 patients with IPF/NSIP

**Table 2. CT visual and quantitative analysis**

	<b>Chronic HP (n=15)</b>	<b>IPF/NSIP (n=17)</b>	<b>p-value</b>
<i>Visual analysis</i>			
<b>Lobular decreased attenuation areas</b>			0.10
Score 0	2(13%)	7(41%)	0.12
Score 1	2(13%)	1(5%)	0.58
Score 2	3(20%)	6(40%)	0.44
Score 3	8(53%)	3(17%)	0.06
<b>Median visual score*</b>	3 (1-3)	2 (0-2)	0.04
<b>Intra/interlobular reticulation</b>	15(100%)	17(100%)	0.48
<b>Ground glass opacities</b>	11(73%)	9(52%)	0.29
<b>Honeycombing</b>	7(46%)	10(58%)	0.72
<b>Craniocaudal distribution</b>			0.26
Homogeneous	12(80%)	10(58%)	0.26
Apical predominance	0(0%)	0(0%)	NA
Basal predominance	3(20%)	7(41%)	0.26
<b>Axial distribution</b>			0.02
Homogeneous	5(33%)	1(5%)	0.07
Central predominance	2(13%)	0(0%)	0.21
Sub pleural predominance	8(53%)	16(94%)	0.01
<i>Quantitative analysis</i>			
<b>Mean %LDAA**</b>	14 ±8	5 ±5	<0.001

Note: \* Data are median with [95% confidence interval]. \*\* Data are means ± SD  
Legends: HP=hypersensitivity pneumonitis; IPF=idiopathic pulmonary fibrosis;  
NSIP=nonspecific interstitial pneumonitis; %LDAA= percentage of lobular decreased  
attenuation areas

**Table 3. Reproducibility of visual and quantitative analysis**

	<b>Kappa</b>	
<b>Visual analysis</b>		
Intra-observer	0.98 [0.95; 1]	
Inter-observer	0.91 [0.80; 1]	
	<b>ICC</b>	<b>BA mean difference</b>
<b>Quantitative analysis</b>		
Intra-observer	0.98 [0.97;0.99]	0.0 [-0.03; 0.02]
Inter-observer	0.89 [0.77;0.95]	0.0 [-0.07; 0.07]

Note: For agreement, data correspond to Kappa Cohen coefficient and data between brackets to the 95% confidence interval. For concordance, data correspond to the intraclass correlation coefficient and data between brackets to the 95% confidence interval. For Bland-Altman analysis, data correspond to the mean difference and data between brackets to the limits of agreement.

Legend: ICC=intraclass correlation coefficient; BA= Bland Altman analysis

## References

1. Lacasse Y, Girard M, Cormier Y. Recent advances in hypersensitivity pneumonitis. *Chest*. juill 2012;142(1):208-17.
2. Lacasse Y, Selman M, Costabel U, Dalphin J-C, Morell F, Erkinjuntti-Pekkanen R, et al. Classification of hypersensitivity pneumonitis: a hypothesis. *Int Arch Allergy Immunol*. 2009;149(2):161-6.
3. Silva CIS, Churg A, Müller NL. Hypersensitivity pneumonitis: spectrum of high-resolution CT and pathologic findings. *AJR Am J Roentgenol*. févr 2007;188(2):334-44.
4. Hansell DM, Wells AU, Padley SP, Müller NL. Hypersensitivity pneumonitis: correlation of individual CT patterns with functional abnormalities. *Radiology*. avr 1996;199(1):123-8.
5. Buschman DL, Gamsu G, Waldron JA, Klein JS, King TE. Chronic hypersensitivity pneumonitis: use of CT in diagnosis. *AJR Am J Roentgenol*. nov 1992;159(5):957-60.
6. Remy-Jardin M, Remy J, Wallaert B, Müller NL. Subacute and chronic bird breeder hypersensitivity pneumonitis: sequential evaluation with CT and correlation with lung function tests and bronchoalveolar lavage. *Radiology*. oct 1993;189(1):111-8.
7. Lynch DA, Newell JD, Logan PM, King TE, Müller NL. Can CT distinguish hypersensitivity pneumonitis from idiopathic pulmonary fibrosis? *AJR Am J Roentgenol*. oct 1995;165(4):807-11.
8. Patel RA, Sellami D, Gotway MB, Golden JA, Webb WR. Hypersensitivity pneumonitis: patterns on high-resolution CT. *J Comput Assist Tomogr*. déc 2000;24(6):965-70.
9. Silva CIS, Müller NL, Lynch DA, Curran-Everett D, Brown KK, Lee KS, et al. Chronic hypersensitivity pneumonitis: differentiation from idiopathic pulmonary fibrosis and nonspecific interstitial pneumonia by using thin-section CT. *Radiology*. janv 2008;246(1):288-97.
10. Fink JN, Ortega HG, Reynolds HY, Cormier YF, Fan LL, Franks TJ, et al. Needs and Opportunities for Research in Hypersensitivity Pneumonitis. *Am J Respir Crit Care Med*. 1 avr 2005;171(7):792-8.
11. Raghu G, Remy-Jardin M, Myers JL, Richeldi L, Ryerson CJ, Lederer DJ, et al. Diagnosis of Idiopathic Pulmonary Fibrosis. An Official ATS/ERS/JRS/ALAT Clinical Practice Guideline. *Am J Respir Crit Care Med*. 01 2018;198(5):e44-68.
12. Adler BD, Padley SP, Müller NL, Remy-Jardin M, Remy J. Chronic hypersensitivity pneumonitis: high-resolution CT and radiographic features in 16 patients. *Radiology*. oct 1992;185(1):91-5.
13. Zompatori M, Calabrò E, Chetta A, Chiari G, Marangio E, Olivieri D. [Chronic hypersensitivity pneumonitis or idiopathic pulmonary fibrosis? Diagnostic role of high resolution Computed Tomography (HRCT)]. *Radiol Med (Torino)*. sept 2003;106(3):135-46.

14. Myers JL. Hypersensitivity pneumonia: the role of lung biopsy in diagnosis and management. *Mod Pathol Off J U S Can Acad Pathol Inc.* janv 2012;25 Suppl 1:S58-67.
15. Travis WD, Matsui K, Moss J, Ferrans VJ. Idiopathic nonspecific interstitial pneumonia: prognostic significance of cellular and fibrosing patterns: survival comparison with usual interstitial pneumonia and desquamative interstitial pneumonia. *Am J Surg Pathol.* janv 2000;24(1):19-33.
16. Austin JH, Müller NL, Friedman PJ, Hansell DM, Naidich DP, Remy-Jardin M, et al. Glossary of terms for CT of the lungs: recommendations of the Nomenclature Committee of the Fleischner Society. *Radiology.* août 1996;200(2):327-31.
17. Picture Thresholding Using an Iterative Selection Method. *IEEE Trans Syst Man Cybern.* août 1978;8(8):630-2.
18. Lynch DA, Al-Qaisi MA. Quantitative computed tomography in chronic obstructive pulmonary disease. *J Thorac Imaging.* sept 2013;28(5):284-90.
19. von Luxburg U. A tutorial on spectral clustering. *Stat Comput.* 1 déc 2007;17(4):395-416.
20. Bland JM, Altman DG. Measuring agreement in method comparison studies. *Stat Methods Med Res.* juin 1999;8(2):135-60.
21. Landis JR, Koch GG. The measurement of observer agreement for categorical data. *Biometrics.* mars 1977;33(1):159-74.
22. Sahin H, Brown KK, Curran-Everett D, Hale V, Cool CD, Vourlekis JS, et al. Chronic hypersensitivity pneumonitis: CT features comparison with pathologic evidence of fibrosis and survival. *Radiology.* août 2007;244(2):591-8.
23. Walsh SLF, Sverzellati N, Devaraj A, Wells AU, Hansell DM. Chronic hypersensitivity pneumonitis: high resolution computed tomography patterns and pulmonary function indices as prognostic determinants. *Eur Radiol.* août 2012;22(8):1672-9.
24. O'Donnell D. Physiology of interstitial lung disease. In: Schwarz M, King T Jr, editors. *Interstitial lung disease.* Hamilton, ON, Canada: Marcel Dekker; 1998. pp. 51–70. In.
25. Small JH, Flower CD, Traill ZC, Gleeson FV. Air-trapping in extrinsic allergic alveolitis on computed tomography. *Clin Radiol.* oct 1996;51(10):684-8.
26. Zúñiga SG, Hernández JS, Toledo HM, Ávila MM, Gochicoa-Rangel L, Reyes JLM, et al. Small airway dysfunction in chronic hypersensitivity pneumonitis. *Respirology.* 2017;22(8):1637-42.
27. Fukuoka J, Franks TJ, Colby TV, Flaherty KR, Galvin JR, Hayden D, et al. Peribronchiolar metaplasia: a common histologic lesion in diffuse lung disease and a rare cause of interstitial lung disease: clinicopathologic features of 15 cases. *Am J Surg Pathol.* juill 2005;29(7):948-54.
28. MacDonald SL, Rubens MB, Hansell DM, Copley SJ, Desai SR, du Bois RM, et al. Nonspecific interstitial pneumonia and usual interstitial pneumonia: comparative

- appearances at and diagnostic accuracy of thin-section CT. *Radiology*. déc 2001;221(3):600-5.
29. Hunninghake GW, Lynch DA, Galvin JR, Gross BH, Müller N, Schwartz DA, et al. Radiologic findings are strongly associated with a pathologic diagnosis of usual interstitial pneumonia. *Chest*. oct 2003;124(4):1215-23.
  30. Oguma T, Niimi A, Hirai T, Jinnai M, Matsumoto H, Ito I, et al. Assessment of Small Airways with Computed Tomography: Mosaic Attenuation or Lung Density? *Respir Int Rev Thorac Dis*. 2015;89(6):539-49.

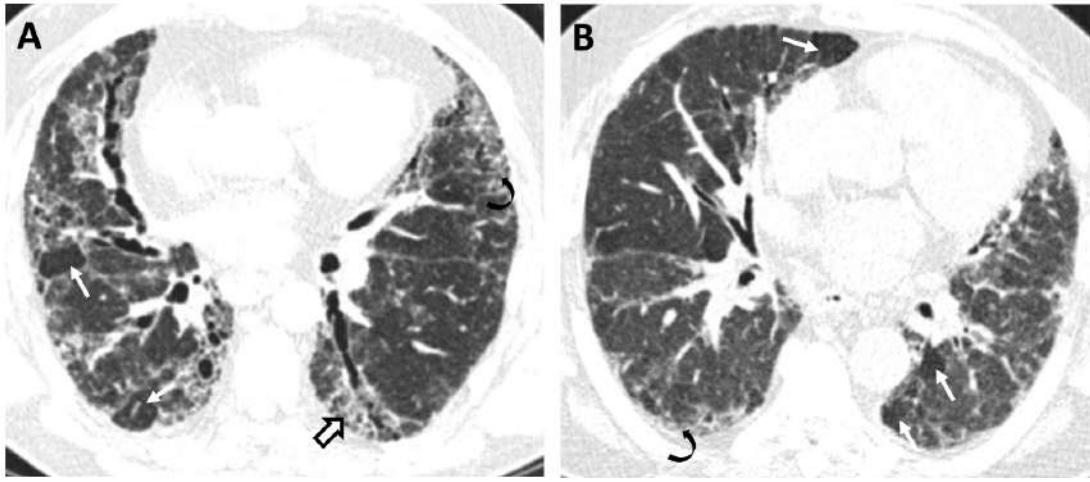


Figure 1. Transverse thin section CT in (A) chronic HP patient and (B) IPF patient. Note lobular decreased attenuation areas (white thin arrows), reticulations (black arrows) and honeycombing (thick arrow).

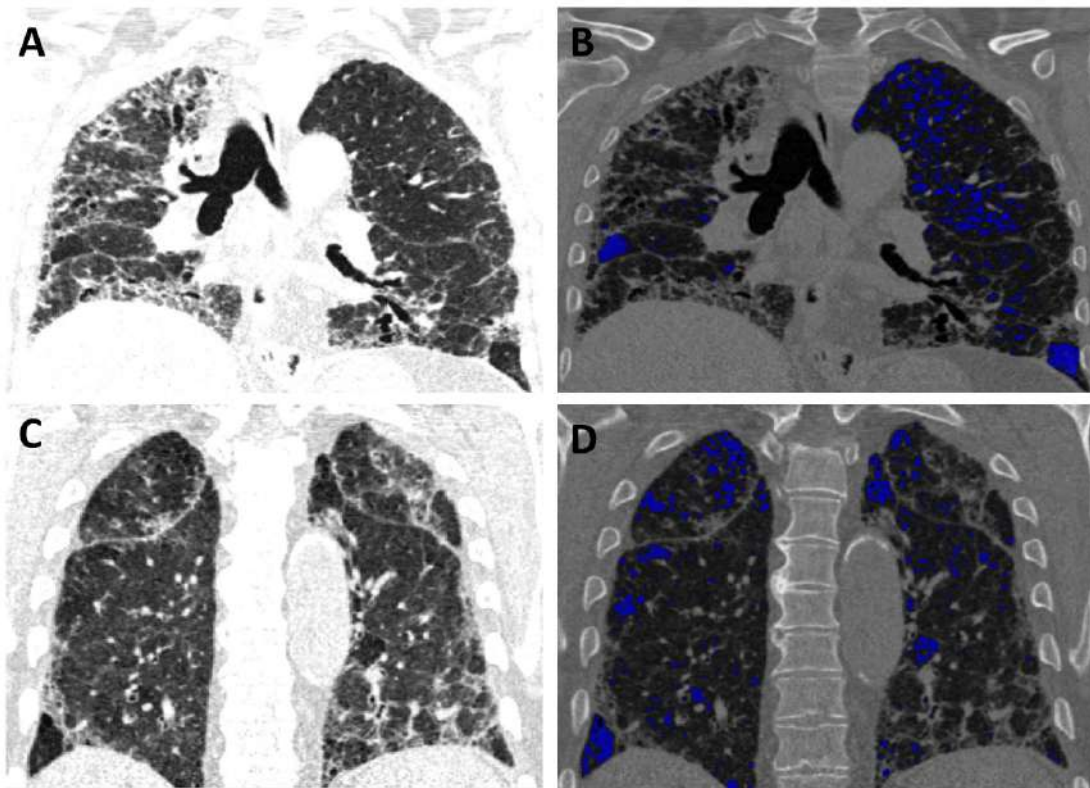
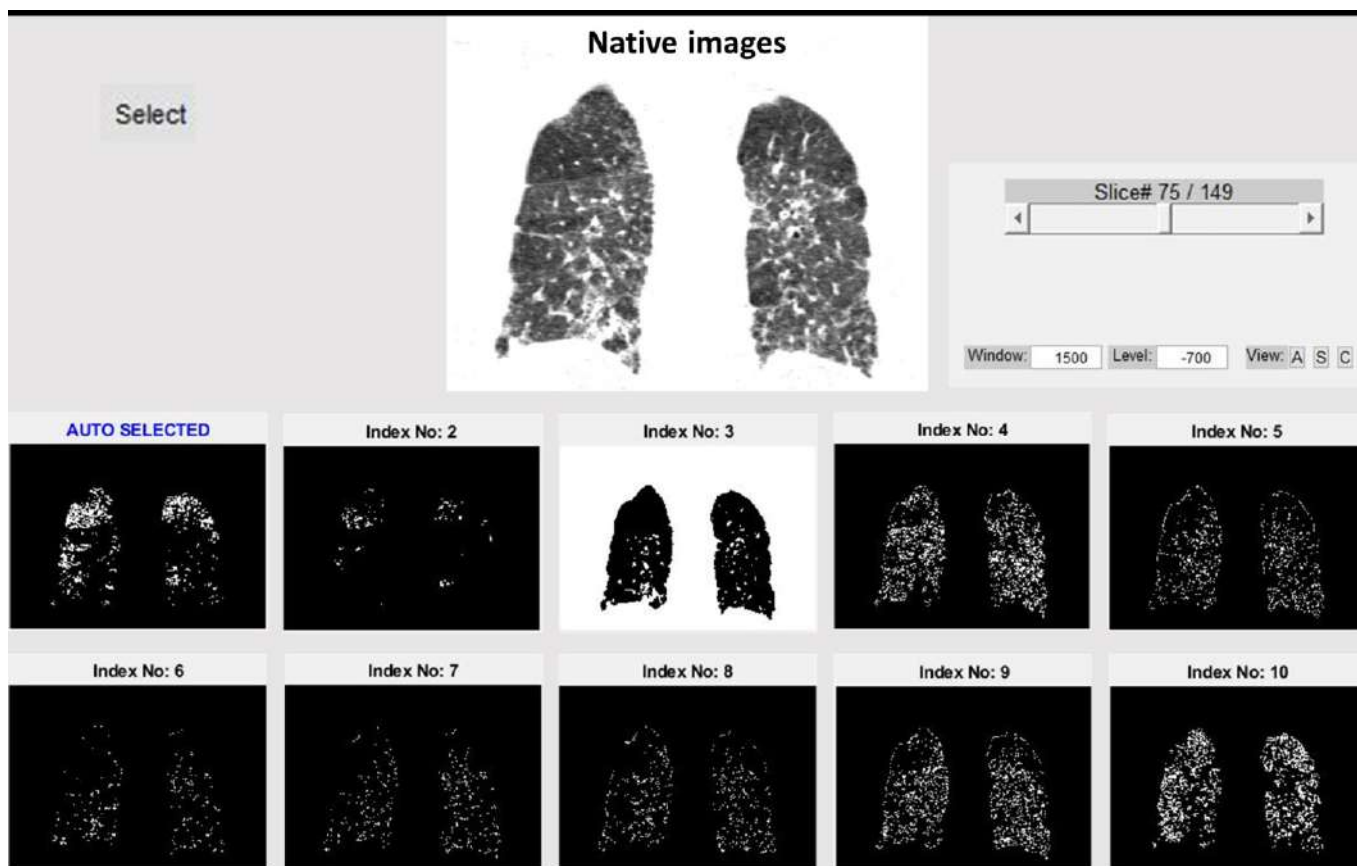


Figure 2. Coronal thin section CT in (A, B) chronic HP patient and (C, D) IPF patient. Semi-automated quantification of lobular decreased attenuation areas (%LDAA) (blue mask) showed 15% in (B) and 8% in (D)



Supplemental Figure E1. Spectral clustering (Number of clusters 10 )

### **3. Contribution à l'IRM quantitative des maladies obstructives chroniques des voies aériennes**

### **3.1 Publication n°3 : Comparaison d'un motif spiralé et d'un motif sphérique d'acquisition de l'espace de Fourier en IRM 3D à temps d'écho ultracourt**

Depuis l'avènement des séquences IRM à temps d'écho ultra court (UTE), il est possible d'obtenir des images IRM pulmonaire morphologiquement proches de celle de la TDM. Actuellement, les deux séquences d'IRM 3D UTE les plus utilisées sont basée soit sur un remplissage sphérique de l'espace k, soit sur un remplissage cylindrique spiralé. La séquence PETRA (pointwise encoding time reduction with radial acquisition) combine une acquisition cartésienne du centre de l'espace k avec une acquisition radiale volumétrique sphérique. La séquence SpiralVibe est basée sur l'empilement d'acquisitions spiralées avec une acquisition cartésienne dans le sens des coupes associée à une interpolation volumétrique. Grace aux acquisitions à temps d'écho ultra court de ces deux séquences et à une résolution spatiale millimétrique voire sous millimétrique, les éléments structuraux du poumon sont facilement identifiables et le signal du parenchyme pulmonaire se trouve augmenté. Cependant, des problématiques telles que la robustesse de la synchronisation respiratoire ainsi que la réduction du temps d'acquisition restent à résoudre. Une comparaison de la qualité des images issues de ces deux motifs d'acquisition est indispensable avant d'étudier l'applicabilité aux pathologies humaines et les développements futurs de l'IRM 3D UTE. Dans cette étude, nous avons évalué les images IRM pulmonaires issues des deux types d'acquisition chez des volontaires sains et des patients atteints de mucoviscidose ou de pneumopathie interstitielle diffuse. L'évaluation comportait une analyse visuelle de la qualité d'image et une analyse quantitative du signal/bruit et du contraste apparent des images. Egalement, la description et l'évaluation des altérations structurales ont été faites en utilisant les scores cliniques dédiés. Les résultats ont démontré une meilleure qualité d'image et un signal/bruit plus élevée lorsque l'acquisition était réalisée en mode sphérique. Néanmoins, la reproductibilité de l'évaluation des altérations structurales était comparable entre les deux motifs d'acquisition. En outre, le motif d'acquisition spiralé offrait une meilleure synchronisation respiratoire et une diminution du temps d'acquisition par deux. Ainsi, la synchronisation respiratoire automatisée et robuste de la technique d'acquisition en motif spiralé permettrait une utilisation fiable de l'IRM 3D UTE dans le cadre du soin courant.

# 3D Ultrashort Echo Time MRI of the Lung Using Stack-of-Spirals and Spherical $k$ -Space Coverages: Evaluation in Healthy Volunteers and Parenchymal Diseases

Gaël Dournes, MD, PhD,<sup>1,2,3\*</sup> Joseph Yazbek, MD,<sup>3</sup> Wadie Benhassen, PhD,<sup>4</sup>  
 Ilyes Benlala, MD,<sup>1,2,3</sup> Elodie Blanchard, MD,<sup>3</sup> Marie-Elise Truchetet, MD,<sup>3</sup> Julie Macey, MD,<sup>3</sup>  
 Patrick Berger, MD, PhD,<sup>1,2,3</sup> and François Laurent, MD<sup>1,2,3</sup>

**Background:** Ultrashort echo time (UTE) has been shown to improve lung MRI quality in three dimensions. The evaluation of 3D-UTE stack-of-spirals VIBE (3D-USV) sequence for parenchymal diseases and a comparison of performance with that of a spherical mode of acquisition is needed.

**Purpose:** To assess MRI quality using a prototypical 3D-USV sequence and to compare performance with that of a spherical acquisition using Pointwise Encoding Time Reduction with Radial Acquisition (PETRA).

**Study Type:** Monocenter, prospective.

**Population:** Twelve healthy volunteers and 32 adult patients with either cystic fibrosis (CF;  $n = 16$ ) or interstitial lung disease (ILD;  $n = 16$ ).

**Field Strength/Sequence:** Both free-breathing 3D-USV and PETRA were completed at 1.5T.

**Assessment:** In healthy volunteers, visual analysis of imaging quality was scored using a Likert scale. Quantitative evaluation of apparent signal ratio (Sr) and contrast ratio (Cr) was measured. Patients with CF and ILD completed both computed tomography (CT) and MRI. Depiction of structural alterations was assessed using dedicated clinical scores. All evaluations were done in consensus by two readers.

**Statistical Tests:** Comparison of means was assessed using the Wilcoxon signed rank test. Concordance and agreement between CT and MRI were assessed using the intraclass correlation coefficient (ICC) and kappa test.

**Results:** In controls, 3D-USV yielded lower artifacts owing to better automatic respiratory synchronization than PETRA ( $P < 0.001$ ). However, Sr and Cr of 3D-USV were found significantly lower by 2.25- and 2.36-fold, respectively ( $P < 0.001$ ). In patients, 3D-USV and PETRA showed comparable performances to assess airway severity in CF (Bhalla score, ICC = 0.89 and ICC = 0.92, respectively) and presence of structural alterations in ILD such as honeycombing (kappa = 0.68 and kappa = 0.69, respectively).

**Data Conclusion:** 3D-USV enables high-resolution morphological imaging of the lung without need of an external device to compensate respiratory motions. Automation and robustness of the method may facilitate clinical application for both airway and interstitial lung investigations.

**Level of Evidence:** 2

**Technical Efficacy:** Stage 1

J. MAGN. RESON. IMAGING 2018;00:000–000.

Morphological magnetic resonance imaging (MRI) of the lung parenchyma remains a technical challenge to get sufficient signal and contrast that would be of clinical interest and applicability.<sup>1,2</sup> Indeed, lung MRI suffers from the very fast

decay of the lung signal related to susceptibility artifacts, the low proton content, and the need of synchronization due to cardiac and respiratory motions.<sup>3</sup> Recent advances in the use of ultrashort echo time (UTE) has been able to improve

View this article online at [wileyonlinelibrary.com](http://wileyonlinelibrary.com). DOI: 10.1002/jmri.26212

Received Mar 15, 2018, Accepted for publication May 18, 2018.

\*Address reprint requests to: G.D., Centre de Recherche Cardio-thoracique de Bordeaux, INSERM U1045, Université Bordeaux Segalen, 146 rue Léo Saignat, 33076 Bordeaux Cedex, France. E-mail: [gael.dournes@chu-bordeaux.fr](mailto:gael.dournes@chu-bordeaux.fr)

From the <sup>1</sup>University of Bordeaux, Centre de Recherche Cardio-Thoracique de Bordeaux, Bordeaux, France; <sup>2</sup>Inserm, Centre de Recherche Cardio-Thoracique de Bordeaux, Bordeaux, France; <sup>3</sup>CHU de Bordeaux, Service d'Imagerie Thoracique et Cardiovasculaire, Service des Maladies Respiratoires, Service de Rhumatologie, Service d'Exploration Fonctionnelle Respiratoire, Pessac, France; and <sup>4</sup>Siemens HealthCare, Erlangen, Germany

Additional supporting information may be found in the online version of this article.

pulmonary MR image quality in 3D.<sup>4–9</sup> An increase in signal and contrast was shown in both healthy volunteers and patients with pulmonary diseases, from neonate<sup>10</sup> to adulthood.<sup>11</sup> However, several drawbacks remain. First, spatial resolution is inferior to that of computed tomography (CT). Second, most MRI requires several minutes and hence there is a need for respiratory motion compensation. That is why various sequence schemes have been proposed to optimize 3D-UTE MRI of the lung.

Although all 3D sequences seek to decrease the echo time down to the microsecond, variable schemes are used to sample the  $k$ -space. The two main  $k$ -space variants consist in acquiring the  $k$ -space either radially into a sphere<sup>4</sup> or into a cylinder using stack-of-discs such as stack-of-stars<sup>5</sup> or stack-of-spirals.<sup>12</sup> In our institution, a novel prototype dedicated to 3D-UTE imaging using VIBE (volume interpolated breath-hold examination) and stack-of-spirals (3D-USV) has been released for testing. Although a few reports exist regarding the rationale and the feasibility of 3D-USV for lung MRI,<sup>12,13</sup> a more exhaustive assessment might be beneficial. In addition, we hypothesized that spherical and cylindrical  $k$ -space coverage using 3D-UTE acquisitions may be different in terms of imaging quality and artifacts. Therefore, the main objective of this study was to assess imaging quality of lung MRI using a prototype 3D-USV sequence in both healthy volunteers and patients suffering from airway and interstitial diseases. Our secondary objective was to compare the results of the 3D-USV sequence with that of the previously published pointwise encoding time reduction with radial acquisition (PETRA) sequence using spherical mode of acquisition.<sup>14,15</sup>

## Materials and Methods

### Description of the Respiratory-Gated 3D-UTE Spiral-VIBE Sequence (3D-USV)

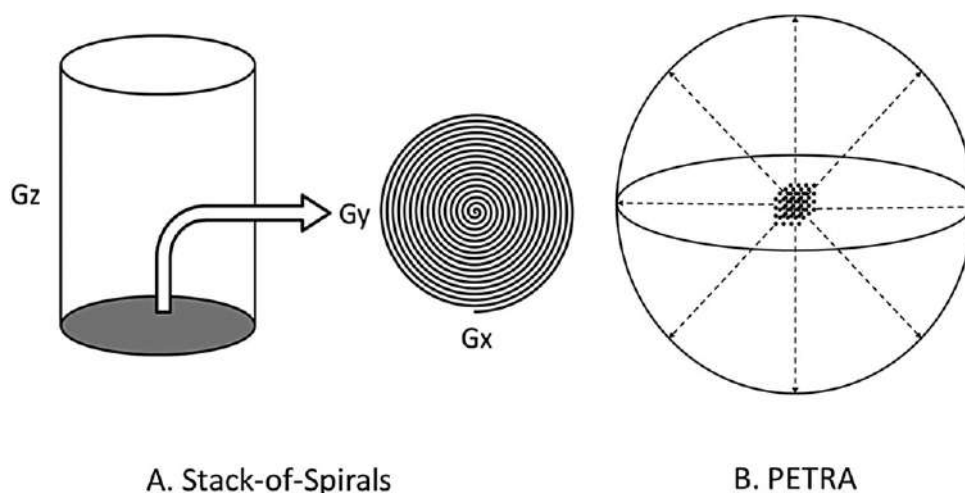
**PULSE SEQUENCE PRINCIPLES.** The prototypical UTE Spiral VIBE sequence was derived from a 3D gradient-echo (GRE) sequence. For slice selection, standard Cartesian phase encoding was performed while in-plane encoding was performed with spiral sampling for efficient  $k$ -space coverage (“stack of spirals,” Fig. 1). Each spiral readout starts immediately after the 3D phase-encoding gradient<sup>13</sup> in order to achieve UTEs, which compensates decaying of transverse relaxation time related to susceptibility artifacts. For further minimization of the echo time, a short nonselective excitation pulse was used, which saves time for the slice refocusing gradient. To account for gradient imperfections and eddy currents,<sup>16</sup> a Tan-Meyer correction was applied, which is based on parameters depending on the scanner type.<sup>17</sup>

**SPECIFIC FEATURES RELATED TO LUNG IMAGING.** MRI was performed with a 1.5T system (MAGNETOM Aera,

Siemens Healthcare, Erlangen, Germany) with an 18-channel anterior body coil in combination with a 32-channel posterior spine coil. To avoid fold-in artifacts and prolonged reconstruction times, coil elements close to the lungs were manually selected. No iterative reconstructions were used. Patients were positioned in the supine position with arms along the body. The basic sequence parameters were as follows: repetition time / echo time (TR/TE) / flip angle = 4.1/0.07 msec/5°. Pulse duration was 60  $\mu$ s, duration of readouts 1800  $\mu$ s, and bandwidth was 2800 Hz/pixel. Field of view (FOV) was (320  $\times$  320 mm) and matrix size 320  $\times$  320. Slice thickness was 1 mm to reach an isotropic voxel dimension of (1  $\times$  1  $\times$  1 mm). Number of slices had to be adapted to the patient size along the slice direction and ranged from 200–240. Partial Fourier acquisition of 6/8 was applied along the slice direction (Supplemental Methods). Because the slice plane was encoded in Cartesian mode, native acquisition was performed in the coronal plane with FOV adapted to overpass the anterior and posterior chest edges to prevent aliasing. To avoid artifacts due to chest motion, prospective respiratory gating was used. Although the original VIBE acronym indicates a “Breathold Examination,”<sup>18</sup> the acquisition time of 3D-USV was several minutes and, thus, additional motion compensation was implemented. The necessary motion information was acquired during the scan with a Cartesian navigator readout which is performed in the head–feet direction. The user had to check which coil element was the closest to the area of maximum respiratory motion, typically the diaphragm. When sufficient  $k$ -space data were acquired in the expiratory state, the scan stopped automatically and corresponding images were reconstructed on the scanner.

### Description of the PETRA Sequence

For comparison purposes, imaging quality of the PETRA sequence was also investigated in this study, as described previously.<sup>14,15</sup> Because respiratory-gated PETRA was not available on MAGNETOM Aera MR scan, PETRA was completed on a MAGNETOM Avanto MR Scan (Siemens Healthcare). Patients were placed in the supine position with arms along the body and a 16-channel body coil/8-channel spine coil was used. TR/TE were 4.1/0.07 msec and flip angle was 5°. FOV was (320  $\times$  320  $\times$  320 mm) and matrix size 320  $\times$  320  $\times$  320 to get isotropic voxel dimensions of (1  $\times$  1  $\times$  1 mm). Pulse duration was 14  $\mu$ s, readout duration 600  $\mu$ s and bandwidth 440 Hz/pixel. Using PETRA, gradients were already switched on before a hard low-flip angle nonselective excitation. After the excitation, 3D spherical acquisition of radial half-projections was begun as early as allowed by the hardware at time  $t =$  echo time after the middle of the excitation pulse. Because encoding of spins already effectively starts at the middle of the pulse, points in the center of  $k$ -space are missed. These points are acquired singlepoint-wise on a Cartesian grid (Fig. 1). To take lung motion into account, an adaptive respiratory gating method involving a respiratory bellows signal was used. In this study we used a 30% threshold to accept end-expiratory data and reject inspiratory data.



A. Stack-of-Spirals

B. PETRA

**FIGURE 1: 3D UTE Spiral VIBE (3D-USV) (A) and PETRA (B) sequence schemes.** Using 3D-USV, each spiral readout starts in the center of  $k$ -space along  $x$  and  $y$  in-plane axes. Slice encoding along the  $z$ -axis is performed with a phase-encoding gradient. Using PETRA, dashed arrows are representative of some radial spokes in every direction to fulfill  $k$ -space into a sphere. The center of  $k$ -space is acquired point-by-point.

For image reconstruction, the  $k$ -space has to be filled on a Cartesian grid. Points acquired in the Cartesian part are simply gridded to their corresponding positions, whereas data for the radial part have to be weighted with a density matrix. This density matrix was adapted to the density of points in the Cartesian center of  $k$ -space with methods that have been previously described.<sup>19,20</sup>

### Qualitative and Quantitative Assessment of 3D-USV Imaging Quality in Healthy Volunteers

The study was performed between September 2016 and December 2017 at a single center and was approved by the local Ethics Committee. All participants gave written informed consent. Twelve healthy volunteers (mean age  $24 \pm 11$ ), seven males and five females, with no history of smoking and no visible abnormalities on an MR scan using the PETRA sequence<sup>15</sup> were included. All patients had to complete both the prototype 3D-USV and the previously published PETRA sequences (Fig. 1) without contrast product injection. Parameters of 3D-USV and PETRA are described in Supplemental Table 1. Before analysis, all examinations were anonymized and analyzed in random order. Two readers with 3 and 9 years of experience in thoracic imaging analyzed the examinations independently, blinded from any clinical data. The two independent readings were combined together and the mean of evaluations was chosen as consensus and interobserver reproducibility was assessed.

#### QUALITATIVE ASSESSMENT OF IMAGING QUALITY.

Visual imaging quality was assessed using a Likert scale as previously described.<sup>4,15</sup> Briefly, each individual score was dedicated to the visibility of fissures (0 = not present, 1 = uninterpretable, 2 = fair visibility, 3 = good partial visibility, 4 = good complete visibility), airways, and vessels (0 = lobar level, 1 = segmental, 2 = subsegmental, 3 = superior to the subsegmental, 4 = up to the distal lung periphery). Sharpness of structures was scored as 1 = blurred, 2 = intermediate, 3 = sharp. A scoring of artifacts was also performed dedicated to motion artifacts (blurring, streaks) related to the thorax and the heart (0 = no lung

structure recognizable, 1 = important artifact, 2 = moderate artifact, 3 = slight artifact, 4 = no artifact). An overall quality score was defined as the sum of these items.

#### QUANTITATIVE ASSESSMENT OF LUNG SIGNAL INTENSITY.

Quantitative evaluation of apparent signal ratio (Sr) and apparent contrast ratio (Cr) were determined as previously described.<sup>15</sup> Briefly, regions of interest (ROIs) were manually placed to represent signal within airways ( $SI_{\text{airway}}$ ), lung ( $SI_{\text{lung}}$ ), and vessels ( $SI_{\text{vessel}}$ ). Three ROIs were placed in the trachea and right and left main bronchus and averaged to calculate  $SI_{\text{airway}}$ . Three ROIs were placed in the pulmonary trunk, right and left main pulmonary arteries and averaged to calculate  $SI_{\text{vessel}}$ . Three axial sections were selected for the assessment of the lung parenchyma, one at the level of the aorta crossing, one at the level of the carina, and one at the level of the pulmonary inferior veins. At each location, ROIs were placed in the anterior and posterior parts of both right and left lung, at least 2 cm from the pleura and after careful avoidance of the lung vessels. The 12 ROIs were averaged to calculate  $SI_{\text{lung}}$ . Thus, apparent Cr and apparent Sr were calculated as follows:  $Cr = (SI_{\text{lung}} - SI_{\text{airway}}) / SI_{\text{vessel}} \cdot 100\%$  and  $Sr = (SI_{\text{lung}} / SI_{\text{airway}}) \cdot 100\%$ .

#### Initial Evaluation in Human Airway and Interstitial Diseases

Data are preliminary results from ongoing studies aiming at comparing CT and MRI in the field of cystic fibrosis (CF) (clinical trial identifier: NCT03357562) and interstitial lung disease (ILD) (clinical trial identifier: NCT03078426). All patients completed unenhanced CT (Supplemental Table 2) and MRI using both 3D-USV and PETRA (Supplemental Table 1) the same day. Clinical and functional patient characteristics are given in Supplemental Tables 3 and 4. The same readers who analyzed the MRI of healthy volunteers also analyzed the anonymized MR examinations of patients.

**TABLE 1. Imaging Quality Comparison Between 3D-USV and PETRA in 12 Healthy Volunteers**

		<u>3D-USV</u>	<u>PETRA</u>	<u>P-value</u>
		(n = 12)	(n = 12)	
Quantitative analysis	Sr	134.2 ± 6.8	302.3 ± 50.7	<0.001
	Cr	13.1 ± 2.3	31 ± 19	<0.001
Qualitative analysis	Fissure	1.0 ± 0.9	2.7 ± 0.5	<0.001
	Bronchi visibility	2.3 ± 0.5	3.0 ± 0.1	<0.001
	Bronchi sharpness	1.8 ± 0.4	2.4 ± 0.3	<0.001
	Vessel visibility	4.0 ± 0.0	4.0 ± 0.0	>0.99
	Vessel sharpness	2.1 ± 0.2	2.8 ± 0.3	<0.001
Artifacts	Streak	4.0 ± 0.0	3.0 ± 0.0	<0.001
	Blurring	3.3 ± 0.5	2.3 ± 0.5	<0.001
	Shading	4.0 ± 0.0	3.0 ± 0.0	<0.001
	Aliasing	3.7 ± 0.2	2.7 ± 0.5	<0.001
	Cardiac	3.0 ± 0.0	3.0 ± 0.0	>0.99

Data are mean ± standard deviation for continuous variables. Sr = signal ratio; Cr = contrast ratio.  $P < 0.05$  was considered statistically significant.



**FIGURE 2:** 3D-USV examination in a healthy volunteer in axial (A), sagittal (B) reformations, and native coronal (C) acquisition. Segmental and some subsegmental bronchi are visible, whereas vessels are depictable up to the lung periphery. There are no artifacts such as streaks, shading, or aliasing. There is slight blurring artifact towards the diaphragm.

In 16 adults with CF (median age = 21 years; seven males and nine females), quantification of structural abnormalities was performed by using the scoring system of Bhalla et al.<sup>11,21</sup> This scoring system is composed of nine items related to the segmental presence of airway wall thickening, lumen bronchiectasis, intraluminal mucous plugs, collapse/consolidation, bulla, emphysema, sacculations/abscess, and mosaic.<sup>22</sup>

Adult patients with ILD (median age = 67 years; 11 males and 5 females) were referred for idiopathic pulmonary fibrosis ( $n = 5$ ), nonspecific interstitial disease ( $n = 2$ ), sarcoidosis ( $n = 1$ ), asbestosis ( $n = 3$ ), Churg and Strauss syndrome ( $n = 1$ ), cryptogenic organizing pneumonia ( $n = 1$ ), and scleroderma ( $n = 3$ ). The presence of structural abnormalities was scored at the segmental level (present = 1) and comprised honeycombing, septal lines, reticulation, ground-glass opacity, nodules, cysts, traction bronchiectasis, and pleural plaque as defined by the glossary of terms from the Fleischner Society.<sup>22</sup>

### Statistical Analysis

The results are expressed as means  $\pm$  standard deviation for continuous variables and absolute numbers for categorical variables. Comparison of means was performed using the Wilcoxon signed rank test, and comparison of categorical variables was performed using the McNemar test.  $P < 0.05$  was considered to indicate a significant difference. Interobserver variability of quantitative measurements of Sr and Cr were assessed using Bland–Altman analysis.<sup>23</sup> Agreement between readers, as well as CT and MRI, was assessed by using the kappa test for categorical variable and concordance using intraclass correlation coefficients (ICC) with 95% confidence interval (CI). Kappa and ICC values were classified as null (0), slight (0–0.20), fair (0.21–0.40), moderate (0.41–0.60), good (0.61–0.80), and very good (0.81–1).<sup>11</sup>

## Results

### Imaging Quality of 3D-USV and PETRA in Healthy Volunteers

Supplemental Table 5 demonstrates the results of a pilot study dedicated to explore 3D-USV intrinsic properties in order to find optimum sequence parameters. By decreasing voxel size down to  $(0.8 \times 0.8 \times 0.8)\text{mm}^3$  there was no increase in visual imaging quality as compared to  $(1 \times 1 \times 1)\text{mm}^3$ , owing to the subsequent decrease in Sr and Cr ( $P < 0.001$ ). In addition, there were no significant differences between full Fourier and partial 6/8 Fourier acquisition regarding all imaging quality markers ( $P$  ranging from 0.2–0.5), although acquisition time was reduced from  $8 \pm 1$  to  $6 \pm 1$  minutes ( $P < 0.001$ ). Finally, there was a significant improvement between imaging quality using 160 spiral interleaves (SI) and 320 or 480, but not between 320 and 480 SI. Therefore, parameters were chosen herein as a voxel dimension of  $(1\text{ mm})^3$ , 320 SI and a partial 6/8 Fourier acquisition.

Table 1 shows a comparison of image quality with that of the previously validated PETRA sequence. PETRA performed better than 3D-USV regarding Sr and Cr by 2.25-fold and 2.36-fold, respectively. At Bland–Altman analysis, the mean



**FIGURE 3:** CT (A), 3D-USV (B), and PETRA (C) noncontrast-enhanced examinations in a 23-year-old male with cystic fibrosis. White arrows indicate a moderate bronchiectasis and black arrows a peripheral mucoid impaction. Despite subjective less sharpness of contours on 3D-USV examination (B) as compared to PETRA (C), both severity scorings to depict structural alterations were rated the same.

difference (MD) between readers of Sr and Cr were 3.2 [limits of agreement:  $-6; 13$ ] and 1.2 [ $-2; 5$ ] using 3D-USV. Using PETRA, MD of Sr was  $-18 [-54; 77]$ , whereas MD of Cr was 4 [ $-6; 18$ ]. There was also significantly better visibility of fissures, bronchi, but not vessels. However, 3D-USV had significantly better scores of imaging artifacts. There were no streaks, no shading, less blurring, and less aliasing than that reported with PETRA (Fig. 2; Supplemental Fig. 1). Interobserver concordance of these qualitative evaluations were good to very good (Supplemental Table 6).

### Preliminary Results in CF and ILD

**CONCORDANCE BETWEEN 3D-USV AND CT IN CF.** 3D-USV examinations were successfully completed in 16 adults with CF (Fig. 3). Structural evaluation was performed in all

**TABLE 2. Concordance between MRI and CT to assess CT-Bhalla score in 16 adults with CF**

	3D-USV ( <i>n</i> = 16)		PETRA ( <i>n</i> = 16)	
	ICC	95% CI	ICC	95% CI
Wall thickening	0.60	[0.21–0.84]	0.70	[0.32–0.76]
Bronchiectasis	Severity	0.78	0.81	[0.64–0.90]
	Extent	0.86	0.84	[0.61–0.91]
Muroid impaction	0.79	[0.74–0.84]	0.85	[0.78–0.92]
Bronchial generation	0.84	[0.72–0.89]	0.83	[0.74–0.91]
Sacculation/abscess	NA	NA	NA	NA
Consolidation/atelectasis	0.93	[0.86–0.98]	0.94	[0.85–0.97]
Bulla	NA	NA	NA	NA
Emphysema	NA	NA	NA	NA
Global score	0.89	[0.81–0.94]	0.92	[0.84–0.97]

Legend: ICC=intraclass correlation coefficient; CI=confidence interval; NA=non applicable

288 segments and then integrated to assess a score in each of the 16 patients. ICC values were good to very good for all analyzed items, ranging from 0.60 [0.21–0.84] for wall thickening to 0.93 [0.86–0.98] for consolidation/atelectasis. The concordance between 3D-USV and CT overall Bhalla score

was found very good (ICC = 0.89 [0.81–0.94]) (Table 2). Interobserver concordance ranged from good (ICC = 0.74 for wall thickening) to very good (ICC = 0.92 for muroid impaction) (Supplemental Table 7).

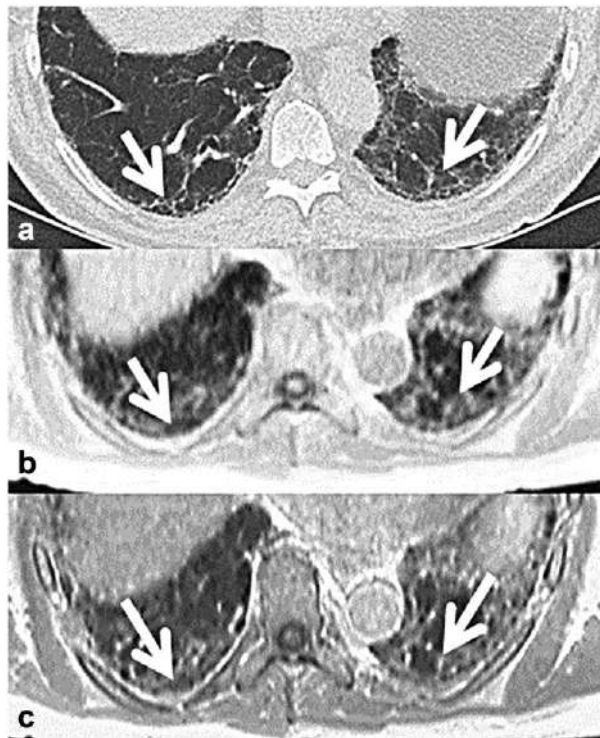


**FIGURE 4: CT (A), 3D-USV (B), and PETRA (C) noncontrast-enhanced examinations in a 60-year-old female with idiopathic pulmonary fibrosis. Magnification on lung bases indicates areas of honeycombing (white arrows).**

**CONCORDANCE BETWEEN 3D-USV AND CT IN ILD.** All 16 patients with ILD completed the 3D-USV examination (Fig. 4). No attempt to integrate the structural alteration was made to calculate a patient score. At the segmental level (*n* = 288 segments of 16 patients), agreement to assess the presence of interstitial-related morphological alteration was found moderate (kappa = 0.44 [0.34–0.54] for traction bronchiectasis) to almost perfect (kappa = 1 for nodules) (Table 3). Interobserver concordance ranged from moderate (ICC = 0.45 for traction bronchiectasis) to almost perfect (ICC = 1 for nodules) (Supplemental Table 8).

**ASSESSMENT OF STRUCTURAL ABNORMALITIES IN PARENCHYMAL DISEASES USING BOTH 3D-USV AND PETRA WITH CT AS REFERENCE.** The results between 3D-USV showed close similarities in the clinical context of both CF and ILD (Tables 2–3). However, in patients with ILD the respiratory belt using PETRA failed at synchronizing respiratory motions in 3 out of 16 patients and, thus, analyses were made in 13 patients only (Table 3, Supplemental Fig. 2). Conversely, all examinations were diagnostically acceptable in disease condition using 3D-USV (Figs. 3–4).

**TABLE 3. Agreement between MRI and CT at the segmental level in patients with lung interstitial disease**

	3D-USV		PETRA	
	(n = 288 segments Cof 16 patients)		(n = 234 segments Cof 13 patients)	
	Kappa	95% CI	Kappa	95% CI
Honeycombing	0.68	[0.56–0.79]	0.69	[0.58–0.81]
Septal lines	0.68	[0.45–0.92]	0.68	[0.44–0.91]
Reticulation	0.65	[0.55–0.75]	0.62	[0.52–0.73]
Ground glass opacity	0.58	[0.46–0.69]	0.48	[0.33–0.63]
Traction bronchiectasis	0.44	[0.34–0.54]	0.47	[0.37–0.58]
Nodule	1.00	[1.00–1.00]	1.00	[1.00–1.00]
Cyst	0.83	[0.70–0.96]	0.87	[0.75–0.99]
Pleural plaque	0.96	[0.91–1.00]	0.96	[0.91–1.00]

Legend: CI=confidence interval

## Discussion

The study demonstrates that high-resolution isotropic 3D imaging of the lung is feasible in humans using UTE Spiral VIBE. Applicability in human airway and pulmonary interstitial diseases showed good imaging quality with clinical information comparable to that of CT.

Lung MRI has recently benefited from the emergence of UTE sequences to reach morphological information close to that of a CT scan.<sup>4,6,14,24</sup> The two main procedures consist of acquiring  $k$ -space either radially into a sphere or into a cylinder using stack-of-discs, although several variants exist. 3D-USV using a stack-of-spirals has been recently described and applied in patients with lung cancer.<sup>12</sup> It could be noticed that in the previous study by Du et al,<sup>16</sup> a higher signal-to-noise ratio was obtained using 2D spiral trajectories than with 2D radial trajectories in static organs such as the brain or bones, which was ascribed to a more time-efficient coverage of the  $k$ -space. On the contrary, by comparing 3D-USV with PETRA, apparent signal and contrast ratios of 3D-USV were found lower in healthy volunteers than that obtained using a radial spherical coverage of  $k$ -space. Indeed, using a stack-of-discs to move from 2D to 3D,  $k$ -space center is displaced at each step along the  $z$ -axis during acquisition. Conversely, using a pure radial acquisition over the same sphere,  $k$ -space center is kept the same all along the acquisition. In addition, PETRA is not composed of pure radial acquisitions and it was demonstrated that complementary pointwise acquisition of the center itself was associated with a subsequent encoding time reduction and, thus, to increase signal.<sup>13</sup> Another point of discussion is that both spiral and radial trajectories are sensitive to gradient imperfections. PETRA mitigates this by sampling the  $k$ -space center in a Cartesian scheme.<sup>14</sup>

Therefore, a narrower bandwidth was available using PETRA than with 3D-USV, which could contribute to the differences measured herein regarding apparent signal ratio. Nevertheless, a lower bandwidth was not possible using 3D-USV because of imaging distortions.<sup>17</sup> Therefore, the results appear to be concordant with the physical principles of these two different schemes, since  $k$ -space center is expected to contain signal and contrast information.

In addition, 3D is obtained as a stack-of-discs using 3D-USV and not as pure 3D. Therefore, careful adherence to isotropic dimensions was checked owing to the theoretical possibility of blurring from contours whether a voxel would not be perfectly isotropic for multiplanar reformation. Nevertheless, the VIBE principle also requires a volumetric interpolation<sup>18</sup> and, in this study, sharpness of lung structures such as airways and vessels were found lower using 3D-USV than with PETRA. Our findings are consistent with previous reports showing a higher level of blurring using a 2D spiral UTE sequence as compared to 2D radial UTE sequences. Indeed, radial trajectory enables reaching the furthest distance from the center of  $k$ -space per unit time, and therefore allows the rapidly decaying MR signal to be sampled at higher spatial frequencies than with spiral trajectory.<sup>16,25</sup>

However, the stack-of-spiral principle benefited from the possibility of fully automatic respiratory gating, whereas respiratory-trigger using a belt was still needed with PETRA.<sup>15</sup> In addition, to fulfill a whole 3D sphere in several minutes may be more challenging in synchronization demand than stack-of-discs with Cartesian steps along the  $z$ -axis. Our results demonstrate that 3D-USV with prospective respiratory gating was robust to motion without the need of an external belt placement. Although the clinical applicability of a

respiratory triggering with belt did not seem impaired in 16 adults with CF, there was a failure to synchronize three ILD patients with BMI level >30. Consequently, three PETRA acquisitions were found nondiagnostic in the ILD group. In both CF and ILD, all 32 3D-USV examinations were diagnostically acceptable. Moreover, we found a lower rate of artifacts using 3D-USV than with PETRA. For instance, streak was absent, since streaks are generated from radial ray during  $k$ -space acquisition. In addition, signal homogeneity was better without shading at the FOV extremum. 3D-USV was also free from aliasing artifact, since a coronal acquisition was used. However, one could remark that folding of the head and abdomen regions would have occurred whether a native axial acquisition would have been used. Indeed, a native axial acquisition would have supposed applying a Cartesian slice encoding along a craniocaudal direction, leading to an aliasing from these neighborhood regions.

Finally, clinical application in CF found that 3D-USV showed similar concordance than PETRA to calculate a CT severity score. In addition, agreements between CT and MRI to describe interstitial disease were found moderate to good and, thus, in the range of that reported between observers using CT alone. For instance, in the study by Watadani et al,<sup>26</sup> the interobserver reproducibility to assess honeycombing between expert readers was moderate only ( $\kappa = 0.40$ ) using CT. Although preliminary, these results may promote the use of UTE as a radiation-free imaging modality in chronic airway and interstitial lung diseases that would require iterative and long-term imaging exposures.<sup>27,28</sup>

The study had several limitations. First, the optimum parameters reported for 3D-USV herein are not meant to be generalizable. Indeed, UTE sequences are sensitive to field inhomogeneities and gradient hardware setup and, thus, local adaptations may be required. In addition, a relatively large panel but not all factors that may influence signal-to-noise ratio were tested herein, such as TR, TE, or flip angle. Moreover, 3D-USV and PETRA sequences were not completed on the same MR scanner, since PETRA was not available on the Siemens Aera MR scanner at the time of the study. However, PETRA was performed on an older Siemens Avanto MR scanner with standard 16-channel body coil / 8-channel spine coil, whereas 3D-USV benefited from the last generation of 18-channel body coil / 32-channel spine coil. Thus, better results in signal ratio and contrast ratio of PETRA are not likely to be explained by an update in MR hardware technology. Third, one could argue that the imaging time of PETRA was  $12 \pm 2$  minutes as compared to  $6 \pm 1$  minutes for 3D-USV. Nevertheless, optimal parameters for both PETRA and 3D-USV were carefully checked using a wide range of parameter variations. Specifically, improvement in 3D-USV imaging quality at both quantitative and qualitative evaluations were not found significant by increasing the number of spiral

interleaves from 320 to 480 and, thus, the mean acquisition time from 8 to 12 minutes. In this study, we did not explore whether this result might be related to hardware capacities or clinical tolerability of volunteers to long acquisition times. Indeed, 3D-USV was not silent, whereas the quiet PETRA sequence might improve acceptability of the MR examination, especially in the pediatric population.<sup>15,29</sup> Finally, evaluation in human diseases was performed in a few adult patients only and requires evaluation in larger multicenter cohorts from childhood to adulthood.

To conclude, 3D-USV is a promising pulse sequence for 3D-UTE imaging of the lung. Although signal and contrast were found lower than that obtained using spherical  $k$ -space coverage, the better respiratory synchronization yielded lower artifact and a lower rate of nondiagnostic imaging acquisition. Automation of respiratory synchronization may enhance the clinical applicability of this newly developed imaging modality in the field of either airway or interstitial lung diseases, for both routine and research investigations.

## Acknowledgments

The study was completed within the context of the Laboratory of Excellence TRAIL, ANR-10-LABX-57. The study was funded by Centre Hospitalier Universitaire de Bordeaux and Le Nouveau Souffle Foundation. Furthermore, the authors thank Alto Stemmer, Thomas Benkert, and David Grodzki from Siemens Healthcare for providing the UTE Spiral VIBE and the PETRA sequence.

## References

- Biederer J, Beer M, Hirsch W, et al. MRI of the lung (2/3). Why ... when ... how? *Insights Imaging* 2012;3:355–371.
- Biederer J, Wielpütz MO, Jobst BJ, Dinkel J. [MRI of interstitial lung diseases: what is possible?] *Radiologe* 2014;54:1204–1212.
- Doumes G, Macey J, Blanchard E, Berger P, Laurent F. [MRI of the pulmonary parenchyma: Towards clinical applicability?] *Rev Pneumol Clin* 2017;73:40–49.
- Johnson KM, Fain SB, Schiebler ML, Nagle S. Optimized 3D ultrashort echo time pulmonary MRI. *Magn Reson Med* 2013;70:1241–1250.
- Chen L, Liu D, Zhang J, et al. Free-breathing dynamic contrast-enhanced MRI for assessment of pulmonary lesions using golden-angle radial sparse parallel imaging. *J Magn Reson Imaging* 2018 [Epub ahead of print].
- Higano NS, Fleck RJ, Spielberg DR, et al. Quantification of neonatal lung parenchymal density via ultrashort echo time MRI with comparison to CT. *J Magn Reson Imaging* 2017;46:992–1000.
- Froidevaux R, Weiger M, Brunner DO, Dietrich BE, Wilm BJ, Pruessmann KP. Filling the dead-time gap in zero echo time MRI: Principles compared. *Magn Reson Med* 2018;79:2036–2045.
- Wielpütz MO, Mall MA. MRI accelerating progress in functional assessment of cystic fibrosis lung disease. *J Cyst Fibros* 2017;16:165–167.
- Togao O, Tsuji R, Ohno Y, Dimitrov I, Takahashi M. Ultrashort echo time (UTE) MRI of the lung: assessment of tissue density in the lung parenchyma. *Magn Reson Med* 2010;64:1491–1498.

10. Walkup LL, Tkach JA, Higano NS, et al. Quantitative magnetic resonance imaging of bronchopulmonary dysplasia in the neonatal intensive care unit environment. *Am J Respir Crit Care Med* 2015;192:1215–1222.
11. Dournes G, Menut F, Macey J, et al. Lung morphology assessment of cystic fibrosis using MRI with ultra-short echo time at submillimeter spatial resolution. *Eur Radiol* 2016;26:3811–3820.
12. Kumar S, Rai R, Stemmer A, et al. Feasibility of free breathing Lung MRI for Radiotherapy using non-Cartesian k-space acquisition schemes. *Br J Radiol* 2017;90:20170037.
13. Qian Y, Boada FE. Acquisition-weighted stack of spirals for fast high-resolution three-dimensional ultra-short echo time MR imaging. *Magn Reson Med* 2008;60:135–145.
14. Grodzki DM, Jakob PM, Heismann B. Ultrashort echo time imaging using pointwise encoding time reduction with radial acquisition (PETRA). *Magn Reson Med* 2012;67:510–518.
15. Dournes G, Grodzki D, Macey J, et al. Quiet submillimeter MR imaging of the lung is feasible with a PETRA sequence at 1.5 T. *Radiology* 2015; 276:258–265.
16. Du J, Bydder M, Takahashi AM, Chung CB. Two-dimensional ultrashort echo time imaging using a spiral trajectory. *Magn Reson Imaging* 2008; 26:304–312.
17. Tan H, Meyer CH. Estimation of k-space trajectories in spiral MRI. *Magn Reson Med* 2009;61:1396–1404.
18. Rofsky NM, Lee VS, Laub G, et al. Abdominal MR imaging with a volumetric interpolated breath-hold examination. *Radiology* 1999;212: 876–884.
19. Pipe JG. Reconstructing MR images from undersampled data: data-weighting considerations. *Magn Reson Med* 2000;43:867–875.
20. Pipe JG, Menon P. Sampling density compensation in MRI: rationale and an iterative numerical solution. *Magn Reson Med* 1999;41:179–186.
21. Bhalla M, Turcios N, Aponte V, et al. Cystic fibrosis: scoring system with thin-section CT. *Radiology* 1991;179:783–788.
22. Hansell DM, Bankier AA, MacMahon H, McLoud TC, Müller NL, Remy J. Fleischner Society: Glossary of terms for thoracic imaging. *Radiology* 2008;246:697–722.
23. Bland JM, Altman DG. Measuring agreement in method comparison studies. *Stat Methods Med Res* 1999;8:135–160.
24. Zha W, Kruger SJ, Johnson KM, et al. Pulmonary ventilation imaging in asthma and cystic fibrosis using oxygen-enhanced 3D radial ultra-short echo time MRI. *J Magn Reson Imaging* 2018;47:1287–1297.
25. Rahmer J, Börner P, Groen J, Bos C. Three-dimensional radial ultrashort echo-time imaging with T2 adapted sampling. *Magn Reson Med* 2006; 55:1075–1082.
26. Watadani T, Sakai F, Johkoh T, et al. Interobserver variability in the CT assessment of honeycombing in the lungs. *Radiology* 2013;266:936–944.
27. Leuraud K, Richardson DB, Cardis E, et al. Ionising radiation and risk of death from leukaemia and lymphoma in radiation-monitored workers (INWORKS): an international cohort study. *Lancet Haematol* 2015;2: e276–281.
28. Dournes G, Marthan R, Berger P, Laurent F. Excess risk of cancer from computed tomography scan is small but not so low as to be incalculable. *Am J Respir Crit Care Med* 2015;192:1396–1397.
29. Niwa T, Nozawa K, Aida N. Visualization of the airway in infants with MRI using pointwise encoding time reduction with radial acquisition (PETRA). *J Magn Reson Imaging* 2017;45:839–844.

**Title. 3D-UTE MRI of the lung using stack-of-spirals: evaluation in healthy volunteers and parenchymal diseases.**

**SUPPLEMENTAL MATERIAL**

**Supplemental Method**

A pilot study was performed to determine the intrinsic properties of the 3D Spiral VIBE ultra-short echo time sequence (3D-USV) in human lungs *in vivo*. Repetition time (TR), echo time (TE) and flip angle were those previously published for PETRA (1) and thus TR/TE/flip angle=4.1ms/0.07ms/5°. 3D isotropic millimeter imaging was used for human lung imaging because of the presence of fine structures such as bronchi and vessels. For this, field-of-view (FOV) of (320x320mm) was used to cover the entire lung in the native coronal plane. A matrix resolution of 320x320 was used to reach millimeter pixel resolution. The slice thickness was adapted to FOV size and matrix size to get isotropic voxel dimension of (1x1x1mm). The number of slices had to be adapted to the patient size and ranged from 200 to 240. The number spiral interleaves (SI) was arbitrarily chosen to find a compromise between resolution and acquisition time. Using 320 SI, the mean acquisition time to get 3D millimeter isotropic imaging of human lung was found to be 8 minutes under respiratory motion compensation and thus, this number of SI was thought clinically acceptable.

Three main factors of variations in imaging quality, signal and contrast were investigated: voxel size, number of spiral interleaves and partial Fourier acquisition along the slice direction. First, the effect of voxel size variation was investigated. Isotropic voxel dimension of (1.2x1.2x1.2mm) was obtained by using FOV=(312x312mm) and matrix size=260x260 and slice thickness=1.2mm. Isotropic voxel dimension of (0.8x0.8x0.8mm) was obtained by using FOV=320x320mm and matrix size=400x400 and slice thickness=0.8mm.

Second, the effect of SI variations was investigated using a 3D isotropic millimeter acquisition [FOV=(320x320mm), matrix=320x320, slice thickness=1mm]. A fifty percent variation was applied starting from 320 SI and thus, 160 SI and 480 SI were also tested.

Third, the effect of partial Fourier acquisition was applied to the 3D isotropic millimeter acquisition [FOV=(320x320mm), matrix=320x320, slice thickness=1mm, 320 SI]. Both full Fourier acquisition and partial 6/8 Fourier acquisition were tested.

Twelve healthy volunteers (mean age  $24 \pm 11$ , 7 male and 5 females) completed all eight 3D-USV examinations the same day. No contrast product injection or inhalation was used.

Acquisition time, imaging quality and quantitative assessments of signal ratio and contrast ratio (1) were calculated. Comparison of multiple paired means was done using Friedman test. Wilcoxon signed rank test was used for comparisons between each paired means.

#### Supplemental Reference

1. Dournes G, Grodzki D, Macey J, et al.: Quiet Submillimeter MR Imaging of the Lung Is Feasible with a PETRA Sequence at 1.5 T. *Radiology* 2015; 276:258–265.

**Supplemental Table 1. 3D-USV and PETRA sequence parameters**

	3D-USV	PETRA
<b>Sequence parameters</b>		
TR/TE (ms)	4.1/0.07	4.1/0.07
Flip angle (°)	5	5
Bandwidth (Hz/Px)	2800	440
Pulse duration (µs)	60	14
Readout length (µs)	1800	600
Tacq (minutes)	6 ± 1	12 ± 2
Voxel size (mm <sup>3</sup> )	1x1x1	1x1x1
Acquisition	320 SI	80 000 RS
Synchronisation	Prospective gating	Belt
Silent	No	Yes
<b>MR scan</b>	AERA (Siemens®)	AVANTO (Siemens®)
<b>Coil</b>	18-channel body coil/32- channel spine coil	16-channel body coil/8-channel spine coil
<b>Contrast product injection</b>	None	None

Legends: Data are mean ± standard deviation for continuous variables. TR=repitition time; TE=echo time; Hz=Hertz; Px=pixel; Tacq=acquisition time; SI:spiral interleave; RS=radial spoke.

**Supplemental Table 2. CT protocol**

---

<b>Machine</b>	SOMATOM DEFINITION 64 (Siemens HealthCare®)
<b>Tube voltage</b>	110 kV
<b>Tube current</b>	Modulating CareDose4D (Siemens Medical Solutions®)
<b>Effective reference tube current</b>	50 mAs
<b>Rotation time</b>	75 ms
<b>Collimation</b>	1 mm
<b>Field-of-view</b>	Patient size dependent
<b>Matrix</b>	512x512
<b>Voxel size</b>	(0.6-0.7mm) <sup>3</sup>
<b>Effective dose</b>	1.2 to 1.5 mSv

---

**Supplemental Table 3. Characteristics of 16 adults with cystic fibrosis**

<b>Age</b>		21	[18.9-31.1]
<b>Male / Female</b>		7 / 9	
<b>BMI</b>		20	[17.6-21.3]
<b>DeltaF508 mutation</b>	(HomoZ/HeteroZ)	7 / 9	
<b>Smoker</b>	(yes /no)	0 / 16	
<b>ABPA</b>	(yes/no)	3 / 13	
<b>PFT</b>	FEV1 (%)	70.0	[56.0-97.9]
	FVC (%)	80.0	[75.0-98.0]
	Tiffeneau	75.5	[67.5-87.3]
	RV (%)	111.0	[96.3-146.8]
	TLC (%)	95.0	[93.2-103.7]

Legends: Data are medians with [95% confidence interval]; BMI=body mass index; HomoZ=homozygous; HeteroZ=heterozygous; ABPA=allergic bronchopulmonary disease; PFT=pulmonary function test; FEV1=forced expiratory volume in 1 second; FVC=forced vital capacity; RV=residual volume; TLC=total lung capacity.

**Supplemental Table 4. Characteristics of 16 adults with pulmonary infiltrative diseases.**

<b>Age</b>		67.0	[53.4-80.0]
<b>Male / Female</b>		11 / 5	
<b>BMI</b>		24.0	[19.2-26.9]
<b>Smoker</b>	(yes/no)	10 / 6	
<b>ILD</b>	Scleroderma	3	
	IPF	5	
	NSIP	2	
	COP	1	
	Sarcoidosis	1	
	Churg and Strauss	1	
	Asbestos	3	
<b>PFT</b>	FEV1 (%)	78.0	[57.0-88.0]
	FVC (%)	69.5	[49.6-99.0]
	Tiffeneau	83.9	[62.5-91.4]
	TLC (%)	66.0	[55.0-86.0]
	TLCO (%)	41.0	[34.0-47.5]
<b>Arterial blood gases</b>	PaO <sub>2</sub> (mmHg)	84.0	[75.2-86.0]

Legends: Data are median with [95% confidence interval]; BMI=body mass index; ILD=interstitial lung disease; PFT=pulmonary function test; IPF=idiopathic pulmonary fibrosis; ; NSIP=non-specific interstitial pattern; COP=; FEV1=forced expiratory volume in 1 second; FVC=forced vital capacity; TLC=total lung capacity; TLCO=transfer lung capacity of oxygen; PaO<sub>2</sub>=partial blood arterial pressure in oxygen.

**Supplemental Table 5. Intrinsic 3D-USV properties assessed in 12 healthy volunteers**

<b>Fixed parameters: F=full; SI=320</b>	<b>Variables</b>	<b>V=(1.2mm)<sup>3</sup></b>	<b>V=(1mm)<sup>3</sup></b>	<b>V=(0.8mm)<sup>3</sup></b>	<b>Friedman test</b>
	Tacq (minutes)	6 ± 2*,**	8 ± 1†	10 ± 2	<0.001
	Sr	155.9 ± 9.8*,**	136.3 ± 5.5†	128.4 ± 3.5	<0.001
	Cr	15.8 ± 1.5*,**	13.4 ± 2.1†	10.6 ± 1.4	<0.001
	Quality score	20.3 ± 3.4*	25.3 ± 4.2†	20.3 ± 5.7	<0.001

<b>Fixed parameters: FOV, F=full; V=(1mm)<sup>3</sup></b>	<b>Variables</b>	<b>SI=160</b>	<b>SI=320</b>	<b>SI=480</b>	<b>Friedman test</b>
	Tacq (minutes)	4 ± 1*,**	8 ± 1†	12 ± 3	<0.001
	Sr	117.8 ± 3.3*,**	136.3 ± 5.5	138.0 ± 2.4	<0.001
	Cr	10.0 ± 1.9*,**	13.4 ± 2.1	13.6 ± 1.9	<0.001
	Quality score	21.3 ± 6.2*,**	25.3 ± 4.2	25.6 ± 2.2	<0.001

<b>Fixed parameters: FOV, SI=320, V=(1mm)<sup>3</sup></b>	<b>Variables</b>	<b>F=full</b>	<b>F=6/8</b>	<b>Friedman test</b>
	Tacq (minutes)	8 ± 1*	6 ± 1	<0.001
	Sr	136.3 ± 5.5	134.2 ± 6.8	0.2
	Cr	13.4 ± 2.1	13.1 ± 2.3	0.5
	Quality score	25.8 ± 4.4	24.3 ± 4.1	0.4

Legendes: Data are mean±standard deviation. Tacq=acquisition time; V=voxel size; SI=number of spiral interleaves; F=k-space filling  
Sr=signal ratio; Cr=contrast ratio

Comparisons between means was performed using Wilcoxon's signed rank test. \* indicates significant difference between 1st and 2nd testing, \*\* between 1st and 2nd testing and † between 2nd and 3rd testing. A risk alpha inferior to 0.05 was considered significant between groups.

**Supplemental Table 6. Interobserver concordance to assess imaging quality of 3D-USV and PETRA**

			<b>3D-USV</b>	<b>PETRA</b>
<b>Quantitative analysis</b>	Sr	Mean difference	3.2	-38
		Limit of agreement	[-6; 13]	[-154; 77]
	Cr	Mean difference	1.2	4
		Limit of agreement	[-2; 5]	[-6; 18]
<b>Qualitative analysis</b>	Fissure	ICC	0.81	0.84
	Bronchi visibility	ICC	0.75	0.86
	Bronchi sharpness	ICC	0.68	0.72
	Vessel visibility	ICC	0.92	0.90
	Vessel sharpness	ICC	0.74	0.82
<b>Artefacts</b>	Streak	ICC	1	0.86
	Blurring	ICC	0.88	0.84
	Shading	ICC	0.92	0.92
	Aliasing	ICC	0.90	0.76
	Cardiac	ICC	0.88	0.91

Legends: ICC=intraclass correlation coefficient; Sr=signal ratio; Cr=contrast ratio.

**Supplemental Table 7. Interobserver concordance to assess CT-Bhalla score in 16 adults with CF**

		<b>3D-USV (n=16)</b>	<b>PETRA (n=16)</b>
		<b>ICC</b>	<b>ICC</b>
<b>Wall thickening</b>		0.74	0.68
<b>Bronchiectasis</b>	Severity	0.82	0.78
	Extent	0.72	0.70
<b>Mucoid impaction</b>	Extent	0.79	0.79
<b>Bronchial generation</b>		0.81	0.78
<b>Sacculation/Abscess</b>		NA	NA
<b>Consolidation/Atelectasis</b>		0.92	0.95
<b>Bulla</b>		NA	NA
<b>Emphysema</b>		NA	NA
<b>Global score</b>		0.90	0.93

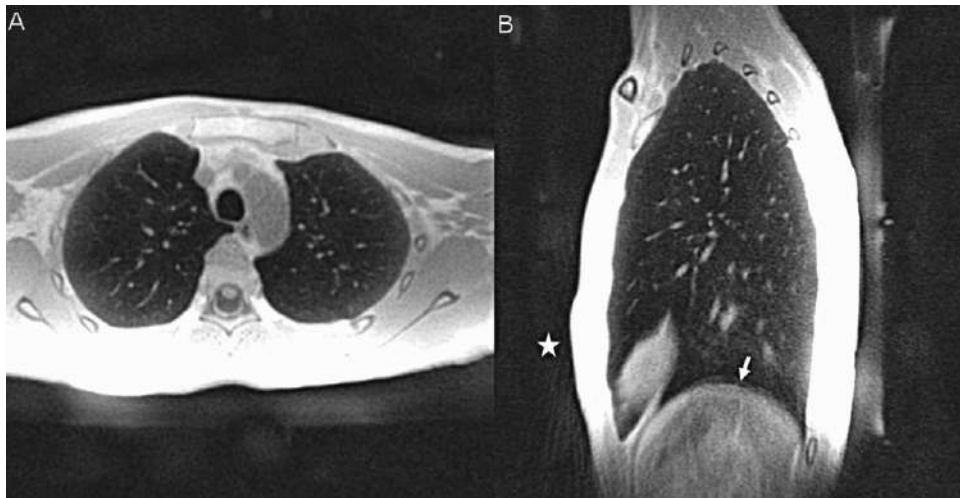
Legend: ICC=intraclass correlation coefficient; NA=non applicable

**Supplemental Table 8. Interobserver agreement to assess the presence of structural abnormalities at the segmental level in patients with lung interstitial disease**

	<b>3D-USV</b>	<b>PETRA</b>
	<b>Kappa</b>	<b>Kappa</b>
<b>Honeycombing</b>	0.51	0.45
<b>Septal lines</b>	0.62	0.67
<b>Reticulation</b>	0.51	0.59
<b>Ground glass opacity</b>	0.59	0.51
<b>Traction bronchiectasis</b>	0.45	0.47
<b>Nodule</b>	0.96	0.96
<b>Cyst</b>	0.71	0.84
<b>Pleural plaque</b>	0.92	0.96

Legend: CI=confidence interval

## SUPPLEMENTAL FIGURES



**Supplemental Figure 1.** PETRA examination in a healthy volunteer in native axial (A) and sagittal reformation (B). There is good depiction of both intrapulmonary bronchi and small vessels up to the lung periphery. On sagittal reformation (B), white star indicate streaks radiating from the sternum and white arrow shows moderate blurring of the diaphragm due to non-perfect respiratory synchronization.



**Supplemental Figure 2.** CT (A), 3D-USV (B) and PETRA (C) non-contrast enhanced examinations in a 63-year-old male with pulmonary idiopathic fibrosis. Black arrows indicate areas of honeycombing, visible on both CT (A) and 3D-USV (B). There was failure of respiratory synchronization using a belt during PETRA examination leading to a non-diagnostic examination.

### **3.2 Publication n°4 : Quantification volumétrique automatique de la sévérité de l'emphysème à l'IRM à temps d'écho ultra court chez des patients atteints de BPCO**

La quantification de l'extension de l'emphysème à l'IRM 3D UTE souffre de problématiques inhérentes au signal IRM (normalisation/calibration) mais également de l'absence d'automatisation disponible en scanner. Dans cette étude nous avons développé une méthode totalement automatique pour la quantification de l'extension de l'emphysème et nous avons essayé d'apporter des solutions nouvelles à la problématique posée de la normalisation du signal IRM. L'objectif de cette étude était donc d'évaluer les capacités de l'IRM 3D-UTE à quantifier l'extension de l'emphysème, avec une analyse visuelle et quantitative automatisée. La méthode a été comparée à la méthode de quantification de l'emphysème en scanner thoracique chez 28 patients BPCO et 10 volontaires sains. Les résultats ont montré une bonne concordance de l'évaluation visuelle de l'emphysème entre IRM 3D UTE et TDM. Le pourcentage d'emphysème quantifié automatiquement en IRM était significativement plus élevé chez les BPCO comparativement aux volontaires sains. Nous avons démontré une corrélation significative entre la quantification de l'emphysème en 3D IRM UTE et la quantification TDM. Également, des corrélations similaires des deux modalités ont été retrouvées avec les paramètres obstructifs aux explorations fonctionnelles respiratoires. Enfin, la performance de l'IRM quantitative dans le diagnostic de l'emphysème était parfaite dans notre série. Ainsi, notre méthode automatique de quantification de l'emphysème est fiable et reproductible chez les patients atteints de BPCO.

# Automated Volumetric Quantification of Emphysema Severity by Using Ultrashort Echo Time MRI: Validation in Participants with Chronic Obstructive Pulmonary Disease

Ilyes Benlala, MD • Patrick Berger, MD, PhD • Pierre-Olivier Girodet, MD, PhD • Claire Dromer, MD • Julie Macey, MD • François Laurent, MD • Gaël Dournes, MD, PhD

From the Université Bordeaux, Centre de Recherche Cardio-Thoracique de Bordeaux, U1045, CIC 1401, Bordeaux, France (I.B., P.B., P.O.G., F.L., G.D.); Centre de Recherche Cardio-Thoracique de Bordeaux, INSERM U1045, Université Bordeaux Segalen, 146 rue Léo Saignat, 33076 Bordeaux Cedex, France (I.B., P.B., P.O.G., F.L., G.D.); and CHU de Bordeaux, Service d'Imagerie Thoracique et Cardiovasculaire, Service des Maladies Respiratoires, Service d'Exploration Fonctionnelle Respiratoire, CIC 1401, France (I.B., P.B., P.O.G., C.D., J.M., F.L., G.D.). Received January 14, 2019; revision requested March 5; revision received March 18; accepted April 9. Address correspondence to G.D. (e-mail: [gael.dournes@chu-bordeaux.fr](mailto:gael.dournes@chu-bordeaux.fr)).

Study supported by University Hospital of Bordeaux (NCT02100800); I.B. supported by Société Française de Radiologie.

Conflicts of interest are listed at the end of this article.

Radiology 2019; 00:1–11 • <https://doi.org/10.1148/radiol.2019190052> • Content code: 

**Background:** The validity of three-dimensional (3D) ultrashort echo time (UTE) MRI for the assessment of emphysema in patients with chronic obstructive pulmonary disease (COPD) at high spatial resolution is, to the knowledge of the authors, unknown.

**Purpose:** To assess whether noncontrast agent-enhanced 3D UTE MRI at submillimeter spatial resolution can be used to determine the extent of emphysema by using both qualitative visual scoring and fully automated volumetric quantification.

**Materials and Methods:** Twenty-eight participants with COPD and 10 control participants (mean age, 70 years  $\pm$  7 [standard deviation] and 64 years  $\pm$  4, respectively) were prospectively enrolled between 2015 and 2017. Participants underwent pulmonary function testing, CT, and MRI. CT was used as the reference standard. Qualitative scoring of emphysema extent was performed by two readers. Fully automated quantification of percentage of low-attenuation volume by using a threshold of  $-950$  HU (%LAV<sub>-950HU</sub>) at CT and percentage of low-signal-intensity volume by using an adaptive threshold of 0.20 (%LSV<sub>0.20</sub>) at MRI were the respective emphysema indexes. Comparison of means was performed by using Student *t* test, correlation was determined by using Pearson test, agreement was found by using weighted  $\kappa$  index, and reproducibility was determined by using intraclass correlation coefficient. Diagnostic performance was assessed by calculating the area under the receiver operating characteristics curve (AUC).

**Results:** With qualitative scoring, agreement between UTE MRI and CT was good (weighted  $\kappa$ , 0.79; 95% confidence interval: 0.71, 0.83). With automated volumetric quantification, %LSV<sub>0.20</sub> was significantly correlated with %LAV<sub>-950HU</sub> in participants with COPD ( $r$ ,  $-0.80$ ;  $P < .001$ ) and correlated with forced expiratory volume in 1 second percentage predicted ( $r$ ,  $-0.55$ ;  $P = .002$ ). %LSV<sub>0.20</sub> was significantly higher in participants with COPD than in control participants ( $P < .001$ ). The diagnostic performance and reproducibility of %LSV<sub>0.20</sub> were good (AUC, 1.00 [95% confidence interval: 0.88, 1.00], and intraclass correlation coefficient,  $> 0.99$ , respectively).

**Conclusion:** A fully automated method with three-dimensional ultrashort echo time MRI reproducibly quantified the volumetric extent of emphysema in participants with chronic obstructive pulmonary disease.

© RSNA, 2019

Online supplemental material is available for this article.

Chronic obstructive pulmonary disease (COPD) is characterized by persistent respiratory symptoms and airflow limitation (1) and is the third leading cause of mortality worldwide (2). In the past decades, chest CT has helped to provide valuable insights into COPD. Indeed, CT enables noninvasive, in vivo, and three-dimensional (3D) quantification of the key components of the disease, such as bronchial remodeling (3) and emphysema (4). Evidence of COPD subtypes (1), relationship with genetic variants (5), longitudinal follow-up (6), and mortality (7) have been investigated at CT. More recently, in an era where the advent of artificial intelligence may allow intricate combinations of

both morphologic and functional information, lung MRI has emerged as a radiation-free modality for the longitudinal follow-up of lung diseases and (8) to help better identify participant phenotype or predict disease outcomes (9). Studies related to ventilation (10), perfusion (11), dynamic biomarkers (12), and coupling between the cardiovascular and pulmonary systems (13,14) at MRI have been performed. However, there are few studies that evaluated the regional extent of emphysema by using MRI (15–18). Recent advances with ultrashort echo times (UTES) have been shown to enable submillimeter resolution with good contrast in three dimensions (19,20). Precursor studies were

## Abbreviations

%LAV<sub>-950HU</sub> = percentage of low-attenuation volume by using a threshold of -950 HU, %LSV<sub>0.20</sub> = percentage of low-signal-intensity volume by using an adaptive threshold of 0.20, 3D = three-dimensional, COPD = chronic obstructive pulmonary disease, GOLD = Global Initiative for Chronic Obstructive Lung Disease, UTE = ultrashort echo time

## Summary

In this pilot study, we validated an automated method to reliably quantify the severity of emphysema from three-dimensional ultrashort echo time lung MRI.

## Key Points

- Quantitative volumetric emphysema indexes obtained by using three-dimensional ultrashort echo time (UTE) MRI showed strong correlation ( $r = 0.84$ ,  $P < .001$ ); visual analysis showed good agreement between UTE MRI and CT for the assessment of the regional extent (weighted  $\kappa$  index, 0.79).
- Quantitative volumetric emphysema indexes by using UTE MRI were different between participants with chronic obstructive pulmonary disease (COPD) and control participants ( $27\% \pm 9$  and  $9\% \pm 4$ , respectively;  $P < .001$ ) and correlated with forced expiratory volume in 1 second percentage predicted ( $r = -0.55$ ;  $P < .001$ ) in study participants with COPD.
- For UTE MRI, the intraclass correlation coefficients for the intra- and interobserver reproducibility were greater than 0.99, and intraclass correlation coefficient of short-term repeatability was 0.97.

performed by using two-dimensional techniques, but those methods were enabled to analyze a single two-dimensional section (16,17) or required a total acquisition time of up to 1 hour per participant (17). One early feasibility study (18) used 3D UTE MRI but involved only 10 participants with COPD. Although all precursor MRI methods were semiautomated, they still required interventions such as manual measurements of standards (16–18), visual matching between CT and MRI sections (16,17), or user oversight of lung segmentation (18). Therefore, the capacity of 3D UTE MRI to depict emphysema, with 3D methods, remained to be further investigated.

We hypothesized that 3D UTE MRI could be a valid and reproducible method to help quantify the severity of emphysema in participants with COPD.

The purpose of this validation study was to assess whether noncontrast agent-enhanced 3D UTE MRI can help determine the extent of emphysema by using both visual scoring and a fully automated volumetric quantification method. Three-dimensional (volumetric) CT was used as the reference standard. Secondary objectives were to assess correlation with lung function, to compare COPD stages of severity, to evaluate the diagnostic performance of MRI in the detection of emphysema, and to determine the reproducibility of evaluation.

## Materials and Methods

### Study Population

Our prospective single-center study was performed between January 2015 and December 2017. The local ethics committee approved the study, and all participants were required to

give written informed consent (*ClinicalTrials.gov* registration number NCT02100800). The study received academic funding from the University Hospital of Bordeaux and the French Society of Radiology. All authors had full control over the data. Details regarding the calculation of the number of participants are provided in Appendix E1 (online). Briefly, we calculated that a minimum of 26 participants with COPD and five control participants were enough to assess the validity of the method with type I rate of 2.5% and power of 90%. According to the study design, the first 10 participants were asked to undergo repeat MRI 10 minutes after the first MRI examination to assess repeatability as a secondary end point. Inclusion criteria were adults older than age 40 years. Participants had to undergo CT, MRI, and pulmonary function testing within a maximum interval of 30 days. COPD was diagnosed according to Global Initiative for Chronic Obstructive Lung Disease (GOLD) guidelines (21–23). The recruitment of participants with COPD was consecutive, and the latest exacerbation had to occur at least 4 weeks from the study inclusion. Control participants were nonsmokers, did not have respiratory symptoms, had visually healthy chest CT scans, had normal results at pulmonary function testing, and were selected to be sex-matched with participants with COPD. Both participants with COPD and control participants were excluded if they had a history of asthma, lung fibrosis, pulmonary hypertension, or cystic fibrosis; if they had contraindications to MRI; or, for control participants, if they had undergone any respiratory treatment (Fig 1).

### CT and MRI Examinations

Noncontrast-enhanced chest CT images were acquired with a 64-section multi-detector row CT scanner (Somatom Definition; Siemens Healthcare, Erlangen, Germany) at full inspiration and with an isotropic voxel size of 0.625 mm<sup>3</sup>; images were reconstructed by using standard (B30f) and sharp (B70f) algorithms. CT doses ranged from 120 to 150 mGy · cm. Details are provided in Appendix E1 (online).

Three-dimensional UTE lung MRI was performed with a 1.5-T system (Magnetom Avanto; Siemens Healthcare, Erlangen, Germany) by using pointwise encoding time reduction with radial acquisition (20) and a submillimeter voxel size of 0.93 mm<sup>3</sup>. Acquisition time was about 12 minutes with respiratory binning to reconstruct only those k-space data acquired at end-tidal respiration (eg, functional residual capacity).

CT images and images obtained by using MRI were anonymized. Image quality was initially assessed by the senior reader (G.D.). Blurring artifacts at the level of the diaphragm and ribs, streaks, and beam-hardening artifacts were scored as follows (19): 0, minimal or none; 1, mild; 2, moderate; and 3, severe.

Signal-to-noise ratio and contrast-to-noise ratio were calculated as follows (24; Appendix E1 [online]): signal-to-noise ratio =  $(S_{vessel}/\sigma_{air})$ ; contrast-to-noise ratio =  $[(S_{vessel} - S_{bronchus})/\sigma_{air}]$ , where signal intensity measurements were performed in pulmonary artery truncus ( $S_{vessel}$ ), extrathoracic air ( $S_{air}$ ), and the trachea ( $S_{bronchus}$ ).  $\sigma_{air}$  corresponds to the standard deviation of  $S_{air}$ .

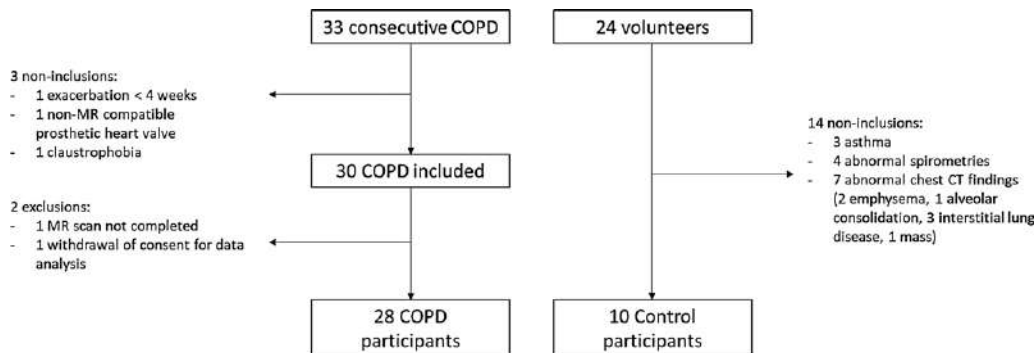


**Figure 1:** Study flowchart. COPD = chronic obstructive pulmonary disease.

## Validation of MRI in the Assessment of Emphysema Severity

**Qualitative visual evaluation of emphysema extent.**—Three-dimensional UTE MRI and CT reconstructed with the sharp algorithm (B70f) were part of the visual evaluation (Fig 2). Multiplanar reformations were allowed in three dimensions. A total of 20 segments were considered (10 segments per lung) (3). A four-point scale was used to determine the extent of emphysema for each segment, as follows: 0, no emphysema; 1, mild emphysema (<25%); 2, moderate emphysema (25%–50%); and 3, severe emphysema (>50%). Scoring was recorded in each segment and then a participant score was calculated as the sum of all scorings.

Qualitative scorings were independently evaluated by two observers blinded to any other data (I.B. and G.D., with 4 and 10 years of experience in thoracic imaging, respectively). Images were read in random order. At the segment level, the mean of two qualitative evaluations was chosen as consensus. Emphysema was considered visually present when both observers assigned a score of 1 or greater.

**Automatic quantification of emphysema extent.**—By using 3D CT images, two emphysema indexes were calculated with software (Myrian; Intracense, Montpellier, France) from the histogram of attenuation distribution: the percentage of low-attenuation volume by using a threshold of  $-950$  HU ( $\%LAV_{-950HU}$ ) and the 15th percentile of the voxel attenuation distribution (1).

At 3D UTE MRI (Figs 3, E1 [online]), two emphysema indexes were determined from the histogram of signal intensity distribution by using an in-house software program written in Matlab (MathWorks, Natick, Mass): the percentage of low-signal-intensity volume and the skewness, which describes the histogram asymmetry and shift. The rationale and method for calculating the relative low signal volume is extensively described in the supplemental Methods section (Appendix E1 [online]). Briefly, after filtering of images obtained at MRI to enhance contours, a segmentation of the lung volume was automatically obtained after calculation of a soft-tissue threshold from the histogram of signal intensity distribution by using the curve-fitting method (25,26). Second, voxel signal intensities contained within the lung volume were normalized between 0 and 1, with native signal intensity from lung air

as minimum and native signal intensity from soft-tissue threshold as maximum. Finally, the percentage of low-signal-intensity volume by using an adaptive threshold of 0.20 ( $\%LSV_{0.20}$ ) was calculated with an equation similar to that used by Zhang et al (17), as follows:

$$\%LSV_{0.20} = \left( \frac{\sum_{i=0}^{0.20} V_i}{\sum_{i=0}^{1.00} V_i} \right) \times 100$$

where  $V$  is the voxel,  $i$  indicates signal intensity value, and  $\Sigma$  is a sum. For each participant,  $i$  corresponds to a normalization of the absolute value of signal intensity into a percentage  $i$  from the minimum (ie, 0) to maximum (ie, 1) signal intensity distribution. Thresholds other than 0.20 were also empirically tested (ie, 0.10, 0.12, 0.15, and 0.25). In addition, the mean paraspinal muscle signal intensity was determined manually by averaging measurements from two regions of interest in right and left paraspinal muscles at the level of the carina.

Automated CT and MRI quantifications lasted about 30 seconds and 5 minutes, respectively.

## Supportive Evaluations of MRI Validity

First, correlations were searched between  $\%LSV_{0.20}$  and pulmonary function tests. Second, differences in  $\%LSV_{0.20}$  were tested between either GOLD stages 1, 2, 3, and 4 or GOLD groups A, B, C, and D (21,22). Third, the diagnostic performance of MRI to discriminate those participants with COPD and emphysema was assessed. For this, we followed the recently published statement from the Fleischner Society to define CT emphysema by using  $\%LAV_{-950HU}$  of at least 6% and/or visual identification (1). Therefore, we identified the following three possible methods of diagnosis at CT: visual identification of emphysema alone; quantification of  $\%LAV_{-950HU}$  of at least 6% alone; and visual identification and  $\%LAV_{-950HU}$  of at least 6%, wherein both methods were required to confirm the diagnosis.

## Reproducibility Assessment

Qualitative and quantitative independent measurements (I.B. and G.D.) were analyzed to assess interobserver reproducibility and repeatability over time. The senior reader (G.D.) evaluated all blinded images 2 months later, in random order, to prevent recall bias and assess intraobserver reproducibility.

## Statistical Analysis

Statistical analyses were performed by using software (NCSS 2001; NCSS, Kaysville, Utah). Normality was assessed by using the Shapiro-Wilk test. For paired variables, comparisons of parametric data were performed by using the paired  $t$  test. For independent variables, comparisons of parametric

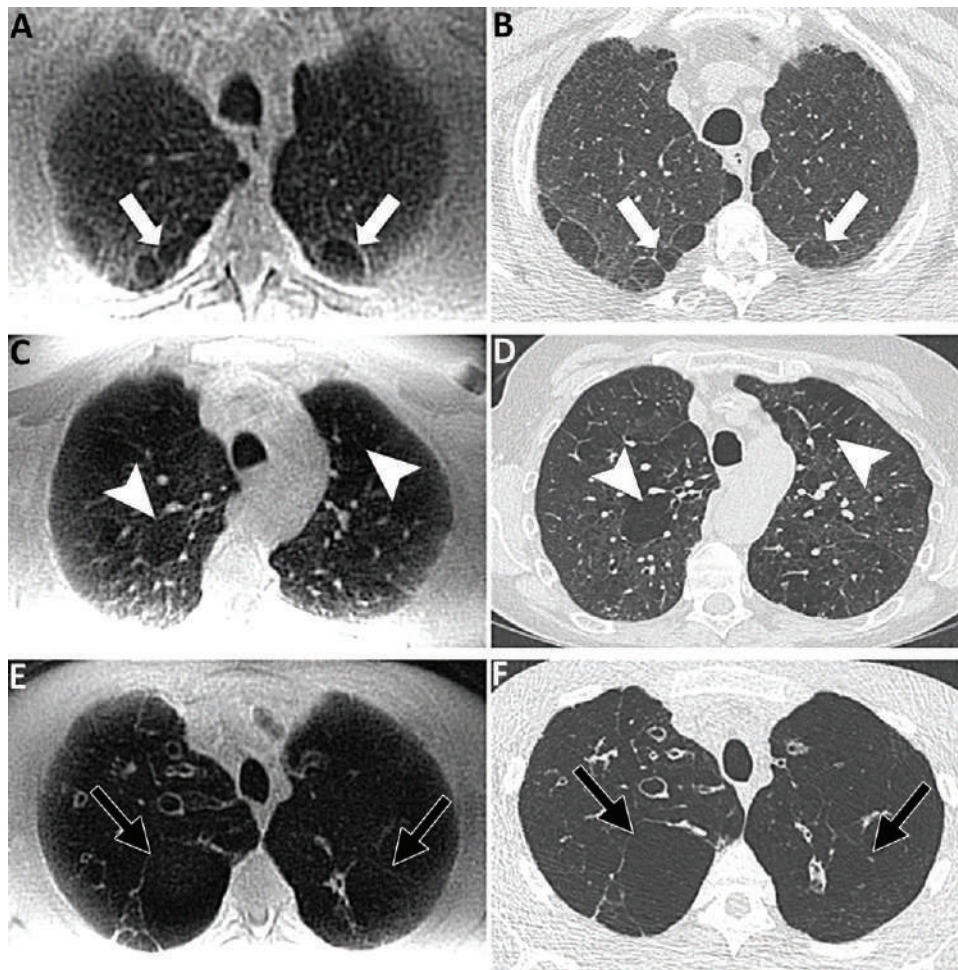


**Figure 2:** Three-dimensional images obtained at A, C, E, ultrashort echo time MRI and B, D, F, CT in three study participants with chronic obstructive pulmonary disease. A, B, Images in the first participant show mild paraseptal emphysema (arrows). C, D, Images in the second participant show moderate emphysema (arrowheads indicate areas of centrilobular emphysema). E, F, Images in the third participant show severe panlobular emphysema; there are conspicuous fine septal lines delineating hyperinflated lobules (arrows).

and nonparametric data were performed by using the Student *t* test and Mann-Whitney test, respectively. Comparison of categorical variables was performed by using the Fisher exact test. Multiple comparisons were performed by using Kruskal-Wallis test with Bonferroni correction. Univariate correlations were assessed by using the Pearson test for parametric variables and the Spearman test for nonparametric variables. The strength of the relationship between %LAV<sub>-950HU</sub> and %LSV<sub>0,20</sub> as an independent variable was assessed by using linear regression analysis. A *P* value less than .05 was considered to indicate statistical significance. Agreement was assessed by using weighted  $\kappa$  index. Reproducibility was assessed by using intraclass correlation coefficients with 95% confidence intervals and Bland-Altman analysis (27). Weighted  $\kappa$  and intraclass correlation coefficient values were classified from null (ie, 0), slight (>0 to  $\leq$ 0.20), fair (>0.20 to  $\leq$ 0.40), moderate (>0.40 to  $\leq$ 0.60), good (>0.60 to  $\leq$ 0.80), and very good (>0.80) according to Landis et al (28). Diagnostic performance was measured by calculating sensitivity, specificity, and area under the receiver operating characteristic curve.

in artifact score, signal-to-noise ratio, or contrast-to-noise ratio between COPD and control participants (Table 2).

### Validation of MRI in the Assessment of Emphysema Severity

**Qualitative visual evaluation.**—A total of 760 segments were evaluated for emphysema severity. Of those 760 segments, 334 and 321 were classified in consensus as devoid of emphysema by using MRI and CT, respectively (Table E3 [online]). There was good agreement between CT and MRI visual categories (weighted  $\kappa$ , 0.79; 95% confidence interval: 0.71, 0.83). At the participant level ( $n = 38$ ), the CT total visual score ranged from 0 ( $n = 2$ ) to more than 50 ( $n = 6$ ). The mean scores for CT and MRI were not significantly different ( $P = .89$ ). The correlation between CT and MRI total visual score was significant ( $r = 0.44$ ;  $P = .005$ ).

**Automatic quantification.**—Both CT and MRI metrics of emphysema extent were significantly higher in participants

## Results

### Study Population

Thirty participants with COPD were included in the study; however, two were excluded from data analysis because they withdrew consent. One participant started to undergo MRI but refused to complete the procedure after 8 minutes. The final population of 28 participants with COPD was primarily composed of heavy smokers, older adults, and men (Table 1). The control population had a similar sex distribution but was slightly younger. All but one participant underwent CT, MRI, and pulmonary function testing examinations on the same day. One participant with COPD underwent CT 20 days before MRI and pulmonary function testing. In addition, 10 participants (seven participants with COPD and three control participants) consented to undergo repeat MRI the same day (Table E1 [online]).

### CT and MRI Examinations

All examinations were of diagnostic quality (Table E2 [online]). There was no difference

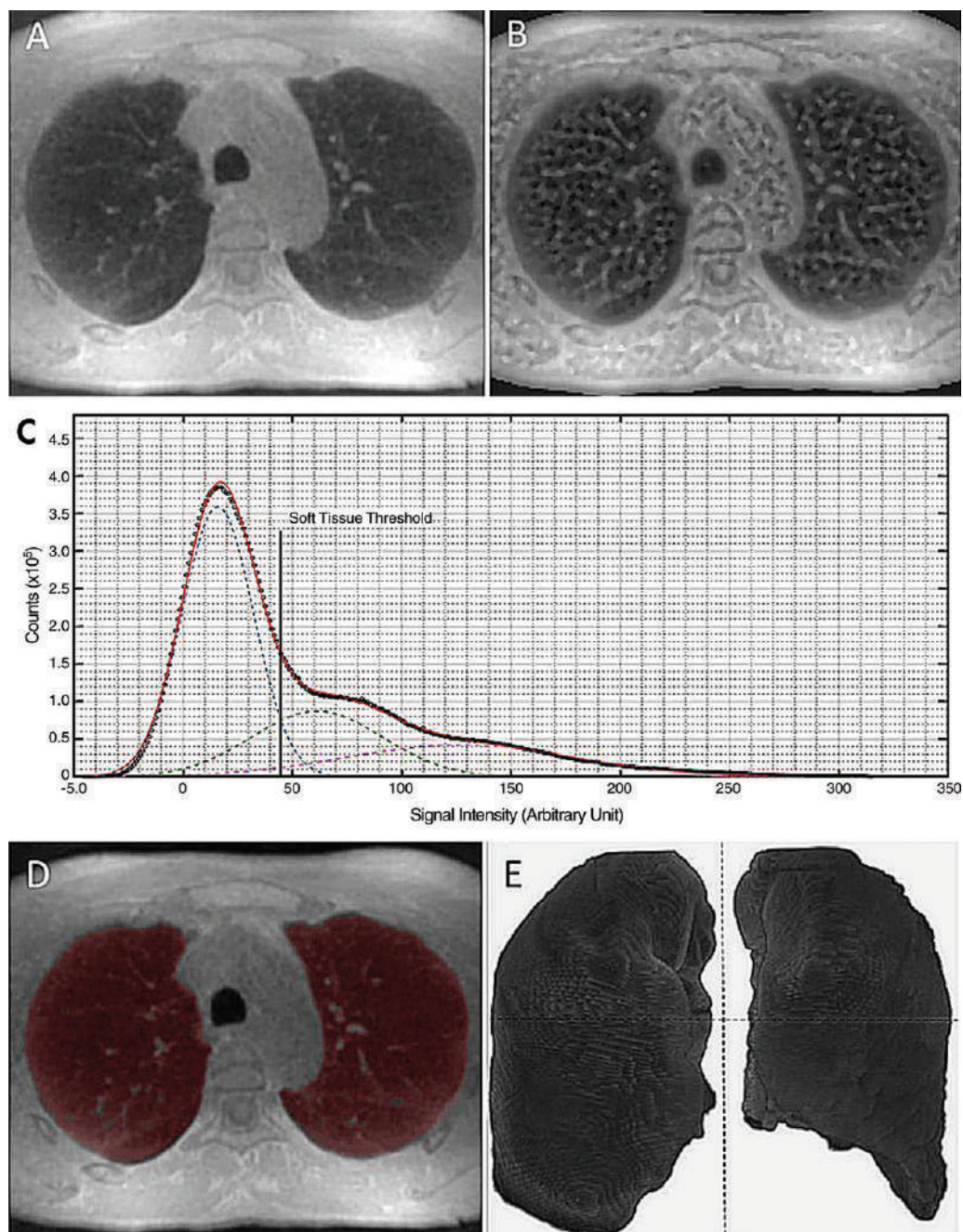


**Figure 3:** Automatic volumetric lung segmentation method. A, Gaussian smoothing is first applied to the image obtained with pointwise encoding time reduction with radial acquisition for denoising at MRI. B, Local enhancement filter is then applied to enable more accurate enhancement of contours. C, The curve-fitting method is applied to the voxel frequency distribution histogram of the, B, locally enhanced image by using three Gaussian-like functions to automatically determine the soft-tissue threshold at the cross point between the curves representative of low and intermediate signal intensities. Finally, the lung volume is segmented by using the soft-tissue threshold and displayed by using either, D, a two-dimensional mask overlaid in red or, E, volume rendering.

with COPD ( $P < .001$ ); skewness was significantly left-shifted toward the lowest normalized signal intensities in participants with COPD (Table 2, Fig 4).

Moreover, %LSV<sub>0.20</sub> showed a strong significant correlation with %LAV<sub>-950HU</sub> ( $r = 0.84$ ;  $P < .001$ ). The slope of the linear regression model was 1.1 (95% confidence interval: 0.9, 1.3) ( $R^2 = 0.71$ ;  $P < .001$ ). At Bland-Altman analysis, the mean difference between %LAV<sub>-950HU</sub> and its linear estimate by using

%LSV<sub>0.20</sub> as independent predictor variable was 0.2 (limits of agreement:  $-15.6, 16.1$ ).

When considering the population of 28 participants with COPD, all correlations between %LAV<sub>-950HU</sub> and percentage of low-signal-intensity volume with various thresholds were significant ( $P \leq .002$ ), although %LSV<sub>0.20</sub> had the highest correlation ( $r = -0.80$ ;  $P < .001$ ) (Fig 5, Table E4 [online]). By using mean paraspinous muscle signal to

**Table 1: Study Participant Characteristics**

Parameter	Participants with COPD (n = 28)	Control Participants (n = 10)	P Value
Age (y)	70 ± 7	64 ± 4	.02
Sex*			.39
M	20	9	
F	8	1	
BMI (kg · m <sup>-2</sup> )	27 (24, 34)	24 (21, 25)	.08
Tobacco use			
Ever smoker*			<.001
Yes	23	0	
No	3	10	
Current smoker*			.55
Yes	4	0	
No	21	10	
Pack-years	42 ± 25	0 (0, 0)	<.001
Pulmonary function testing			
FEV <sub>1%</sub> (%)	56 ± 18	102 ± 9	<.001
FVC (%)	89 (82, 95)	101 (94, 113)	<.001
FEV <sub>1</sub> /FVC (%)	49 ± 13	78 ± 4	<.001
FEF <sub>25%-75%</sub> (%)	23 ± 12	89 ± 16	<.001
TLC (%)	115 ± 17	103 ± 11	.06
RV (%) <sup>†</sup>	158 ± 40	107 ± 30	<.001
TLCO (%) <sup>‡</sup>	55 ± 25	109 ± 24	<.001
PaO <sub>2</sub> (mm Hg)	74 (65, 84)	74 (68, 80)	.26
PaCO <sub>2</sub> (mm Hg)	38 ± 7	38 ± 3	.67

Note.—Unless otherwise indicated, data are mean ± standard deviation for continuous normal variables, or median with 95% confidence interval in parentheses for nonnormal distribution. Arterial blood gases were acquired in the supine position. BMI = body mass index, COPD = chronic obstructive pulmonary disease, FEF<sub>25%-75%</sub> = forced expiratory flow at 25%–75%, FEV<sub>1%</sub> = forced expiratory volume in 1 second, FEV<sub>1</sub> = forced expiratory volume in 1 second, FVC = forced volume capacity, PaCO<sub>2</sub> = arterial partial pressure of carbon dioxide, PaO<sub>2</sub> = arterial partial pressure of oxygen, RV = residual volume, TLC = total lung capacity, TLCO = TLC of carbon monoxide.

\* Data are numbers of participants.

<sup>†</sup> Measurement was missing in one participant with chronic obstructive pulmonary disease.

<sup>‡</sup> Measurements were missing in two participants with chronic obstructive pulmonary disease.

determine emphysema index, we found no correlation to %LAV<sub>-950HU</sub>.

There was no statistically significant relationship between age and quantitative emphysema index by using either CT ( $r = 0.31$ ;  $P = .10$ ) or MRI ( $r = 0.33$ ;  $P = .07$ ). In addition, similar correlations were noticed between the %LSV<sub>0.20</sub> and 15th percentile ( $r = -0.82$ ;  $P < .001$ ) and skewness and CT metrics of emphysema (Fig 5).

### Supportive Evaluations of MRI Validity

**Correlations between UTE MRI and lung functional impairment.**—By using the visual scores, the correlation between MRI and obstruction as indicated by forced expiratory volume in 1 second (percentage predicted) at pulmonary function testing was statistically significant ( $r = -0.33$ ;  $P = .042$ ).

By using quantitative MRI, statistically significant correlations were found between %LSV<sub>0.20</sub> and pulmonary function testing parameters related to airway obstruction, residual volume, and transfer lung carbon monoxide diffusing capacity (Table E5 [online]). Age did not correlate to pulmonary function

testing results in patients with COPD ( $P > .20$ ). Correlations to pulmonary function tests were similar between CT and MRI.

**Comparison of GOLD stages by using quantitative MRI.**—Significant differences in %LSV<sub>0.20</sub> were found between GOLD stage 1 ( $n = 4$ ) and GOLD stage 3 ( $n = 10$ ) or GOLD stage 4 ( $n = 2$ ) ( $P < .01$ ), but not GOLD stage 2 ( $n = 12$ ) (Table E6 [online]). However, no significant differences were found between GOLD groups A, B, C, and D (Table E7 [online]) or by using %LAV<sub>-950HU</sub>.

**Diagnostic accuracy of UTE MRI.**—By using both qualitative analysis and %LAV<sub>-950HU</sub> of at least 6% to define emphysema, the optimal threshold of %LSV<sub>0.20</sub> was greater than 17.8%, with a sensitivity of 24 of 24 (100%; 95% confidence interval: 86%, 100%) and a specificity of four of four (100%; 95% confidence interval: 40%,

100%). Diagnostic accuracy by using the automated detection threshold of %LSV<sub>0.20</sub> was better than visual analysis (Table 3).

### Assessment of Reproducibility

Good interobserver reproducibility (intraclass correlation coefficient,  $>0.60$ ) and very good intraobserver reproducibility (intraclass correlation coefficient,  $>0.90$ ) were obtained with use of qualitative scores. Because CT and MRI quantitative measurements were fully automated, intraclass correlation coefficients were greater than 0.99 and the mean difference at Bland-Altman analysis was equal to 0% (Table 4). The repeatability of %LSV<sub>0.20</sub> was almost perfect (intraclass correlation coefficient, 0.97; 95% confidence interval: 0.88, 0.99).

Reproducibility of manual measurement of mean paraspinal muscle signal was moderate to good, with intraclass correlation coefficients ranging from 0.58 to 0.72.

### Discussion

This prospective study analyzed the qualitative and quantitative performance of three-dimensional (3D) ultrashort echo time (UTE) MRI for the quantitative assessment of the re-

gional extent and severity of emphysema severity with an automated method. By using CT as the reference standard, a good agreement was found to categorize the segmental extent of emphysema by using a qualitative visual score (weighted  $\kappa$ , 0.79). By using fully automated quantification, a strong linear correlation was found to be significant between percentage of low-signal-intensity volume by using an adaptive threshold of 0.20 (%LSV<sub>0.20</sub>) and percentage of low-attenuation volume by using a threshold of -950 HU (%LAV<sub>-950HU</sub>;  $r = 0.84$ ;  $P < .001$ ). To support the validity of the method, there were significant correlations between MR emphysema indexes and pulmonary function testing results related to airway obstruction, pulmonary distension, and alteration in gas exchanges ( $P < .05$ ). Moreover, %LSV<sub>0.20</sub> was significantly different between the spirometric Global Initiative for Chronic Obstructive Lung Disease (GOLD) stages ( $P < .01$ ). In addition, %LSV<sub>0.20</sub> was found

to help diagnose the manifestation of emphysema with an area under the receiver operating characteristic curve of up to 1.00 (95% confidence interval: 0.88, 1.00). Finally, fully automated measurement of %LSV<sub>0.20</sub> was reproducible (intra-class correlation coefficient,  $>0.99$ ) whereas the short-term

**Table 2: Qualitative and Quantitative Analyses of Emphysema at CT and MRI**

Parameter	Participants with COPD ( $n = 28$ )	Control Participants ( $n = 10$ )	$P$ Value
<b>Qualitative analysis</b>			
CT			
Emphysema score	26 (17, 37)	0 (NA)	$<.001$
Artifact score	$1.2 \pm 0.5$	$1.1 \pm 0.3$	.31
MRI			
Emphysema score	22 (4, 37)	0 (0, 15)	$<.001$
Artifact score	$1.9 \pm 0.5$	$1.6 \pm 0.7$	.16
<b>Quantitative analysis</b>			
CT			
%LAV <sub>-950HU</sub>	$22 \pm 15$	$4 \pm 2$	$<.001$
15th percentile (HU)	$-956 \pm 27$	$-918 \pm 11$	$<.001$
SNR	$2.5 \pm 1.5$	$2.7 \pm 1.1$	.63
CNR	$66 \pm 17$	$67 \pm 20$	.83
MRI			
%LSV <sub>0.20</sub>	$27 \pm 9$	$9 \pm 4$	$<.001$
Skewness	$0.7 \pm 0.2$	$0.3 \pm 0.2$	$<.001$
SNR	$12 \pm 4$	$16 \pm 5$	.34
CNR	10 (9, 11)	11 (7, 14)	.35

Note.—Data are mean  $\pm$  standard deviation for continuous normal variables, or median with 95% confidence interval in parentheses for nonnormal distribution. Fifteenth percentile indicates the 15th percentile of the voxel attenuation distribution. %LAV<sub>-950HU</sub> = percentage of low-attenuation volume by using a threshold of -950 HU, %LSV<sub>0.20</sub> = percentage of low-signal-intensity volume by using an adaptive threshold of 0.20, CNR = contrast-to-noise ratio, COPD = chronic obstructive pulmonary disease, NA = not applicable, SNR = signal-to-noise ratio.

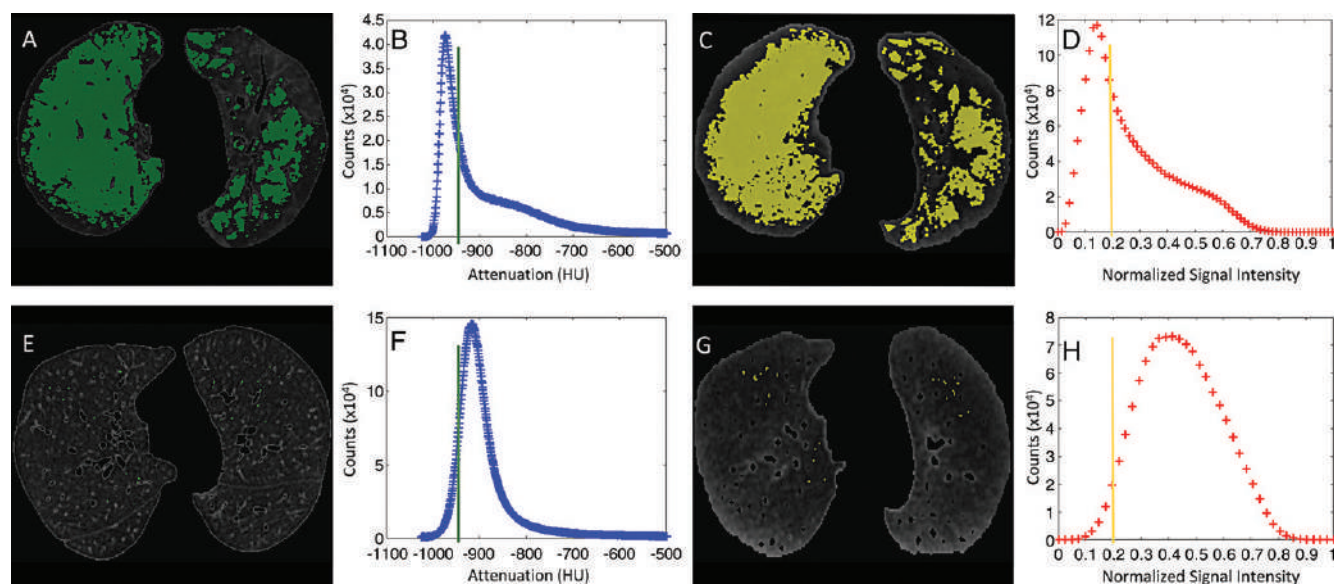


**Figure 4:** Examples of CT and MRI volumetric quantification of emphysema indexes in a participant with chronic obstructive pulmonary disease (COPD) with, *A–D*, severe emphysema and, *E–H*, a control participant without COPD. *A, E*, On CT scans, voxels with attenuation lower than -950 HU are in green. *B, F*, Corresponding CT histograms; green line indicates the emphysema index threshold and blue indicates the histogram of lung attenuations. *C, G*, At MRI, voxels with signal intensity lower than an adaptive threshold of 0.20 are in yellow. *D, H*, Corresponding MRI normalized histograms; yellow line indicates the emphysema index threshold and red indicates the histogram of lung normalized intensities.

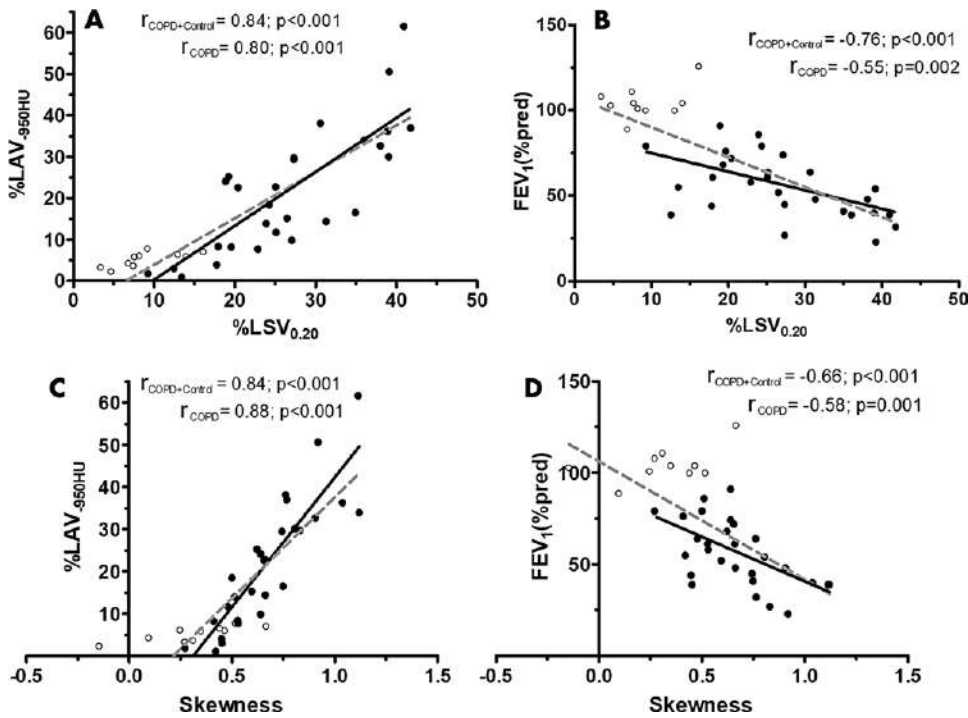


**Figure 5:** Graphs show Pearson correlation ( $r$ ) between, A, C, quantitative three-dimensional (3D) MRI emphysema indexes and 3D CT and, B, D, lung function. Black dots represent data in the 28 participants with chronic obstructive pulmonary disease (COPD) and white dots represent data in the 10 control participants. Solid lines represent the regression line in participants with COPD, and the dashed line represents the regression line in participants with COPD and control participants.  $\%LAV_{-950HU}$  = percentage of low-attenuation volume by using a threshold of  $-950$  HU;  $\%LSV_{0.20}$  = percentage of low-signal-intensity volume by using an adaptive threshold of 0.20;  $FEV_1$  = forced expiratory volume in 1 second; pred = predicted.

repeatability of the method was very good (intraclass correlation coefficient, 0.97).

Three-dimensional UTE MRI has been shown to increase the imaging quality of the lung (19). However, UTE sequences are prone to be sensitive to gradient imperfections or eddy currents. The pointwise encoding time reduction with radial acquisition sequence has been shown to overcome these technical issues (29). By combining both a radial and a Cartesian acquisition, no discontinuity was reported in the encoding time over  $k$ -space, leading to an increase in signal-to-noise ratio and stability against  $B_0$  inhomogeneities. These characteristics may be beneficial to enable a reliable quantification of emphysema.

Because MRI examinations were not calibrated, we used an adaptive approach for the normalization of the lung voxel intensity histogram similar to that used in previous studies (16–18). However, to normalize intensities, it has been demonstrated that muscle density is prone to variation between patients with COPD (30,31). Conversely, the curve-fitting method enabled us to automatically segment the lung and to calculate the so-called soft-tissue threshold value by integrating all signals at 3D imaging (25,26). Another critical point of discussion is that any analysis of a distribution requires two boundaries (32). However, at submillimeter resolution, the minimum intensity value in the human lung must be representative of air. By using our MRI method, a good concordance was found between the

raw lung minimum intensity value and the raw minimum of extrathoracic air. We also found no difference between participants with COPD and control participants within the absolute range of raw intensity values. Conversely, the skewness was significantly shifted toward the lowest normalized intensities in COPD.

Our study had several limitations. First, this was a single-center study and we were unable to match participants with and participants without COPD according to age. Nevertheless, correlations between age and pulmonary function testing results or emphysema metrics were not significant. Second, all participants were in stable condition, without supplemental oxygen, and mild artifacts were noticed. Respiratory synchronization would possibly have been less efficient in participants who had baseline dyspnea from their COPD. Third,  $\%LAV_{-950HU}$  was measured

at end inspiration whereas  $\%LSV_{0.20}$  was measured at functional residual capacity (17,18). This large difference in the inspiration could adversely affect the severity of emphysema depicted at MRI, whereas the study was not sampled to assess whether the correlations would be different between each GOLD group of participants with COPD. That the findings of emphysema at CT were similar to those at MRI is an interesting result because MRI should be better at depicting emphysema if a full inspiration was used. Moreover, we were not able to explain why quantitative MRI was different between the spirometry GOLD stages, whereas quantitative CT was not different. Nevertheless, this result may promote the use of more advanced MR protocols to better understand COPD beyond morphologic imaging. Fourth, we did not perform a direct comparison of  $\%LSV_{0.20}$  with pathologic findings. However, CT has been previously validated versus pathologic examination (33). Fifth, we used only pointwise encoding time reduction with radial acquisition for 3D UTE MRI (34). Therefore, the threshold of 0.20 to calculate percentage of low-signal-intensity volume cannot be thought of as generalizable. Nonetheless, recent data have demonstrated that adaptation of thresholds may also be necessary with CT techniques of dose reduction (35). Sixth, the spatial resolution of MRI is still lower than that of CT and we did not perform a lobar evaluation. Thus, quantification of a whole-lung index cannot supplant visual or regional assessment of lung

**Table 3: Diagnostic Performance of MRI in Depiction of Emphysema in Participants with Chronic Obstructive Pulmonary Disease**

Method of Diagnosis	MRI Qualitative Analysis		MRI Quantitative Analysis (%LSV <sub>0.20</sub> )			
	Sensitivity	Specificity	Sensitivity	Specificity	AUC	Best Threshold (%)
CT qualitative	23/26 (88) [70, 98]	1/2 (50)	24/26 (92) [80, 99]	2/2 (100) [16, 100]	0.96 [0.87, 1.00]	>13.5
CT quantitative	22/24 (92) [73, 98]	2/4 (50)	24/24 (100) [86, 100]	4/4 (100) [40, 100]	1.00 [0.88, 1.00]	>17.8
CT qualitative + quantitative	22/24 (92) [73, 98]	2/4 (50) [6, 93]	24/24 (100) [86, 100]	4/4 (100) [40, 100]	1.00 [0.88, 1.00]	>17.8

Note.—CT was used as the reference standard. Data are numerator/denominator; data in parentheses are percentages and data in brackets are 95% confidence intervals. The best threshold corresponded to the optimal cut-off for diagnosis and was calculated as the optimal Youden *J* index between sensitivity and specificity of percentage of low-signal-intensity volume by using an adaptive threshold of 0.20 (%LSV<sub>0.20</sub>). AUC = area under the receiver operating characteristic curve.

abnormalities. Finally, a longitudinal design would be worth performing in a larger multicenter cohort.

In conclusion, we demonstrated that an automated method with three-dimensional ultrashort echo time lung MRI reproducibly quantified the volumetric extent and severity of emphysema in participants with chronic obstructive pulmonary disease.

**Acknowledgments:** The study was funded by the University Hospital of Bordeaux and the French Society of Radiology and was achieved within the context of Laboratory of Excellence TRAIL (ANR-10-LABX-57). The authors thank Quentin d'Acremont, PhD, for advice regarding MRI segmentation methods. The authors are grateful to clinical research assistant Ms Virginie Niel for invaluable help during the participant recruitment and data collection.

**Author contributions:** Guarantors of integrity of entire study, I.B., J.M., G.D.; study concepts/study design or data acquisition or data analysis/interpretation, all authors; manuscript drafting or manuscript revision for important intellectual content, all authors; approval of final version of submitted manuscript, all authors; agrees to ensure any questions related to the work are appropriately resolved, all authors; literature research, I.B., P.B., P.O.G., J.M., F.L., G.D.; clinical studies, all authors; experimental studies, I.B., P.B., G.D.; statistical analysis, I.B., P.B., G.D.; and manuscript editing, I.B., P.B., P.O.G., J.M., F.L., G.D.

**Disclosures of Conflicts of Interest:** I.B. disclosed no relevant relationships. P.B. Activities related to the present article: disclosed no relevant relationships. Activities not related to the present article: disclosed money paid to author for board memberships from Boehringer Ingelheim, Novartis, AstraZeneca, Sanofi-Genzyme, Menarini, and Circassia; disclosed money paid to author for consultancy from Novartis, AstraZeneca, and Sanofi-Genzyme; disclosed money paid to author for grants/grants pending from Novartis and Boehringer-Ingelheim; disclosed payment to author for lectures including service on speak-

**Table 4: Reproducibility of Qualitative and Quantitative Analysis**

Parameter	Intraclass Correlation Coefficient*	Mean Difference <sup>†</sup>
Qualitative analysis		
CT visual		
Intraobserver	0.79 (0.64, 0.89)	5.1 (−24.7, 34.8)
Interobserver	0.67 (0.45, 0.81)	4.1 (−30.8, 39.1)
MRI visual		
Intraobserver	0.99 (0.99, 0.99)	0.3 (−4.4, 5.0)
Interobserver	0.68 (0.47, 0.82)	6.8 (−25.4, 38.9)
Quantitative analysis		
%LAV <sub>−950HU</sub>		
Intraobserver	>0.99	0
Interobserver	>0.99	0
%LSV <sub>0.20</sub>		
Intraobserver	>0.99	0
Interobserver	>0.99	0
Reproducibility over time		
MRI visual		
MRI visual	0.95 (0.92, 0.98)	−0.4 (−7.8, 5.2)
%LSV <sub>0.20</sub>	0.97 (0.88, 0.99)	−0.6 (−6.1, 4.9)

Note.—Reproducibility of qualitative and quantitative analyses was performed in 38 participants, whereas repeatability over time was assessed in 10 participants. The time interval for repeatability was 10 minutes. %LAV<sub>−950 HU</sub> = percentage of low-attenuation volume by using a threshold of −950 HU, %LSV<sub>0.20</sub> = percentage of low-signal-intensity volume by using an adaptive threshold of 0.20.

\* Data in parentheses are 95% confidence intervals.

<sup>†</sup> Data in parentheses are the limits of agreement.

ers bureaus from Circassia, Menarini, AstraZeneca, and Boehringer-Ingelheim; disclosed travel expenses paid to author from European Respiratory Society and Congrès de Pneumologie de Langue Française. Other relationships: disclosed money to author's institution for patents pending from Aquitaine Science Transfert. P.O.G. Activities related to the present article: disclosed no relevant relationships. Activities not related to the present article: disclosed money paid to author for lectures including service on speakers bureaus from Novartis, AstraZeneca, and Boehringer-Ingelheim; disclosed travel expenses paid to author from Chiesi, AstraZeneca, and Boehringer-Ingelheim. Other relationships: disclosed no relevant relationships. C.D. disclosed no relevant relationships. J.M. disclosed no relevant relationships. F.L. Activities related to the present article: disclosed no relevant relationships. Activities not related to the present article: disclosed money paid to author for lectures including service on speakers bureaus from Boehringer-Ingelheim, Chiesi, Roche, Basilea, and Novartis. Other relationships: disclosed no relevant relationships. G.D. disclosed no relevant relationships.

## References

- Lynch DA, Austin JHM, Hogg JC, et al. CT-definable subtypes of chronic obstructive pulmonary disease: A statement of the Fleischner Society. *Radiology* 2015;277(1):192–205.
- Lozano R, Naghavi M, Foreman K, et al. Global and regional mortality from 235 causes of death for 20 age groups in 1990 and 2010: a systematic analysis for the Global Burden of Disease Study 2010. *Lancet* 2012;380(9859):2095–2128.
- Montaudon M, Berger P, de Dietrich G, et al. Assessment of airways with three-dimensional quantitative thin-section CT: in vitro and in vivo validation. *Radiology* 2007;242(2):563–572.
- Bankier AA, De Maertelaer V, Keyzer C, Gevenois PA. Pulmonary emphysema: subjective visual grading versus objective quantification with macroscopic morphometry and thin-section CT densitometry. *Radiology* 1999;211(3):851–858.
- Cho MH, Castaldi PJ, Hersh CP, et al. A genome-wide association study of emphysema and airway quantitative imaging phenotypes. *Am J Respir Crit Care Med* 2015;192(5):559–569.
- Diaz AA, Strand M, Coxson HO, et al. Disease severity dependence of the longitudinal association between CT lung density and lung function in smokers. *Chest* 2018;153(3):638–645.
- Oelsner EC, Carr JJ, Enright PL, et al. Per cent emphysema is associated with respiratory and lung cancer mortality in the general population: a cohort study. *Thorax* 2016;71(7):624–632.
- Leuraud K, Richardson DB, Cardis E, et al. Ionising radiation and risk of death from leukaemia and lymphoma in radiation-monitored workers (INWORKS): an international cohort study. *Lancet Haematol* 2015;2(7):e276–e281.
- Nielsen A, Hansen MB, Tietze A, Mouridsen K. Prediction of tissue outcome and assessment of treatment effect in acute ischemic stroke using deep learning. *Stroke* 2018;49(6):1394–1401.
- Kirby M, Eddy RL, Pike D, et al. MRI ventilation abnormalities predict quality-of-life and lung function changes in mild-to-moderate COPD: longitudinal TINCan study. *Thorax* 2017;72(5):475–477.
- Hueper K, Vogel-Claussen J, Parikh MA, et al. Pulmonary microvascular blood flow in mild chronic obstructive pulmonary disease and emphysema. The MESA COPD Study. *Am J Respir Crit Care Med* 2015;192(5):570–580.
- Capaldi DPI, Eddy RL, Svenningsen S, et al. Free-breathing pulmonary MR imaging to quantify regional ventilation. *Radiology* 2018;287(2):693–704.
- Dournes G, Laurent F, Coste F, et al. Computed tomographic measurement of airway remodeling and emphysema in advanced chronic obstructive pulmonary disease. Correlation with pulmonary hypertension. *Am J Respir Crit Care Med* 2015;191(1):63–70.
- Bhatt SP, Vegas-Sánchez-Ferrero G, Rahaghi FN, et al. Cardiac Morphometry on Computed Tomography and Exacerbation Reduction with  $\beta$ -Blocker Therapy in Chronic Obstructive Pulmonary Disease. *Am J Respir Crit Care Med* 2017;196(11):1484–1488.
- Ley-Zaporozhan J, Ley S, Eberhardt R, Kauczor HU, Heussel CP. Visualization of morphological parenchymal changes in emphysema: comparison of different MRI sequences to 3D-HRCT. *Eur J Radiol* 2010;73(1):43–49.
- Ma W, Sheikh K, Svenningsen S, et al. Ultra-short echo-time pulmonary MRI: evaluation and reproducibility in COPD subjects with and without bronchiectasis. *J Magn Reson Imaging* 2015;41(5):1465–1474.
- Zhang WJ, Hubbard Cristinacce PL, Bondesson E, et al. MR quantitative equilibrium signal mapping: a reliable alternative to CT in the assessment of emphysema in patients with chronic obstructive pulmonary disease. *Radiology* 2015;275(2):579–588.
- Roach DJ, Crémillieux Y, Serai SD, et al. Morphological and quantitative evaluation of emphysema in chronic obstructive pulmonary disease patients: A comparative study of MRI with CT. *J Magn Reson Imaging* 2016;44(6):1656–1663.
- Johnson KM, Fain SB, Schiebler ML, Nagle S. Optimized 3D ultrashort echo time pulmonary MRI. *Magn Reson Med* 2013;70(5):1241–1250.
- Dournes G, Grodzki D, Macey J, et al. Quiet submillimeter MR imaging of the lung is feasible with a PETRA sequence at 1.5 T. *Radiology* 2015;276(1):258–265.
- Rabe KF, Hurd S, Anzueto A, et al. Global strategy for the diagnosis, management, and prevention of chronic obstructive pulmonary disease: GOLD executive summary. *Am J Respir Crit Care Med* 2007;176(6):532–555.
- Vestbo J, Hurd SS, Agustí AG, et al. Global strategy for the diagnosis, management, and prevention of chronic obstructive pulmonary disease: GOLD executive summary. *Am J Respir Crit Care Med* 2013;187(4):347–365.
- Leivseth L, Brumpton BM, Nilsen TIL, Mai XM, Johnsen R, Langhammer A. GOLD classifications and mortality in chronic obstructive pulmonary disease: the HUNT Study, Norway. *Thorax* 2013;68(10):914–921.
- Börnert P, Stuber M, Botnar RM, et al. Direct comparison of 3D spiral vs. Cartesian gradient-echo coronary magnetic resonance angiography. *Magn Reson Med* 2001;46(4):789–794.
- Cheng DC, Jiang X, Schmidt-Trucksäss A. Image segmentation using histogram fitting and spatial information. In: Perner P, Salvetti O, eds. *Advances in Mass Data Analysis of Signals and Images in Medicine, Biotechnology and Chemistry*. Berlin, Germany: Springer, 2007; 47–57.
- Biswas S, Ghoshal D, Hazra R. A new algorithm of image segmentation using curve fitting based higher order polynomial smoothing. *Optik (Stuttg)* 2016;127(20):8916–8925.
- Bland JM, Altman DG. Measuring agreement in method comparison studies. *Stat Methods Med Res* 1999;8(2):135–160.
- Landis JR, Koch GG. The measurement of observer agreement for categorical data. *Biometrics* 1977;33(1):159–174.
- Grodzki DM, Jakob PM, Heismann B. Ultrashort echo time imaging using pointwise encoding time reduction with radial acquisition (PETRA). *Magn Reson Med* 2012;67(2):510–518.
- Wallbridge P, Parry SM, Das S, et al. Parasternal intercostal muscle ultrasound in chronic obstructive pulmonary disease correlates with spirometric severity. *Sci Rep* 2018;8(1):15274.
- Vivodtzev I, Moncharmont L, Tamisier R, et al. Quadriceps muscle fat infiltration is associated with cardiometabolic risk in COPD. *Clin Physiol Funct Imaging* 2018;38(5):788–797.
- Li G, Luo S, You C, et al. A novel calibration method incorporating nonlinear optimization and ball-bearing markers for cone-beam CT with a parameterized trajectory. *Med Phys* 2019;46(1):152–164.
- Madani A, Van Muylem A, de Maertelaer V, Zanen J, Gevenois PA. Pulmonary emphysema: size distribution of emphysematous spaces on multidetector CT images—comparison with macroscopic and microscopic morphometry. *Radiology* 2008;248(3):1036–1041.
- Dournes G, Yazbek J, Benhassen W, et al. 3D ultrashort echo time MRI of the lung using stack-of-spirals and spherical  $k$ -Space coverages: Evaluation in healthy volunteers and parenchymal diseases. *J Magn Reson Imaging* 2018;48(6):1489–1497.
- den Harder AM, de Boer E, Lagerweij SJ, et al. Emphysema quantification using chest CT: influence of radiation dose reduction and reconstruction technique. *Eur Radiol Exp* 2018;2(1):30.

## Appendix E1

### Supplemental Methods

#### Calculation of Number of Subjects

According to previous CT and MR literature, the number of subjects necessary to assess the validity of MRI to assess emphysema volumetric extent was calculated to take into account the following conditions: risk alpha = 2.5%; power = 90%; good agreement between CT and MR visual scorings (weighted-kappa index  $\geq 0.62$ ) (4) and strong correlation between CT and MR quantitative emphysema indexes (Pearson correlation coefficient  $\geq 0.80$ ) (17). The number of subjects to obtain this result, related to the main objective, was found to be at least twenty-six. In addition, we determined the relative proportion between COPD and controls on the basis of their difference in emphysema indexes as follows: type I rate = 2.5%, power = 90%, CT or MR emphysema index mean difference = 18 between COPD and controls with standard deviation (SD) = 15 in COPD and SD = 5 in controls (36). Thus, we determined that at least five controls would be necessary. To determine the minimum number of participants who had to repeat MRI, to assess reproducibility over time (short term interscan reproducibility), we used the following hypotheses: risk alpha = 2.5%, power = 90%, and intraclass correlation coefficient  $\geq 0.90$  (2). We estimated that nine participants would be enough to complete this secondary endpoint. Finally, we arbitrarily estimated that 1/10 patients may be lost to follow-up or would not be able to complete the study.

Therefore, we aimed at including thirty COPD subjects and ten controls, and the first ten participants were asked to repeat MRI the same day.

#### Image Acquisition

Chest CT scans were acquired with a 64-section multidetector CT scanner (Somatom Definition; Siemens, Erlangen, Germany) by using the following parameters: 110-kV tube voltage, 50-mAs tube current and 75-msec rotation time, 0.75-mm collimation, no contrast injection. Data were acquired in the supine position at full inspiration and reconstructed with both high-spatial-frequency and standard algorithm, with a 0.625-mm reconstruction section thickness, 1-mm reconstruction interval,  $320 \times 320\text{-mm}^2$  field-of-view, pixel size  $0.625 \times 0.625\text{ mm}^2$ , and  $512 \times 512$  matrix.

Lung MRI was performed with a 1.5 Tesla system (MAGNETOM AVANTO, was used. An active 2nd order shimming was used to correct B0 inhomogeneities. Pointwise encoding time reduction with radial acquisition (PETRA) 3D-UTE sequence parameters were as follow: TR/TE were 4.1/0.07 msec and flip angle was  $5^\circ$ , FOV was ( $360 \times 360 \times 360\text{ mm}^3$ ) and matrix size  $384 \times 384 \times 384$  with an isotropic voxel dimensions of ( $0.93 \times 0.93 \times 0.93\text{ mm}^3$ ), acquisition time about 12 minutes. Respiratory motion artifacts were avoided by using a respiratory-trigger belt with data acquisition at functional residual capacity (FRC).

#### Analysis of Imaging Quality

Imaging quality of CT and MR examinations was also assessed qualitatively and quantitatively. First, the respiratory motion artifacts (blurring, streaks) was assessed by the senior reader (GD) using a Likert scale as proposed by Johnson et al (19): 0 = minimal/none; 1 = present but mild, ie, local and does not obscure normal lung anatomy; 2 = moderate, local and obscures normal

lung anatomy; 3 = severe, diffuse and renders images nondiagnostic. We used anatomic structures that were expected to be readily visible in all imaging modalities to assess normal lung anatomy, ie, the diaphragm, and the rib cage contours. For CT imaging, additional assessment of beam hardening artifacts was performed using the same visual grading. An overall artifact score was calculated as the sum of all artifact scorings. Second, Signal-to-noise ratio (SNR) and contrast-to-noise ratio (CNR) were derived from the formula proposed by Börnert and colleagues

(24) and adapted to the lung as follows:  $SNR = S_{\text{vessel}}/\sigma_{\text{air}}$  and  $CNR = (S_{\text{vessel}} - S_{\text{bronchus}})/\sigma_{\text{air}}$ .

In these formula,  $S_{\text{vessel}}$  correspond to a signal intensity measurement in the pulmonary artery truncus;  $S_{\text{air}}$  correspond to a signal intensity measurement of extrathoracic air measured on the same slice as  $S_{\text{vessel}}$ ;  $\sigma_{\text{air}}$  corresponds to the standard deviation of  $S_{\text{air}}$ ;  $S_{\text{bronchus}}$  corresponds to the signal intensity measured in the trachea. Regions-of-interest of 50 mm<sup>2</sup> were used for each measurement. In this study, CT reconstructed with standard reconstruction algorithm (B30f) was analyzed for SNR and CNR measurements, and we used the same formula to calculate SNR and CNR at both CT and MR examinations.

In this study using MRI, results showed no difference in SNR between 28 COPD and 10 control participants (mean SNR = 12 ± 4 and 16 ± 5, respectively;  $P = .34$ ) and CNR (median CNR = 10 [9–11] and 11 [7–4], respectively;  $P = .35$ ).

## Qualitative Analysis

Emphysema visual extent evaluation was performed by two observers with 4 years (I.B.) and 10 years (G.D.) of experience in thoracic imaging blinded to the patient characteristics, other imaging results and the other reader's evaluation. To assess intra observer agreement the expert reader performed each reading twice with a 2-months interval between evaluations. Window settings for the visual analysis of emphysema on CT datasets were: window width 1500 Hounsfield Units (HU) and window level–700 HU. For UTE MRI datasets brightness and contrast were enhanced to detect low signal areas of the lung. a four-point scale was used to determine the extent of emphysema for each segment: 0 = no emphysema, 1 = mild emphysema (< 25%), 2 = moderate emphysema (25%–50%), 3 = severe emphysema (> 50%).

## Automated Quantitative Analysis

To segment lungs from the rest of thoracic structures and large pulmonary vessels on CT images, attenuation values of -500 and -1024 HU were used in a threshold-based technique. Percentage low-attenuation volume using a threshold of -950 Hounsfield Units (%LAV<sub>-950HU</sub>) was calculated as the proportion of lung voxels between -1024HU and -950 HU over the total lung voxels, as previously described (37,38). 15th percentile was also derived from the voxel frequency distribution histogram.

For 3D-UTE MRI, 3D fully automated quantitative analysis was performed using a homemade software program written in MATLAB (The MathWorks, Inc., Natick, Massachusetts, USA) (see Fig E1). In our approach, we did not correct for B1 inhomogeneities. Regarding B1 inhomogeneities, the study was performed at 1.5 T and the flip was 5° and thus, we did not expect any issue related to this point. Second, the PETRA sequence was used to acquire the 3D UTE MRI examination. PETRA combines a radial acquisition and a Cartesian acquisition of the center of k-space. Using this technical principle, it was reported no discontinuity in the development of phases also in the presence chemical shifts or B0 inhomogeneities. In addition, the gap in k-space center is completely filled with data measured at the absolute shortest encoding time. This might help to increase SNR and stability compared with projection methods. PETRA is not sensitive to gradient imperfections, gradient delays, or eddy currents during gradient ramping and has low demands on fast gradient switching and

ramping times. This often leads to problems in UTE imaging. Therefore, the combination of a 2nd order shimming and the use of PETRA allowed us to minimize data inconsistencies related to B0 inhomogeneities before post processing.

In this setting, the user had to first click inside the trachea to both start the process and plant a seed for further segmentation of large airways. For lung segmentation, after a Gaussian smoothing (Fig E1–1,2), local enhancement filter was first applied to all images to delineate lung boundaries, then a 3D median filter was used to de-noise enhanced images (Fig E1–3). The voxel frequency distribution histogram of the local enhanced images was derived from these images and a curve fitting method was performed using Gaussian-like functions based on the assumption that different tissues in medical images have a Gaussian-like distribution in the histogram (25). After investigating different Gaussian-like functions, the best fitting curve was found using three functions (Fig E1–4). In addition, the histogram showed three peaks that correspond to lung/background voxels, soft tissue with intermediate intensities voxels (typically vessels, bone marrow and muscles) and soft tissue with high intensities voxels (typically subcutaneous fat), respectively. The optimal threshold for lung segmentation was considered as the cross point of the two first Gaussian-like distributions and called the soft tissue threshold (STT). Using this automatic STT threshold, connected lungs voxels were isolated from the extrapulmonary structures and from large pulmonary vessels (Fig E1–5) to create a lung mask, after trachea and main bronchi were removed (Fig E1–6,7) using region growing algorithm segmentation (3). Then, the lung mask was applied to the native, unfiltered MR images to segment the lung MR volume. To determine percentage low-signal-intensity volume (%LSV), the range of native lung signal intensity values was first normalized between 0 and 1 with 0 corresponding to the minimum signal intensity value of the lung and 1 corresponding to the maximum signal intensity value within the lung mask which was determined automatically from the STT measurement (Fig E1–8,9). Therefore, the lung signal intensities were normalized using the following formula:

$$NLSI_j = (LSI_j - \min_j) / (\max - \min) ,$$

where  $NLSI_j$  corresponds to the normalized lung signal intensity of a voxel  $j$ ,  $LSI_j$  corresponds to the native signal intensity of the voxel  $j$ ,  $\min$  corresponds to the minimum native signal intensity value in the segmented lung volume, and  $\max$  corresponds to the native signal intensity value of STT.

Since no MRI calibration was performed, this normalization was needed to keep a constant threshold level with respect to minimum and maximum lung signal intensities, similarly to CT -950HU threshold where -1024HU and -500HU are constantly the minimum and maximum of lung attenuations. Moreover, our since the 3D PETRA acquisition allows submillimetric isotropic voxel dimension, the minimum signal intensity in the lung is expected to be representative of lung air in all patients.

In this study, we used the percentage of low-signal-intensity volume using an adaptive threshold of 0.20 (%LSV<sub>0.20</sub>) which was calculated with a similar equation to that used by Zhang and colleagues (17), as follows:

$$\%LSV_{0.20} = \left( \frac{\sum_{i=0}^{0.20} Vi}{\sum_{i=0}^{1.00} Vi} \right) \times 100 ,$$

where  $Vi$  is the voxels with the  $i$  intensity value. For each participant, “ $i$ ” corresponds to a normalization of the absolute value of intensity “ $I$ ” into a percentage “ $i$ ” from the minimum (= 0) to maximum (= 1) intensity distribution. Thus, %LSV<sub>0.20</sub> corresponds to the proportion of lung voxels ranging below an adaptive threshold of 0.20 of normalized lung intensity histogram. Skewness, which describes histogram asymmetry and shift, was also calculated and depicted left shifted histogram (toward lowest values) in patients with emphysema.

To support the methodology, several additional statistical tests were performed. First several thresholds were empirically investigated from the normalized range of signal values (ie, 0.10, 0.12, 0.15, 0.20 and 0.25). Indeed, the best correlation with CT %LAV<sub>-950HU</sub> was found using %LSV below the adaptative threshold of 0.20 (Table E4). The linear regression model between %LAV<sub>-950HU</sub> and %LSV<sub>0.20</sub> was as follows: [%LAV<sub>-950HU</sub>] = 1.1 x [%LSV<sub>0.20</sub>] - 7.3 ( $R^2 = 0.71$ ;  $P < .001$ ).

Second, to support the use of a normalization between the minimum-to-maximum lung signal intensity values, we found very high agreement between the absolute value of the minimum of lung intensity and the minimum of extrathoracic air, with a mean difference of 0.9 [-1.7; 3.6] at Bland-Altman analysis and a Pearson correlation coefficient of 0.86 ( $P < .001$ ). As mentioned above, there was no difference between COPD and controls in SNR and CNR. In addition, before normalization from 0 to 1, we found no significant difference between COPD and controls in the absolute range of raw signal values (Table E1). We also found no correlation of this absolute range with lung function, nor with CT measurement of emphysema (Table E8).

## References

36. Lederlin M, Laurent F, Dromer C, Cochet H, Berger P, Montaudon M. Mean bronchial wall attenuation value in chronic obstructive pulmonary disease: comparison with standard bronchial parameters and correlation with function. *AJR Am J Roentgenol* 2012;198(4):800–808.
37. Dournes G, Laurent F, Coste F, et al. Computed tomographic measurement of airway remodeling and emphysema in advanced chronic obstructive pulmonary disease. Correlation with pulmonary hypertension. *Am J Respir Crit Care Med* 2015;191(1):63–70.
38. Coste F, Dournes G, Dromer C, et al. CT evaluation of small pulmonary vessels area in patients with COPD with severe pulmonary hypertension. *Thorax* 2016;71(9):830–837.

**Table E1. Characteristics of 10 participants who repeated MRI the same day**

		<b>COPD (n = 7)</b>	<b>Controls (n = 3)</b>
<b>Age</b>	Years	71 ± 8	62 ± 2
<b>Sex ratio</b>	Men/Women	5/2	3/0
<b>BMI</b>	kg.m <sup>-2</sup>	27 ± 5	23 ± 2
<b>Tobacco</b>	smoking status (yes/no)	7/3	0/3
	curent smoker (yes/no)	2/5	
<b>PFT</b>	FEV <sub>1</sub> (% pred)	63 ± 12	102 ± 6
	FVC (% pred)	91 ± 10	101 ± 10
	FEV <sub>1</sub> /FVC (%)	55 ± 9	80 ± 3
	TLC (% pred)	112 ± 14	108 ± 14
	FEF <sub>25-75</sub> (% pred)	29 ± 11	101 ± 10
	RV (% pred)	150 ± 31	121 ± 38
	TLCO (% pred)	67 ± 16	109 ± 24
<b>Arterial blood gases (ambient air)</b>	PaO <sub>2</sub> (mmHg)	77 ± 13	85 ± 2
	PaCO <sub>2</sub> (mmHg)	37 ± 5	41 ± 2

CT	%LAV-950HU	14 ± 11	5 ± 1
----	------------	---------	-------

Note.—Data are means ± SD. COPD = chronic obstructive pulmonary disease; BMI = body mass index; FEV<sub>1</sub> = forced expiratory volume in 1 second; FVC = forced volume capacity; FEF<sub>25-75</sub> = forced expiratory flow at 25%–75%; TLC = total lung capacity; RV = residual volume; TLCO = transfer lung capacity of carbon monoxide; PaO<sub>2</sub> = arterial partial pressure of oxygen; PaCO<sub>2</sub> = arterial partial pressure of carbon dioxide; % pred = percentage predicted; CT = computed tomography; %LAV-950HU = percentage low-attenuation volume using a threshold of -950 HU.

**Table E2. Comparison of artifacts between CT and MRI**

	CT (n = 38)	MRI (n = 38)	P value
Streak	NA	1 ± 0	NA
Beam Hardening	1 ± 0	NA	NA
Rib blurring	0.1 ± 0.2	0.1 ± 0.3	0.64
Diaphragm blurring	0.4 ± 0.5	0.8 ± 0.5	0.01
Total score	1.3 ± 0.5	1.8 ± 0.6	<0.001

Note.—Data are mean ± SD. A 4-point scale was used from 0 = minimal/none to 3 = severe, diffuse. CT = computed tomography; MRI = magnetic resonance imaging; NA = not applicable.

**Table E3. Qualitative segmental scoring of emphysema extent using CT and MRI.**

MR segmental scoring	CT segmental scoring							
	0	0.5	1	1.5	2	2.5	3	
0	263	55	9	7	0	0	0	334
0.5	38	25	9	7	1	7	0	87
1	9	5	9	17	17	7	1	65
1.5	2	1	4	20	10	22	12	71
2	5	12	4	15	8	14	13	71
2.5	0	3	7	7	7	14	23	61
3	4	1	1	3	1	17	44	71
	321	102	43	76	44	81	93	760

Note.—Data are the absolute number of segments that were classified into each qualitative category at consensus analysis. Twenty segments were scored in each of the 38 participants. At the segmental level, the extent of emphysema was determined on a visual basis as follows: 0 = no emphysema, 1 = mild emphysema (< 25%), 2 = moderate emphysema (25%–50%), and 3 = severe emphysema (> 50%). At the segmental level, the mean of 2 independent readers was chosen as consensus.

**Table E4. Univariate analysis of CT emphysema index with quantitative MRI and PFT parameters in COPD patients.**

		n	Coefficient	P value
	%LSV <sub>0.20</sub>	28	0.801	<0.001
	%LSV <sub>0.25</sub>	28	0.771	<0.001
	%LSV <sub>0.15</sub>	28	0.711	<0.001
	%LSV <sub>0.12</sub>	28	0.591	<0.001
	%LSV <sub>0.10</sub>	28	0.541	0.002
	Skewness	28	0.881	<0.001
	MeanMuscle <sub>0.10</sub>	28	0.312	0.10
	MeanMuscle <sub>0.20</sub>	28	0.261	0.16
%LAV <sub>-950HU</sub>	FEV <sub>1</sub> (% pred)	28	-0.421	0.02
	FVC (% pred)	28	0.042	0.81
	FEV <sub>1</sub> /FVC (%)	28	-0.701	<0.001
	FEF <sub>25-75</sub> (% pred)	28	-0.411	0.02
	TLC (% pred)	28	0.501	0.01
	RV (% pred)	27	0.331	0.08
	TLCO (% pred)	26	-0.391	0.045
	PaO <sub>2</sub> (mmHg)	28	0.012	0.94
	PaCO <sub>2</sub> (mmHg)	28	-0.312	0.10

Note.—Data are Pearson correlation coefficients<sup>1</sup> for continuous normal variables, or Spearman correlation coefficients<sup>2</sup> if their distribution was not normal.

BMI = body mass index; PFT = pulmonary function test; %LAV<sub>-950HU</sub> = percentage low-attenuation volume using a threshold of -950 Hounsfield Units; %LSV<sub>0.20</sub> = percentage low-signal-intensity volume using an adaptive threshold of 0.20; MeanMuscle<sub>0.10</sub> = threshold at 10% from mean paraspinal muscle signal intensity; MeanMuscle<sub>0.20</sub> = threshold at 20% from mean paraspinal muscle signal intensity; FEV<sub>1</sub> = forced expiratory volume in 1 second; FVC = forced volume capacity; FEF<sub>25-75</sub> = forced expiratory flow at 25%–75%; TLC = total lung capacity; RV = residual volume; TLCO = transfer lung capacity of carbon monoxide; PaO<sub>2</sub> = arterial partial pressure of oxygen, PaCO<sub>2</sub> = arterial partial pressure of carbon dioxide; % pred = percentage predicted.

**Table E5. Univariate analysis of quantitative MR emphysema indexes with PFT parameters**

		n	Coefficient	P value
	<b>FEV<sub>1</sub> (% pred)</b>	28	-0.551	0.002
	<b>FVC (% pred)</b>	28	-0.092	0.63
	<b>FEV<sub>1</sub>/FVC (%)</b>	28	-0.731	<0.001
	<b>FEF<sub>25-75</sub> (% pred)</b>	28	-0.531	0.003
<b>%LSV<sub>0.20</sub></b>	<b>TLC (% pred)</b>	28	0.571	0.001
	<b>RV (% pred)</b>	27	0.461	0.02
	<b>TLCO (% pred)</b>	26	-0.491	0.01
	<b>PaO<sub>2</sub> (mmHg)</b>	28	-0.252	0.19
	<b>PaCO<sub>2</sub> (mmHg)</b>	28	-0.092	0.63
	<b>FEV<sub>1</sub> (% pred)</b>	28	-0.581	0.001
	<b>FVC (% pred)</b>	28	-0.072	0.71
	<b>FEV<sub>1</sub>/FVC (%)</b>	28	-0.741	<0.001
	<b>FEF<sub>25-75</sub> (% pred)</b>	28	-0.571	0.001
	<b>TLC (% pred)</b>	28	0.491	0.01
<b>Skewness</b>	<b>RV (% pred)</b>	27	0.401	0.041
	<b>TLCO (% pred)</b>	26	-0.511	0.008
	<b>PaO<sub>2</sub> (mmHg)</b>	28	-0.152	0.43
	<b>PaCO<sub>2</sub> (mmHg)</b>	28	-0.042	0.81

Note.—Data are Pearson correlation coefficients<sup>1</sup> for continuous normal variables, or Spearman correlation coefficients<sup>2</sup> if their distribution was not normal.

PFT = pulmonary function test; %LSV<sub>0.20</sub> = percentage low-signal-intensity volume using an adaptative threshold of 0.20; FEV<sub>1</sub> = forced expiratory volume in 1 second; FVC = forced volume capacity; FEF<sub>25-75</sub> = forced expiratory flow at 25%–75%; TLC = total lung capacity; RV = residual volume; TLCO = transfer lung capacity of carbon monoxide; PaO<sub>2</sub> = arterial partial pressure of oxygen; PaCO<sub>2</sub> = arterial partial pressure of carbon dioxide; %pred = percentage predicted.

**Table E6. Comparison of spirometric GOLD grades using quantitative MRI and CT**

		GOLD1 (n = 4)		GOLD2 (n = 12)		GOLD3 (n = 10)		GOLD4 (n = 2)		P value
<b>MRI Analysis</b>										
	%LSV <sub>0.20</sub>	21	[11–24]£¥	24	[19–27]	35	[25–39]\$	38	[27–39]\$	0.042
	Skewness	0.5	[0.3–0.6]£¥	0.6	[0.5–0.7]£¥	0.8	[0.6–1.0]\$\$	0.8	[0.8–0.9]\$\$	0.01
<b>CT Analysis</b>										
	%LAV <sub>-950HU</sub>	16	[5–23]	14	[9–25]	31	[12–37]	41	[30–51]	0.14

(\$) Different from GOLD1 (&) Different from GOLD2 (£) Different from GOLD3 (¥) Different from GOLD4.

Note.—Data are medians with [95% confidence interval]. Comparisons of nonparametric variables were performed using Kruskal-Wallis test, with Bonferroni correction. GOLD = global initiative for chronic obstructive lung disease; CT = computed tomography; MRI = magnetic resonance imaging; %LAV<sub>-950HU</sub> = percentage lowattenuation volume using a threshold of -950 Hounsfield Units; %LSV<sub>0.20</sub> = percentage low-signal-intensity volume using an adaptative threshold of 0.20.

**Table E7. Comparison of GOLD ABCD groups using quantitative MRI and CT**

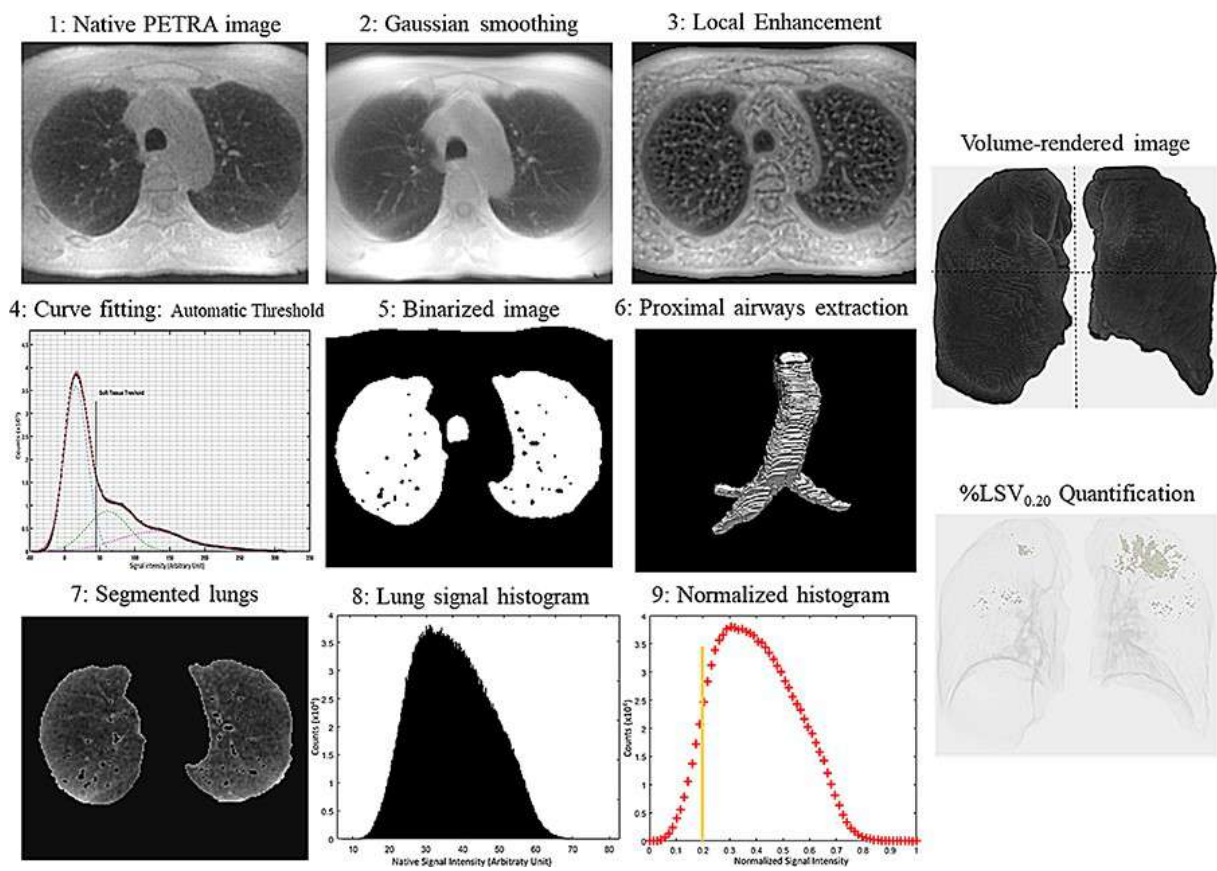
		GOLD A (n = 5)		GOLD B (n = 16)		GOLD C (n = 2)		GOLD D (n = 5)		P value
<b>MRI Analysis</b>										
	%LSV <sub>0.20</sub>	19	[11–37]	25	[20–34]	23	[19–27]	31	[25–39]	0.44
	Skewness	0.6	[0.3–1.1]	0.6	[0.5–0.7]	0.7	[0.6–0.7]	0.8	[0.6–0.9]	0.39
<b>CT Analysis</b>										
	%LAV <sub>-950HU</sub>	25	[2–35]	15	[9–23]	27	[24–30]	30	[19–45]	0.35

Note.—Data are medians with [95% confidence interval]. Comparisons of nonparametric variables were performed using Kruskal-Wallis test with Bonferroni correction. GOLD = global initiative for chronic obstructive lung disease; CT = computed tomography; MRI = magnetic resonance imaging; %LAV<sub>-950HU</sub> = percentage low-attenuation volume using a threshold of -950 Hounsfield Units; %LSV<sub>0.20</sub> = percentage low-signal-intensity volume using an adaptative threshold of 0.20.

**Table E8. Statistical analysis of the absolute range of lung signal intensity values (ARSV)**

ARSV	
	P value
T-test between 28 COPD versus 10 Controls	0.10
Pearson test with FEV <sub>1</sub> (%pred) (n = 38)	0.19
Pearson test with %LAV <sub>-950HU</sub> (n = 38)	0.82

COPD, chronic obstructive pulmonary disease; FEV<sub>1</sub>, forced expiratory volume in 1 second; %pred = percentage predicted; %LAV<sub>-950HU</sub> = percentage low-attenuation volume using a threshold of -950 HU.



### **3.3 Publication n°5 : Quantification du remodelage bronchique à l'IRM 3D UTE chez des patients atteint de mucoviscidose**

L'intérêt de la quantification du remodelage bronchique dans la mucoviscidose est bien établi. Plusieurs études ont rapporté que les mesures bronchiques à la TDM dans la mucoviscidose corrélaient à la fonction pulmonaire et aux scores visuels. De plus, ces mesures permettaient une détection précoce et une évaluation longitudinale des altérations structurales dans la mucoviscidose. La répétition des scanners dans une population jeune voire pédiatrique est problématique. Ainsi, l'IRM pulmonaire peut être une alternative non irradiante dans le suivi de ces malades. Le développement de l'IRM 3DUTE a permis une amélioration de la résolution spatiale avec une imagerie morphologique proche de celle de la TDM. La question à laquelle nous devons répondre est alors : les méthodes de quantification du remodelage bronchique à la TDM sont-elles transposables à l'IRM 3DUTE ?

Dans cette étude, notre objectif était d'évaluer la concordance des mesures bronchiques faites à l'IRM 3DUTE et au scanner. Nous avons inclus 27 patients qui ont bénéficié d'une TDM et d'une IRM 3DUTE ainsi que des explorations fonctionnelles respiratoires. La comparaison des mesures bronchiques faites en IRM et au scanner a montré une bonne à très bonne concordance. La mesure de l'épaisseur pariétale bronchique corrélait avec la fonction respiratoire et les scores visuels de sévérité. Les mesures TDM corrélaient de façon similaire avec la fonction respiratoire, ce qui peut être un appui supplémentaire à la concordance entre les deux modalités. La reproductibilité de ces mesures était bonne. En conclusion, la transposition des techniques de quantification du remodelage bronchique à l'IRM 3DUTE est faisable avec des résultats similaires à ceux du scanner dans la mucoviscidose.

**Title: Quantitative measurements of bronchial dimensions using 3D-MRI with ultrashort echo times: a pilot study in cystic fibrosis**

**Article Type: Original research**

**Authors**

Shafey Elahee<sup>3</sup>, Fabien Baldacci<sup>4</sup>, Ilyes Benlala<sup>1,2,3</sup>, Julie Macey<sup>3</sup>, Sophie Bui<sup>3</sup>, Patricck Berger<sup>1,2,3</sup>, François Laurent<sup>1,2,3</sup>, Gael Dournes<sup>1,2,3</sup>

**Affiliations**

<sup>1</sup> Univ. Bordeaux, Centre de Recherche Cardio-Thoracique de Bordeaux, U1045, CIC 1401, F-33000 Bordeaux, France

<sup>2</sup> Inserm, Centre de Recherche Cardio-Thoracique de Bordeaux, U1045, CIC 1401, F-33000 Bordeaux, France

<sup>3</sup> CHU de Bordeaux, Service d'Imagerie Thoracique et Cardiovasculaire, service des Maladies respiratoires, service d'explorations Fonctionnelles respiratoires, CIC 1401, F-33600 Pessac, France

<sup>4</sup>Université de Bordeaux, LaBri, F-33405 Talence Cedex, France

**Contact author :**

Dr Gael Dournes, Centre de Recherche Cardio-thoracique de Bordeaux, INSERM U1045, Université Bordeaux, 146 rue Léo Saignat, 33076 Bordeaux Cedex, France

E-mail: [gael.dournes@chu-bordeaux.fr](mailto:gael.dournes@chu-bordeaux.fr)

## ABSTRACT

**Background:** Using CT, three dimensional airway quantification of bronchial lumen and wall dimensions have been proven useful to investigate cystic fibrosis (CF) severity and understand the underlying mechanisms in vivo. The feasibility of a transposition of the quantitative method to high resolution morphological 3D MRI is unknown.

**Purpose:** The main objective of our study was to assess the concordance between 3D-CT and 3D-MRI in order to quantify bronchial measurements in CF patients. Secondary objectives were to correlate the MR bronchial measurements in CF patients with results from pulmonary function test (PFT) and the Bhalla score, to discriminate between CF groups of severity, and to assess the reproducibility of the technique.

**Material and Methods:** The pilot study was retrospective. CF participants underwent chest MRI using a 3D UTE sequence, CT and PFT. Cross-sectional wall area (WA), lumen area (LA), percentage wall area (%WA), and wall thickness (WT) were measured both on 3D-CT and 3D-UTE MRI at the third and fourth bronchial generation of the upper and lower pulmonary lobes. The visual Bhalla score was assessed on 3D-UTE MRI. CF were classified as mild based on a  $FEV1\% \geq 80\%$  at PFT. Concordance and agreement were assessed by using intraclass correlation and Bland-Altman analysis, correlations were assessed by using Spearman test, and comparisons were done using repeated ANOVA.

**Results:** 27 patients with CF (mean age, 27.2 years) were included. The concordance between 3D-UTE MRI and 3D-CT to quantify WA was good (ICC=0.77) and very good to quantify LA (ICC=0.84), although 3D-UTE systematically underestimated the measurements (mean difference=-1.9 and -1.5, respectively). The wall thickness significantly correlated to FEV1% and the Bhalla score ( $\rho=-0.32$ ,  $p<0.001$  and  $\rho=-0.41$ ,  $p<0.001$ , respectively). %WA was significantly different between CF groups of severity ( $p<0.001$ ). The interobserver reproducibility of WA and LA measurements was good (ICC>0.62)

**Conclusion:** MR quantitative metrics assessed with dedicated software showed good concordance to CT metrics of bronchial measurements. Both MRI and CT metrics correlated similarly to pulmonary function tests and imaging indices of CF severity.

**Key words:** Cystic fibrosis, MRI, CT.

## INTRODUCTION

Cystic fibrosis (CF) is the most frequent genetic disorder in Caucasian population (1–3). Despite increased longevity, pulmonary dysfunction causes major morbidity in cystic fibrosis, and accounts for more than 90% of the mortality (4). The structural lung disease (SLD) is characterized by progressive bronchiectasis (BE) and airway wall thickening (AWT).

The standard for assessment of lung disease in cystic fibrosis was initially pulmonary function tests (PFTs). However, PFTs are not sensitive enough to detect early lung damage and correlate weakly with morphologic abnormalities.

Therefore, computed tomography (CT) has become the standard reference to assess bronchi morphometric data. In 1990, Bhalla et al. (4) published a visual scoring system designed to quantify structural lung abnormalities in CF patients by using thin-section CT. Since then, a number of additional visual scoring systems and modifications of scoring systems have been proposed, and they were frequently used for both clinical treatment and research purposes (5).

Later on, in 2004, De Jong et al. (6) evaluated five of the visual scoring systems and found that they correlated with PFTs. However, these visual scoring systems are subjective (7) with increased variability between observers especially on the lower end of the scoring scale. For instance, using visual scorings, assessment of bronchial wall thickening is either not reproducible (8) or defined on a pure subjective basis (9). Definition of bronchiectasis is also not consensual (10) and appears to differ between various scoring systems (11–13).

Hence, three-dimensional measurement of bronchial thickness at multi-detector row CT were introduced (14–16). Indeed, automated CT bronchial measurement is objective, reproducible and allows for early detection and longitudinal assessment of lung abnormalities in cystic fibrosis (17–19). Early detection of SLD is considered important for clinical studies and for treatment guidance to prevent irreversible SLD or progression.

However, a limitation of 3D-CT is the inherent patient exposure to ionizing radiation. Unfortunately, MRI, as a radiation free technique, has not been used yet to get 3D imaging of bronchi, since none of conventional techniques has been reported to get sufficient signal and contrast from the lung parenchyma and/or the airway wall (20). Recent advances have been proposed to solve these technical issues that may eventually enable MRI to get morphological information close to that of CT (21).

In this article we propose a method to extract the human airway tree from a 3D MRI sequence with ultrashort echo time (3D-UTE). Indeed, 3D-UTE has been demonstrated to improve

imaging quality, especially to discriminate the bronchial lumen and the bronchial wall from the surrounding lung parenchyma (22,23).

In this study, we hypothesized that the bronchial metrics obtained from a 3D high resolution UTE MRI sequence should be concordant with those obtained at 3D CT scan chosen as reference, and would provide similar information on the disease severity. Thus, the main objective of this feasibility, pilot study was to assess the concordance between 3D-UTE MRI and 3D CT scans to assess quantitative measurements of bronchial dimensions in patients with CF. Secondary objectives were to assess correlation with lung function, to assess correlation with the Bhalla score, to discriminate between CF groups of severity and to evaluate the reproducibility of the method.

## **MATERIALS AND METHODS**

### **2.1. Study population**

The study was a retrospective analysis of prospectively collected data (Clinical Trial registration number: NCT02449785). The local ethic committee approved the study and all participants gave written informed consent.

Inclusion criteria were an age superior to 18 years old, a diagnosis of CF proven by a positive sweat test and/or genotypic test. Clinical examination, biological evaluation, pulmonary function tests (PFT), and CT and MR imaging were performed during a routine annual visit (1). Non-inclusion criteria were pregnant women, pulmonary transplant patients and the basic contraindication of an MR exam which includes pacemakers, implantable defibrillators, metal foreign bodies and claustrophobia. In this study, we also excluded MR exams with respiratory motion artefacts that would prevent clear delineation of bronchial contours.

### **2.2. Imaging techniques**

*Thin section CT.*

Volumetric acquisition of the whole lungs was performed during a breath hold at functional residual capacity with a 64-section multi-detector row CT scanner (Definition 64; Siemens, Erlangen, Germany) and with the following parameters: 140 kV, 5mAs, and 0.75-mm native

section thickness. Images were reconstructed with 1-mm reconstruction thickness, 300–380-mm<sup>2</sup> field of view, and 1mm reconstruction interval.

### *3D MRI with ultra short echo time*

The chest MR was carried out on a 1.5 Tesla machine (Avanto 1.5T, Siemens) by using a 3D submillimeter isotropic radial ultra-short echo (UTE) acquisition. Furthermore, this is a free breathing MRI technique, without any contrast agent. The parameters of the sequence were a TR/TE value of 4.1/0.07ms, a flip angle of 6° and 80 000 radial shots. The respiratory synchronization was obtained by using a respiratory belt for end normal expiration acquisition. The acquisition time of the sequence ranged from 10 to 15 minutes.

## **2.3. Quantitative measurements of bronchial dimensions by using 3D-CT and 3D-MRI**

### *2.3.1. Bronchial measurements from 3D- CT*

The first step of the process pipeline consists in extracting the 3D airway tree. Most of the common segmentation approaches are based on a region growing algorithm initialized in the trachea, that will aggregate the voxels corresponding to the airway lumen (*i.e.* air voxels) and stop on the voxels corresponding to the airway wall. The main difficulty consists in finding bronchi which are getting smaller at each generation without leaking into the lung parenchyma. The segmentation process is thus always combined with a preprocessing filtering step.

The classical filtering methods are composed of a noise removal step, typically by using a Gaussian kernel, and an airway enhancement step. Two types of airway enhancement steps are commonly used, those based on morphological operators (in order to highlight black structure surrounded by white structure) (24) and those relying on Hessian-based operators in order to highlight dark tubular structure.

Once the airway tree has been extracted, the first step of the analysis consists in computing the curveskeleton of the binary volume (see Figure 2E). This simplification of the volume into a set of curves is used both for the geometrical or topological analysis of the airway tree and to estimate the crosssections along the volume.

In order to analyze a tubular shape such as the bronchial tree, it is required to reconstruct a crosssection orthogonally to the shape, to be able to estimate its diameter (see Figure 2F). This orthogonal cross-section is usually estimated from the skeleton which will locally represent the tangential direction to the orthogonal plane. The software provided fully automated segmentation of the skeleton (*i.e.*, airway central axis of the bronchial tree), and two dimensional reformatted images strictly perpendicular to the central axis were automatically obtained. The rest of the procedure was semiautomatic: The observer chose the bronchus and determined the bronchial generation and reformatted cross section on which measurements were to be obtained. The precise location where a measurement was obtained was determined by the observer in order to have the minimal percentage of bronchial cross section circumference in contact with a pulmonary artery section.

### *2.3.2 Bronchial measurements from 3D-UTE MRI*

In this section, we detail our method to extract the human airway tree from MRI image. We used the PETRA sequence which is a MRI 3D, submillimeter, isotropic radial ultra-short echo acquisition. Our method is first based on a dedicated preprocessing filtering step required to avoid the leakage of the segmentation into the lung parenchyma and then it is followed by a region growing segmentation algorithm. From this 3D segmented airway tree, the same post processing analysis is realized by extracting the curve-skeleton from which cross-section is reconstructed to make quantitative measurements.

#### *Pre-filtering Step*

The first step consists in filtering the image to help the segmentation of the airway lumen. Both kind of classical CT scan methods (morphological and Hessian-based) does not provide accurate results on MRI data. Though the PETRA sequence has been reported effective to get infra-pulmonary imaging with high resolution, the signal/noise ratio is still very low compared to CT scan, and those algorithms failed to go further than the first generation of bronchi without leaking into the parenchyma. This is why we developed a dedicated algorithm for MRI data. The acquisition does not include an automatic signal correction in order to make the signal homogeneous over the 3D volume, such as shown on Figure 3a. In order to make the signal intensity more homogeneous all across the lung volume, we apply a signal correction based on a Gaussian of the image with a large  $\sigma$ :

$$I' = I - G\sigma=25(I) + \text{Mean}(G\sigma=25(I))$$

The Gaussian image  $G\sigma$  represents the local brightness. Figure 1 shows the result of the corrected image  $I'$ . The image is still corrupted by noise, and the overall quality is not necessarily better, but the airway lumen is more homogeneous over the 3D volume.

The noise includes some dark voxels inside the airway wall, which induce leakage during the segmentation process, and bright voxels inside the airway lumen which can stop the segmentation process early. In order to filter the noise, a Gaussian based approach was not deemed effective because a large kernel size would blur small structures, whereas a small kernel size could be disturbed by the extreme noisy values.

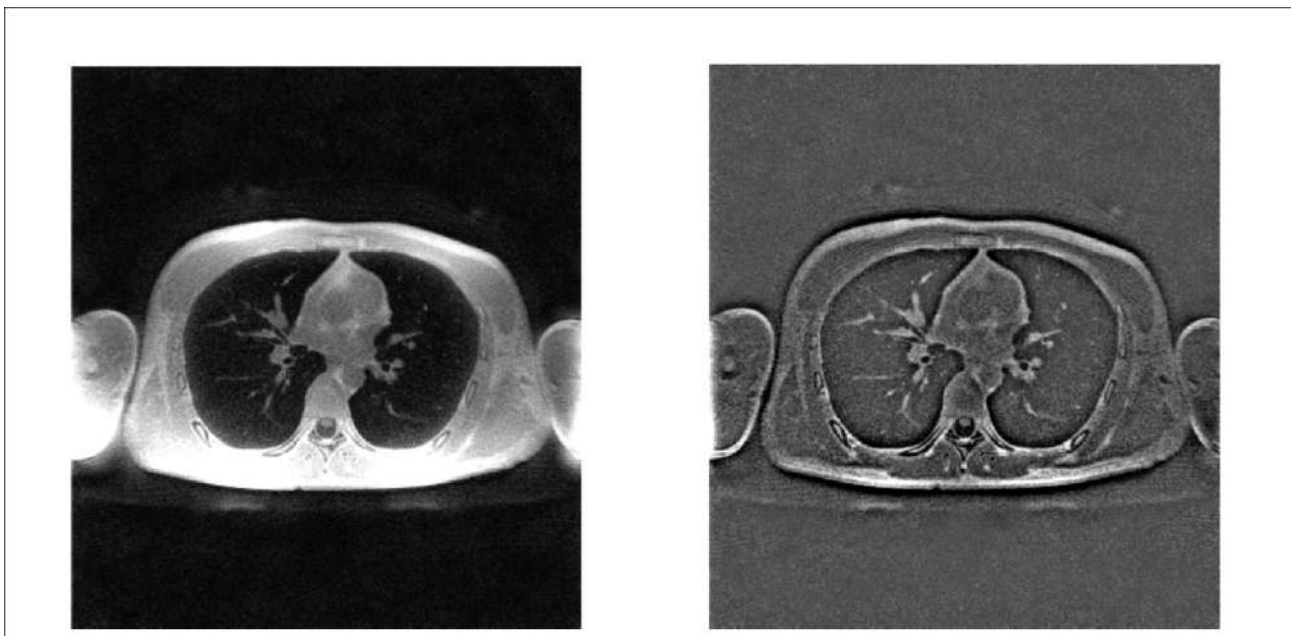


Figure 1. 3D-UTE lung MRI before correction (left image) and after correction (right image) of signal intensity values.

Therefore, we have chosen to use a median based filter in order not to be influenced by the extreme noisy values. Since we are working on a tubular shaped organ, we developed an anisotropic median filter not to consider values outside the airway. We use a  $5 \times 1 \times 1$  kernel placed according to seven different orientations in the  $5 \times 5 \times 5$  cube, which according to our experiments is enough to always get a good direction. Among those orientations we choose the one for which the standard deviation is the lowest and then compute the median value. This approach allows to remove the bright voxels from the airway lumen, and the dark voxels from the airway wall. The filtered image we obtain is suitable for a region growing segmentation approach, since we can distinguish precisely the airway lumen from the airway wall.

### Segmentation of the airway tree

A simple region growing directly applied on our filtered images gives acceptable results (see Figure 2D), and satisfying enough to realize a clinical analysis (Figure 2).

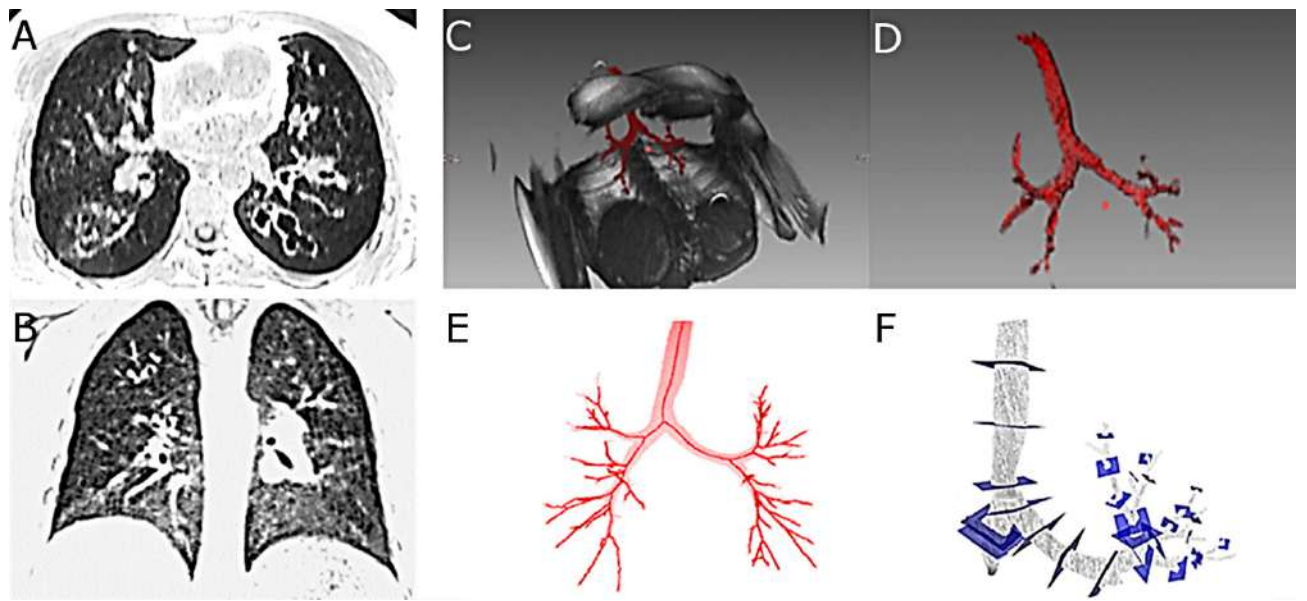


Figure 2. 3D-UTE lung MRI acquired in a patient with cystic fibrosis (A, B). Owing to the 3D isotropic voxel size, reformations are allowed in both axial (A) and coronal (B) planes. In C and D, an extraction of the bronchial tree (red color) volume is shown, from the rest of the lung parenchyma and soft tissue of the thorax (grey colors). In E, the segmented bronchial volume is skeletonized (red lines) in order to allow orthogonal reformations along the bronchial paths (blue colored cross sections in F).

### Post-Analysis of the airway tree

The analysis of the human bronchial tree requires to compare the lumen area to the airway wall area measured orthogonally to the airway. In order to get the 2D cross-section we used the same methods as the one presented in Section 2 to extract the curve-skeleton and estimate the orthogonal plane. Those methods only rely on a segmented tubular organ and can be applied similarly to segmented airway trees obtained from CT data or MRI data. On a 2D cross-section, the lumen area can be directly computed from the segmented volume, while the airway wall requires another segmentation process. On cross-sections reconstructed from our filtered image,

many methods used on CT scan data allow to extract the airway wall properly. We choose the method used in (25) based on a Laplacian of Gaussian operator with  $\sigma = 0.5$ . (Figure 3).

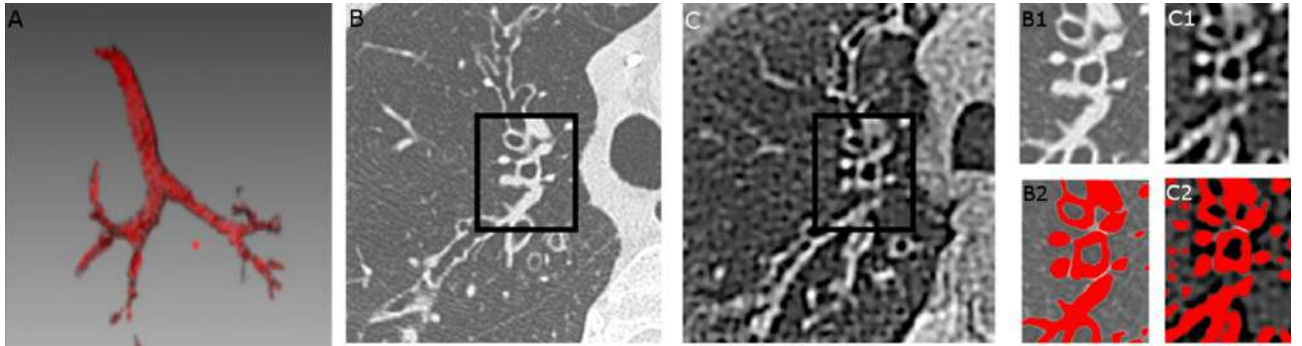


Figure 3. A bronchial tree volume is displayed in A. The right upper lobe of a cystic fibrosis male is displayed using CT (B) and corresponding UTE MRI (C). The black rectangle represents a magnification of the apical right upper lobe bronchus and shown using CT (B1) and UTE MRI (C1). A segmentation of the bronchial wall area is shown in B2 and C2, by using the Laplacian-of-Gaussian algorithm.

### 2.3.3. Imaging analysis

Two radiologists with 2 and 10 years of experience in chest MRI measured the bronchial dimensions on both 3D-CT and 3D-UTE MRI. The same set of four bronchi was chosen at the segmental (3rd generation) and corresponding sub-segmental level (4th generation): the apical right and left upper lobes (RB1, LB1) and the posterior right and left inferior bronchi (RB10, LB10).

The bronchial wall area and the bronchial lumen area were measured on orthogonal cross sections of bronchi and normalized to the body surface area to calculate WA and LA, respectively. Percentage wall area was calculated as follows:  $\%WA = WA / (WA + LA) \times 100$ .

All analyses were made independently, after anonymization of data sets and blinded from any clinical data or the other observer results. The mean of each bronchial measurement was chosen as consensus.

We also calculated wall thickness (WT) as follows:  $WT = \sqrt{\left[ \frac{(WA + LA)}{\pi} \right]} - \sqrt{\frac{LA}{\pi}}$ .

## 2.4. Pulmonary function tests

Pulmonary function tests (PFT) were obtained with body plethysmography (Jaeger; Master lab, Geispolsheim-Gare, France). PFT was performed before multi– detector row CT and the 3D-MRI on the same day.

## 2.5. Statistical analysis

Concordance was assessed by using intraclass correlation and agreement was evaluated by using Bland-Altman analysis. Correlation were assessed by using Spearman test. Comparison of means was assessed by using repeated ANOVA, with CF severity status as the group factor, participant identifier as the subject factor and the bronchus as the within factor.

## 3. RESULTS:

### 3.1. Patient characteristics

Thirty patients were included and 3 datasets of MR images were excluded because of motion artefacts that did not allowed to clearly assess the bronchial contours.

The mean age of the patients included was 27.23 years. There were 16 males for 11 females and only 4 patients were smokers. Their mean BMI was 21.62 kg/m<sup>2</sup>. Twenty-three patients had the mutation deltaF508 either in its homozygous or heterozygous form.

The patients had a mean exacerbation rate of 1.91 per person during the study year versus 1.17 the previous year. Most of the exacerbations were treated with antibiotics.

It is important to note that 24 patients were colonized with *Pseudomonas Aeruginosa*, 17 with methicillin sensitive *Staphylococcus aureus* and only 4 with methicillin resistant *Staphylococcus aureus*. 22 patients had an exocrine pancreatic deficiency while 5 patients were suffering from diabetes. The spirometry data analysis showed that the mean FEV<sub>1</sub> was at 63.57%, the FVC at 80.5% and FEV<sub>1</sub>/FVC at 0.66. The mean TLC was found to be at 103.5%. The characteristics of the population are illustrated in Table 1.

**Table 1. Characteristics of study participants**

<b>n</b>	<b>27</b>
<b>Age (years)</b>	27.2 ± 7.1
<b>Gender (Male/Female)</b>	16/11
<b>Weight (kg)</b>	60.6 ± 10.8
<b>Body Mass Index (kg/m<sup>2</sup>)</b>	21.6 ± 2.9
<b>Active smoker (yes/no)</b>	4/23
<b>Mutation DF508 (homozygote ou hétérozygote) (yes/no)</b>	20/7
<b>Exocrine panereatic insufficiency (yes/no)</b>	22/8
<b>Diabetes (yes/no)</b>	5/25
<b>FEV1 (%pred)</b>	63.5± 19.9
<b>FEV1/FVC (%)</b>	66.5 ± 11.5
<b>RV (%pred)</b>	150 ± 30
<b>TLC (%pred)</b>	103.5 ± 13.45

Legends: FEV1=forced expiratory volume in 1 second; FVC=forced vital capacity; RV=residual volume; TLC=total lung capacity; %pred=percentage of predicted value

### **3.2. Concordance and agreement between 3D-CT and 3D-MRI**

Good concordance was found between 3D-UTE and 3D-CT to assess bronchial dimensions (ICC>0.62), while the highest concordance was found for LA measurement (ICC=0.84) (Figure 4). At Bland-Altman analysis, the mean difference of WA was -1.9 [-19.7; 16] and -1.5 [-8; 4.9] for LA, without heterogeneity of distribution from the low to the high values and thus, indicating a systematic underestimation (Figure 5).

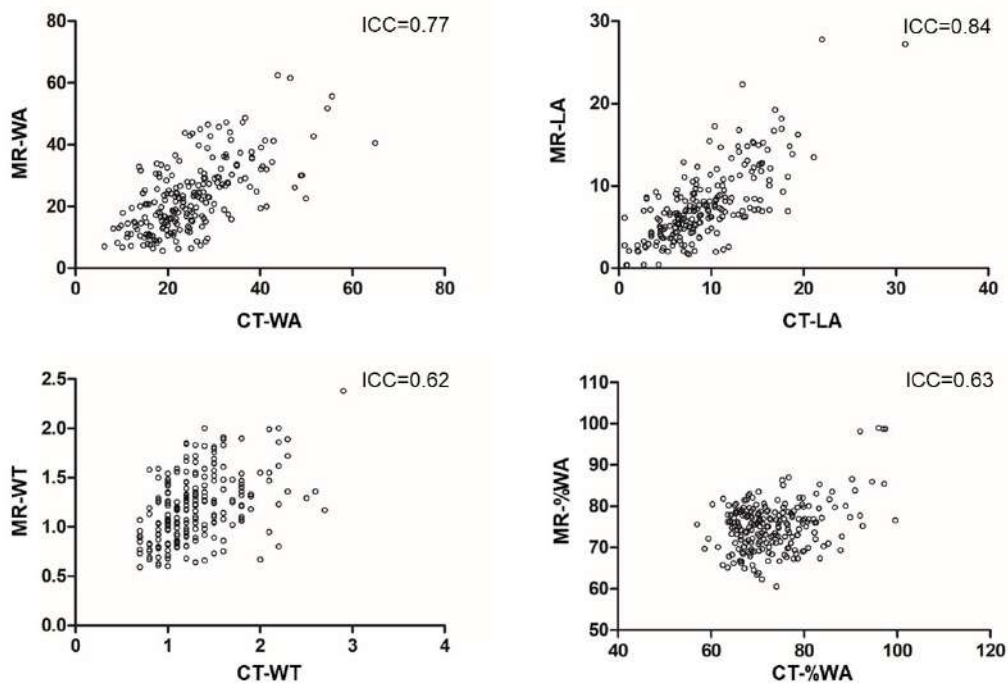


Figure 4. Concordance between CT and MRI bronchial dimensions. WA, LA, WT and %WA represent the normalized wall area, lumen area, wall thickness and percentage wall area, respectively. ICC indicates the intraclass correlation value between CT and 3D-UTE MRI measurements, as represented by white circles.

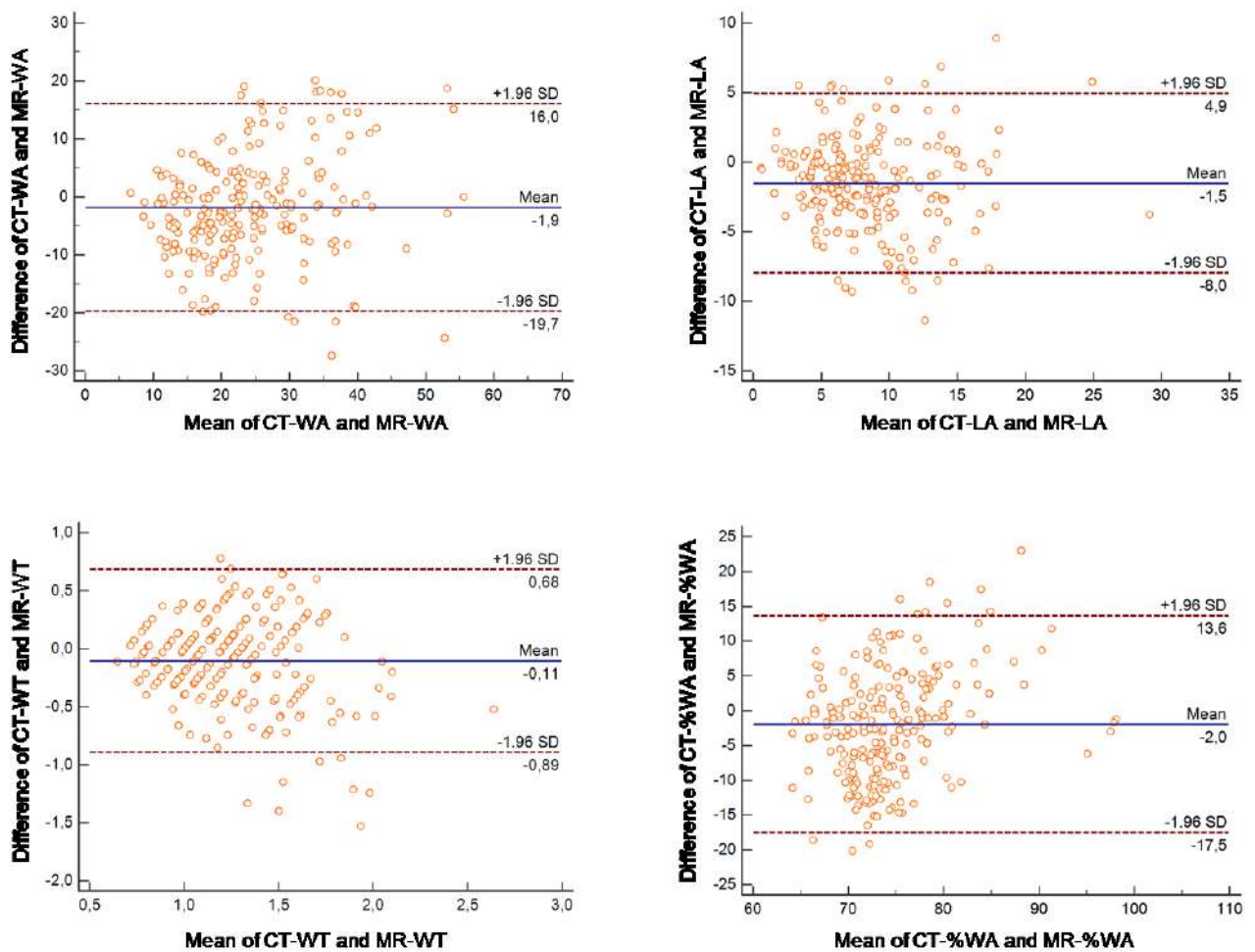


Figure 5. Bland-Altman analysis between CT and MRI bronchial dimensions. WA, LA, WT and %WA represent the normalized wall area, lumen area, wall thickness and percentage wall area, respectively. The blue line indicates the mean difference and the dashed lines indicates the limits of agreement.

### 3.3. Correlations to PFT and Bhalla score.

Quantitative bronchial measurements as assessed by 3D-UTE and 3D-CT were found to share similar correlations to PFTs and the Bhalla score. For instance, WA, WT and %WA but not LA correlated to PFT obstructive indexes ( $p < 0.01$ ). WA and WT were also found to consistently correlate to the MR Bhalla score ( $p < 0.001$ ) (Table 2).

**Table 2. Correlation between bronchial measurements, pulmonary functional tests and the MR Bhalla score**

All bronchi		FEV1%		FEV1/FVC		RV%		MR Bhalla score	
		$\rho$	p-value	$\rho$	p-value	$\rho$	p-value	$\rho$	p-value
<b>MRI</b>	<b>WA</b>	0.18	<b>0.008</b>	-0.13	<b>0.049</b>	0.16	<b>0.03</b>	-0.31	<b>&lt;0.001</b>
	<b>LA</b>	0.03	0.60	0.06	0.36	-0.01	0.86	-0.12	0.07
	<b>WT</b>	-0.30	<b>&lt;0.001</b>	-0.24	<b>&lt;0.001</b>	0.29	<b>&lt;0.001</b>	-0.41	<b>&lt;0.001</b>
	<b>%WA</b>	-0.32	<b>&lt;0.001</b>	-0.25	<b>&lt;0.001</b>	0.36	<b>&lt;0.001</b>	-0.23	<b>&lt;0.001</b>
<b>CT</b>	<b>WA</b>	-0.30	<b>&lt;0.001</b>	-0.24	<b>&lt;0.001</b>	0.23	<b>0.001</b>	-0.34	<b>&lt;0.001</b>
	<b>LA</b>	0.00	0.96	0.03	0.61	0.09	0.22	-0.09	0.20
	<b>WT</b>	-0.42	<b>&lt;0.001</b>	-0.29	<b>&lt;0.001</b>	0.34	<b>&lt;0.001</b>	-0.38	<b>&lt;0.001</b>
	<b>%WA</b>	-0.20	<b>0.003</b>	-0.16	<b>0.02</b>	0.26	<b>&lt;0.001</b>	-0.12	0.07

Note: data are rho coefficient of correlation of Spearman. A p-value<0.05 was considered significant

Legend: WA=normalized wall area; LA=normalized lumen area; WT=normalized wall thickness;

%WA=wall area divided by total area x 100; FEV1=forced expiratory volume in 1 second;

FVC=forced vital capacity; RV=residual volume; TLC=total lung capacity; %=percentage predicted

### 3.4. Comparison between CF groups of severity.

CF with mild FEV1% $\geq$ 80% were discriminated from those with moderate to severe FEV1%<80%. There was a significant difference in %WA between groups using either MRI (F-ratio=2.47, p<0.001) or CT (F-ratio=2.28, p<0.001) (Table 3).

**Table 3. Comparison of bronchial parameters between CF groups according to their functional impairment severity.**

		<b>Group A</b> (n=72)	<b>Group B</b> (n=144)	<b>Repeated ANOVA</b>	
				F-ratio	p-value
<b>MRI</b>	<b>WA</b>	22.6 ± 2.5	23.5 ± 1.7	0.92	0.64
	<b>LA</b>	8.4 ± 0.8	7.2 ± 0.6	1.08	0.36
	<b>WT</b>	1.1 ± 0.08	1.2 ± 0.06	0.97	0.54
	<b>%WA</b>	70.0 ± 1.7	75.0 ± .2	2.47	<b>&lt;0.001</b>
<b>CT</b>	<b>WA</b>	22.9 ± 2.1	26.1 ± 1.5	0.80	0.84
	<b>LA</b>	9.9 ± 1.0	8.7 ± 0.7	1.22	0.17
	<b>WT</b>	1.1 ± 0.06	1.2 ± 0.04	1.23	0.16
	<b>%WA</b>	72.7 ± 1.4	76.6 ± 1.0	2.28	<b>&lt;0.001</b>

Note: Data are mean ± standard deviation. Group A and B were defined according to FEV1% $\geq$ 80% and FEV1% $<$ 80%, respectively. A p-value inferior to 0.05 was considered significant.

Legend: WA=normalized wall area; LA=normalized lumen area; WT=normalized wall thickness; %Wall Area=wall area divided by total area x 100.

### **3.5. Reproducibility of evaluation.**

Interobserver reproducibility of bronchial measurements was moderate to good, ranging from 0.52 for WT, to 0.62 for both WA and LA, as measured by 3D-UTE MRI. Similar level of reproducibility was found using 3D-CT, with ICC values ranging from 0.53 to 0.67 (Table 4).

**Table 4. Reproducibility of MRI and CT bronchial measurements**

	MRI		CT	
	ICC	95%CI	ICC	95%CI
WA	0.62	[0.54-0.70]	0.67	[0.58-0.60]
LA	0.62	[0.53-0.69]	0.65	[0.58-0.73]
WT	0.52	[0.41-0.61]	0.57	[0.44-0.67]
%WA	0.55	[0.44-0.65]	0.53	[0.39-0.64]

Legend: ICC=intraclass correlation coefficient; CI=confidence interval; WA=normalized wall area; LA=normalized lumen area; WT=normalized wall thickness; %WA=wall area divided by total area x 100

## DISCUSSION

The results of our study indicate that MR metrics with dedicated software shows good to very good concordance to CT in assessing the quantitative measurements of wall and lumen area in a population of adults with CF. Moreover, significant correlations were found between the MR metrics and PFT obstructive indices or the MR Bhalla score, in the range of that of CT. In addition, quantitative MR metric was able to discriminate between CF groups of severity, while the reproducibility of evaluation was good.

CF is characterised by increased WT and BE due to inflammatory changes (26,27). Up to now, the standard of reference to assess the structural airway remodeling in CF is high resolution Computed Tomography (CT) and visual scoring methods such as Helbich-Bhalla score are still widely used in routine. However, visual scores are inherently subjective and thus, for more objective and more precise airway measurements, automated quantification of bronchial dimensions have been investigated.

In 2007, Montaudon et al. (14) showed that WT and WA assessed quantitatively from 3D-CT correlated to CF visual scores and PFT and thus, could be used to assess the severity of CF quantitatively.

In 2017, Kuo et al. (28) demonstrated objective quantification of BE and AWT in children with CF by using an objective airway-artery quantification (AA') from a 3D-CT. The study revealed that the number of AA' pairs found on 3D-CTs could reflect the severity of CF and that their number increases with each segmental generation in CF. This objective measurement of BE parameter allowed to differentiate between CF and controls. The same author later revealed that the A/A' ratio could be used to assess BE longitudinally (29). In this study, we did not normalize the bronchial dimensions by the artery dimension but provided bronchial dimensions only. It could be discussed that, in the study by Kuo and colleagues, the artery dimension were significantly lower in CF than in controls and thus, the higher AA' ratio in CF was driven by both airway and vessel relative balance in CF (30,31). Nevertheless, further assessment of both airway and airway to vessel may be developed as a next step.

The major benefit of our study is the radiation free technique of MRI. The substitution of a radiation technique by a radiation free method yielding comparable results as proposed is one of the fundamentals of radioprotection. We must bear in mind that CF patients are young and are thus prone to be more radio sensitive than the general population. They are also subjected to repeated imaging evaluation which means that their cumulated radiation exposure is far from being negligible (32). Besides, with the development of new therapies (potentiators and correctors of CFTR), CF patients have greater life expectancy. All these factors make the CF population an ideal target for a radiation free imaging technique. We shall be able to do imaging follow-ups more frequently. Hence, any progression of the disease under a particular treatment would be more quickly detected and the therapy promptly adjusted accordingly. Thus, this study may suggest that automated quantification of bronchial dimensions using 3D MRI may be a complementary tool to standard visual scores, for precise and objective airway evaluations.

The study has limitations. First, the feasibility study was retrospective and the population was small. Second, the automated method required some manual interventions, especially to disconnect the wall area from the neighboring vessel contour. Third, the bronchial volume obtained from 3D MRI was still inferior to that obtained from 3D CT and thus, only a set of four bronchi were tested. However, correlations with disease severity and differences between CF groups of severity status were achieved, similarly to CT. Fourth, 3D UTE MRI using the PETRA sequence lasts longer than CT. Nevertheless, new 3D UTE sequences have been shown to decrease the acquisition time.

## CONCLUSION

The study indicates that MR metrics with dedicated software shows good to very good concordance to CT in assessing the quantitative measurements of wall and lumen area in a population of adults with CF. Being able to perform such study with a non-ionizing technique leads to many perspectives in CF patients whose lung deficiency is a chronic state requiring frequent follow-ups by a reliable, sensitive and objective imaging method. It could also be extended to other chronic obstructive lung diseases such.

## REFERENCES

1. pnds\_2017\_vf1.pdf [Internet]. [cité 13 août 2019]. Disponible sur: [https://www.hassante.fr/upload/docs/application/pdf/2017-09/pnds\\_2017\\_vf1.pdf](https://www.hassante.fr/upload/docs/application/pdf/2017-09/pnds_2017_vf1.pdf)
2. Cystic Fibrosis - an overview | ScienceDirect Topics [Internet]. [cité 14 août 2019].
3. Maffessanti M, Candusso M, Brizzi F, Piovesana F. Cystic fibrosis in children: HRCT findings and distribution of disease. *J Thorac Imaging*. 1996;11(1):27-38.
4. Bhalla M, Turcios N, Aponte V, Jenkins M, Leitman BS, McCauley DI, et al. Cystic fibrosis: scoring system with thin-section CT. *Radiology*. juin 1991;179(3):783-8.
5. Nasr SZ, Kuhns LR, Brown RW, Hurwitz ME, Sanders GM, Strouse PJ. Use of computerized tomography and chest x-rays in evaluating efficacy of aerosolized recombinant human DNase in cystic fibrosis patients younger than age 5 years: a preliminary study. *Pediatr Pulmonol*. mai 2001;31(5):377-82.
6. de Jong PA, Ottink MD, Robben SGF, Lequin MH, Hop WCJ, Hendriks JJE, et al. Pulmonary disease assessment in cystic fibrosis: comparison of CT scoring systems and value of bronchial and arterial dimension measurements. *Radiology*. mai 2004;231(2):434-9.
7. Calder AD, Bush A, Brody AS, Owens CM. Scoring of chest CT in children with cystic fibrosis: state of the art. *Pediatr Radiol*. déc 2014;44(12):1496-506.

8. Ernst CW, Basten IA, Ilsen B, Bult N, Van Gompel G, De Wachter E, et al. Pulmonary disease in cystic fibrosis: assessment with chest CT at chest radiography dose levels. *Radiology*. nov 2014;273(2):597-605.
9. Rosenow T, Oudraad MCJ, Murray CP, Turkovic L, Kuo W, de Bruijne M, et al. PRAGMACF. A Quantitative Structural Lung Disease Computed Tomography Outcome in Young Children with Cystic Fibrosis. *Am J Respir Crit Care Med*. 15 mai 2015;191(10):1158-65.
10. Brody A, Chang A. The imaging definition of bronchiectasis in children: Is it time for a change? *Pediatr Pulmonol*. 2018;53(1):6-7.
11. Bhalla M, Turcios N, Aponte V, Jenkins M, Leitman BS, McCauley DI, et al. Cystic fibrosis: scoring system with thin-section CT. *Radiology*. juin 1991;179(3):783-8.
12. Brody AS, Tiddens HAWM, Castile RG, Coxson HO, de Jong PA, Goldin J, et al. Computed tomography in the evaluation of cystic fibrosis lung disease. *Am J Respir Crit Care Med*. 15 nov 2005;172(10):1246-52.
13. Eichinger M, Optazait D-E, Kopp-Schneider A, Hintze C, Biederer J, Niemann A, et al. Morphologic and functional scoring of cystic fibrosis lung disease using MRI. *Eur J Radiol*. juin 2012;81(6):1321-9.
13. Montaudon M, Berger P, Cangini-Sacher A, de Dietrich G, Tunon-de-Lara JM, Marthan R, et al. Bronchial measurement with three-dimensional quantitative thin-section CT in patients with cystic fibrosis. *Radiology*. févr 2007;242(2):573-81.
14. Kuo W, Soffers T, Andrinopoulou E-R, Rosenow T, Ranganathan S, Turkovic L, et al. Quantitative assessment of airway dimensions in young children with cystic fibrosis lung disease using chest computed tomography. *Pediatr Pulmonol*. nov 2017;52(11):1414-23.
15. de Jong PA, Nakano Y, Hop WC, Long FR, Coxson HO, Paré PD, et al. Changes in airway dimensions on computed tomography scans of children with cystic fibrosis. *Am J Respir Crit Care Med*. 15 juill 2005;172(2):218-24.
16. Brody AS, Sucharew H, Campbell JD, Millard SP, Molina PL, Klein JS, et al. Computed tomography correlates with pulmonary exacerbations in children with cystic fibrosis. *Am J Respir Crit Care Med*. 1 nov 2005;172(9):1128-32.
17. Thia LP, Calder A, Stocks J, Bush A, Owens CM, Wallis C, et al. Is chest CT

- useful in newborn screened infants with cystic fibrosis at 1 year of age? *Thorax*. avr 2014;69(4):320-7.
19. Roach DJ, Crémillieux Y, Fleck RJ, Brody AS, Serai SD, Szczesniak RD, et al. Ultrashort Echo-Time Magnetic Resonance Imaging Is a Sensitive Method for the Evaluation of Early Cystic Fibrosis Lung Disease. *Ann Am Thorac Soc*. 2016;13(11):1923-31.
  20. Altes TA, Eichinger M, Puderbach M. Magnetic resonance imaging of the lung in cystic fibrosis. *Proc Am Thorac Soc*. 1 août 2007;4(4):321-7.
  21. Dournes G, Grodzki D, Macey J, Girodet P-O, Fayon M, Chateil J-F, et al. Quiet Submillimeter MR Imaging of the Lung Is Feasible with a PETRA Sequence at 1.5 T. *Radiology*. avr 2016;279(1):328.
  21. Dournes G, Grodzki D, Macey J, Girodet P-O, Fayon M, Chateil J-F, et al. Quiet Submillimeter MR Imaging of the Lung Is Feasible with a PETRA Sequence at 1.5 T. *Radiology*. juill 2015;276(1):258-65.
  22. Pennati F, Roach DJ, Clancy JP, Brody AS, Fleck RJ, Aliverti A, et al. Assessment of pulmonary structure-function relationships in young children and adolescents with cystic fibrosis by multivolume proton-MRI and CT. *J Magn Reson Imaging JMRI*. 2018;48(2):531-42.
  23. Aykac D, Hoffman EA, McLennan G, Reinhardt JM. Segmentation and analysis of the human airway tree from three-dimensional X-ray CT images. *IEEE Trans Med Imaging*. août 2003;22(8):940-50.
  24. Lederlin M, Laurent F, Dromer C, Cochet H, Berger P, Montaudon M. Mean bronchial wall attenuation value in chronic obstructive pulmonary disease: comparison with standard bronchial parameters and correlation with function. *AJR Am J Roentgenol*. avr 2012;198(4):800-8.
  25. Davis SD, Fordham LA, Brody AS, Noah TL, Retsch-Bogart GZ, Qaqish BF, et al. Computed tomography reflects lower airway inflammation and tracks changes in early cystic fibrosis. *Am J Respir Crit Care Med*. 1 mai 2007;175(9):943-50.
  26. Sly PD, Gangell CL, Chen L, Ware RS, Ranganathan S, Mott LS, et al. Risk factors for bronchiectasis in children with cystic fibrosis. *N Engl J Med*. 23 mai 2013;368(21):1963-70.
  27. Kuo W, de Bruijne M, Petersen J, Nasserinejad K, Ozturk H, Chen Y, et al. Diagnosis of bronchiectasis and airway wall thickening in children with cystic

- fibrosis: Objective airway-artery quantification. *Eur Radiol.* nov 2017;27(11):4680-9.
28. Kuo W, Soffers T, Andrinopoulou E-R, Rosenow T, Ranganathan S, Turkovic L, et al. Quantitative assessment of airway dimensions in young children with cystic fibrosis lung disease using chest computed tomography. *Pediatr Pulmonol.* nov 2017;52(11):1414-23.
  29. de Jong PA, Nakano Y, Hop WC, Long FR, Coxson HO, Paré PD, et al. Changes in airway dimensions on computed tomography scans of children with cystic fibrosis. *Am J Respir Crit Care Med.* 15 juill 2005;172(2):218-24.
  30. Long FR, Williams RS, Castile RG. Structural airway abnormalities in infants and young children with cystic fibrosis. *J Pediatr.* févr 2004;144(2):154-61.
  31. O'Reilly R, Ryan S, Donoghue V, Saidlear C, Twomey E, Slattery DM. Cumulative radiation exposure in children with cystic fibrosis. *Ir Med J.* févr 2010;103(2):43-6.

### **3.4 Publication n°6 : Evaluation de la quantification des hyper et hypo signaux en IRM 3DUTE comme marqueurs de la sévérité de l'atteinte pulmonaire dans la mucoviscidose**

L'atteinte pulmonaire de la mucoviscidose est caractérisée par des phénomènes destructifs comme les broncheectasies, les sacculations et l'emphysème mais aussi par des phénomènes inflammatoires productifs comme les impactions mucoïdes, les consolidations et les épaissements des parois bronchiques. Tous ces phénomènes peuvent se traduire par des hypodensités et des hyperdensités à l'imagerie TDM. L'IRM 3DUTE a l'avantage d'être une modalité non irradiante qui peut être utile dans le suivi de l'atteinte pulmonaire de la mucoviscidose. Dans cette étude, nous avons développé une méthode quantitative dérivée des méthodes quantitatives des hypo et hyper densités en TDM, afin d'évaluer la sévérité des altérations structurales pulmonaires chez des patients atteints de mucoviscidose. Nous avons inclus 30 patients qui ont bénéficié d'une TDM, d'une IRM et d'épreuves fonctionnelles respiratoires (EFR) le même jour ainsi que d'une IRM et d'EFR de contrôle un an plus tard. Les résultats ont montré une bonne corrélation des hypo et hyper signaux quantifiés à l'IRM avec les hypo et hyper densités quantifiées au scanner. Les données quantitatives des deux modalités ont montré, de façon, similaire des corrélations significatives avec la fonction respiratoire. La variation du volume expiratoire maximale en une seconde corrélait avec la variation des hyper signaux mais pas avec les hypo signaux, ce qui suggère que la part inflammatoire productifs de la maladie (impactions mucoïdes, consolidations et épaissements bronchiques) pourrait être suivi de façon objective et reproductible à l'IRM 3DUTE. Ainsi, les quantifications automatiques en IRM 3D UTE des hypo signaux et des hyper signaux permettent d'évaluer de manière fiable la sévérité de la maladie chez des patients atteints de mucoviscidose sans aucune irradiation et peuvent aider à objectiver les altérations liées aux processus destructifs et productifs secondaires à l'inflammation bronchiques chronique.

**Automated quantification of high and low signal-intensity volumes using MRI with ultrashort echo times in cystic fibrosis: a cross-sectional and longitudinal study.**

**Article Type: Original research**

**Authors**

Ilyes Benlala<sup>1,2,3</sup>, Cedric Leung<sup>3</sup>, Sophie Point<sup>3</sup>, Chantal Raheison<sup>1,2,3</sup>, Patrick Berger<sup>1,2,3</sup>, François Laurent<sup>1,2,3</sup>, Julie Macey<sup>2,3\*</sup>, Gaël Dournes<sup>1,2,3\*</sup>

\* indicates that both authors contributed equally

**Affiliations**

<sup>1</sup> Univ. Bordeaux, Centre de Recherche Cardio-Thoracique de Bordeaux, U1045, CIC 1401, F-33000 Bordeaux, France

<sup>2</sup> Inserm, Centre de Recherche Cardio-Thoracique de Bordeaux, U1045, CIC 1401, F-33000 Bordeaux, France

<sup>3</sup> CHU de Bordeaux, Service d'Imagerie Thoracique et Cardiovasculaire, Service des Maladies Respiratoires, Service d'Exploration Fonctionnelle Respiratoire, Unité de Pneumologie Pédiatrique, CIC 1401, F-33600 Pessac, France

**Contact author :**

Dr Gaël Dournes, Centre de Recherche Cardio-thoracique de Bordeaux, INSERM U1045, Université Bordeaux Segalen, 146 rue Léo Saignat, 33076 Bordeaux Cedex, France

Tel: +33 5 57 57 46 02 Fax: +33 5 57 57 16 95

E-mail: [gael.dournes@chu-bordeaux.fr](mailto:gael.dournes@chu-bordeaux.fr)

## **Abstract**

**Objectives.** The aim of the study was to validate the automated quantification of high and low signal-intensity volumes using MRI with ultrashort echo time with CT as reference, to assess the disease severity in cystic fibrosis (CF).

**Methods.** The study was prospective and was performed in a single center between May 2015 and September 2017. Participants with CF had to complete clinical examination, CT, MRI and pulmonary function test (PFT) the same day during their routine follow-up (M0), and then 1-year after (M12) except for CT. Using MRI, percentage high (%MR-HSV), low (%MR-LSV) and total abnormal (%MR-TSV) signal-intensity volumes were recorded, as well as their corresponding attenuation measurements using CT (%CT-HAV, %CT-LAV, %CT-TAV, respectively). Automated quantifications and visual Bhalla score were evaluated independently by two observers. Correlations were assessed using Spearman test, comparison using Mann-Whitney test, and reproducibility using intraclass correlation coefficient (ICC).

**Results.** 30 participants were enrolled (median age 27 years, 18 men). At M0, there was a good correlation between %MR-HSV and %CT-HAV ( $\rho=0.70$ ;  $p<0.001$ ) and %MR-LSV and %CT-LAV ( $\rho=0.60$ ;  $p<0.001$ ). Automated MR metrics correlated to PFTs and Bhalla score at both M0 and M12 ( $p<0.05$ ) while %MR-TSV was significantly different between CF with and without respiratory exacerbation ( $p=0.01$ ). The variation of %MR-HSV correlated to the variation of FEV1% at PFT ( $\rho=-0.49$ ;  $p=0.008$ ) but not the visual MR-Bhalla score ( $\rho=0.05$ ;  $p=0.78$ ). The reproducibility was almost perfect ( $ICCs>0.95$ )

**Conclusions.** Automated quantification of abnormal signal-intensity volumes allows reproducible assessment of CF severity at both cross-sectional and longitudinal analysis.

**Word count of Abstract:** 248

**Word count of main manuscript:** 2992

### **Key points:**

- At cross-sectional analysis, the automated quantifications of high and low signal-intensity volumes correlated to the quantification of high and low attenuation using CT as reference, and

also the visual Bhalla score and pulmonary function test, while a composite index of both high and low signal-intensity volume enabled to discriminate CF with exacerbation.

- At longitudinal analysis, the variation of high-signal-intensity volume correlated to the variation of pulmonary function test, and was significantly reduced in CF with an improvement in exacerbation status.

- Automated quantification of abnormal signal-intensity volumes should be worth complementing the conventional visual analysis to assess the disease severity in CF and follow-up longitudinally, for both research and routine purposes.

### **Abbreviation list:**

PFT=pulmonary function test

%CT-HAV=percentage high attenuation volume

%CT-LAV=percentage low attenuation volume

%CT-TAV=percentage total abnormal attenuation volume

%MR-HSV=percentage high-signal-intensity volume

%MR-LSV=percentage low-signal-intensity volume

%MR-TSV=percentage total abnormal signal-intensity volume

### **Introduction**

Cystic fibrosis (CF) is the most common genetic disorder in Caucasians [1] and the lung disease is the major site responsible for exacerbations and deaths. However, the life expectancy has

increased and thus, the majority of CF patients are nowadays adults [2]. In the last few years, quantitative imaging has gained in interest owing to the advent of novel therapies, to assess response to treatment [3]. Indeed, imaging allows to assess both structural [4–6] and functional information [7–9], and despite correlations to pulmonary function test (PFT), it is known that the information are different [6, 10]. Using CT, several visual scorings have been proposed [4–6]. However, visual scores are inherently subjective [11], time consuming [12] and may lack precision to depict lung findings [11]. Recently, other methods have been investigated [13–15]. Previous authors have proposed to quantify the lung disease severity using CT attenuation values, instead of morphological depiction. This refers to the concept of “plus pathology” and “minus pathology”, where the lung alterations are discriminated according to a productive process (such as airway wall thickening, mucus plugs, or consolidation/atelectasis) on the one hand, and to those alterations related to a destructive process (such as airway lumen dilatation and emphysema) on the other hand [16]. For instance, Wielputz et al showed that, using a threshold of -950HU, the CT quantification of percentage low attenuation volume (%LAV) could be used as a quantification of the lung destructive damages [14]. Conversely, recent publication has shown that CT quantification of percentage high attenuation volume (%HAV) could be used as a tool to assess alterations related to a high productive content [15]. However, owing to the need to repeat imaging over time, a radiation-free and contrast-free imaging modality is desirable [17]. To date, MRI of the lung has been demonstrated to provide three-dimensional high resolution morphology using ultrashort echo-times (3D-UTE) [18–20], with similar information than CT to assess the visual CF scorings [20–22]. Recent publications have also demonstrated that the quantification of percentage low-signal-intensity volume (%LSV) at MRI can be used as a surrogate of %LAV at CT [23]. However, to the knowledge of the authors, there is no literature that would aim at quantifying the high-signal-intensity volume using 3D-UTE MRI in CF. There is also no literature that would demonstrate that the correlates at a single

time point would be consistently found valid over time. We hypothesize that the quantitative measurement of MRI high-signal-intensity volume using 3D-UTE may be clinically relevant and reproducible to assess CF severity. In addition, we aimed at building a composite quantification of both high and low signal-intensity volumes to assess a total abnormal signal-intensity volume. Thus, the aim of the study was to validate the quantitative measurement of MR high-signal-intensity volume, using CT as reference. Secondary endpoints were to assess correlations to the visual Bhalla score, to assess correlations with lung function, to assess longitudinal variations over time after 1-year follow-up, to assess variations in CF with pulmonary exacerbation, to assess the added value of low-signal-intensity volume and to assess reproducibility of evaluation.

## **Material and methods**

### *Study population*

The study was prospective and performed in a single center between May 2015 and September 2017 (ClinicalTrial identifier: NCT02449785). The study was approved by the local ethics committee, and all participants gave written informed consent. All co-authors had full control over the data. Inclusion criteria were adults CF of more than 18-year-old, with a diagnosis of CF proven by genetic and/or sweat chloride test. All participants were included during their routine yearly follow-up and had to undergo clinical examinations, pulmonary function test (PFT), CT and MRI on the same day [24]. According to the study protocol, the exacerbation status was recorded, which was determined according to the Fuchs criteria [25]. Participants were also asked to perform the same set of examinations except for CT after one year, during their next routine yearly follow-up. During the 1-year period, management of patients were done according to standard of care [24]. Exclusion criteria were pregnancy and any

contraindications to MRI such as claustrophobia or pacemaker. The number of subjects was calculated to find a good correlation between MRI and CT quantification of CF severity, *i.e.* a correlation coefficient of  $\geq 0.60$ , with a risk alpha of 5% and a power of 90%. Thus, 25 subjects were calculated as enough to meet the criteria and it was planned to include 30 CF participants.

#### *CT and MRI examinations*

Chest CT scans were performed using a 64-slice multidetector CT scanner (Somatom Definition®; Siemens Healthcare, Erlangen, Germany) at end inspiration without contrast product enhancement. Tube voltage was adapted to patient weight with a modulating tube current (CareDose4D; Siemens Medical Solutions). Effective reference tube current was equal to 50 mAs. The effective exam dose ranged from 1.2 to 1.5 mSv. Voxel size was equal to 0.625 mm<sup>3</sup>. Both standard (B30f) and sharp (B70f) algorithms were used for image reconstruction.

Three-dimensional UTE lung MRI was performed with a 1.5 Tesla system (Magnetom Avanto®; Siemens Healthcare, Erlangen, Germany) using pointwise encoding time reduction with radial acquisition [21, 26]. A 16-channel body coil/8-channel spine coil was used. Sequence parameters were as follow: TR/TE were 4.1/0.07ms and flip angle was 5°, FOV was (360x360x360mm<sup>3</sup>) and matrix size 384x384x384 with an isotropic voxel dimension of (0.93x0.93x0.93mm<sup>3</sup>). Acquisition time was about 12 minutes synchronized to end tidal respiration using a respiratory-trigger belt (e.g. Functional Residual Capacity).

#### *Automated quantification of CT high attenuation and MRI high signal-intensity volumes*

Using CT, automated measurement of percentage high attenuation volume (%CT-HAV) was performed using previously published method [15] using the commercially available Syngo.via

Pulmo CT software (Siemens, Erlangen, Germany). Briefly, the software automatically recognize the lung, traces lung contours, determine histograms of attenuation values, and calculates the lung volume occupied by voxels with a predetermined range of attenuation values. The mode of the lung density histogram and its standard deviation (SD) were automatically determined. %CT-HAV was calculated by dividing the volume of those intrapulmonary voxels with an attenuation higher than Mode+3SD by the lung volume [15].

Using MRI, percentage the high-signal-intensity volume (%MR-HSV) was measured similarly, using in-house software written in MatLab. First, the lung volume was segmented from the rest of the thoracic structures which was further enclosed by morphological operators to fill holes to obtain a hollow-free mask. Then, the mode of the histogram signal intensities was calculated as well as the standard deviation (SD). Thus, %MR-HSV was calculated similarly than with CT, that is a normalization of the high-signal-intensity volume by the lung volume, and expressed as a percentage. In addition, as a first attempt study, several thresholds of mode + n\*SD (i.e. n= 3; 4; 5; 6) were empirically tested to find the best correlate with %CT-HAV, chosen as reference.

#### *Automated quantification of CT low attenuation and MRI low signal-intensity volumes*

Using CT images, the percentage low attenuation volume (%CT-LAV) was automatically quantified using the Syngo.via Pulmo CT software (Siemens HealthCare, Erlangen, Germany). For this, a common threshold of below -950HU was used to determine the low attenuation volume and normalized by the lung volume [14, 27].

Using MRI, the percentage of low-signal-intensity volume (%MR-LSV) was automatically determined from the 3D-UTE MR images using previously validated method [23]. This MR

measurement has been previously reported to provide similar information using 3D-UTE than %CT-LAV using 3D-CT.

#### *Evaluation of a global automated score using CT and MRI*

Using CT, a composite index was built by adding the information provided by both high and low attenuation volumes. This index was called the percentage total abnormal attenuation volume (%TAV) and was calculated as follows:  $\%CT-TAV = \%CT-HAV + \%CT-LAV$

Similarly, the MR percentage total abnormal signal-intensity volume (%MR-TSV) was calculated as follows:  $\%MR-TSV = \%MR-HSV + \%MR-LSV$

#### *Visual scoring using the Bhalla score*

Visual semi-quantitative evaluation of the structural lung damages was performed using the Bhalla score [4] at both CT and 3D-UTE MRI [21]. For this, scorings of airway wall thickening, bronchiectasis, mucus plugs, bronchial generation involved, consolidation/atelectasis, sacculation/abcess, bulla and emphysema were done (Supplemental Table E1). The sum of these scorings was calculated to define the visual score, and the Bhalla score was calculated as follows:  $Bhalla\ score = 25 - (visual\ scoring)$ .

#### *Imaging analysis.*

All CT and MR images were anonymized and evaluated independently in random order by two observers with 4 years and 10 years of experience in thoracic imaging, blinded to demographic, clinical and functional data. For quantitative measurement of attenuation values, CT

reconstructed with the B30f algorithm were used whereas CT reconstructed with B70f algorithm were used for visual semi-quantitative analyses. In addition, the junior reader repeated the evaluation 1 month later to avoid recall bias and assess intra-observer reproducibility.

### *Statistical analysis*

Statistical analyses were performed using NCSS software (NCSS 2001, Kaysville, UT, USA). Data were expressed as medians with [95% confidence interval] for continuous variables and absolute number for categorical variable. Comparisons of medians was performed using the Mann Whitney test, comparison of categorical variables was performed using the Fisher's Exact test. Comparison of paired medians were done using the Wilcoxon signed rank test and paired percentages using the McNemar test. Correlations were assessed using Spearman test. A p-value < 0.05 was considered statistically significant. Reproducibility was assessed using intraclass correlation coefficients (ICCs). ICC values were classified as null (=0), slight (>0 and <0.20), fair  $\geq 0.20$  and <0.40), moderate ( $\geq 0.40$  and <0.60), good ( $\geq 0.60$  and <0.80), very good ( $\geq 0.80$  and <0.95) and almost perfect ( $\geq 0.95$ ) according to Landis and colleagues [28].

## **Results**

### *Study population.*

At initial evaluation (M0), thirty CF participants were prospectively enrolled (median age 27 [22-28] years, 18 men) (Table 1). The median FEV1%p was 63 [52-73] . At M0, 11 participants were in a period of pulmonary exacerbation (Supplemental Tables E2) and among them, 4/11 were also in exacerbation during their routine visit at 1-year follow-up (M12). Conversely, 19

participants were in stable condition at M0 (Supplemental Table E2) and 4 of them were found in exacerbation at M12. Thus, there was a total of 8/20 participants with exacerbation at M12 (Supplemental Table E3). Moreover, 2 CF participants did not perform the MR examination at M12, because of pregnancy (n=1) and loss of follow-up (n=1) (Figure 1).

#### *Validation of MR quantification of high-signal-intensity volumes with CT as reference*

First, the threshold of Mode+3SD was confirmed to be the most relevant to define %CT-HAV in cystic fibrosis (Supplemental Table E4). Using MRI, several thresholds from Mode+1SD to Mode+8SD to define %MR-HSV were tested (Supplemental Table E5). The best correlate to %CT-HAV as the CT reference was found for a threshold of more than Mode+5SD of the lung MRI parenchymal intensity histogram ( $\rho=0.70$ ;  $p<0.001$ ) (Figure 2-3).

#### *Correlations to the Bhalla score and PFT*

At M0, there was a very good correlation between CT and MRI to assess the Bhalla score ( $\rho=0.95$ ;  $p<0.001$ ). The threshold of Mode+5SD to define %MR-HSV was found the best to correlate to the CT-Bhalla score, the MR-Bhalla score and FEV1%p from PFT ( $p<0.05$ ) (Figure 3; Supplemental Table E5). The correlation between FEV1%p and %MR-HSV or %CT-HAV were found similar (Figure 3, Table 2). At M12, the same threshold of Mode+5SD was also found the best to correlate to both FEV1%p ( $\rho=-0.50$ ;  $p=0.006$ ) and MR-Bhalla score ( $\rho=-0.53$ ;  $p=0.002$ ) (Table 2; Supplemental Table E5).

#### *Additional evaluations of MR low-signal-intensity and automated total score*

Using CT as reference, a significant correlations between %MR-LSV with %CT-LAV ( $\rho=0.60$ ;  $p<0.001$ ) and between %MR-TSV and %CT-TAV ( $\rho=0.68$ ;  $p<0.001$ ). There were significant correlations between these two additional MR metrics to PFTs, the CT-Bhalla score and the MR-Bhalla score ( $p<0.05$ ) (Table 2; Supplemental Table E6). The median time duration to acquire %MR-TSV and %CT-TAV was 4 minutes.

#### *Assessment of MR metrics variations between initial evaluation and 1-year follow-up*

First, when assessing the 28 participants who completed both initial and 1-year follow-up MRI, the sole MR quantitative or visual metric of CF severity who was found to correlate to the variation in FEV1%p was %MR-HSV ( $\rho=-0.49$ ;  $p=0.008$ ) (Table 3).

Second, at M0, %MR-TSV and %MR-LSV were significantly higher between participants with ( $n=11$ ) and without ( $n=19$ ) exacerbation ( $p<0.05$ ), but not %MR-HSV (Figure 4). All CT quantitative and visual metrics were not found significantly different between these two groups (Supplemental Table E2). Conversely, at M12, %MR-TSV and %MR-HSV were significantly higher between CF with ( $n=8$ ) and without ( $n=20$ ) exacerbation, but not %MR-LSV (Figure 4).

Third, the longitudinal evaluation of 11 CF participants with exacerbation at M0 showed that, at M12, 7/11 were found in stable condition ( $p=0.01$ ) (Supplemental Table E7). At paired analysis, %MR-HSV was the sole MR metric to show a significant reduction in median value ( $p=0.004$ ) whereas FEV1%p, %MR-LSV and %MR-TSV were not found different (Figure 5; Supplemental Table E7).

#### *Assessment of reproducibility*

Very good intra and inter observer reproducibility were obtained for visual scores (ICC>0.80). Reproducibility of quantitative measurements at CT and MRI were almost perfect, with ICCs >0.97 (Table 5)

## **Discussion**

To the best of our knowledge, this study is the first to demonstrate that the quantitative measurement of %MR-HSV is feasible in CF using 3D-UTE MRI. At cross-sectional analysis, the threshold of Mode+5SD was found the best to correlate to %CT-HAV chosen as standard of reference, and also to the visual Bhalla score and pulmonary function test. The same threshold was confirmed when repeating the examination after 1-year. Moreover, %MR-HSV could be combined with the quantification of %MR-LSV to calculate a total abnormal signal-intensity volume (%MR-TSV), the latter being able to discriminate between CF participants with and without exacerbation at two time points. At longitudinal analysis, the variation of %MR-HSV showed significant correlation with the variation of lung obstruction while a significant reduction was observed in CF experiencing a decline in rate of exacerbation status. The reproducibility of the method was almost perfect.

Scoring of the lung severity in CF usually relates to visual morphological features. However, several issues have been recently pointed out [11]. Despite publication of a glossary of terms, it is noticeable that items such as “Sacculation” or “Infiltrate” are currently not defined [29]. There is also variability in the literature to use either the bronchial inner diameter [12] or the outer diameter [30] to define a bronchial dilatation, which is prone to impair the reproducibility of evaluations across expert centers. There is also a lack of precision to depict variations. For instance, using the Bhalla score [4], all extents of lesion of more than 9/18 pulmonary segments

share the same score of 3 points, meaning that all variations within 9 pulmonary segments (=1 lung) are missed.

Recently, alternative quantitative methods have emerged. Using the PRAGMA-CF score in infants and children [13], it has been proposed to manually color structural alterations over 10 CT slices. However, in adults, the use of 10 CT slices only may be prone to under sampling of data. Otherwise, previous authors have shown that the lung abnormalities at CT could be categorized into two settings, *i.e.* those related to an increase of material content [15], and those related to a destruction of the airways and/or lung parenchyma [14]. In this study, we demonstrated that these quantitative measurements could be transposed to 3D-UTE MRI. Moreover, imaging was repeated after 1-year follow-up, demonstrating that the results are accountable at several time points instead of a single cross-sectional analysis.

Since visual scores are calculated as the sum of several scorings [4–6], we investigated the ability of %MR-HSV to build a total abnormal signal-intensity volume, as the sum of high and low signal intensity volumes. In this study, %MR-TSV was found able to discriminate those patients with pulmonary exacerbations, whereas %CT-TAV did not. This result may be similar to previous report in chronic obstructive broncho-pulmonary disease (COPD) where %MR-LSV was found able to discriminate between COPD groups of severity, but not %CT-LAV [23]. In this study, it was discussed that the signal intensity at MRI may have additional functional information than the attenuation at CT. Interestingly, the differences in %MR-HSV and %MR-LSV between CF with and without exacerbation were not similar between M0 and M12. This suggests that, beyond global measurements, the quantitative methods may allow to unravel phenotypes of patients. In addition, %MR-HSV may not discriminate between fixed fibrotic alterations and active lung inflammation. However, the quantitative measurement could be also analyzed over time, and the longitudinal analysis of %MR-HSV, but not the visual

Bhalla score, demonstrated significant relationship to the variable part of the disease process, including the reversible ones.

The study has limitations. First, this is a single monocenter study, using a single MR sequence scheme. Second, CT and MRI were not acquired at the same volume [23], suggesting that results may be even better whether MRI could be acquired at full inspiration. Third, the study involved adults CF only, which is similar to previous study related to %CT-HAV [15]. Thus, the performance in younger populations is currently unknown, although MRI could be used as a radiation-free technique to investigate this point. Fourth, the measurement of %MR-HSV and %CT-HAV does not allow to discriminate the vessel tree; further technical innovation enabling black-blood weighted MRI [31] or removal of vessels at CT [32] should be worth testing to further improve this quantitative measurement. Fifth, the global %MR-TSV measurement did not include air trapping. This is similar to the Bhalla score, where air trapping is not part of the evaluation [4]. Indeed, %MR-LSV was validated with %CT-LAV using a threshold of -950HU, which is a measurement of pure air but not air trapped within lung parenchyma and thus, does not refer to the same range of CT attenuation [33]. Nevertheless, additional assessment of air trapping using either dynamic MRI [34] or inhalation of contrast agents [35] may be valuable to further refine the quantification of the total abnormal signal-intensity score.

To conclude, automated quantification of lung signal-intensity volumes using 3D-UTE MRI are reproducible and correlate to the lung disease severity in CF at both cross-sectional and longitudinal analyses. Automated objective quantifications may be worthwhile complementing the conventional visual analyses for both routine and research purposes in CF.

## Acknowledgement

The study was funded by the French Society of Radiology and was achieved within the context of Laboratory of Excellence TRAIL, ANR-10-LABX-57.

## References

1. Jain M, Goss CH (2014) Update in cystic fibrosis 2013. *Am J Respir Crit Care Med* 189:1181–1186. <https://doi.org/10.1164/rccm.201402-0203UP>
2. Kuehn BM (2014) Progress in treating cystic fibrosis means that many patients may now reach midlife and beyond. *JAMA* 312:1182–1183. <https://doi.org/10.1001/jama.2014.12285>
3. Ronan NJ, Einarsson GG, Twomey M, et al (2018) CORK Study in Cystic Fibrosis: Sustained Improvements in Ultra-Low-Dose Chest CT Scores After CFTR Modulation With Ivacaftor. *Chest* 153:395–403. <https://doi.org/10.1016/j.chest.2017.10.005>
4. Bhalla M, Turcios N, Aponte V, et al (1991) Cystic fibrosis: scoring system with thin-section CT. *Radiology* 179:783–788. <https://doi.org/10.1148/radiology.179.3.2027992>
5. Helbich TH, Heinz-Peer G, Eichler I, et al (1999) Cystic fibrosis: CT assessment of lung involvement in children and adults. *Radiology* 213:537–544. <https://doi.org/10.1148/radiology.213.2.r99nv04537>
6. Brody AS, Klein JS, Molina PL, et al (2004) High-resolution computed tomography in young patients with cystic fibrosis: distribution of abnormalities and correlation with pulmonary function tests. *J Pediatr* 145:32–38. <https://doi.org/10.1016/j.jpeds.2004.02.038>
7. Eichinger M, Optazait D-E, Kopp-Schneider A, et al (2012) Morphologic and functional scoring of cystic fibrosis lung disease using MRI. *Eur J Radiol* 81:1321–1329. <https://doi.org/10.1016/j.ejrad.2011.02.045>
8. Bates AJ, Higano NS, Hysinger EB, et al (2018) Quantitative Assessment of Regional Dynamic Airway Collapse in Neonates via Retrospectively Respiratory-Gated 1 H Ultrashort Echo Time MRI. *J Magn Reson Imaging*. <https://doi.org/10.1002/jmri.26296>
9. Woods JC, Conradi MS (2018) 3He diffusion MRI in human lungs. *J Magn Reson* 292:90–98. <https://doi.org/10.1016/j.jmr.2018.04.007>
10. Brody AS, Sucharew H, Campbell JD, et al (2005) Computed tomography correlates with pulmonary exacerbations in children with cystic fibrosis. *Am J Respir Crit Care Med* 172:1128–1132. <https://doi.org/10.1164/rccm.200407-989OC>
11. Calder AD, Bush A, Brody AS, Owens CM (2014) Scoring of chest CT in children with cystic fibrosis: state of the art. *Pediatr Radiol* 44:1496–1506. <https://doi.org/10.1007/s00247-013-2867-y>

12. Chassagnon G, Hubert D, Fajac I, et al (2016) Long-term computed tomographic changes in cystic fibrosis patients treated with ivacaftor. *Eur Respir J* 48:249–252. <https://doi.org/10.1183/13993003.01918-2015>
13. Rosenow T, Oudraad MCJ, Murray CP, et al (2015) PRAGMA-CF. A Quantitative Structural Lung Disease Computed Tomography Outcome in Young Children with Cystic Fibrosis. *Am J Respir Crit Care Med* 191:1158–1165. <https://doi.org/10.1164/rccm.201501-0061OC>
14. Wielpütz MO, Weinheimer O, Eichinger M, et al (2013) Pulmonary emphysema in cystic fibrosis detected by densitometry on chest multidetector computed tomography. *PLoS ONE* 8:e73142. <https://doi.org/10.1371/journal.pone.0073142>
15. Chassagnon G, Martin C, Burgel P-R, et al (2018) An automated computed tomography score for the cystic fibrosis lung. *Eur Radiol* 28:5111–5120. <https://doi.org/10.1007/s00330-018-5516-x>
16. Wielpütz MO, Eichinger M, Biederer J, et al (2016) Imaging of Cystic Fibrosis Lung Disease and Clinical Interpretation. *Rofo* 188:834–845. <https://doi.org/10.1055/s-0042-104936>
17. Leuraud K, Richardson DB, Cardis E, et al (2015) Ionising radiation and risk of death from leukaemia and lymphoma in radiation-monitored workers (INWORKS): an international cohort study. *Lancet Haematol* 2:e276-281. [https://doi.org/10.1016/S2352-3026\(15\)00094-0](https://doi.org/10.1016/S2352-3026(15)00094-0)
18. Johnson KM, Fain SB, Schiebler ML, Nagle S (2013) Optimized 3D ultrashort echo time pulmonary MRI. *Magn Reson Med* 70:1241–1250. <https://doi.org/10.1002/mrm.24570>
19. Dournes G, Grodzki D, Macey J, et al (2015) Quiet Submillimeter MR Imaging of the Lung Is Feasible with a PETRA Sequence at 1.5 T. *Radiology* 276:258–265. <https://doi.org/10.1148/radiol.15141655>
20. Roach DJ, Crémillieux Y, Fleck RJ, et al (2016) Ultrashort Echo-Time Magnetic Resonance Imaging Is a Sensitive Method for the Evaluation of Early Cystic Fibrosis Lung Disease. *Ann Am Thorac Soc* 13:1923–1931. <https://doi.org/10.1513/AnnalsATS.201603-203OC>
21. Dournes G, Menut F, Macey J, et al (2016) Lung morphology assessment of cystic fibrosis using MRI with ultra-short echo time at submillimeter spatial resolution. *Eur Radiol* 26:3811–3820. <https://doi.org/10.1007/s00330-016-4218-5>
22. Dournes G, Yazbek J, Benhassen W, et al (2018) 3D ultrashort echo time MRI of the lung using stack-of-spirals and spherical  $k$ -Space coverages: Evaluation in healthy volunteers and parenchymal diseases: Lung MRI With 3D UTE Spiral VIBE Sequence. *Journal of Magnetic Resonance Imaging*. <https://doi.org/10.1002/jmri.26212>
23. Benlala I, Berger P, Girodet P-O, et al (2019) Automated Volumetric Quantification of Emphysema Severity by Using Ultrashort Echo Time MRI: Validation in Participants with Chronic Obstructive Pulmonary Disease. *Radiology* 292:216–225. <https://doi.org/10.1148/radiol.2019190052>

24. Centre de Reference Mucoviscidose (2017). Protocole National de Diagnostic et de Soins (PNDS) Mucoviscidose. Haute Autorité de Santé, France. Available via [https://www.has-sante.fr/portail/upload/docs/application/pdf/2017-09/pnds\\_2017\\_vf1.pdf](https://www.has-sante.fr/portail/upload/docs/application/pdf/2017-09/pnds_2017_vf1.pdf). Accessed 20 October 2019.
25. Fuchs HJ, Borowitz DS, Christiansen DH, et al (1994) Effect of aerosolized recombinant human DNase on exacerbations of respiratory symptoms and on pulmonary function in patients with cystic fibrosis. The Pulmozyme Study Group. *N Engl J Med* 331:637–642. <https://doi.org/10.1056/NEJM199409083311003>
26. Grodzki DM, Jakob PM, Heismann B (2012) Ultrashort echo time imaging using pointwise encoding time reduction with radial acquisition (PETRA). *Magn Reson Med* 67:510–518. <https://doi.org/10.1002/mrm.23017>
27. Lynch DA, Austin JHM, Hogg JC, et al (2015) CT-Definable Subtypes of Chronic Obstructive Pulmonary Disease: A Statement of the Fleischner Society. *Radiology* 277:192–205. <https://doi.org/10.1148/radiol.2015141579>
28. Landis JR, Koch GG (1977) The measurement of observer agreement for categorical data. *Biometrics* 33:159–174
29. Hansell DM, Bankier AA, MacMahon H, et al (2008) Fleischner Society: Glossary of Terms for Thoracic Imaging. *Radiology* 246:697–722. <https://doi.org/10.1148/radiol.2462070712>
30. Kuo W, Soffers T, Andrinopoulou E-R, et al (2017) Quantitative assessment of airway dimensions in young children with cystic fibrosis lung disease using chest computed tomography. *Pediatr Pulmonol* 52:1414–1423. <https://doi.org/10.1002/ppul.23787>
31. Altbach MI, Bilgin A, Li Z, et al (2005) Processing of radial fast spin-echo data for obtaining T2 estimates from a single k-space data set. *Magnetic Resonance in Medicine* 54:549–559. <https://doi.org/10.1002/mrm.20611>
32. Milanese G, Eberhard M, Martini K, et al (2018) Vessel suppressed chest Computed Tomography for semi-automated volumetric measurements of solid pulmonary nodules. *Eur J Radiol* 101:97–102. <https://doi.org/10.1016/j.ejrad.2018.02.020>
33. Matsuoka S, Kurihara Y, Yagihashi K, et al (2008) Quantitative assessment of air trapping in chronic obstructive pulmonary disease using inspiratory and expiratory volumetric MDCT. *AJR Am J Roentgenol* 190:762–769. <https://doi.org/10.2214/AJR.07.2820>
34. Higano NS, Hahn AD, Tkach JA, et al (2017) Retrospective respiratory self-gating and removal of bulk motion in pulmonary UTE MRI of neonates and adults. *Magn Reson Med* 77:1284–1295. <https://doi.org/10.1002/mrm.26212>
35. Rayment JH, Couch MJ, McDonald N, et al (2019) Hyperpolarised <sup>129</sup>Xe MRI to monitor treatment response in children with cystic fibrosis. *Eur Respir J*. <https://doi.org/10.1183/13993003.02188-2018>

## Table Legends

Table 1. Clinical, functional and imaging characteristics of study participants.

Table 2. Correlation between MRI and CT metrics of CF severity with pulmonary function test at initial evaluation and 1-year follow-up.

Table 3. Correlation between the variation of MR metrics of CF severity and the variation of pulmonary function test between initial evaluation and 1-year follow-up.

Table 4. Reproducibility of quantitative and visual analyses

## Figure Legends.

**Figure 1. Flow chart of the study.** CF=cystic fibrosis.

**Figure 2.** Axial CT lung section (A, C) and corresponding MRI 3D UTE lung section (B, D) in a 14-year old female with cystic fibrosis. White arrows show an emphysema lesion in the right inferior lobe. Green arrows show a bronchiectasis and peri-bronchial thickening in the left inferior lobe, on both CT and MRI. On C image, blue areas indicate CT volumetric quantification of low attenuation volume and red areas display segmentation of high attenuation volume. On D image, blue and red images shows the quantification of low signal-intensity volume and high-signal intensity volume, respectively.

**Figure 3. Correlation between automated quantification of MR high-signal-intensity volumes with CT quantitative score (A), CT visual score (B) and pulmonary function test (C, D).** %MR-HSV=percentage high-signal-intensity volume; %CT-HAV=percentage high attenuation volume; FEV1=forced expiratory volume in 1 second, %p=percentage of predicted value.

**Figure 4. Comparison of MR quantitative metrics in CF with and without respiratory exacerbation at initial evaluation (M0, n=30) (A, B, C) and at 1-year follow-up (M12, n=28) (D, E, F).** There were 11/19 CF with exacerbation at M0 and 8/20 CF with exacerbation at M12. The center line of the box plot represent the median value and the whiskers the range of minimum to maximum values. %MR-HSV (A, D), %MR-LSV (B, E) and %MR-TSV (C, F) represent the quantitative measurements of percentage high-signal-intensity volume, low-signal-intensity volume and total abnormal signal-intensity volume, respectively. There was significantly higher %MR-TSV value in CF with exacerbation at both M0 and M12. Conversely, %MR-LSV was significantly higher at M0 only, and %MR-HSV at M12 only.

**Figure 5. Comparison of MR metrics in 11 CF participants with pulmonary exacerbation at initial evaluation (M0) and 1-year follow-up (M12).** At M12, 7/11 of these study participants were found in stable condition during their routine yearly follow-up. Black points indicates the each individual measurements and the horizontal lines represent the median values. There was a significant reduction over time in percentage high-signal-

intensity value (%MR-HSV, panel A) but not in percentage low-signal-intensity volume (%MR-LSV, panel B) nor percentage total abnormal signal-intensity volume (%MR-TSV, panel C).

**Table 1. Clinical, functional and imaging characteristics of study participants**

		M0 (n=30)	M12 (n=28)
<b>Age</b>	Years	27 [22-28]	25 [22-28]
<b>Sex ratio</b>	Men/Women	18 / 12	17 / 11
<b>BMI</b>	kg.m <sup>-2</sup>	21 [20-22]	21 [20-23]
<b>Tobacco consumption</b>	Yes/no	4 / 26	4 / 24
<b>Mutation ΔF508</b>	Homozygous (yes/no)	18 / 12	17 / 11
<b>ABPA</b>	Yes/no	2 / 28	2 / 26
<b>Exacerbation</b>	Yes/no	11 / 19	8 / 20
<b>PFT</b>	FEV <sub>1</sub> (%p)	63 [52-73]	59 [49-80]
	FEV <sub>1</sub> /FVC	68 [63-73]	68 [62-74]
	FEF <sub>25-75</sub> (%p)	33 [23-43]	36 [21-47]
	TLC (%p)	100 [94-108]	105 [99-111]
<b>Arterial blood gases (ambient air)</b>	PaO <sub>2</sub> (mmHg)	80 [74-91]	74 [59-91]
	PaCO <sub>2</sub> (mmHg)	38 [36-40]	43 [39-46]
<b>Quantitative imaging</b>			
<b>MRI</b>	%MR-HSV	4.9 [2.9-6.1]	3.9 [3.0-5.1]
	%MR-LSV	12.8 [9.6-16.9]	18.9 [13.2-24.4]
	%MR-TSV	15.6 [13.3-25.4]	22 [15.8-28.3]
<b>CT</b>	%CT-HAV	3.6 [3.4-4.1]	NA
	%CT-LAV	5.7 [3.9-7.8]	NA
	%CT-TAV	9.5 [7.1-12.1]	NA
<b>Visual imaging</b>	MR-Bhalla score	13 [12-14]	13 [12-15]
	CT-Bhalla score	13 [12-14]	NA

Note: Data are median with [95% confidence interval] for continuous variables and absolute number for categorical variables. Legends: CF= cystic fibrosis; M0=initial evaluation; M12=evaluation at 1-year follow-up; BMI=body mass index; ABPA=allergic broncho-pulmonary aspergillosis; FEV<sub>1</sub>=forced expiratory volume in 1 second; FVC=forced volume capacity; FEF<sub>25-75</sub>=forced expiratory flow at 25%-75%; TLC=total lung capacity; %p=percentage of predicted value; PaO<sub>2</sub>=arterial partial pressure of oxygen; PaCO<sub>2</sub>=arterial partial pressure of carbon dioxide; %HSV= percentage of high signal intensity volume; %LSV=percentage low-signal-intensity volume; %TSV=percentage total abnormal signal intensity volume; %HAV= percentage of high attenuation; %LAV =percentage low-attenuation volume; %TAV=percentage total abnormal attenuation volume; NA=not applicable

**Table 2. Correlation between MRI and CT metrics of CF severity with pulmonary function test at initial evaluation and 1-year follow-up**

					FEV1%p		FEV1/FVC		FEF25-75%p		TLC%p		
					$\rho$	p-value	$\rho$	p-value	$\rho$	p-value	$\rho$	p-value	
<b>MRI</b>	<b>Quantitative</b>	<b>%MR-HSV</b>	M0	n=30	-0.49	<b>0.006</b>	-0.49	<b>0.005</b>	-0.48	<b>0.008</b>	0.00	0.97	
			M12	n=28	-0.50	<b>0.006</b>	-0.43	<b>0.01</b>	-0.50	<b>0.004</b>	0.00	>0.99	
		<b>%MR-LSV</b>	M0	n=30	-0.46	<b>0.01</b>	-0.60	<b>&lt;0.001</b>	-0.51	<b>0.004</b>	0.10	0.64	
			M12	n=28	-0.48	<b>0.009</b>	-0.53	<b>0.003</b>	-0.52	<b>0.004</b>	-0.04	0.84	
		<b>%MR-TSV</b>	M0	n=30	-0.48	<b>0.007</b>	-0.61	<b>&lt;0.001</b>	-0.55	<b>0.005</b>	0.16	0.43	
			M12	n=28	-0.54	<b>0.002</b>	-0.45	<b>0.01</b>	-0.50	<b>0.005</b>	-0.03	0.88	
	<b>Visual</b>	<b>MR-Bhalla score</b>	M0	n=30	0.62	<b>&lt;0.001</b>	0.58	<b>&lt;0.001</b>	0.70	<b>&lt;0.001</b>	-0.07	0.75	
			M12	n=28	0.58	<b>0.001</b>	0.36	<b>0.03</b>	0.59	<b>0.001</b>	-0.03	0.88	
	<b>CT</b>	<b>Quantitative</b>	<b>%CT-HAV</b>	M0	n=30	-0.43	<b>0.01</b>	-0.45	<b>0.01</b>	-0.56	<b>0.001</b>	-0.01	0.94
				M12	n=28	NA	NA	NA	NA	NA	NA	NA	NA
<b>%CT-LAV</b>			M0	n=30	-0.38	<b>0.047</b>	-0.51	<b>0.003</b>	-0.56	<b>0.001</b>	-0.14	0.51	
			M12	n=28	NA	NA	NA	NA	NA	NA	NA	NA	
<b>%CT-TAV</b>			M0	n=30	-0.42	<b>0.02</b>	-0.55	<b>0.001</b>	-0.46	<b>0.01</b>	-0.12	0.56	
			M12	n=28	NA	NA	NA	NA	NA	NA	NA	NA	
<b>Visual</b>		<b>CT-Bhalla score</b>	M0	n=30	0.56	<b>0.001</b>	0.56	<b>0.001</b>	0.62	<b>&lt;0.001</b>	-0.10	0.62	
			M12	n=28	NA	NA	NA	NA	NA	NA	NA	NA	

Note: data rho correlation coefficient of Spearman.

Legend: CF=cystic fibrosis; M0=initial evaluation; M12=follow-up at 1 year; %HSV=percentage high-signal-intensity volume; %LSV=percentage low-signal-intensity volume; %TSV=percentage total signal intensity volume; %HAV=percentage high attenuation volume; %LAV=percentage low attenuation volume; %TAV=percentage total attenuation volume; FEV1=forced expiratory volume in 1 second; FVC=forced vital capacity;FEF25-75=forced expiratory flow at 25%-75%; TLC=total lung capacity; %p=percentage of predicted value.

**Table 3. Correlation between the variation of MR metrics of CF severity and the variation of pulmonary function test between initial evaluation and 1-year follow-up.**

				$\Delta$ FEV1%p		$\Delta$ FEV1/FVC		$\Delta$ FEF25-75%p		$\Delta$ TLC%p	
				$\rho$	p-value	$\rho$	p-value	$\rho$	p-value	$\rho$	p-value
<b>MRI</b>	<b>Quantitative</b>	$\Delta$ %MR-HSV	n=28	-0.49	<b>0.008</b>	-0.51	<b>0.004</b>	-0.56	<b>0.001</b>	0.57	<b>0.02</b>
		$\Delta$ %MR-LSV	n=28	-0.12	0.55	-0.14	0.48	-0.18	0.36	0.14	0.60
		$\Delta$ %MR-TSV	n=28	-0.26	0.16	-0.29	0.11	-0.34	0.07	0.17	0.51
	<b>Visual</b>	$\Delta$ MR-Bhalla score	n=28	0.05	0.78	0.06	0.74	0.08	0.66	-0.61	<b>0.01</b>

Note: data are rho correlation coefficient of Spearman.  $\Delta$  indicates the variation of measurements and was calculated as the relative difference between measurement at initial evaluation and 1-year follow-up.

Legend: CF=cystic fibrosis; %HSV=percentage high-signal-intensity volume; %LSV=percentage low-signal-intensity volume; %TSV=percentage total signal intensity volume; FEV1=forced expiratory volume in 1 second; FVC=forced vital capacity; FEF25-75=forced expiratory flow at 25%-75%; TLC=total lung capacity; %p=percentage of predicted value.

**Table 4. Reproducibility of quantitative and visual analyses**

	M0 (n=30)	M12 (n=28)
<b>Quantitative analysis</b>		
<b>MRI</b>		
<b>%MR-HSV</b>		
Intra-observer	0.98	0.98
Inter-observer	0.97	0.97
<b>%MR-LSV</b>		
Intra-observer	>0.99	>0.99
Inter-observer	>0.99	>0.99
<b>CT</b>		
<b>%CT-HAV</b>		
Intra-observer	0.98	NA
Inter-observer	0.97	NA
<b>%CT-LAV</b>		
Intra-observer	>0.99	NA
Inter-observer	>0.99	NA
<b>Visual analysis</b>		
<b>MR-Bhalla score</b>		
Intra-observer	0.97	0.98
Inter-observer	0.84	0.91
<b>CT-Bhalla score</b>		
Intra-observer	0.93	NA
Inter-observer	0.86	NA

Note: data are intraclass correlation coefficients.

Legend: %HSV percentage high signal intensity volume; %LSV=percentage low-signal-intensity volume;

%HAV= percentage high attenuation volume; %LAV=percentage low-attenuation volume; NA=not applicable

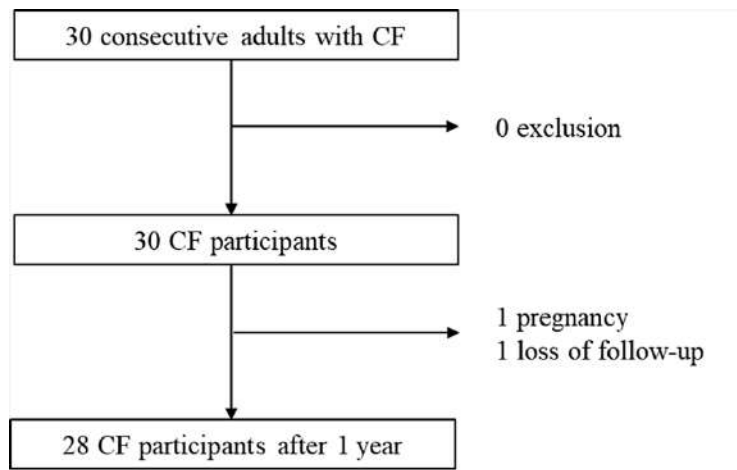


**Figure 1. Flow chart of the study.** CF=cystic fibrosis.

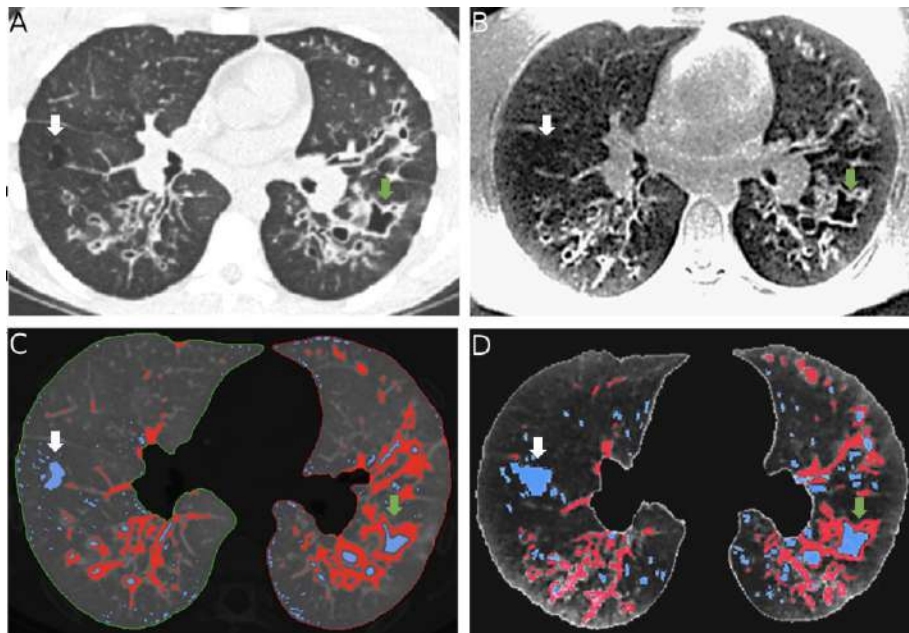


**Figure 2.** Axial CT lung section (A, C) and corresponding MRI 3D UTE lung section (B, D) in a 14-year old female with cystic fibrosis. White arrows show an emphysema lesion in the right inferior lobe. Green arrows show a bronchiectasis and peri-bronchial thickening in the left inferior lobe, on both CT and MRI. On C image, blue areas indicate CT volumetric quantification of low attenuation volume and red areas display segmentation of high attenuation volume. On D image, blue and red images shows the quantification of low signal-intensity volume and high-signal intensity volume, respectively.

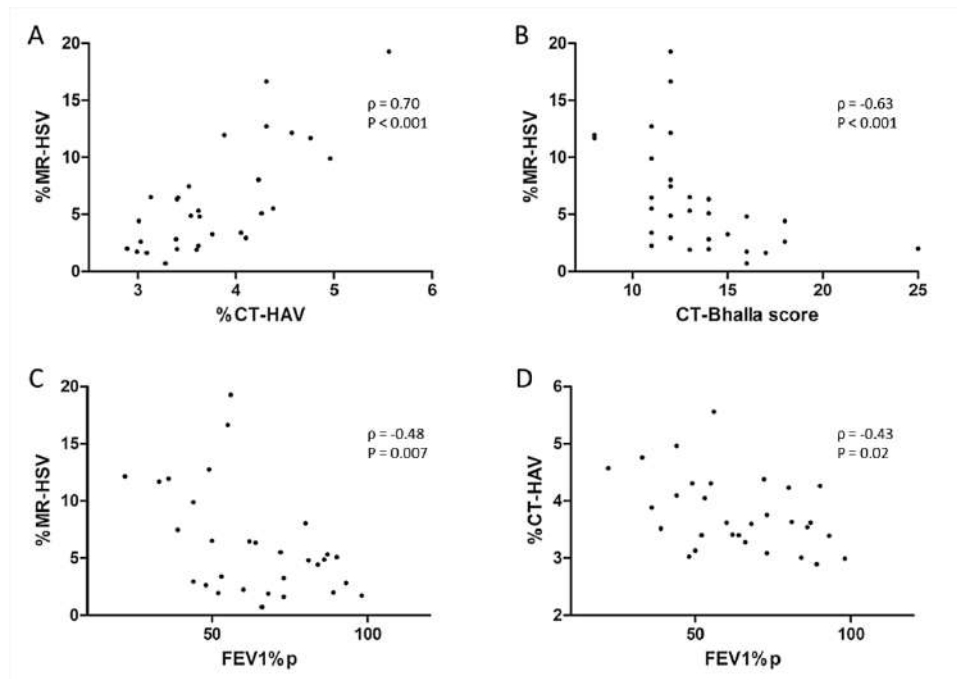


**Figure 3. Correlation between automated quantification of MR high-signal-intensity volumes with CT quantitative score (A), CT visual score (B) and pulmonary function test (C, D).** %MR-HSV=percentage high-signal-intensity volume; %CT-HAV=percentage high attenuation volume; FEV1=forced expiratory volume in 1 second, %p=percentage of predicted value.

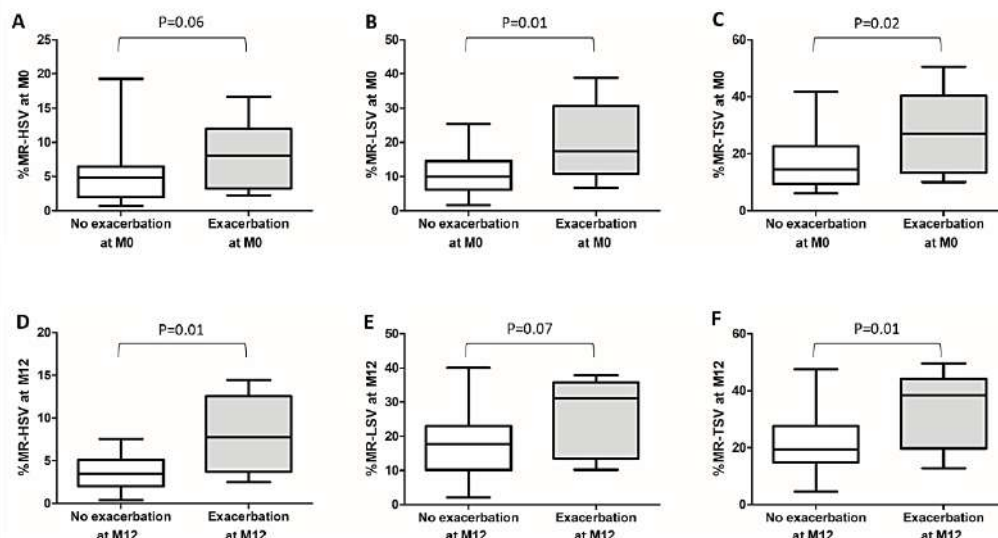


**Figure 4. Comparison of MR quantitative metrics in CF with and without respiratory exacerbation at initial evaluation (M0, n=30) (A, B, C) and at 1-year follow-up (M12, n=28) (D, E, F).** There were 11/19 CF with exacerbation at M0 and 8/20 CF with exacerbation at M12. The center line of the box plot represent the median value and the whiskers the range of minimum to maximum values. %MR-HSV (A, D), %MR-LSV (B, E) and %MR-TSV (C, F) represent the quantitative measurements of percentage high-signal-intensity volume, low-signal-intensity volume and total abnormal signal-intensity volume, respectively. There was significantly higher %MR-TSV value in CF with exacerbation at both M0 and M12. Conversely, %MR-LSV was significantly higher at M0 only, and %MR-HSV at M12 only.

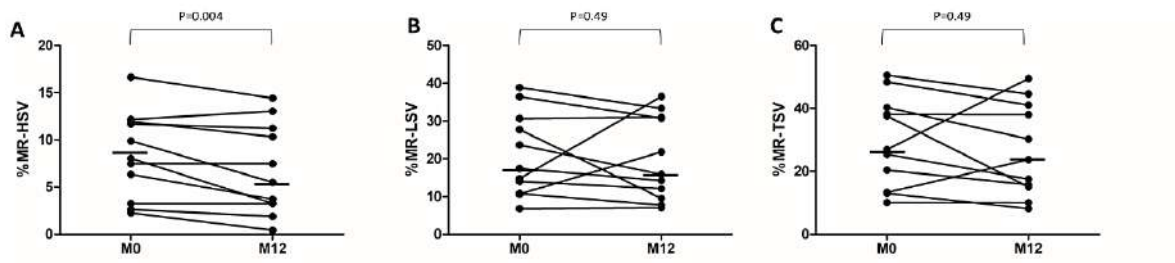


**Figure 5. Comparison of MR metrics in 11 CF participants with pulmonary exacerbation at initial evaluation (M0) and 1-year follow-up (M12).** At M12, 7/11 of these study participants were found in stable condition during their routine yearly follow-up. Black points indicates the each individual measurements and the horizontal lines represent the median values. There was a significant reduction over time in percentage high-signal-intensity value (%MR-HSV, panel A) but not in percentage low-signal-intensity volume (%MR-LSV, panel B) nor percentage total abnormal signal-intensity volume (%MR-TSV, panel C).

## SUPPLEMENTAL MATERIAL

**Supplemental Table E1. Bhalla score** (reproduced from the original publication by *M. Bhalla et al.*)

Category	Scores			
	0	1	2	3
<b>Severity of bronchiectasis</b>	Absent	Mild	Moderate	Severe
<b>Peribronchial thickening</b>	Absent	Mild	Moderate	Severe
<b>Extent of bronchiectasis (no. of segments)</b>	Absent	1-5	6-9	>9
<b>Extent of mucus plugging (no. of segments)</b>	Absent	1-5	6-9	>9
<b>Sacculatoins or abscesses (no. of segments)</b>	Absent	1-5	6-9	>9
<b>Generation of bronchial divisions involved (bronchiectasis/plugging)</b>	Absent	Up to 4 <sup>th</sup> generation	Up to 5 <sup>th</sup> generation	Up to 6 <sup>th</sup> generation and distal
<b>No. of bullae</b>	Absent	Unilateral (not>4)	Bilateral (not >4)	>4
<b>Emphysema (no. of segments)</b>	Absent	1-5	>5	
<b>Collapse/consolidation</b>	Absent	Subsegmental	Segmental/lobar	

**The score is calculated as follows: Total Bhalla score = 25 – (sum of scorings)**

Bronchiectasis severity: Absent (0), luminal diameter slightly greater than diameter of adjacent vessel (Mild (1)), luminal diameter 2-3X the adjacent vessel (Moderate (2)), luminal diameter >3X the adjacent vessel (Severe (3))  
 Peribronchial thickening severity: Absent (0), wall thickness equal to the diameter of adjacent vessel (Mild (1)), wall thickness 2X the adjacent vessel (Moderate (2)), wall thickness >2X the adjacent vessel (Severe (3))

### Parameters' definitions

1. Bronchiectasis: luminal size of bronchi compared with the diameter of an adjacent blood vessel roughly equidistant from the hilum
2. Peribronchial thickening: bronchial wall thickness compared with the diameter of an adjacent blood vessel roughly equidistant from the hilum
3. Mucus plugging: tubular structures with or without branching pattern or rounded opacities differentiated from blood vessels by their position relative to adjacent patent bronchi and blood vessels
4. Abscesses: differentiated from plugged bronchi by their nonbranching appearance and their lack of direct continuity with bronchi
5. Bullae: identified by their peripheral location, their long pleural attachment and their lack of direct communication or continuity with bronchi

*Note: bronchioles with the tree-in-bud pattern are scored as mucus plugs*

**Table E2. Characteristics of CF participants with and without respiratory exacerbation at initial evaluation.**

		<b>CF with exacerbation at M0 (n=11)</b>	<b>CF without exacerbation at M0 (n=19)</b>	<b>p-value</b>
<b>Age</b>	Years	27.5 [23-32]	26 [21-28]	0.27
<b>Sex ratio</b>	Men/Women	8 / 3	10 / 9	0.44
<b>BMI</b>	kg.m <sup>-2</sup>	21.5 [20-22]	21.5 [17-23]	0.64
<b>Tobacco use</b>	Yes/no	3 / 8	1 / 18	0.12
<b>Mutation ΔF508</b>	homozygous (yes/no)	6 / 5	12 / 7	0.71
<b>ABPA</b>	Yes/no	1 / 10	1 / 18	>0.99
<b>PFT</b>	FEV1%p	48 [35-65]	72 [55-86]	<b>0.006</b>
	FEV <sub>1</sub> /FVC	62 [47-69]	72 [66-76]	<b>0.007</b>
	FEF25-75%p	20 [8-42]	43 [31-54]	<b>0.006</b>
	TLC%p	100 [91-123]	100 [94-110]	0.82
<b>CT quantitative</b>	%CT-HAV	3.8 [3.4-4.4]	3.5 [3.2-4.0]	0.10
	%CT-LAV	7.9 [3.4-20.8]	5.2 [3.9-7.4]	0.30
	%CT-TAV	12.2 [6.9-24]	9 [6.9-10]	0.15
<b>CT visual</b>	CT-Bhalla score	12 [10-14]	14 [12-16]	0.11
<b>MR visual</b>	MR-Bhalla score	11 [10-14]	14 [12-16]	0.06

Note: data are median with 95% confidence interval.

Legends: CF=cystic fibrosis; M0=initial evaluation; BMI=body mass index; ABPA=allergic bronchopulmonary aspergillosis; PFT=pulmonary function test; FEV1=forced expiratory volume in 1 second; FVC=forced vital capacity; FEF25-75=forced expiratory flow 25%-75%; TLC=total lung capacity; %p=percentage predicted; %CT-HAV=percentage high attenuation volume; %CT-LAV=percentage low attenuation volume; %CT-TAV=percentage total abnormal attenuation volume; NA=not applicable.

**Table E3. Characteristics of CF participants with and without respiratory exacerbation at 1-year follow-up**

		<b>CF with exacerbation at M12 (n=8)</b>	<b>CF without exacerbation at M12 (n=20)</b>	<b>p-value</b>
<b>Age</b>	Years	25.5 [20-34]	27 [22-28]	0.81
<b>Sex ratio</b>	Men/Women	2 / 6	10 / 10	0.40
<b>BMI</b>	kg.m <sup>-2</sup>	21 [20-22]	20 [18-24]	0.58
<b>Tobacco use</b>	Yes/no	2 / 6	2 / 18	0.55
<b>Mutation ΔF508</b>	Homozygous (yes/no)	3 / 5	13 / 7	0.23
<b>ABPA</b>	Yes/no	1 / 7	1 / 19	0.49
<b>PFT</b>	FEV1%p	36.5 [24-54]	78.5 [58-86]	<b>&lt;0.001</b>
	FEV <sub>1</sub> /FVC	58 [49-64]	71 [67-77]	<b>0.002</b>
	FEF25-75%p	14.5 [9-24]	45 [34-61]	<b>&lt;0.001</b>
	TLC%p	104 [97-126]	105 [94-119]	>0.99
<b>CT quantitative</b>	%CT-HAV	NA	NA	
	%CT-LAV	NA	NA	
	%CT-TAV	NA	NA	
<b>CT visual</b>	CT-Bhalla score	NA	NA	
<b>MR visual</b>	MR-Bhalla score	11 [8-13]	14 [12-17]	<b>0.009</b>

Note: data are median with 95% confidence interval.

Legends: CF=cystic fibrosis; M12=evaluation at 1-year follow-up; BMI=body mass index; ABPA=allergic bronchopulmonary aspergillosis; PFT=pulmonary function test; FEV1=forced expiratory volume in 1 second; FVC=forced vital capacity; FEF25-75=forced expiratory flow 25%-75%; TLC=total lung capacity; %p=percentage predicted; %CT-HAV=percentage high attenuation volume; %CT-LAV=percentage low attenuation volume; %CT-TAV=percentage total abnormal attenuation volume; NA=not applicable.

**Table E4. Correlations between CT quantification of high attenuation volume and pulmonary function test according to five thresholds**

		<b>FEV1%p</b>	
		$\rho$	p-value
<b>%CT-HAV</b>	Mode+1SD	-0.32	0.08
	Mode+2SD	-0.33	0.07
	Mode+3SD	-0.43	0.01
	Mode+4SD	-0.31	0.08
	Mode+5SD	-0.25	0.17

Note: data are rho correlation coefficient of Spearman

Legends: %CT-HAV=percentage high attenuation volume; SD=standard deviation of the lung parenchyma attenuation values; FEV1=forced expiratory volume in 1 second; %p=percentage of predicted value.

**Table E5. Correlations between MRI quantification of high-signal-intensity values and quantitative CT, visual CT, visual MRI and pulmonary function test**

M0		%CT-HAV		CT-Bhalla score		MR-Bhalla score		FEV1%p	
		$\rho$	p-value	$\rho$	p-value	$\rho$	p-value	$\rho$	p-value
%MR-HSV	Mode+1SD	-0.32	0.08	0.22	0.25	0.20	0.29	0.33	0.07
	Mode+2SD	-0.33	0.07	0.31	0.09	0.31	0.10	0.38	0.04
	Mode+3SD	0.26	0.15	-0.39	<b>0.03</b>	-0.10	0.56	-0.23	0.22
	Mode+4SD	0.60	<b>0.005</b>	-0.51	<b>0.003</b>	-0.53	<b>0.002</b>	-0.40	<b>0.02</b>
	Mode+5SD	0.70	<b>&lt;0.001</b>	-0.63	<b>&lt;0.001</b>	-0.64	<b>&lt;0.001</b>	-0.49	<b>0.006</b>
	Mode+6SD	0.51	<b>0.003</b>	-0.54	<b>0.001</b>	-0.51	<b>0.004</b>	-0.33	0.07
	Mode+7SD	0.47	<b>0.008</b>	-0.40	<b>0.02</b>	-0.49	<b>0.005</b>	-0.31	0.08
	Mode+8SD	0.40	<b>0.02</b>	-0.11	0.56	0.40	<b>0.02</b>	-0.25	0.17
<hr/>									
M12		%CT-HAV		CT-Bhalla score		MR-Bhalla score		FEV1%p	
		$\rho$	p-value	$\rho$	p-value	$\rho$	p-value	$\rho$	p-value
%MR-HSV	Mode+1SD	NA	NA	NA	NA	0.22	0.25	0.33	0.07
	Mode+2SD	NA	NA	NA	NA	0.31	0.09	0.38	0.04
	Mode+3SD	NA	NA	NA	NA	-0.10	0.56	-0.23	0.22
	Mode+4SD	NA	NA	NA	NA	-0.39	<b>0.03</b>	-0.42	<b>0.02</b>
	Mode+5SD	NA	NA	NA	NA	-0.53	<b>0.002</b>	-0.50	<b>0.006</b>
	Mode+6SD	NA	NA	NA	NA	-0.51	<b>0.004</b>	-0.43	<b>0.03</b>
	Mode+7SD	NA	NA	NA	NA	-0.49	<b>0.005</b>	-0.31	0.08
	Mode+8SD	NA	NA	NA	NA	0.40	<b>0.02</b>	-0.25	0.17

Note: data are rho correlation coefficients of Spearman

Legends: M0=initial evaluation; M12=evaluation of 1-year follow-up; Mode=mode of the lung parenchyma histogram of signal intensity distribution frequency; SD=standard deviation of the lung parenchyma signal-intensity histogram; %MR-HSV=percentage high-signal-intensity volume; %CT-HAV=percentage high attenuation volume; FEV1=forced expiratory volume in 1 second; %p=percentage predicted; NA=not applicable.

**Table E6. Correlation between MRI and CT metrics of CF severity with the Bhalla score**

<b>M0</b>			<b>MR-Bhalla score</b>		<b>CT-Bhalla score</b>	
			$\rho$	p-value	$\rho$	p-value
<b>MRI</b>	<b>Quantitative</b>	%MR-HSV	-0.64	< <b>0.001</b>	-0.63	< <b>0.001</b>
		%MR-LSV	-0.40	<b>0.03</b>	-0.39	<b>0.03</b>
		%MR-TSV	-0.46	<b>0.01</b>	-0.52	<b>0.003</b>
	<b>Visual</b>	MR-Bhalla score	NA	NA	0.95	< <b>0.001</b>
<b>CT</b>	<b>Quantitative</b>	%CT-HAV	-0.77	< <b>0.001</b>	-0.72	< <b>0.001</b>
		%CT-LAV	-0.40	<b>0.03</b>	-0.43	<b>0.01</b>
		%CT-TAV	-0.42	<b>0.02</b>	-0.43	<b>0.02</b>
	<b>Visual</b>	CT-Bhalla score	0.95	< <b>0.001</b>	NA	NA

Note: data are rho coefficient correlation of Spearman

Legends: CF=cystic fibrosis; M0=initial evaluation; %MR-HSV=percentage high-signal-intensity volume; %MR-LSV=percentage low-signal-intensity volume; %MR-TSV=percentage total abnormal signal intensity volume; %CT-HAV=percentage high attenuation volume; %CT-LAV=percentage low attenuation volume; %CT-TAV=percentage total abnormal attenuation volume; NA=not applicable.

**Table E7. Longitudinal analysis of CF participants with and without respiratory exacerbation between initial evaluation and 1-year follow-up.**

		CF with exacerbation at M0			CF without exacerbation at M0		
		M0	M12	P-value	M0	M12	P-value
<b>Exacerbation</b>	Yes/No	11 / 0	4 / 7	<b>0.01</b>	0 / 19	4 / 12	0.12
<b>PFT</b>	FEV1%p	48 [35-65]	46 [25-80]	0.57	72 [55-86]	74 [54-86]	0.13
	FEV <sub>1</sub> /FVC	62 [47-69]	67 [51-76]	0.10	72 [66-76]	69 [63-76]	0.12
	FEF25-75%p	20 [8-42]	21 [11-49]	0.20	43 [31-54]	40 [24-57]	0.28
	TLC%p	100 [91-123]	100 [92-137]	0.43	100 [94-110]	100 [95-113]	0.45
<b>MR quantitative</b>	%MR-HSV	8 [3-12]	5.5 [2-11]	<b>0.004</b>	5 [2-8]	5 [2-7]	0.73
	%MR-LSV	17 [10-31]	16 [10-33]	0.49	10 [8-18]	19.3 [12-25]	<b>0.009</b>
	%MR-TSV	27 [13-41]	24 [15-44]	0.49	15 [12-24]	24 [16-28]	<b>0.01</b>
<b>MR visual</b>	MR-Bhalla score	11 [10-14]	11 [9-15]	0.81	14 [12-17]	13 [12-17]	0.62

Note: data are median with 95% confidence interval.

Legends: CF=cystic fibrosis; M0=initial evaluation; M12=evaluation at 1-year follow-up; PFT=pulmonary function test; FEV1=forced expiratory volume in 1 second; FVC=foced vital capacity; FEF25-75=forced expiratory flow 25%-75%; TLC=total lung capacity; %p=percentage predicted; %MR-HSV=percentage high-signal-intensity volume; %MR-LSV=percentage low-signal-intensity volume; %MR-TSV=percentage total abnormal signal-intensity volume.

### **3.5 Publication n°7 : Quantification de l'atteinte inflammatoire des voies aériennes dans la mucoviscidose à l'aide de séquence IRM T2 Mapping**

L'analyse morphologique des altérations structurales dans la mucoviscidose ne permet pas de distinguer les phénomènes inflammatoires actifs, potentiellement réversibles sous traitement, de ceux qui correspondent à des phénomènes cicatriciels. Avec l'avènement de nouvelles thérapies dans la mucoviscidose, le besoin de répéter les imageries est primordial pour suivre la réponse au traitement et cibler les altérations susceptibles d'être traitées. La quantification des phénomènes productifs/inflammatoires par les hyperdensités au scanner ou les hypersignaux à l'IRM 3DUTE reste parasitée par l'inclusion inévitable de structures normales (i.e. vaisseaux ou bronches saines) mais également par le manque de spécificité pour l'atteinte inflammatoire active.

Dans cette étude de faisabilité, nous avons développé une méthode de quantification des hypersignaux T2 à l'IRM comme marqueurs des phénomènes inflammatoires actifs de l'atteinte des voies aériennes dans la mucoviscidose. Dix volontaires sains et 12 patients atteints de mucoviscidose ont bénéficié d'une IRM incluant la séquence T2 mapping ainsi que des explorations fonctionnelles respiratoires. De plus, six patients ont été contrôlés par IRM après traitement antibiotique. Les résultats ont montré une quantification nulle chez les volontaires sains. De fortes corrélations significatives ont été retrouvées avec la fonction respiratoire. Par ailleurs, les mesures d'hypersignaux T2 ont diminué après traitement. Ainsi, cette étude a permis de mettre en évidence l'apport du contraste en IRM afin de caractériser l'inflammation des voies aériennes dans la mucoviscidose.

# Quantification of MRI T2-weighted High Signal Volume in Cystic Fibrosis: A Pilot Study

Ilyes Benlala, MD • François Hocke, MD • Julie Macey, MD • Stéphanie Bui, MD • Patrick Berger, MD, PhD • François Laurent, MD • Gaël Dournes, MD, PhD

From the Univ. Bordeaux, Centre de Recherche Cardio-Thoracique de Bordeaux, U1045, CIC 1401, F-33000 Bordeaux, France (I.B., P.B., F.L., G.D.); Inserm, Centre de Recherche Cardio-Thoracique de Bordeaux, U1045, CIC 1401, F-33000 Bordeaux, France (I.B., P.B., F.L., G.D.); and CHU de Bordeaux, Service d'Imagerie Thoracique et Cardiovasculaire, Service des Maladies Respiratoires, Service d'Exploration Fonctionnelle Respiratoire, Unité de Pneumologie Pédiatrique, CIC 1401, F-33600 Pessac, France (I.B., F.H., J.M., S.B., P.B., F.L., G.D.). Received April 6, 2019; revision requested June 6, 2019; revision received August 25; accepted September 10. **Address correspondence to** G.D. (e-mail: [gael.dournes@chu-bordeaux.fr](mailto:gael.dournes@chu-bordeaux.fr)).

Conflicts of interest are listed at the end of this article.

See also the editorial by Revel and Chassagnon in this issue.

Radiology 2019; 00:1–11 • <https://doi.org/10.1148/radiol.2019190797> • Content codes: **CH** **MR**

**Background:** In patients with cystic fibrosis (CF), pulmonary structures with high MRI T2 signal intensity relate to inflammatory changes in the lung and bronchi. These areas of pathologic abnormalities can serve as imaging biomarkers. The feasibility of automated quantification is unknown.

**Purpose:** To quantify the MRI T2 high-signal-intensity lung volume and T2-weighted volume-intensity product (VIP) by using a black-blood T2-weighted radial fast spin-echo sequence in participants with CF.

**Materials and Methods:** Healthy individuals and study participants with CF were prospectively enrolled between January 2017 and November 2017. All participants underwent a lung MRI protocol including T2-weighted radial fast spin-echo sequence. Participants with CF also underwent pulmonary function tests the same day. Participants with CF exacerbation underwent repeat MRI after their treatment with antibiotics. Two observers supervised automated quantification of T2-weighted high-signal-intensity volume (HSV) and T2-weighted VIP independently, and the average score was chosen as consensus. Statistical analysis used the Mann-Whitney test for comparison of medians, correlations used the Spearman test, comparison of paired medians used the Wilcoxon signed rank test, and reproducibility was evaluated by using intraclass correlation coefficient.

**Results:** In 10 healthy study participants (median age, 21 years [age range, 18–27 years]; six men) and 12 participants with CF (median age, 18 years [age range, 9–40 years]; eight men), T2-weighted HSV was equal to 0% and 4.1% (range, 0.1%–17%), respectively, and T2-weighted VIP was equal to 0 msec and 303 msec (range, 39–1012 msec), respectively ( $P < .001$ ). In participants with CF, T2-weighted HSV or T2-weighted VIP were associated with forced expiratory volume in 1 second percentage predicted ( $\rho = -0.88$  and  $\rho = -0.94$ , respectively;  $P < .001$ ). In six participants with CF exacerbation and follow-up after treatment, a decrease in both T2-weighted HSV and T2-weighted VIP was observed ( $P = .03$ ). The intra- and interobserver reproducibility of MRI were good (intraclass correlation coefficients,  $>0.99$  and  $>0.99$ , respectively).

**Conclusion:** In patients with cystic fibrosis (CF), automated quantification of lung MRI high-signal-intensity volume was reproducible and correlated with pulmonary function testing severity, and it improved after treatment for CF exacerbation.

© RSNA, 2019

Online supplemental material is available for this article.

Automated quantification of lung structural alterations is a challenge in chronic airway diseases such as cystic fibrosis (CF) (1). Imaging has a pivotal role for monitoring the response to treatment in the young patients with this disease (2). There is also the need for repeated testing (3). Because more recent therapies are expected to increase life expectancy, a nonionizing (4) noncontrast agent-enhanced (5) imaging modality is desirable. To assess the severity of lung structural damages, several visual scoring systems have been proposed (6–10). However, visual scoring systems have many limitations, as follows: they are inherently subjective, they depend on the training of the reader (11), they are time consuming (12), and they often lack precision to detect lung findings (11). For instance, by using the Helbich-Bhalla score (13), up to two pulmonary lobes must be involved to get a single point of variation. Recently, alternative methods have been investigated. By

using CT, it has been proposed to manually color structural alterations over a grid to calculate a score known as Cystic Fibrosis–Perth Rotterdam Annotated Grid Morphometric Analysis, or CF-PRAGMA, score (14). Also, an automated CT quantification of high-attenuation lung volume has been reported in adults with advanced CF (12). By using MRI, T2-weighted sequences have been shown to depict structural abnormalities related to an increase in cellular and/or water content, resulting in a high T2 signal, such as lung consolidation, bronchial wall edema, and mucus plugs (15). Renz et al (16) proposed scoring these high T2-weighted areas of signal intensity in terms of visual extent and intensity and demonstrated their correlation with respiratory exacerbation status and biologic markers of inflammation.

Our hypothesis is that the amount of MRI high-signal-intensity T2-weighted pathologic findings in the

## Abbreviations

3D = three-dimensional, CF = cystic fibrosis, FEV<sub>1</sub> = forced expiratory volume in 1 second, HSV = high-signal-intensity volume, RFSE = radial fast spin echo, SD = standard deviation, UTE = ultrashort echo time, VIP = volume-intensity product

## Summary

Automated and reproducible quantification of high-signal-intensity volume of the lungs by using MRI was feasible in participants with cystic fibrosis to monitor inflammation and response to treatment.

## Key Results

- In participants with cystic fibrosis (CF), the median MRI T2-weighted high-signal-intensity volume (HSV) was 4.1% of total lung volume; the median T2-weighted volume-intensity product (VIP) was 303 msec.
- The reproducibility of automated measurements of HSV and VIP was high (intraclass correlation coefficient, 0.99).
- In participants with CF, both T2-weighted HSV and T2-weighted VIP were inversely correlated with forced expiratory volume in 1 second percentage predicted ( $\rho = -0.88$  and  $\rho = -0.94$ , respectively;  $P < .001$ ).
- After antibiotic treatment of CF exacerbation, both T2-weighted HSV and T2-weighted VIP decreased from 8% to 4.2% ( $P = .03$ ) and from 664 msec to 260 msec ( $P = .03$ ), respectively.

lungs related to CF could be quantified in an automated fashion and that this would correlate with pulmonary function. The aim of our study was to build an automated quantification of a high-signal-intensity volume method and to evaluate its feasibility in both participants with CF and healthy volunteers. Secondary end points were to assess a composite volume-intensity product (VIP), to measure correlations with lung function, to assess correlation to conventional visual scores, to evaluate variation under treatment, and to assess the reproducibility of this imaging test.

## Materials and Methods

We received ethics committee approval (local ethical committee registration number: DC 2016/98). Our prospective study received academic financial support from the French Society of Radiology and all authors had control of the data and information submitted for publication. Participants with CF and healthy participants provided oral consent; participants with CF and healthy participants or their parents, in the case of minors, provided written informed consent.

## Study Participants

This was a prospective pilot study conducted between January 2017 and November 2017 at the University Hospital of Bordeaux. A screening visit was performed before inclusion of individuals to check for eligibility criteria and a 1-month interval was used to collect their written informed consent.

From January 2017 to June 2017, the feasibility of the technique was tested in healthy participants. Inclusion criteria were age 18 years or older, no tobacco consumption, no respiratory symptoms, no history of lung disease, and no visible lung abnormalities on a noncontrast three-dimensional (3D) ultrashort echo time (UTE) sequence (17).

Second, from July 2017 to November 2017, preliminary evaluation was performed in the CF group. Participants with CF were screened during a routine visit 3 months before their annual follow-up. Inclusion criteria were consecutive participants age 8 years or older. Clinical and biologic evaluation, pulmonary function tests, CT, and MRI had to be completed the same day during their routine annual follow-up (18). MRI was repeated twice within a 10-minute interval to assess the short-term repeatability. In participants with CF with respiratory exacerbation requiring antibiotic therapy, routine evaluation of MRI and/or CT images was proposed to manage response to treatment (18). In participants with CF and healthy participants, exclusion criteria were any contraindication to MRI. Because this was an exploratory study, no power calculation for the number of participants was performed, and a total number of 10 healthy participants and 12 participants with CF was arbitrarily determined (Fig 1).

## Protocols for MRI, CT, and Pulmonary Function Testing

**MRI protocol.**—MRI was performed on an MRI system (Aera; Siemens, Erlangen, Germany) at 1.5 T (Table E1 [online]). First, a 3D UTE sequence was completed by using the following parameters: repetition time msec/echo time msec, 4.3/0.05; flip angle, 5°; and voxel size, 1 × 1 × 1 mm<sup>3</sup>. Respiratory synchronization at end normal expiration was allowed by an automated navigator-triggered prospective synchronization (17).

T2-weighted radial fast spin-echo (RFSE) sequence is a spin-echo–based two-dimensional sequence with a linear radial k-space trajectory (19). In this study, both section-selective and frequency-selective fat saturation prepulses were implemented. When acquiring radial data, the frequent sampling of center of k-space resulted in an inherent averaging effect, which improved motion artifacts. RFSE motion-insensitive behavior was further reinforced by using a respiratory binning method, prospective acquisition correction, at functional residual capacity (20). Then, to maintain sampling density in rings of increasing radius, radial projections of neighboring echo times were shared by linear interpolation. This process continued until the outer ring was reached by using an algorithm with a pseudo-golden angle ratio (21). Multiple echoes were acquired and could be reconstructed by using a k-space tiering method that preserved the targeted echo time T2 weighting. A composite image of all acquired echo times was enabled from the full k-space data set (ie, all radial views at all echo times throughout k-space), as previously described in the study by Altbach and colleagues (22) and T2 mapping reconstructions from the multiple echo acquisitions (Fig 2).

We used the following free-breathing parameters: repetition time msec/reconstructed echo times msec, 2350/20, 50, 85, 100 and 150; flip angle, 145°; pixel size, 1.6 × 1.6 mm<sup>2</sup>; section thickness, 1.6 mm; no section interleave; respiratory binning method by using prospective acquisition correction at functional residual capacity; and mean acquisition time, 12 minutes. The set of two-dimensional images was subsequently compiled into a 3D volume of isotropic voxels (1.6 mm<sup>3</sup>) that allowed for 3D reformations (Fig 3). This spin-echo sequence had low signal intensity from

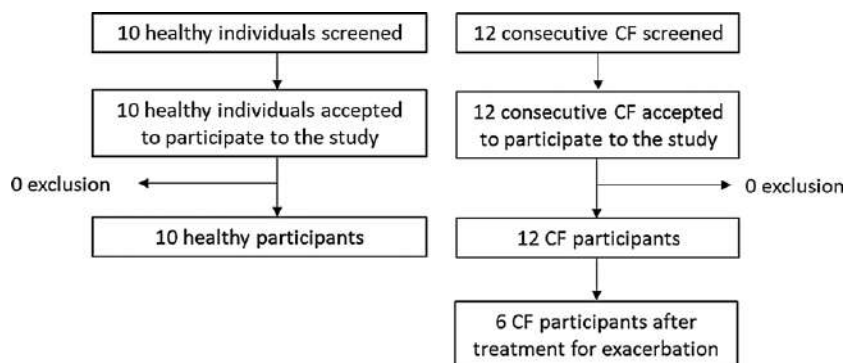


**Figure 1:** Study flowchart. CF = cystic fibrosis.

vessels, and the use of long echo times ( $\leq 150$  msec) in addition to the plane spatial saturation before each echo train helped to further decrease the signal intensity from slow flow (Figs 2–4).

The total acquisition time of the full MRI protocol was 16–18 minutes.

**CT protocol.**—CT examinations were performed by using a CT imager (Somatom Definition 64; Siemens Healthcare) in the supine position, on the axial plane, without contrast agent injection, during a 15-second breath-hold maneuver at end normal expiration (functional residual capacity). The isotropic voxel size was 0.6–0.7 mm<sup>3</sup> (Table E2 [online]).

**Pulmonary function testing.**—Pulmonary function tests were assessed by using body plethysmography (BodyBox, HypAir Compact; Medisoft, Sorinnes, Belgium). The forced expiratory volume in 1 second (FEV<sub>1</sub>), forced vital capacity, functional residual capacity, residual volume, and total lung capacity were measured and expressed as percentage of predicted value for age and sex.

### MRI Evaluation of T2-weighted RFSE Sequence

**Qualitative assessment.**—Lung motion artifact of the lung-liver interface was scored by using a Likert scale as follows: 0, no artifact; 1, minimal; 2, moderate (local, < 10% of the interface); 3, substantial ( $\geq 10\%$  and < 50% of the interface); and 4, severe (diffuse,  $\geq 50\%$  of the interface). The lobar visibility of airways was scored as follows: 0, not visible; 1, segmental; 2, subsegmental; 3, sub-subsegmental; and 4, more than the sub-subsegmental level. The lobar vessel visibility was assessed at 3D UTE as reference in healthy volunteers, and at CT as the reference in CF as follows: 0, not visible; 1, less than 10% visibility; 2, 11%–50% visibility; 3, 51%–75% visibility; and 4, more than 75% visibility. Airways and vessels were scored in every lobe and averaged to get a single mean value per each participant.

**Quantitative assessment.**—The pipeline to quantify T2-weighted high-signal-intensity volume (HSV) is described in Appendix E1 (online). Briefly, the black-blood T2-weighted RFSE pulse sequence could not discriminate the lung parenchyma from heart and vessels and surrounding thoracic soft tissues because of the

use of both spatial and fat saturation. To overcome this issue, both 3D UTE and T2-weighted RFSE were performed at the same lung volume, and 3D UTE was interpolated to match the spatial resolution of T2-weighted RFSE (23) before registration (Table E1 [online]). Therefore, images were registered by using an optimized multimodal intensity-based algorithm (24). First, an iterative algorithm to select the optimal threshold on the basis of splitting the image histogram into two classes was performed on 3D UTE images to create a lung mask (25), which was closed by using a 3D rolling-ball algorithm (26). The lung mask

was then applied to the T2-weighted RFSE-registered images to isolate the lung volume (Fig E1 [online]).

Second, structures with high signal intensity were segmented by using a high-pass filter. For this, the standard deviation (SD) of air was automatically measured on the axial plane in all pixels located at more than 2 cm from the anterior chest surface within the middle third of the stack of sections. Then, the mode of the histogram of the lung parenchyma signal intensity distribution plus 12 SDs of air (hereafter, referred to as mode + 12 SDs of air) was chosen as a low-cut threshold. Because MRI examinations were not calibrated, this approach enabled an adaptive thresholding, similar to that previously reported by using CT (12) (Fig E2 [online]). The HSV could be calculated and displayed by using a volume-rendering technique (Figs 4, E3 [online]). To consider intersubject variability related to different lung volumes, particularly between children and adults, HSV was normalized to the lung volume to calculate T2-weighted HSV.

Third, the 3D HSV mask was fused to the corresponding 3D T2 maps to add the T2 value information at every point of HSV (Fig 4). A composite index was called the T2 VIP and calculated as follows:

$$T2 - VIP = \frac{\left[ \sum_{i=0}^{max} (T2i \times HSVi) \right]}{V_{lung}} \text{ (in milliseconds)},$$

wherein  $T2i$  is the T2 value  $i$ ,  $HSVi$  is the HSV of voxels with a T2i value,  $max$  is the maximum T2 value,  $\Sigma$  indicates a sum, and  $V_{lung}$  is the total lung volume. Thresholds other than mode + 12 SDs of air were also empirically tested (ie, mode + four SDs of air, mode + eight SDs of air, mode + 16 SDs of air, and mode + 20 SDs of air).

Finally, the feasibility of regional evaluation was tested, and automated quantifications were available on right, left, upper, and lower lungs (Appendix E1 [online]).

**Imaging analysis.**—All examinations were anonymized and two readers (F.H. and G.D., with 3 and 10 years of experience, respectively, in chest imaging) qualitatively and quantitatively scored the images independently, in random order, blinded from other clinical data and the results from the other reader. The mean of evaluation per examination was chosen as con-

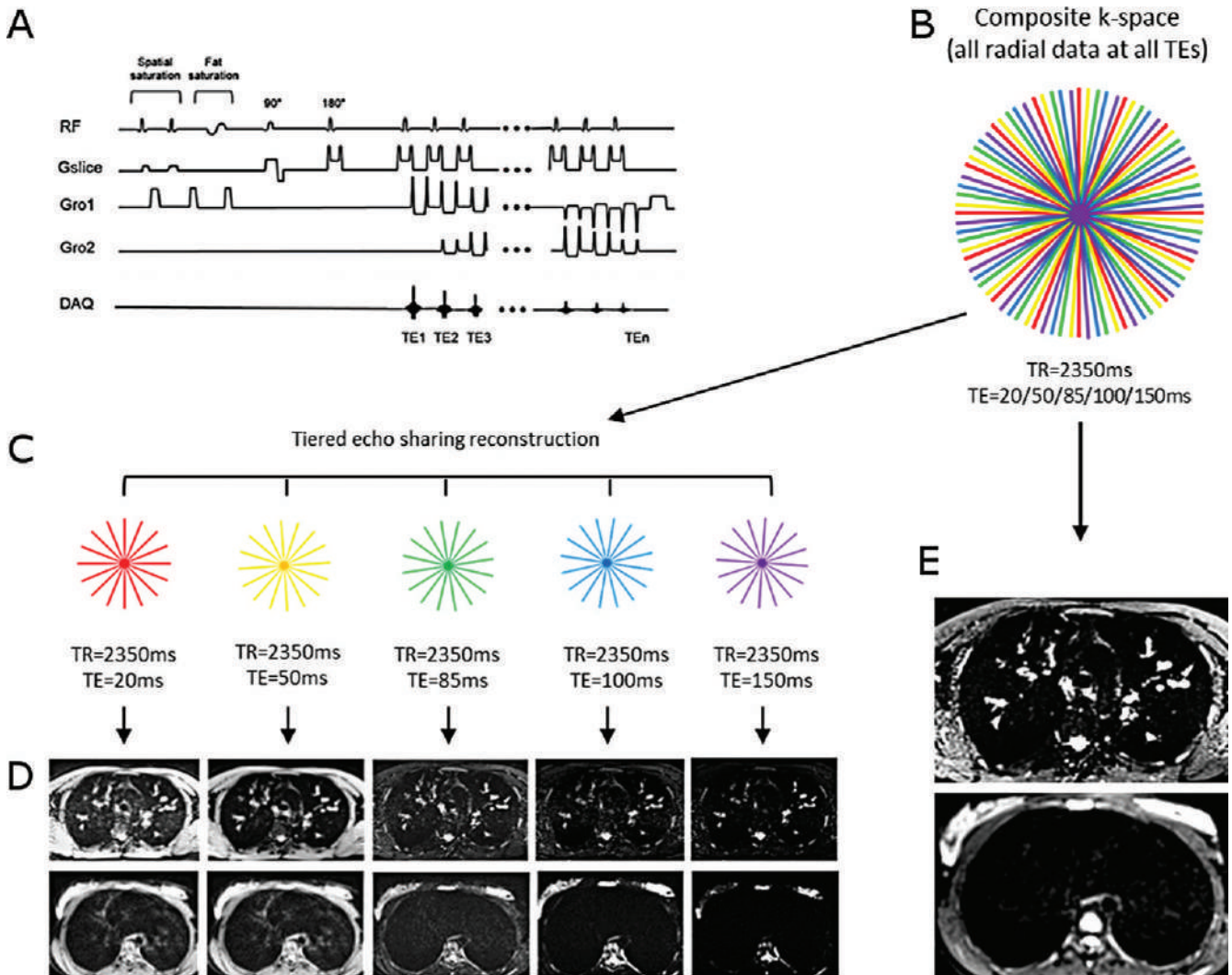


**Figure 2:** Description of the black-blood T2 radial fast spin-echo sequence. **A**, The theoretical principle of the sequence scheme. Each two-dimensional radial fast spin-echo acquisition is acquired on the axial plane after both spatial and fat saturation before each echo train, where the number of echo times (TE<sub>n</sub>) can be freely selected. **B**, **C**, The following parameters were used: repetition time (TR) msec/echo times (TEs) msec, 2350/20 (red), 50 (yellow), 85 (green), 100 (blue), and 150 (purple), which were ordered radially at different angles within the same k-space. By using tiered echo sharing reconstruction, five weighted TEs were obtained. **D**, **E**, Images in the top row were obtained in a male participant with cystic fibrosis (CF), and images in the bottom row were obtained in a healthy female participant. The radial pattern for k-space trajectory is shown, **B**, along with, **E**, a composite image of all five acquired TEs. Therefore, **E**, the contrast is driven by all five TEs with spatial and fat saturation. There is a good visibility of mucus with high signal intensity compared with the background parenchyma in the participant with CF. **E**, Note the lack of lung vessel visibility in participants with CF and healthy participants. A calculation of T2 values with T2 mapping reconstruction is also allowed because of the multiple TE design. DAQ = data acquisition, Gro1 = readout gradient 1, Gro2 = readout gradient 2, Gslice = slice gradient, RF = radiofrequency pulse.

sensus. The visibility of airways and vessels was scored on raw T2-weighted RFSE images and then again after application of the high-signal-intensity mask.

In participants with CF, the interobserver reproducibility of T2-weighted HSV and T2-weighted VIP was calculated. The senior reader (G.D.) repeated the evaluation 1 month later to avoid recall bias, and evaluations from this same reader were used to calculate the intraobserver reproducibility. Finally, data from short-term repeated imaging were used to assess the reproducibility of the consensus evaluation over time only.

#### Additional Assessments of CF Visual Scores by Using MRI and CT

In participants with CF, evaluation of three previously published visual scores were assessed (Tables E3–E5 [online]): the Bhalla

score (7) by using the 3D UTE sequence alone (17), the Eichinger morphologic score (9) by using a combination of both 3D UTE and T2-weighted RFSE, and the Brody II score by using CT (6,10).

MRI and CT visual evaluations were performed randomly by the senior reader (G.D.) in a single session after anonymization of all datasets of images. The senior reader was blinded to any other participant characteristic.

#### Statistical Analysis

Data were expressed as medians with ranges. Medians were compared by using Mann-Whitney test, paired medians were compared by using Wilcoxon signed rank test, and correlations were compared by using Spearman test. Percentage comparison was performed by using Fisher exact test. Reproducibility was

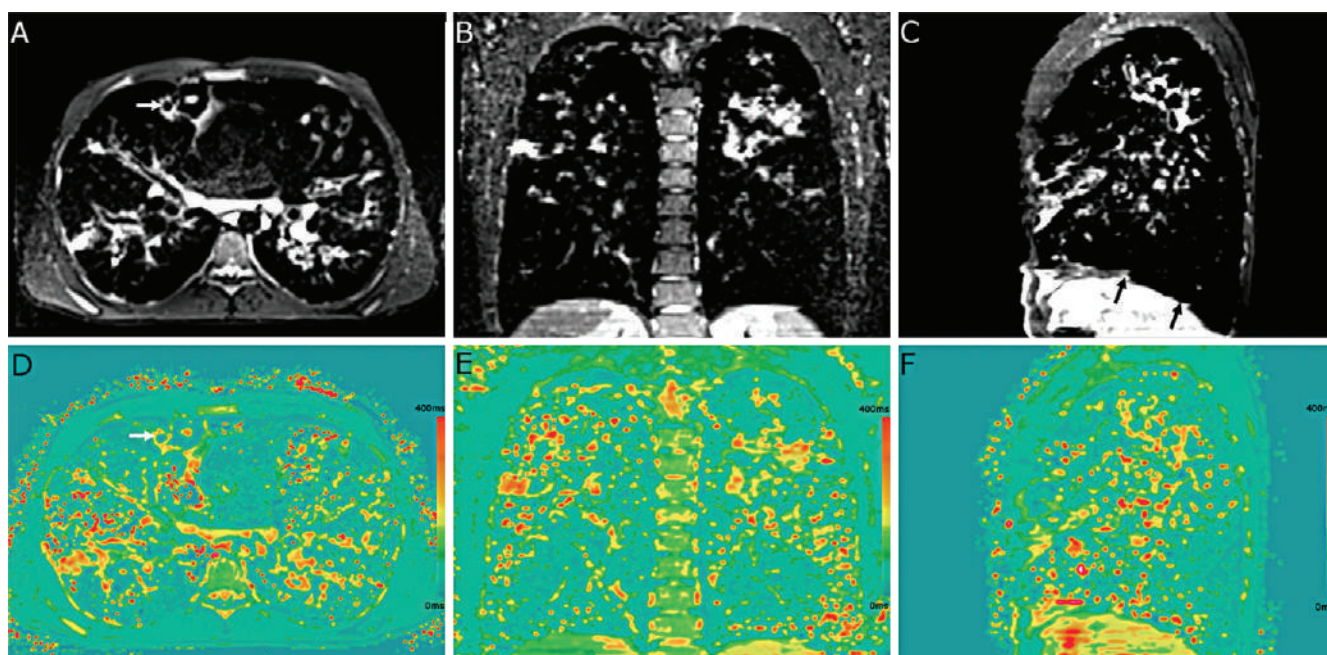


**Figure 3:** Three-dimensional isotropic imaging of the lung (voxel size,  $1.6 \times 1.6 \times 1.6 \text{ mm}^3$ ) by using black-blood contrast T2 radial fast spin-echo sequence (repetition time msec/echo time (TE) msec, 2350/20, 50, 85, 100, 150) with concomitant T2 mapping reconstruction in a 20-year-old man with cystic fibrosis. **A–C**, Images are the composite imaging reconstructed from all five acquired TEs. **D–F**, T2 mapping images that correspond to the images in **A–C**. By adapting the section thickness to the pixel size, three-dimensional isotropic reformations can be reconstructed in the **B, E**, coronal and **C, F**, sagittal planes from the **A, D**, native axial image. Bronchiectasis wall that appears with T2-weighted high signal intensity is shown (white arrows on **A** and **D**). Slight motion artifact toward the diaphragm is shown (black arrows on **C**). **D–F**, The vertical bar indicates the range of T2 values in milliseconds.

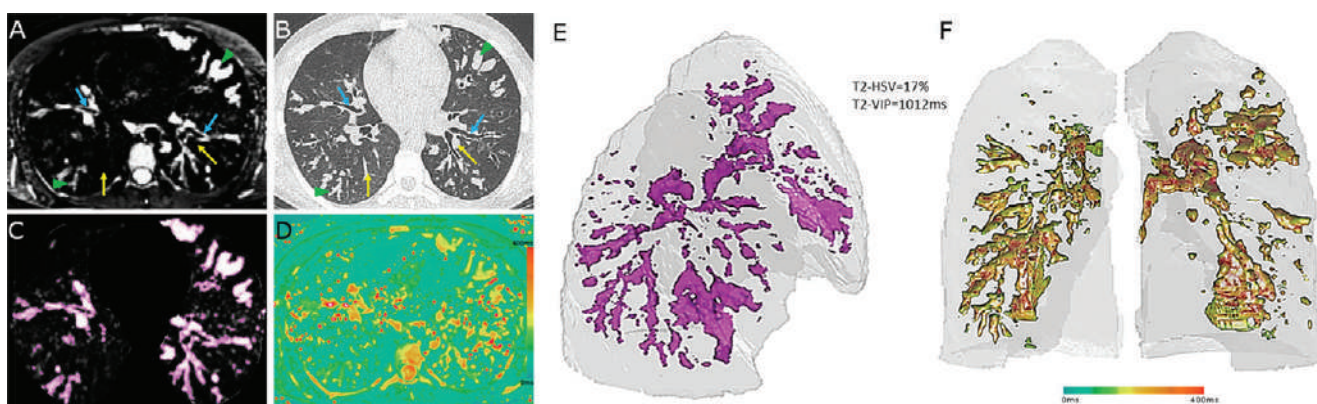


**Figure 4:** Images in a 16-year-old male participant with cystic fibrosis. **A**, Axial black-blood contrast of T2-weighted (T2W) radial fast spin-echo sequence (repetition time msec/echo time msec, 2350/20, 50, 85, 100, 150). **B**, Noncontrast CT scan. **C**, Axial high-signal-intensity mask. Axial T2 mapping, **D**, and volume rendering of **E**, T2W high-signal-intensity volume (HSV) by using an oblique right anterior view and color-coded volume rendering of volume-intensity product (VIP) on coronal view, **F**. Intrapulmonary vessels, **B**, at the segmental level (yellow arrows, left lung) or at further pulmonary artery divisions (yellow arrows, right lung) are shown that are not visible on **A**, an image from MRI. **A, B**, Areas of mucus plugs in large bronchocele (green arrowheads, left lung) or small bronchiolar impaction (green arrowheads, right lung). Areas of bronchial wall thickening are shown (blue arrows on **A** and **B**). A low-cut threshold of mode + 12 standard deviations of extrathoracic air is applied to keep areas of high signal intensity only (purple area on **C**). **E**, This process is extended to every section of the lung acquisition and the final HSV is quantified. A fusion of the high-signal-intensity mask to the corresponding, **D**, T2 map adds information on the T2 value of every pixel of HSV (**D–F**). The vertical bar, **D**, and the corresponding horizontal bar, **F**, indicates the range of T2 values in milliseconds.

assessed by using intraclass correlation coefficients with 95% confidence intervals.

## Results

### Characteristics of Study Participants

First, 10 healthy participants met the inclusion criteria (six men and four women; median age, 21 years; age range, 18–27 years). Next, 12 participants with CF (eight male and four

female participants; median age, 18 years; age range, 9–40 years) were enrolled, and there were no exclusions (Fig 1). The median percentage predicted FEV<sub>1</sub> was 76% (range, 34%–102%). Six of the participants with CF (four male and two female participants; median age, 16 years; age range, 10–24 years) were referred for pulmonary exacerbation and pulmonary function tests, and MRI was repeated after 1 month of treatment. CT was also repeated in one adult (Table 1).

**Table 1: Study Participants Characteristics**

Parameter	Result
Healthy participants ( <i>n</i> = 10)	
Median age (y)	21 (18–27)
Sex	
No. of male participants	6
No. of female participants	4
Body mass index (kg/m <sup>2</sup> )	24 (19–32)
Tobacco consumption	
Yes	0
No	10
Respiratory symptoms	
Yes	0/10
No	
History of lung disease	
Yes	0/10
No	
Lung abnormalities at 3D UTE MRI	
Yes	0/10
No	
Participants with cystic fibrosis ( <i>n</i> = 12)	
Age (y)	18 (9–40)
Sex	
No. of male participants	8
No. of female participants	4
Body mass index (kg/m <sup>2</sup> )	22 (16–31)
Tobacco consumption	
Yes	0
No	12
ΔF508 mutation	
Homozygous	9
Nonhomozygous	3
ABPA status	
Yes	1
No	11
Pulmonary function tests	
Percentage predicted FEV <sub>1</sub>	76 (34–102)
Percentage predicted FEV <sub>1</sub> /FVC	71 (36–83)
Percentage predicted FRC	100 (93–175)
Percentage predicted RV	112 (71–204)
Percentage predicted TLC	96 (86–118)

Note.—For continuous variables, data are medians and data in parentheses are range. For categorical variables, data are absolute value. Data of pulmonary function tests are expressed as percentage of predicted value. 3D = three-dimensional, ABPA = allergic bronchopulmonary aspergillosis, FEV<sub>1</sub> = forced expiratory volume in 1 second, FRC = functional residual capacity, FVC = forced vital capacity, RV = residual volume, TLC = total lung capacity, UTE = ultrashort echo time.

### Initial Evaluation of T2-weighted RFSE in Healthy Participants and Participants with CF

In healthy participants, a few normal airways and vessels were visible, although with low signal intensity. However, because of both the black-blood properties of T2-weighted RFSE and the

**Table 2: Image Quality Characteristics of the T2-weighted Radial Fast Spin-Echo Sequence**

Parameter	Healthy Participants ( <i>n</i> = 10)	Participants with CF ( <i>n</i> = 12)	<i>P</i> Value
Respiratory motion artifact			
Diaphragm blurring (score of 0–4)	1 (1–2)	1 (1–2)	.59
T2-weighted RFSE			
Visibility of airways (score of 0–4)	0.5 (0–1)	3.2 (2–4)	<.001
Visibility of vessels (score of 0–4)	0.2 (0–0.4)	0.1 (0–0.6)	NA
High-signal-intensity mask			
Visibility of airways (score of 0–4)	0	3 (2–4)	<.001
Visibility of vessels (score of 0–4)	0	0	NA
T2-weighted HSV (%)	0	4.1 (0.1–17)	<.001
T2-weighted VIP (msec)	0	303 (39–1012)	<.001

Note.—Unless otherwise indicated, data are medians and data in parentheses are range. A *P* value less than .05 was considered to indicate statistical significance. The average of two independent readings was chosen as consensus. T2-weighted radial fast spin echo (RFSE) corresponds to the raw images from MRI reconstructed from the composite k-space of all radial views at all echo times. The high-signal-intensity mask corresponds to the segmented lung structures within T2-weighted RFSE and with high signal intensity only, defined by using a low-cut threshold of mode of the lung signal intensity histogram plus 12 standard deviations of the signal intensity of extrathoracic air. Motion artifact at the lung-liver interface was scored as follows: 0, no artifact; 1, minimal; 2, moderate (local, <10% of the interface); 3, substantial (≥10% and < 50% of the interface); and 4, severe (diffuse, ≥50% of the interface). Airway visibility was scored in every lobe and averaged per each participant as follows: 0, no depiction; 1, segmental; 2, subsegmental; 3, sub-subsegmental; 4, more than the sub-subsegmental level. Vessel visibility was scored in every lobe and averaged per each participant as follows: 0, no visibility; 1, less than 10% visibility; 2, 11%–50% visibility; 3, 51%–75% visibility; and 4, more than 75% visibility. CF = cystic fibrosis, HSV = high-signal-intensity volume; VIP = volume-intensity product; NA = not applicable.

use of a high-pass filter, no vessels and no airways were visually noticed within a high-signal-intensity mask (vessel visibility score, 0). Therefore, both T2-weighted HSV and T2-weighted VIP were scored as 0 (Table 2, Fig E3 [online]). In patients with CF, the vessel visibility score was also 0 within the high-signal-intensity mask (Fig 5). The median T2-weighted HSV was 4.1% (range, 0.1%–17.0%) and the median T2-weighted VIP was 303 msec (range, 39–1012 msec), whereas both metrics were statistically different from those of the healthy participants (*P* < .001). In participants with CF, T2-weighted VIP was higher in the upper lung than in the lower lung (*P* = .01)

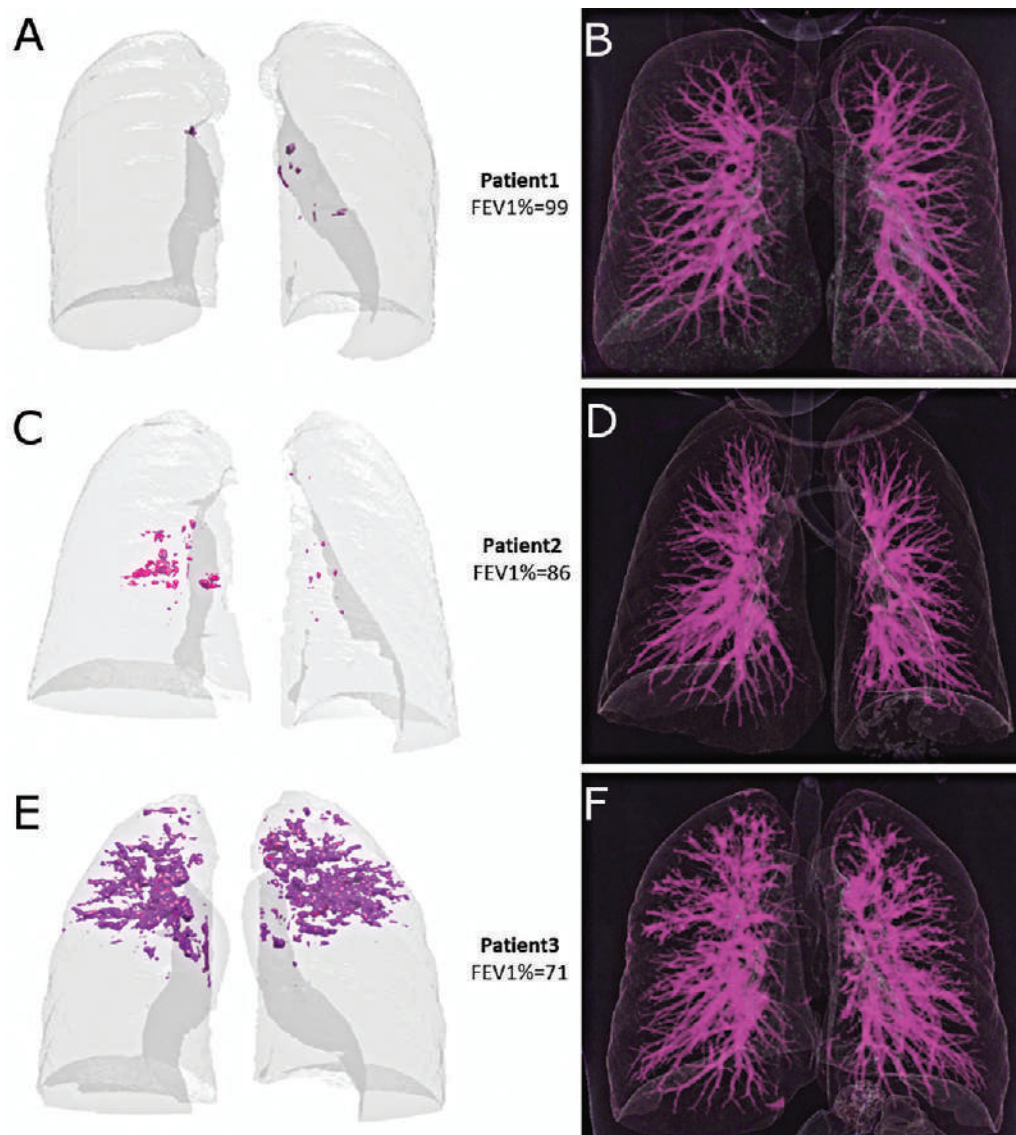


**Figure 5:** High-signal-intensity volume images segmented by using MRI in, **A, B**, a 28-year-old male participant with cystic fibrosis (CF), **C, D**, a 10-year-old female participant with CF, and, **E, F**, a 24-year-old male participant with CF. The three participants with CF with an increasing level of severity are shown from top to bottom (purple areas). In the left column, there are increasing T2-weighted (T2W) high-signal-intensity volumes (HSVs) from top to bottom (**A**, 0.2%; **C**, 2.1%; and **E**, 8%, respectively). In the right column, both normal vessels and CF-related structural alterations are shown by using a volume-rendering technique (**B, D, F**) of the corresponding images in the left column (**A, C, E**). Note the lack of normal pulmonary vessels in the T2W HSV mask (**A, C, E**) compared with those visible on the volume-rendered examination (**B, D, F**). FEV1% = percentage predict forced expiratory volume in 1 second.

(Table E6 [online]). The mean time for the full postprocessing technique was 1 minute.

#### Correlations of Quantitative T2-weighted RFSE

In participants with CF, T2-weighted HSV and T2-weighted VIP correlated to both percentage predicted FEV<sub>1</sub> ( $\rho = -0.88$  and  $\rho = -0.94$ , respectively;  $P < .001$ ), and FEV<sub>1</sub>/forced vital capacity ( $\rho = -0.75$  and  $\rho = -0.76$ ; respectively;  $P \leq .005$ ) (Table 3).

The threshold of mode + 12 SDs of air had the highest correlations with pulmonary function testing (Table E7 [online]). In addition, significant correlations were found between MRI quantitative metrics and total visual scores, and

specific items related to wall thickening and bronchiectasis, mucus plugs, consolidation, and air trapping (Tables 3, E8 [online], E9 [online]).

#### Follow-up at Treatment

In six participants with CF who were treated for a respiratory exacerbation, there was an increase in percentage predicted FEV<sub>1</sub> ( $P = .03$ ) and a decrease in T2-weighted HSV ( $P = .03$ ) and T2-weighted VIP ( $P = .03$ ) after treatment (Fig 6, Table E10 [online]). However, T2-weighted VIP was the sole MRI biomarker that was found to correlate with the variation of percentage predicted FEV<sub>1</sub> ( $P = .01$ ) (Table 4). When the MRI metrics of T2-weighted HSV

**Table 3: Correlation Coefficients and Reproducibility of T2-weighted HSV and T2-weighted VIP Values, Pulmonary Function Testing Indexes, and Visual Scores**

Parameter	T2-weighted HSV(msec) (n = 12)	T2-weighted VIP (n = 12)
Pulmonary function tests		
Percentage predicted FEV <sub>1</sub>		
ρ value	−0.88	−0.94
P value	<.001	<.001
Percentage predicted FEV <sub>1</sub> /FVC		
ρ value	−0.75	−0.76
P value	.005	.004
Percentage predicted FRC		
ρ value	0.52	0.55
P value	.08	.06
Percentage predicted RV		
ρ value	0.80	0.82
P value	.001	.001
Percentage predicted TLC		
ρ value	0.63	0.54
P value	.02	.07
MRI Bhalla score		
ρ value	−0.65	−0.74
P value	.02	<.001
MRI Eichinger M score		
ρ value	0.83	0.79
P value	<.001	.002
CT Brody II score		
ρ value	0.68	0.69
P value	.02	.01
Reproducibility (ICC)		
Intraobserver	>0.99	>0.99
Interobserver	>0.99	>0.99
Interscan	0.98 (0.95, 0.99)	0.97 (0.94, 0.99)

Note.—Correlations were tested by using Spearman correlation coefficient (ρ). Data in parentheses are 95% confidence intervals. FEV<sub>1</sub> = forced expiratory volume in 1 second, FRC = functional residual capacity, FVC = forced vital capacity, HSV = high-signal-intensity volume, ICC = intraclass correlation coefficient, RV = residual volume, VIP = volume-intensity product, TLC = total lung capacity.

and T2-weighted VIP are compared with the existing scoring systems for CF at MRI and CT (Bhalla for MRI, Eichinger for MRI, and Brody II for CT) they are at least equal to or better than other biomarker methods for capturing the degree of pulmonary insufficiency as measured by pulmonary function tests.

### Assessment of Reproducibility

By using the automated method, the intra- and interobserver reproducibility of both T2-weighted HSV and T2-

weighted VIP were almost perfect (intraclass correlation coefficients, >0.99 and >0.99, respectively) and good at short-term reproducibility (intraclass correlation coefficient, 0.98 and 0.97, respectively).

### Discussion

This work demonstrates that a method for the automated quantification of lung MRI parenchymal high-signal-intensity volume (HSV) is feasible for patients with cystic fibrosis (CF) by using a radial fast spin-echo pulse sequence with long echo times. In healthy volunteers, the mean T2-weighted high signal volume was equal to 0%, demonstrating no quantification of normal airways or vessels. However, in participants with CF, T2-weighted HSV and T2-weighted volume-intensity product (VIP) were correlated to pulmonary function testing indexes (ie, percentage predicted forced expiratory volume in 1 second [FEV<sub>1</sub>], ρ = −0.88 and −0.94 for T2-weighted HSV and T2-weighted VIP, respectively; *P* < .001). Decreases of T2-weighted HSV and T2-weighted VIP were shown in six participants with CF after their treatment for respiratory exacerbation (*P* = .03). The intra- and interobserver reproducibility of the automated method was high (intraclass correlation coefficient, >0.99).

Structural abnormalities with high T2 signal intensity are known to relate to an increase in water and/or cellular content (27). Although high T2 value cannot discriminate between mucus plugs, vasogenic edema, cytotoxic edema, cellular infiltration, or pneumonia (28), in the clinical context of CF, all of these features are likely related to CF inflammation (15). Interestingly, recent CF literature has shown that a visual increase in T2-weighted signal intensity allows for the diagnosis of acute respiratory exacerbations (16,29,30). Our study supports the findings of other groups, which is that a significant decrease in the T2-weighted signal intensity was observed after treatment (30). High-signal-intensity T2 structures were also found to correlate to both the disease severity (29,30) and biologic markers of inflammation (11,18). By using our method, the volumetric measurement of T2-weighted HSV was specific for such high-signal-intensity abnormalities. This suggests that our method may be promising for monitoring the many types of inflammatory changes that occur in CF, particularly in patients with mild-to-moderate disease severity. Indeed, the ability of T2-weighted MRI to depict early forms of CF has already been demonstrated by using visual scores (30,31) and thus, because of the correlation of the MRI metrics to the conventional visual methods, a transposition of the quantitative technique is expected. In addition, there is a recent interest in removing the lung vessels to improve imaging evaluation (32). For instance, in patients with CF, the black-blood property of the T2-weighted RFSE is a spin-echo sequence that may help to discriminate between endobronchial mucus plugs and the adjacent pulmonary arterial vessel, which is not possible by using noncontrast two-dimensional imaging (14), particularly in young patients with CF and small bronchi. This method removes vessel contamination from the quantitative airway measurements (33).

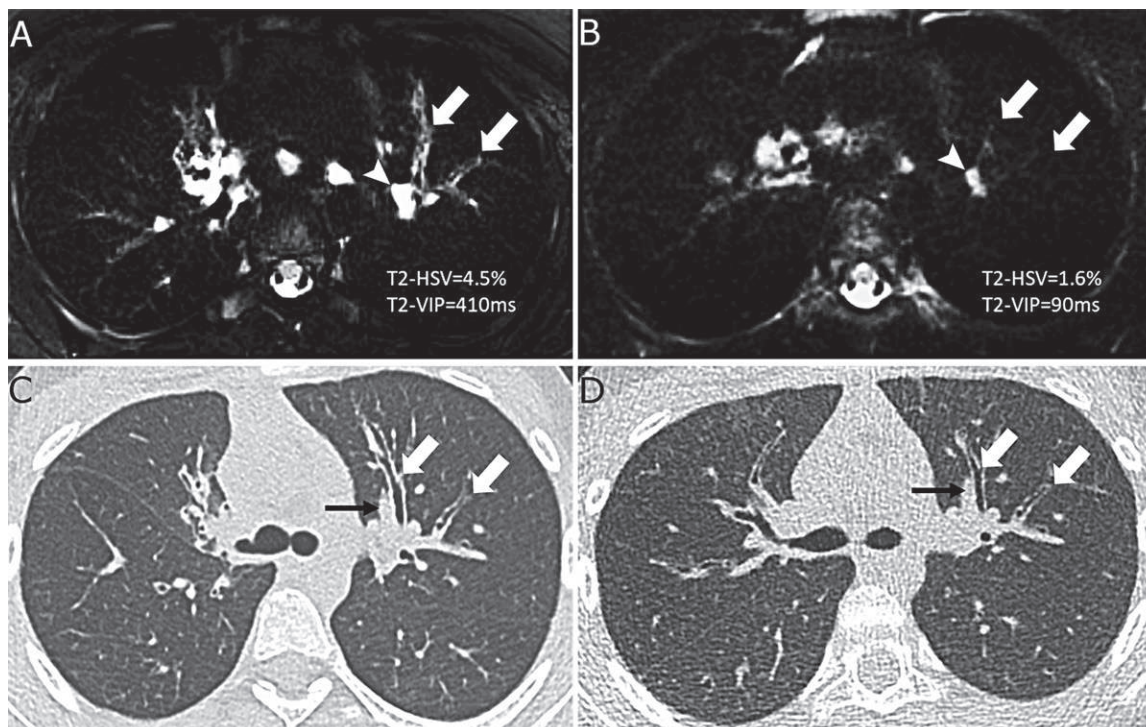


**Figure 6:** Images in a 24-year-old woman with cystic fibrosis before, **A, C**, and after, **B, D**, intravenous antibiotic treatment for a pulmonary exacerbation. Axial black-blood noncontrast-enhanced T2-weighted radial fast spin-echo sequence, **A, B** (repetition time msec/echo time msec, 2350/20, 50, 85, 100, 150), and axial noncontrast-enhanced CT scan, **C, D**. Shown are segmental bronchi in the left upper lobe that have a markedly increased T2-weighted signal intensity contrast during exacerbation (white arrows). Note the lack of normal vessel visibility on **A** and **B**. By using CT, there was subjective bronchial wall thickening on **C** that did not reach the objective threshold of more than 1× the diameter of the adjacent vessel (black arrows), both, **C**, before and, **D**, after treatment. Decreases in size and signal intensity of intrapulmonary lymph nodes (white arrowheads on **A** and **B**) are also shown. Finally, **A, B**, the overall quantification of relative high-signal-intensity volume (HSV) and volume-intensity product (VIP) decreased after treatment by −63% and −78%, respectively.

In our study, we explored the value of T2-weighted signal intensity as an MRI-specific feature. Interestingly, the decrease of lung T2-weighted VIP was related to the improvement in percentage predicted FEV<sub>1</sub> after antibiotic treatment, but not T2-weighted HSV. This suggests that absolute value of the T2-weighted signal intensity may have additional functional information compared with the volume of these T2-weighted lesions. Moreover, pulmonary function tests are not available in infants and preschool children, although lung MRI is available (30,31), and imaging can depict alterations before pulmonary function test modifications (11). In addition, percentage predicted FEV<sub>1</sub> is a global biomarker, whereas imaging allows quantification of the regional distribution of the disease (6,7,9). We showed that automation of lung MRI T2-weighted signal abnormalities is reproducible and may help to simplify and standardize CF evaluations.

We also demonstrated successful registration of 3D UTE and T2-weighted RFSE acquisitions as a single data set. This is similar to the coregistration of PET/CT examinations. Recent studies with CT have demonstrated that whereas bronchiectasis is not reversible (3,34), a decrease in wall thickening and mucus can be found (3,34). In this contemporary context, T2-weighted HSV may be a tool that can monitor potentially reversible alterations, with the ability to follow up their severity quantitatively in a nonionizing and noncontrast-enhanced

manner. Therefore, T2-weighted HSV could be a relevant imaging biomarker for the early diagnosis of CF inflammation in the bronchial wall before the development of bronchiectasis (3,34). We showed that when T2-weighted HSV and T2-weighted VIP are compared with the existing scoring systems for CF at MRI, they were in some instances better than the other imaging-based scoring methods for capturing the degree of pulmonary insufficiency as measured by pulmonary function tests before and after a CF exacerbation (Table 4).

Our study had limitations. This was a single-center feasibility study with a small sample size. In addition, the T2-weighted RFSE spin echo used for this study was recent, although in principle it could be programmed to work on any 1.5-T MRI hardware. Moreover, T2-weighted HSV was not able to capture abnormalities with low signal intensity such as mucus-free bronchiectasis, mucus impaction with a low T2-weighted signal intensity (35), air trapping (6,10,36), or perfusion defects (30). Thus, automated measurements from black-blood T2-weighted images should not supplant a detailed visual analysis with a UTE T1-weighted examination, such as the 3D UTE pulse sequence that we also used (17). Finally, the acquisition time was 18 minutes, which was in the range of or lower than published protocols (9,36). Therefore, additional sequences focused on ventilation and/or perfusion (8,36) may be worthwhile to further enhance the multiparametric lung MRI examination.

**Table 4: Correlation between MRI Quantitative Metrics, Visual Scores, and Pulmonary Function Tests**

Parameter	Percentage Predicted FEV <sub>1</sub>		Percentage Predicted FEV <sub>1</sub> /FVC		Percentage Predicted FRC	
	$\rho$ Value	<i>P</i> Value	$\rho$ Value	<i>P</i> Value	$\rho$ Value	<i>P</i> Value
<b>MRI quantitative</b>						
T2-weighted HSV (%)						
Pretreatment value ( <i>n</i> = 6)	-0.87	.03	-0.69	.13	0.50	.31
Posttreatment value ( <i>n</i> = 6)	-0.83	.04	-0.60	.20	0.49	.32
Variation* ( <i>n</i> = 6)	0.67	.14	-0.36	.48	0.38	.46
T2-weighted VIP (msec)						
Pretreatment value ( <i>n</i> = 6)	-0.92	.008	-0.45	.37	0.66	.15
Posttreatment value ( <i>n</i> = 6)	-0.94	.005	-0.37	.46	0.66	.15
Variation* ( <i>n</i> = 6)	0.90	.01	-0.48	.33	0.73	.10
<b>MRI Bhalla score</b>						
Pretreatment value ( <i>n</i> = 6)	0.69	.13	0.76	.08	-0.76	.08
Posttreatment value ( <i>n</i> = 6)	0.85	.03	0.43	.39	-0.79	.06
Variation* ( <i>n</i> = 6)	0.02	.97	0.23	.65	0.05	.93
<b>MRI Eichinger M score</b>						
Pretreatment value ( <i>n</i> = 6)	-0.45	.37	-0.73	.09	0.63	.18
Posttreatment value ( <i>n</i> = 6)	-0.76	.08	-0.63	.17	0.69	.13
Variation* ( <i>n</i> = 6)	0.16	.75	0.12	.81	0.55	.25
<b>CT Brody II score</b>						
Pretreatment value ( <i>n</i> = 6)	-0.81	.052	0.52	.29	0.50	.30
Posttreatment value ( <i>n</i> = 1)	NA	NA	NA	NA	NA	NA
Variation* ( <i>n</i> = 1)	NA	NA	NA	NA	NA	NA

Note.—Data are Spearman correlation coefficient ( $\rho$ ). Data are before and after treatment with antibiotics in six participants with cystic fibrosis who had pulmonary exacerbation. FEV<sub>1</sub> = forced expiratory volume in 1 second, FRC = functional residual capacity, FVC = forced vital capacity, HSV = high-signal-intensity volume, NA = not applicable, VIP = volume-intensity product.

\* Variation corresponds to the difference of measurement before and after treatment. Pretreatment, posttreatment, and variation of MRI and CT scorings were correlated to pretreatment, posttreatment, and variation of pulmonary function test indexes, respectively. Data of pulmonary function test are expressed as percentage of predicted value.

In this single center pilot study of participants with cystic fibrosis, we found that the automated quantification of lung MRI high-signal-intensity volume was a reproducible imaging biomarker that correlated with pulmonary function testing severity and improved after treatment.

**Acknowledgments:** The study was conducted within the context of the Laboratory of Excellence TRAIL, ANR-10-LABX-57. The authors thank Wadie Benhasen, PhD, and Fei Han, PhD, for technical support.

**Author contributions:** Guarantors of integrity of entire study, F.H., J.M., G.D.; study concepts/study design or data acquisition or data analysis/interpretation, all authors; manuscript drafting or manuscript revision for important intellectual content, all authors; approval of final version of submitted manuscript, all authors; agrees to ensure any questions related to the work are appropriately resolved, all authors; literature research, all authors; clinical studies, all authors; experimental studies, I.B., F.H., G.D.; statistical analysis, I.B., S.B., G.D.; and manuscript editing, I.B., F.H., S.B., P.B., F.L., G.D.

**Disclosures of Conflicts of Interest:** I.B. Activities related to the present article: disclosed grant from the French Society of Radiology. Activities not related to the present article: disclosed no relevant relationships. Other relationships: disclosed no relevant relationships. F.H. disclosed no relevant relationships. J.M. disclosed no relevant relationships. S.B. disclosed no relevant relationships. P.B. Activities related to the present article: disclosed no relevant relationships. Activities not related to the present article: disclosed money paid to author for board memberships from AstraZeneca, Boehringer Ingelheim, Circallia, Menarini, Novartis, and Sanofi;

disclosed money paid to author for consultancy from AstraZeneca, Novartis, and Sanofi; disclosed money to author's institution for grants/grants pending from AstraZeneca, Boehringer Ingelheim, and Novartis; disclosed money paid to author for lectures including service on speakers bureaus from AstraZeneca, Boehringer Ingelheim, Circassia, Menarini, and Novartis; disclosed money to author's institution for patents; disclosed money paid to author for development of education presentations from Boehringer Ingelheim; disclosed travel/accommodations/meeting expenses unrelated to activities already listed from AstraZeneca, Boehringer Ingelheim, and Novartis. Other relationships: disclosed no relevant relationships. F.L. disclosed no relevant relationships. G.D. disclosed no relevant relationships.

## References

- Szczesniak R, Turkovic L, Andrinopoulou ER, Tiddens HAWM. Chest imaging in cystic fibrosis studies: What counts, and can be counted? *J Cyst Fibros* 2017;16(2):175–185.
- Rayment JH, Couch MJ, McDonald N, et al. Hyperpolarised <sup>129</sup>Xe magnetic resonance imaging to monitor treatment response in children with cystic fibrosis. *Eur Respir J* 2019;53(5):1802188.
- Ronan NJ, Einarsson GG, Twomey M, et al. CORK Study in Cystic Fibrosis: Sustained Improvements in Ultra-Low-Dose Chest CT Scores After CFTR Modulation With Ivacaftor. *Chest* 2018;153(2):395–403.
- Leuraud K, Richardson DB, Cardis E, et al. Ionising radiation and risk of death from leukaemia and lymphoma in radiation-monitored workers (INWORKS): an international cohort study. *Lancet Haematol* 2015;2(7):e276–e281.
- Saake M, Schmide A, Kopp M, et al. MRI Brain Signal Intensity and Relaxation Times in Individuals with Prior Exposure to Gadobutrol. *Radiology* 2019;290(3):659–668.
- Brody AS, Klein JS, Molina PL, Quan J, Bean JA, Wilmott RW. High-resolution computed tomography in young patients with cystic fibrosis:

- distribution of abnormalities and correlation with pulmonary function tests. *J Pediatr* 2004;145(1):32–38.
7. Bhalla M, Turcios N, Aponte V, et al. Cystic fibrosis: scoring system with thin-section CT. *Radiology* 1991;179(3):783–788.
  8. Zha W, Nagle SK, Cadman RV, Schiebler ML, Fain SB. Three-dimensional Isotropic Functional Imaging of Cystic Fibrosis Using Oxygen-enhanced MRI: Comparison with Hyperpolarized  $^3\text{He}$  MRI. *Radiology* 2019;290(1):229–237.
  9. Eichinger M, Optazait DE, Kopp-Schneider A, et al. Morphologic and functional scoring of cystic fibrosis lung disease using MRI. *Eur J Radiol* 2012;81(6):1321–1329.
  10. Loeve M, Lequin MH, de Bruijne M, et al. Cystic fibrosis: are volumetric ultra-low-dose expiratory CT scans sufficient for monitoring related lung disease? *Radiology* 2009;253(1):223–229.
  11. Calder AD, Bush A, Brody AS, Owens CM. Scoring of chest CT in children with cystic fibrosis: state of the art. *Pediatr Radiol* 2014;44(12):1496–1506.
  12. Chassagnon G, Martin C, Burgel PR, et al. An automated computed tomography score for the cystic fibrosis lung. *Eur Radiol* 2018;28(12):5111–5120.
  13. Helbich TH, Heinz-Peer G, Eichler I, et al. Cystic fibrosis: CT assessment of lung involvement in children and adults. *Radiology* 1999;213(2):537–544.
  14. Rosenow T, Oudraad MCJ, Murray CP, et al. PRAGMA-CF. A Quantitative Structural Lung Disease Computed Tomography Outcome in Young Children with Cystic Fibrosis. *Am J Respir Crit Care Med* 2015;191(10):1158–1165.
  15. Wielpütz MO, Eichinger M, Biederer J, et al. Imaging of Cystic Fibrosis Lung Disease and Clinical Interpretation. *Rofo* 2016;188(9):834–845.
  16. Renz DM, Scholz O, Böttcher J, et al. Comparison between magnetic resonance imaging and computed tomography of the lung in patients with cystic fibrosis with regard to clinical, laboratory, and pulmonary functional parameters. *Invest Radiol* 2015;50(10):733–742.
  17. Dournes G, Yazbek J, Benhassen W, et al. 3D ultrashort echo time MRI of the lung using stack-of-spirals and spherical  $k$ -Space coverages: Evaluation in healthy volunteers and parenchymal diseases. *J Magn Reson Imaging* 2018;48(6):1489–1497.
  18. Protocole National de Diagnostic et de Soins Mucoviscidose. Haute Autorité de Santé. [https://www.has-sante.fr/portail/upload/docs/application/pdf/2017-09/pnds\\_2017\\_vf1.pdf](https://www.has-sante.fr/portail/upload/docs/application/pdf/2017-09/pnds_2017_vf1.pdf). Published January 1, 2017. Updated September 1, 2017. Accessed May 14, 2019.
  19. Natsuaki Y, Keerthisavan MB, Bilgin A, et al. Flexible and Efficient 2D Radial TSE T2 Mapping with Tiered Echo Sharing and with “Pseudo” Golden Angle Ratio. *International Society of Magnetic Resonance in Medicine*. <http://archive.ismrm.org/2017/0369.html>. Published April 22, 2017. Accessed May 14, 2019.
  20. Klessen C, Asbach P, Kroencke TJ, et al. Magnetic resonance imaging of the upper abdomen using a free-breathing T2-weighted turbo spin echo sequence with navigator triggered prospective acquisition correction. *J Magn Reson Imaging* 2005;21(5):576–582.
  21. Svedin BT, Payne A, Bolster BD Jr, Parker DL. Multiecho pseudo-golden angle stack of stars thermometry with high spatial and temporal resolution using  $k$ -space weighted image contrast. *Magn Reson Med* 2018;79(3):1407–1419.
  22. Altbach MI, Bilgin A, Li Z, Clarkson EW, Trouard TP, Gmitro AF. Processing of radial fast spin-echo data for obtaining T2 estimates from a single  $k$ -space data set. *Magn Reson Med* 2005;54(3):549–559.
  23. Goshtasby A, Turner DA, Ackerman LV. Matching of tomographic slices for interpolation. *IEEE Trans Med Imaging* 1992;11(4):507–516.
  24. Woo J, Stone M, Prince JL. Multimodal registration via mutual information incorporating geometric and spatial context. *IEEE Trans Image Process* 2015;24(2):757–769.
  25. Ridler TW, Calvard S. Picture Thresholding Using an Iterative Selection Method. *IEEE Trans Syst Man Cybern Syst* 1978;8(8):630–632.
  26. Armato SG III, Giger ML, Blackburn JT, Doi K, MacMahon H. Three-dimensional approach to lung nodule detection in helical CT. In: Hanson KM, ed. *Proceedings of SPIE: medical imaging 1999—image processing*. Vol 3661. Bellingham, Wash: International Society for Optical Engineering, 1999; 553–559.
  27. Vogel-Claussen J, Renne J, Hinrichs J, et al. Quantification of pulmonary inflammation after segmental allergen challenge using turbo-inversion recovery-magnitude magnetic resonance imaging. *Am J Respir Crit Care Med* 2014;189(6):650–657.
  28. Moldoveanu B, Otmishi P, Jani P, et al. Inflammatory mechanisms in the lung. *J Inflamm Res* 2009;2:1–11.
  29. Scholz O, Denecke T, Böttcher J, et al. MRI of cystic fibrosis lung manifestations: sequence evaluation and clinical outcome analysis. *Clin Radiol* 2017;72(9):754–763.
  30. Wielpütz MO, Puderbach M, Kopp-Schneider A, et al. Magnetic resonance imaging detects changes in structure and perfusion, and response to therapy in early cystic fibrosis lung disease. *Am J Respir Crit Care Med* 2014;189(8):956–965.
  31. Stahl M, Wielpütz MO, Graeber SY, et al. Comparison of Lung Clearance Index and Magnetic Resonance Imaging for Assessment of Lung Disease in Children with Cystic Fibrosis. *Am J Respir Crit Care Med* 2017;195(3):349–359.
  32. Milanese G, Eberhard M, Martini K, Vittoria De Martini I, Frauenfelder T. Vessel suppressed chest Computed Tomography for semi-automated volumetric measurements of solid pulmonary nodules. *Eur J Radiol* 2018;101:97–102.
  33. de Jong PA, Ottink MD, Robben SGF, et al. Pulmonary disease assessment in cystic fibrosis: comparison of CT scoring systems and value of bronchial and arterial dimension measurements. *Radiology* 2004;231(2):434–439.
  34. Chassagnon G, Hubert D, Fajac I, Burgel PR, Revel MP; investigators. Long-term computed tomographic changes in cystic fibrosis patients treated with ivacaftor. *Eur Respir J* 2016;48(1):249–252.
  35. Dournes G, Berger P, Refait J, et al. Allergic Bronchopulmonary Aspergillosis in Cystic Fibrosis: MR Imaging of Airway Mucus Contrasts as a Tool for Diagnosis. *Radiology* 2017;285(1):261–269.
  36. Veldhoen S, Weng AM, Knapp J, et al. Self-gated Non-Contrast-enhanced Functional Lung MR Imaging for Quantitative Ventilation Assessment in Patients with Cystic Fibrosis. *Radiology* 2017;283(1):242–251.

## Appendix E1

### Quantification of T2-High-Signal Intensity Volume and Volume-Intensity Product

The quantification of MRI metrics were done by using an in-house software program written in MATLAB (The MathWorks, Inc., Natick, Massachusetts, USA). First, 3D-UTE acquired in the coronal plane with an isotropic voxel dimension of  $(1 \times 1 \times 1 \text{ mm})^3$  was reformatted in the axial plane. Since section thickness was slightly different between 3D-UTE (1 mm) and T2 radial turbo spin echo sequence (T2 RTSE images (1.6 mm), an interpolation of 3D-UTE sections was needed to match sections of the T2 TSE sequence (Table E1). Indeed, MR images from 3D-UTE and T2 RTSE sequences were acquired at end normal expiration (functional residual capacity), using navigator-triggered prospective acquisitions and thus lung volumes are expected equal between the two sets. To decrease sections number of 3D-UTE images, a linear interpolation was performed between successive sections and an exact match was found between 3D-UTE section and T2 RTSE section (23) (Fig E1, A). To make lung segmentation feasible on T2 RTSE images, first, image registration using optimized multimodal Intensity-based algorithm was applied to 3D-UTE images and T2 RTSE images (1). For this, correlation metrics were performed to compare intensity patterns in source images (T2 RTSE) and target images (3D-UTE). Mutual information considered as similarity metrics were used to minimize uncertainty between the transformed image and original image (2). To maximize similarity, One Plus One Evolutionary algorithm with small initial radius and 100 iterations was used as an optimizer for image registration process Fig E1, B).

Lung segmentation on T2 TSE fat-saturated images using threshold-based techniques is almost impossible since there is no contrast difference between soft tissue structures (muscle, fat and vessels) or cortical bone and the lungs. Conversely, isolating lungs from the rest of thoracic structures on 3D-UTE images is feasible. To do so, a threshold based method was chosen and an iterative algorithm to select the optimal threshold was used. The algorithm is based on splitting image histogram into two classes (background/foreground). A threshold value is computed as the average of the two sample means. This process is repeated until the threshold value does not change anymore and considered as the optimal threshold (25). The created lung mask was further closed by using a 3D rolling ball algorithm based on mathematical morphology operators was applied to the created mask (26). Thus, the hollow-free lung mask was applied to T2 TSE registered images and lung segmentation became finally feasible (Fig E1, C).

Finally, structures with high-signal-intensity were segmented using a high-pass filter. For this, the standard deviation of air ( $SD_{\text{air}}$ ) was automatically measured in the axial plane in all pixels located at more than 2 cm from the anterior chest surface, within the middle third of the stack of slices. Then, the mode of the histogram of the lung parenchyma signal intensity distribution, plus twelve  $SD_{\text{air}}$  ( $\text{mode}+12SD_{\text{air}}$ ) was chosen as a low-cut threshold after empirically testing other thresholds ie,  $\text{Mode}+4SD_{\text{air}}$ ,  $\text{Mode}+8SD_{\text{air}}$ ,  $\text{Mode}+16SD_{\text{air}}$  and  $\text{Mode}+20SD_{\text{air}}$ . The use of the mode to calculate an adaptative threshold was previously validated (12). The rationale of picking the mode of the histogram was to calculate the low-cut threshold is that the most frequent signal value of the lung voxels would be normal parenchyma

with low signal owing to T2 RTSE parameters (ie, long TE with black-blood contrast). Indeed, in CF participants, voxels of high signal intensity did not exceed 17% of the whole lung (T2-HSV range (0.1–17)) which indicates that more than 80% of voxels may follow similar distribution in both normal and disease condition. To further support this statement, comparisons of mode between 10 healthy participants (median mode of lung histogram = 16 (13–20)) and 12 CF participants (median mode of lung histogram = 15 (13–21)) were not statistically significant (Mann-Whitney test;  $P = .92$ ) (Fig E2). In 6 CF with exacerbation, there was also no statistical difference of the mode before and after antibiotic treatment (Wilcoxon signed rank test;  $P = .89$ ). Furthermore, the mode did not correlate to PFT results (Table E7). Therefore, we found no variability of the mode in relationship with neither CF status nor the disease severity. Moreover, neither the lung volume, the mode nor  $SD_{air}$  were also found to correlate to PFT ( $P > .05$ ).

In addition, the high signal intensity mask was fused to the corresponding 3D T2 mapping cartographies to add the T2 value information at every point of HSV (Fig 4). A composite index was called the T2-VIP (Volume Intensity Product) and calculated as follows:

$$T2 - VIP = \frac{\left[ \sum_{i=0}^{max} (T2_i \times HSV_i) \right]}{V_{lung}} \text{ (in milliseconds)}$$

where  $T2_i$  corresponds to the T2 value “i,”  $HSV_i$  corresponds to the volume of those voxels with the  $T2_i$  value, max represents the maximum T2 value and  $V_{lung}$  the total lung volume.

Regarding the lung volume MRI measurement, an additional analysis was performed versus pulmonary function test. In 12 study participants with cystic fibrosis, there was no difference between the MRI volume (median = 2.1 (1–5) L) and the absolute value of functional residual capacity (median = 1.9 (1.1–4.8) L) as measured by pulmonary function test ( $P = .77$ ). The concordance was found very good (intraclass correlation coefficient: 0.97). At Bland-Altman analysis (3), the mean difference between these two measurements was 0.10 (limits of agreement: [-0.52; 0.71]).

Moreover, for regional evaluation of T2 metrics, right and left lungs were separated. To do so, the two largest 3D connected components starting from the right of the image were automatically labeled as right and left lungs. Along the cranio-caudal direction, the first and the last slice belonging to the lung mask were identified as the upper and the lower boundaries. Therefore, the upper lung was defined as the upper half between these two boundaries, and the lower lung as the lower half part between these two boundaries. Then, both T2-HSV and T2-VIP were automatically calculated within these regional masks.

## References

1. Lu X, Zhang S, Su H, Chen Y. Mutual information-based multimodal image registration using a novel joint histogram estimation. *Comput Med Imaging Graph* 2008;32(3):202–209.
2. Eikvil L, Husy P, Ciarlo A. Adaptive Image Registration. Semantic Scholar. <https://pdfs.semanticscholar.org/9d9c/acf0eebc5ba7dd3ec9a4dff6452e2478a6f7.pdf>. Published 2005. Accessed May 15, 2019.
3. Bland JM, Altman DG. Measuring agreement in method comparison studies. *Stat Methods Med Res* 1999;8(2):135–160.

**Table E1. MRI sequence parameters**

	2D Radial TSE	3D UTE Spiral VIBE
MRI Scan	AERA (Siemens)	
Field strength	1.5 T	
Coil	18-channel body coil/32-channel spine coil	
TR (ms)	2350	4.3
TE (ms)	20/50/85/100/150	0.05
Flip angle (°)	145	5
Bandwidth (Hz/Px)	505	2800
Radial views	390	NA
Spiral interleaves	NA	320
Field of view (mm <sup>2</sup> )	320 × 320	320 × 320
Matrix	200 × 200	320 × 320
Pixel size (mm <sup>2</sup> )	1.6 × 1.6	1 × 1
Slice thickness (mm)	1.6	1
Number of slices	80 to 120	192 to 240
Slice interleaves (%)	0	NA
Concatenations	15	NA
Acquisition plane	Axial	Coronal
Synchronization	PACE	Navigator-triggered prospective acquisition
Tacq (minutes)	8 to 12	4 to 6
Contrast product	None	None

Legends: TR = repetition time; TE = echo time; Hz = Hertz; Px = Pixel; Tacq = acquisition time; mm = millimeter; ms = millisecond; T = Tesla; PACE = prospective acquisition correction.

**Table E2. CT protocol**

Machine	SOMATOM DEFINITION 64 (Siemens Healthcare)
Tube voltage	110 kV
Tube current	Modulating CareDose4D (Siemens Medical Solutions)
Effective reference tube current	50 mAs
Rotation time	75 ms
Collimation	1 mm
Field-of-view	Patient size dependent
Matrix	512 × 512
Voxel size	(0.6–0.7 mm) <sup>3</sup>
Effective dose	1.2 to 1.5 mSv

Legends: kV = kilovoltage; mAs = milliampere.second; ms = millisecond; mm = millimeter; mSv = milliSievert.

**Table E3. Bhalla score (reproduced from reference 7)**

Category	Scores			
	0	1	2	3
Severity of bronchiectasis	Absent	Mild	Moderate	Severe
Peribronchial thickening	Absent	Mild	Moderate	Severe
Extent of bronchiectasis (no. of segments)	Absent	1–5	6–9	>9
Extent of mucus plugging (no. of segments)	Absent	1–5	6–9	>9
Sacculatoins or abscesses (no. of segments)	Absent	1–5	6–9	>9
Generation of bronchial divisions involved (bronchiectasis/plugging)	Absent	Up to 4th generation	Up to 5th generation	Up to 6th generation and distal
No. of bullae	Absent	Unilateral (not > 4)	Bilateral (not > 4)	>4
Emphysema (no. of segments)	Absent	1–5	>5	
Collapse/consolidation	Absent	Subsegmental	Segmental/lobar	

**The score is calculated as follows: Total Bhalla score = 25 – (sum of scorings).**

Bronchiectasis severity: Absent (0), luminal diameter slightly greater than diameter of adjacent vessel (Mild (1)), luminal diameter 2–3× the adjacent vessel (Moderate (2)), luminal diameter > 3× the adjacent vessel (Severe (3)).

Peribronchial thickening severity: Absent (0), wall thickness equal to the diameter of adjacent vessel (Mild (1)), wall thickness 2× the adjacent vessel (Moderate (2)), wall thickness > 2× the adjacent vessel (Severe (3)).

**Parameters’ definitions**

1. Bronchiectasis: luminal size of bronchi compared with the diameter of an adjacent blood vessel roughly equidistant from the hilum.
2. Peribronchial thickening: bronchial wall thickness compared with the diameter of an adjacent blood vessel roughly equidistant from the hilum.
3. Mucus plugging: tubular structures with or without branching pattern or rounded opacities differentiated from blood vessels by their position relative to adjacent patent bronchi and blood vessels.
4. Abscesses: differentiated from plugged bronchi by their nonbranching appearance and their lack of direct continuity with bronchi.
5. Bullae: identified by their peripheral location, their long pleural attachment and their lack of direct communication or continuity with bronchi.

Note.—Bronchioles with the tree-in-bud pattern are scored as mucus plugs.

**Table E4. Eichinger morpho-functional MRI score (reproduced from reference 9)**

Parameter	Right			Left			Maximal Parameter/Global Score
	UL	ML	LL	UL	LG	LL	
1. Bronchiectasis/wall thickening							12
2. Mucus plugging							12
3. Abscesses/sacculations							12
4. Consolidation							12
5. Special findings							12
6. Perfusion size							12
Maximal lobar/global score	12	12	12	12	12	12	72

UL = upper lobe; ML = middle lobe; LL = lower lobe; LG = lingula.

Finding scoring: absent (0), less than 50% of the lobe (1), more than 50% of the lobe (2).

-Global score (GS): sum of all parameters of the whole lung; (0–72).

-Morphology score (MS): sum of morphologic parameter scores of the whole lung; (0–60).

-Function score (FS): perfusion score of the whole lung; (0–12).

**Parameters’ definitions**

1. Bronchiectasis/bronchial wall thickening:

In the central zone: bronchial dilatation with respect to the accompanying pulmonary artery (luminal diameter > corresponding pulmonary artery) and lack of bronchial tapering mostly associated with wall thickening. In the peripheral zone: visibility of bronchi within 1 cm of the pleural surface.

2. Mucus plugging: hyperintensity on the HASTE-images (higher than the signal of the musculature). If mucus plugging was observed in the periphery of a lung segment, this segment was also scored for bronchiectasis.

3. Abscess/sacculations: Circular structures with a minimum diameter of 1.5 cm which are air filled or show an air fluid level.

4. Consolidation: A homogeneous increase in pulmonary parenchymal signal with possible presence of an air bronchogram, size > 2 cm.

5. Special findings: pleural effusion, pleural reaction/pleurisy or pneumothorax.

6. Perfusion size: The size of a perfusion defect.

Note.—In this study, information provided by T1-weighted sequence were assessed by using the 3D-UTE sequence, and information provided by T2-weighted sequence were assessed by using the T2-RTSE sequence.

**Table E5. Brody HRCT score (reproduced from reference 6)**

Parameter	Calculation
Bronchiectasis score (0–12)	(Extent of bronchiectasis in central lung + Extent of bronchiectasis in peripheral lung) × Average bronchiectasis size multiplier [0.5 = 0; 1 = 1; 1.5 = 1.25; 2.0 = 1.5; 2.5 = 1.75; 3 = 2] where Average bronchiectasis size = (Size of largest dilated bronchus + Average size of dilated bronchus)/2
Mucus plugging score (0–6)	Extent of mucous plugging in central lung + Extent of mucous plugging in peripheral lung
Peribronchial thickening score (0–9)	(Extent of peribronchial thickening in central lung + Extent of peribronchial thickening in peripheral lung) × Severity of peribronchial thickening [1 = mild; 1.25 = moderate; 1.5 = severe]
Parenchyma score (0–9)	Extent of dense parenchymal opacity + Extent of ground glass opacity + Extent of cysts or bullae
Air trapping score (0–4.5)	Extent of air trapping × Appearance of air trapping [1 = subsegmental; 1.5 = segmental or larger]

Finding extent scoring: absent (0), 1/3 of the lobe (1), 1/3 to 2/3 of the lobe (2), more than 2/3 of the lobe (3).

Bronchiectasis severity: less than 2× adjacent vessel (1), 2× to 3× adjacent vessel (2), more than 3× adjacent vessel (3).

**Parameters’ definitions**

1. Bronchiectasis: one or more of the following criteria: a bronchoarterial ratio > 1, a nontapering bronchus, a bronchus within 1 cm of the costal pleura, or a bronchus abutting the mediastinal pleura.

2. Peribronchial thickening: bronchial wall thickness > 2 mm in the hila, 1 mm in the central portion of the lung, and 0.5 mm in the peripheral lung.

3. Mucus plugging: Central mucous plugging was defined as an opacity filling a defined bronchus, and peripheral mucous plugging was defined as the presence of either dilated mucous-filled bronchi or peripheral thin branching structures or centrilobular nodules in the peripheral lung.

4. Air trapping: areas of lung on the expiratory images that remained similar in attenuation to the appearance on inspiratory images.

Note.—In this study, CT scans were acquired at end normal expiration only, as suggested by reference 10.

**Table E6. Comparison of regional measurements of T2 high signal volume and intensity in 12 participants with cystic fibrosis.**

	Right lung (n = 12)	Left lung (n = 12)	Mann-Whitney test
T2-HSV (%)	4.6 (0.1–16.1)	1.5 (0.1–17.5)	0.68
T2-VIP (ms)	398 (21–993)	114 (27–1002)	0.81
	Upper lung (n = 12)	Lower lung (n = 12)	Mann-Whitney test
T2-HSV (%)	5.6 (0.1–15.2)	1.2 (0.2–18.7)	0.10
T2-VIP (ms)	426 (47–1351)	60 (10–741)	<b>0.01</b>

Note.—Data are median with range from minimum to maximum between parentheses.

Legend: T2-HSV = high-signal-intensity volume; T2-VIP = volume-intensity product.

**Table E7. Correlation between MRI quantitative parameters and FEV<sub>1</sub>% in 12 participants with cystic fibrosis.**

	FEV <sub>1</sub> %	
	$\rho$	<i>P</i>
<b>Extrathoracic air</b>		
SD <sub>air</sub>	0.41	0.18
<b>Lung</b>		
Mode	0.18	0.56
SD <sub>lung</sub>	–0.81	0.001
Volume	–0.51	0.09
<b>HSV (mL)</b>		
Mode+4SD <sub>air</sub>	–0.76	0.004
Mode+8SD <sub>air</sub>	–0.83	<0.001
Mode+12SD <sub>air</sub>	–0.87	<0.001
Mode+16SD <sub>air</sub>	–0.83	<0.001
Mode+20SD <sub>air</sub>	–0.83	<0.001
<b>T2-HSV (%)</b>		
Mode+4SD <sub>air</sub>	–0.81	0.001
Mode+8SD <sub>air</sub>	–0.83	<0.001
Mode+12SD <sub>air</sub>	–0.88	<0.001
Mode+16SD <sub>air</sub>	–0.83	<0.001
Mode+20SD <sub>air</sub>	–0.81	0.001
<b>Mean T2 (ms)</b>	–0.28	0.60
<b>T2-VIP (ms)</b>		
Mode+4SD <sub>air</sub>	–	
	–	
	–	
	–	
	–	

Note.—Correlations were tested using Spearman test.

Legends: FEV<sub>1</sub>% = forced expiratory volume in 1 second percentage predicted; Mode = most common number in the histogram of signal intensity distribution from lung parenchyma; SD<sub>air</sub> = standard deviation of signal from extra thoracic air; SD<sub>lung</sub> = standard deviation of signal intensity within the lung parenchyma; HSV = high-signal-intensity volume; T2-HSV = relative high-signal-intensity volume; T2-VIP = volume intensity product.

**Table E8. Correlations of T2-HSV and T2-VIP with visual scores in 12 participants with cystic fibrosis.**

		T2-HSV (%)		T2-VIP (ms)	
		$\rho$	<i>P</i> value	$\rho$	<i>P</i> value
<b>MRI</b>	Peribronchial thickening	0.39	0.20	0.37	0.23
<b>Bhalla score</b>	Bronchiectasis severity	0.61	<b>0.03</b>	0.66	<b>0.02</b>
	Bronchiectasis extent	0.48	0.11	0.50	0.09
	Mucus plugs	0.85	<b>&lt;0.001</b>	0.90	<b>&lt;0.001</b>
	Bronchial generation involved	0.65	<b>0.02</b>	0.65	<b>0.02</b>
	Collapse/consolidation	0.56	0.059	0.66	<b>0.02</b>
	Sacculation/Abcess	NA	NA	NA	NA
	Emphysema	0.48	0.11	0.40	0.20
	Bulla	NA	NA	NA	NA
	Total score	-0.65	<b>0.02</b>	-0.74	<b>&lt;0.001</b>
<b>MRI</b>	Wall thickening/bronchiectasis	0.71	<b>0.01</b>	0.70	<b>0.01</b>
<b>Eichinger-M</b>	Mucus plugs	0.69	<b>0.01</b>	0.66	<b>0.02</b>
	Sacculation/Abcess	NA	NA	NA	NA
	Consolidation	0.60	<b>0.040</b>	0.65	<b>0.03</b>
	Special findings	NA	NA	NA	NA
	Total morphologic score	0.83	<b>&lt;0.001</b>	0.79	<b>0.002</b>
<b>Eichinger-P</b>	Perfusion	NA	NA	NA	NA
<b>CT</b>	Wall Thickening	0.30	0.34	0.28	0.38
<b>Brody II</b>	Bronchiectasis	0.66	<b>0.02</b>	0.69	<b>0.01</b>
	Mucus plugs	0.65	<b>0.02</b>	0.75	<b>0.004</b>
	Parenchymal opacities	0.56	0.058	0.52	0.08
	Air trapping	0.81	<b>0.001</b>	0.86	<b>&lt;0.001</b>
	Total score	0.68	<b>0.02</b>	0.69	<b>0.01</b>

Note.—Data are rho coefficient of correlation of Spearman.

Legend: T2-HSV = high-signal-intensity volume; T2-VIP = volume-intensity product; Eichinger-M = morphologic MRI scoring of CF structural alterations; Eichinger-P = scoring of perfusion defects as proposed by Eichinger and colleagues. NA = not applicable.

**Table E9. Correlations of MRI and CT visual scores with pulmonary function tests in 12 participants with cystic fibrosis.**

	(n = 12)		(n = 12)		(n = 12)	
	$\rho$	<i>P</i> value	$\rho$	<i>P</i> value	$\rho$	<i>P</i> value
	0.70		-0.70		-0.55	0.058
	0.62		-0.70		-0.83	
	-0.36	0.24	0.20	0.53	0.52	0.08
	-0.46	0.12	0.60		0.40	0.19
	-0.15	0.64	0.49	0.10	0.59	
	NA	NA	-0.70		-0.66	
	-0.70		NA	NA	0.53	0.07
	-0.66		0.53	0.07	NA	NA

Note.—Correlations were tested by using Spearman test. Data of pulmonary function tests are expressed as percentage of predicted value.

Legend: FEV<sub>1</sub> = forced expiratory volume in 1 second; FVC = forced vital capacity; FRC = functional residual capacity; RV = residual volume; TLC = total lung capacity; Eichinger-M = morphologic MRI scoring of CF structural alterations.

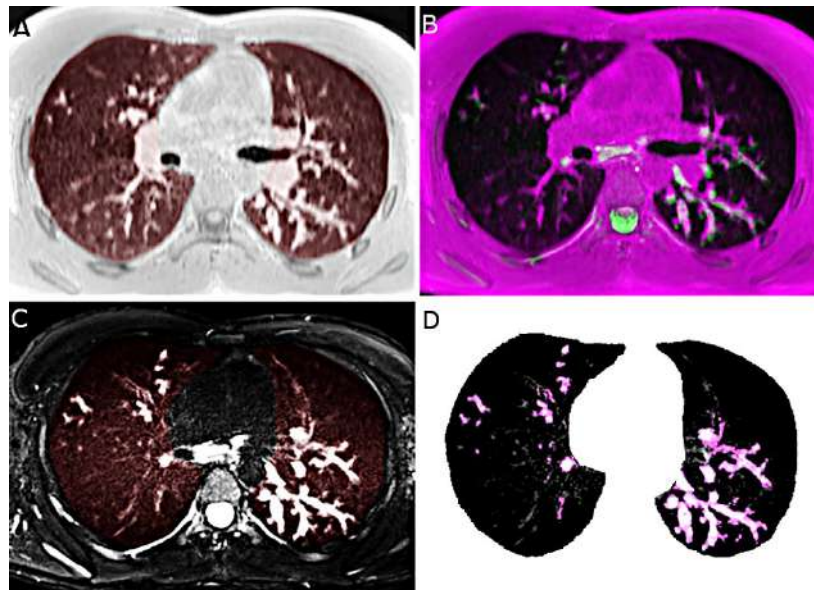
**Table E10. Comparison of pulmonary function test and MRI and CT indexes in 6 participants with CF under respiratory exacerbation, before and after treatment.**

		Before treatment (n = 6)	After treatment (n = 6)	Wilcoxon signed rank test
<b>Pulmonary Function tests</b>				
FEV <sub>1</sub> %	n = 6	68 (34–71)	80 (55–94)	0.03
FEV <sub>1</sub> /FVC (%)	n = 6	64 (36–77)	67 (37–80)	0.10
FRC%	n = 6	118 (95–175)	117 (92–170)	0.16
<b>MRI quantitative</b>				
T2-HSV (%)	n = 6	8 (4.5–17)	4.2 (1.6–10)	0.03
T2-VIP (ms)	n = 6	664 (410–1012)	260 (90–500)	0.03
MRI Bhalla score	n = 6	12 (9–13)	13 (9–16)	0.26
MRI Eichinger-M score	n = 6	14 (11–26)	11 (10–22)	0.09
CT Brody II score	n = 1	102	98	NA

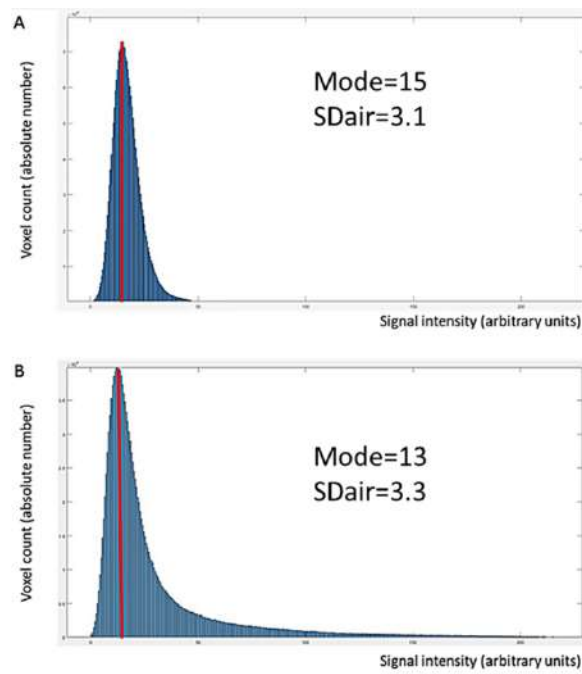
Note.—Data are medians with range from minimum to maximum between parentheses. 6 pulmonary exacerbations were due to a bacterial infection and were treated using intravenous antibiotherapy. Data of pulmonary function tests are expressed as percentage of predicted value.

Legend: Eichinger-M = morphologic MRI scoring of CF structural alterations; FEV<sub>1</sub> = forced expiratory volume in 1 second; FVC = forced vital capacity; FRC = functional residual capacity; T2-HSV = relative high-signal-intensity volume; T2-VIP = volume intensity product.

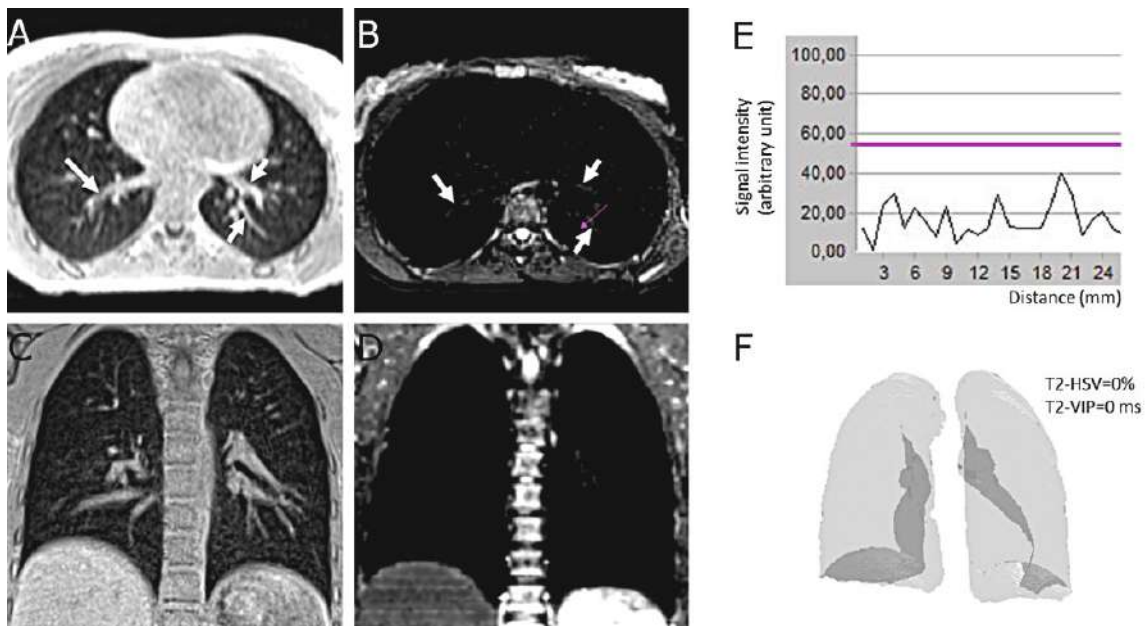
## SUPPLEMENTAL FIGURES



**Supplemental Figure E1. 15-year-old male with cystic fibrosis. Axial non-contrast 3D UTE MRI (A), black-blood contrast T2 radial turbo spin echo sequence (T2-RTSE) (C,D) and imaging registration of both 3D UTE and T2-RTSE (B).** On T2 image (C), lung segmentation is almost impossible since there is no contrast difference between soft tissue structures (muscle, fat and vessels), ribs and the lungs. Conversely, on 3D UTE image (A), isolating low signal intensity of the lungs from the rest of isoT1 or hyperT1 thoracic structures is feasible. Therefore, iterative algorithm to select the optimal threshold based on splitting image histogram into two classes was performed on 3D UTE images. The lung mask was closed to include intrapulmonary vessels and hilum by using a 3D rolling ball algorithm. The resulting lung mask was then applied to T2 Radial TSE registered images (B) and lung segmentation became feasible (C,D). To extract high signal intensity structures from the lung, a threshold was set at mode, derived from the frequency distribution histogram of the segmented lungs from T2 TSE images, plus twelve standard deviation of extra-thoracic air (D).



**Supplemental Figure E2. Histograms of lung voxel intensity frequency distribution in a 18-year-old healthy participant (A) and a 23-year-old participant with cystic fibrosis (B), using T2-radial turbo spin echo sequence.** The proportion of voxels with high signal-intensity is increased on (B) histogram, whereas there is vast majority of voxels of low signal-intensity in both histograms. The mode correspond to the signal intensity value of the most frequent signal value, and SDair indicates the standard deviation of extra-thoracic air.



**Supplemental Figure E3. 22-year-old female healthy participant. Axial (A, B), coronal (C, D) and volume rendering (F) MR images acquired using non-contrast 3 UTE (A, C) and black-blood contrast T2 radial TSE (B, D, F). E represent the profile of signal intensity along the purple arrow visible on (B) image. On axial images, white arrows indicate proximal vessels with some visible vessels on T2 radial TSE image (B), although of low signal intensity. The vessel suppression is almost complete on the black blood T2 radial TSE coronal image (D). E image shows the intensity profile along the purple arrow traced in the left lower lobe in B image. The signal intensity (vertical axis, in arbitrary unit) is plotted along the distance (horizontal axis, in mm). By using a high-pass filter (horizontal purple line, E), set at the mode of the lung histogram of intensity distribution, plus twelve standard deviations of extra-thoracic air, the low signal intensities were removed from the high-signal-intensity volume measurement. Therefore, both relative high-signal-intensity volume (T2-HSV) and T2 volume intensity product (T2-VIP) were equal to 0, as displayed using a volume rendering technique in (F).**

# **DISCUSSION ET PERSPECTIVES**

Les travaux réalisés au cours de cette thèse ont trait à de nouvelles méthodes de quantification TDM et IRM pour l'évaluation des différents compartiments atteints dans les maladies obstructives chroniques des voies aériennes. La complexité des méthodes est variable et leur applicabilité en devenir. Nous avons décrit certaines nouvelles méthodes (quantification des lobules clairs, quantification de l'emphysème en IRM, mapping IRM des hypersignaux T2) ou utilisé des méthodes connues pour mieux préciser leurs potentiels (quantification des vaisseaux dans la BPCO).

#### *Eude du remodelage bronchique et vasculaire à la TDM*

L'imagerie TDM quantitative pulmonaire peut contribuer à déterminer de nouveaux phénotypes de malades atteints de BPCO. En effet, des études récentes menées par notre équipe sur l'hypertension pulmonaire (HTP) secondaire à la BPCO ont montré une association entre le remodelage bronchique, mesuré de façon non invasive à la TDM, et le degré de sévérité de l'HTP chez les patients BPCO (69). En outre, un score prédictif, construit en combinant les données morpho-métriques TDM du remodelage bronchique et vasculaire avec les données fonctionnelles des gaz du sang ( $\text{PaO}_2$ ), permettrait de sélectionner les malades BPCO porteurs d'une HTP sévère afin d'éviter aux patients de subir un cathétérisme cardiaque droit qui est une méthode invasive non dénuée de complications (88). Dans la continuité de ces travaux, l'étude présentée dans ce manuscrit avait pour objectif de comparer les données quantitatives du remodelage bronchique et vasculaire des patients BPCO porteurs d'une HTP sévère et des patients atteints d'HTAP précapillaire sévère ((118)[Publication n°1]). Notre étude a montré des corrélations significatives des données quantitatives du remodelage bronchique et vasculaire avec le degré de sévérité de l'HTP dans le groupe de patients BPCO porteurs d'HTP sévère. En revanche, dans le groupe de patients atteints d'HTAP, seules les données du remodelage vasculaire corrélaient avec le degré de sévérité de l'HTP avec un coefficient de corrélation négatif. Ces résultats, similaires à d'autres déjà publiés (69,88), suggèrent que l'HTP secondaire à la BPCO pourrait être due à une atteinte des compartiments bronchique et vasculaire de façon différente des autres HTAP précapillaires. En effet, la première hypothèse étudiée chez les patients BPCO porteurs d'HTP était celle de la sévérité de l'emphysème qui serait liée à l'apparition d'une HTP. Cependant, cette hypothèse a été écartée par de nombreuses études (69,88,96) et nos résultats qui ne montrent aucune corrélation de la sévérité de l'HTP avec le degré d'emphysème. La coexistence d'une HTAP idiopathique avec la BPCO est une autre hypothèse pour tenter d'expliquer le degré de sévérité de l'HTP secondaire à la BPCO (119,120). Néanmoins, les résultats de notre étude peuvent apporter des éléments de réponse

dans cette incertitude suggérant des phénomènes d'interaction complexes entre les compartiments bronchique et vasculaire dans la BPCO. Toutefois, notre étude présente quelques limitations. Il s'agit d'une étude observationnelle et rétrospective, ce qui ne nous permet pas de conclure quant à la relation de causalité entre l'épaississement de la paroi bronchique ou l'augmentation de la surface des petits vaisseaux et le degré de l'HTP. Un nombre d'effectif réduit dans chaque groupe étudié du fait de la rareté de l'HTP sévère ne nous permet pas de faire des analyses multivariées. Les données du remodelage bronchique restent des données globales sans distinction entre artères et veines ni entre une vasoconstriction de la lumière et un épaississement de la paroi vasculaire. Néanmoins, les patients inclus présentaient tous une HTP précapillaire pure confirmée par le cathétérisme cardiaque droit.

Il serait intéressant de pouvoir confirmer ces résultats dans une nouvelle cohorte prospective et de juger de la pertinence prédictive du score TDM quantitative, voire de l'efficacité des traitements déjà existants de l'HTAP.

Une étude prospective promue par le CHU de Bordeaux, dont le titre est : TDM quantitative en double énergie dans l'hypertension pulmonaire, est en cours. L'objectif de cette étude est de déterminer un score quantitatif morphologique et fonctionnel du remodelage bronchique et vasculaire à l'aide d'acquisition scannographique en double énergie afin de prédire la présence et la sévérité de l'HTP. (Clinical Trial : NCT03901287).

#### *Etude de l'atteinte des voies aériennes distales à la TDM*

Le processus inflammatoire dans les maladies bronchiques obstructives chroniques touche tout l'arbre bronchique y compris les bronchioles périphériques (121). Cette atteinte des voies aériennes distales contribue à l'expression clinique de ces maladies ce qui a poussé au développement de nouveaux dispositifs d'inhalation qui permettent aux médicaments de cibler l'atteinte des voies aériennes distales (122). Dans ce contexte, la quantification de l'atteinte des voies aériennes distales est importante pour classer les malades et les prendre en charge correctement. Les méthodes TDM qui existent actuellement présentent des limites qui peuvent altérer leur fiabilité (73,75,77,78,123). Ainsi, dans notre étude [Publication n°2] nous avons développé une méthode quantitative semi-automatique sous contrôle visuel du radiologue, de l'extension de l'atteinte des voies aériennes distales. Cette méthode appliquée aux images TDM de malades atteints de pneumopathie d'hypersensibilité (PH) chronique a permis de les discriminer des patients contrôles, et surtout de quantifier la sévérité de l'atteinte des voies aériennes distales. En effet, l'atteinte bronchiolaire de la PHS est responsable d'une atteinte obstructive distale similaire à celle retrouvée dans les maladies bronchiques obstructives

chroniques (124,125). Ainsi, l'application de cette méthode afin de quantifier le piégeage d'air expiratoire ou l'aspect en mosaïque des images TDM de ces malades est tout à fait possible. Cependant, notre technique présente également quelques limitations. La méthode a été testée seulement sur des images TDM en inspiration, cependant les zones d'hypodensités lobulaires reflètent l'atteinte obstructive des voies aériennes distales et/ou la vasoconstriction (126). Notre méthode est semi-automatique nécessitant une validation du radiologue ce qui allonge la durée de l'analyse de façon acceptable mais qui reste tout de même nécessaire pour une analyse fiable. De plus, la reproductibilité intra et inter observateur de notre technique était très bonne. Une méthode totalement automatique a été publiée récemment (127) mais à l'heure actuelle elle reste chronophage ou demandeuse en capacité informatique. Les techniques basées sur les méthodes d'apprentissage peuvent constituer des alternatives robustes mais les problématiques liées aux nombres d'exams nécessaires, à la qualité de la segmentation manuelle et au manque de standardisation des paramètres entre les centres font que ces techniques sont difficiles à utiliser plus largement.

L'étape suivante serait d'appliquer cette méthode dans des études sur les maladies bronchiques obstructives chroniques proprement dites. L'utilisation de cette méthode dans une étude prospective qui vient d'être mise en place au CHU de Bordeaux sur les bronchiolites oblitérantes du greffé (Clinical Trial : NCT04080232) sera l'occasion de comparer notre méthode avec les méthodes existantes voire avec les données fonctionnelles de l'IRM pulmonaire à l'oxygène. Enfin, une transposition de cette méthode aux images d'IRM protonique 3DUTE et son utilisation dans l'asthme, la BPCO (Clinical Trial : PIMABOD) et la mucoviscidose (Clinical Trial : NCT03357562) font partie des perspectives de cette étude.

#### *Faisabilité de l'IRM protonique pulmonaire à haute résolution*

Le développement de nouvelles séquences IRM 3DUTE a permis l'obtention d'images morphologiques proches de celle de la TDM. Ces séquences peuvent être séparées en deux catégories selon le motif de remplissage de l'espace k : remplissage sphérique ou remplissage cylindrique spiralé ou radial. Ainsi, la comparaison de ces deux motifs paraît nécessaire afin de juger l'applicabilité de ces séquences en routine et en recherche. Notre étude ((128) [Publication n°3]) avait pour objectif d'évaluer la qualité des images IRM issues des deux séquences. Malgré une meilleure qualité des images acquises par la séquence au motif sphérique et un meilleur signal/bruit, le manque de robustesse de cette séquence surtout chez les patients obèses et /ou dyspnéique et sa durée d'acquisition plus longue font que les séquences au motif cylindrique spiralé soient plus compatibles pour une utilisation en routine et/ou en recherche. De plus, les

scores cliniques évalués dans notre étude ont montré une reproductibilité similaire entre les deux séquences, ce qui suggère que leur qualité diagnostique est comparable. Les résultats de notre étude sont expliqués par le principe physique de chaque motif d'acquisition. Pour le motif sphérique radial purement 3D, le passage répété par le centre de l'espace k fait que le signal/bruit est plus élevé que pour le motif cylindrique composé d'un empilement de coupes 2D. En revanche, cette même propriété fait que la synchronisation respiratoire de l'acquisition en mode sphérique est plus complexe et moins robuste que celle de l'acquisition cylindrique spiralée. Ainsi, ce dernier mode d'acquisition est privilégié dans les études à venir (Clinical Trial : NCT03357562, NCT03089346, PIMABOD).

#### *Quantification de l'emphysème à l'IRM protonique 3DUTE*

Du fait que le signal IRM n'est pas calibré, une normalisation est nécessaire pour pouvoir quantifier l'atteinte parenchymateuse à l'IRM protonique pulmonaire dans la BPCO. Ainsi, dans notre étude ((129)[Publication n°4]) nous avons apporté des solutions aux problématiques de normalisation du signal IRM et d'automatisation de la segmentation pulmonaire. Nous avons utilisé une méthode de fitting des courbes de l'histogramme des signaux thoraciques afin de déterminer un seuil automatique appelé le seuil des tissus mous. Ce seuil nous permet de normaliser le signal IRM de façon objective afin d'éviter un choix arbitraire ou une mesure manuelle plus ou moins variable. Cette normalisation nous permet également de déterminer un seuil bas pour quantifier l'emphysème de façon adaptative. De façon similaire à celle employée en scanner la variation de ce seuil et un double seuillage pourrait nous permettre d'isoler l'atteinte des voies aériennes distales et de l'emphysème. D'une façon toutefois purement quantitative qui ne permet pas de localiser cette atteinte. On voit donc le potentiel de complément avec une méthode de mesure de piégeage visuelle telle que décrite plus haut en scanner et potentiellement transposable en IRM.

S'agissant de l'emphysème, nos résultats ont montré une bonne corrélation avec les données TDM de référence. Aussi, la validité de nos résultats a été renforcée par les corrélations significatives retrouvées avec les données spirométriques. En outre, les données quantitatives de l'emphysème à l'IRM 3DUTE étaient significativement différentes entre les patients BPCO des différents groupe GOLD contrairement aux données TDM, ce qui peut suggérer que le signal IRM 3DUTE renferme des informations fonctionnelles utiles à la compréhension de la maladie (130,131). Notre étude présentait quelques limitations. Les acquisitions TDM et IRM étaient faites à deux volumes pulmonaires différents (i.e. Capacité pulmonaire totale pour la TDM et Volume fonctionnel résiduel pour l'IRM). Cependant, la concordance entre les deux

modalités était bonne ainsi que les corrélations avec la fonction respiratoire qui étaient similaires pour les deux modalités. Les données quantitatives IRM n'ont pas fait l'objet de validation versus les données histologiques de l'emphysème, néanmoins, dans cette étude la TDM était la référence standard en raison de nombreuses études de validation radio-histologiques antérieures (42,45–47). Enfin, la séquence IRM 3DUTE et ses paramètres d'acquisition peuvent influencer les données quantitatives, ainsi le seuil de l'emphysème déterminé dans cette étude ne peut être généralisable.

Une étude longitudinale et multicentrique pourrait être envisagée afin de valider plus largement la méthode. Néanmoins, nous avons retrouvé des résultats similaires dans la mucoviscidose (publication n°6). En perspectives, une cohorte prospective de patients asthmatiques a été constituée (Clinical Trial : NCT03089346) et la mesure des hyposignaux parenchymateux fera l'objet d'une étude prochainement.

#### *Etude du remodelage bronchique à l'IRM protonique 3DUTE*

Plusieurs travaux TDM menés dans notre laboratoire, ont étudié l'intérêt des mesures bronchiques non invasives dans les maladies obstructives chroniques des voies aériennes (66,67,69). Depuis l'avènement de l'IRM 3DUTE et la possibilité d'avoir des images avec une résolution spatiale sous millimétrique, nous nous sommes interrogés sur la possibilité de transposer les techniques de quantification TDM du remodelage bronchique à l'IRM. De plus, du fait du caractère non irradiant de l'IRM, son utilisation dans la population de jeunes adultes voire pédiatrique de la mucoviscidose nous paraît primordiale. Ainsi, l'objectif de cette étude [Publication n°5] était d'évaluer la concordance des mesures bronchiques entre le scanner et l'IRM 3DUTE chez les patients atteints de mucoviscidose. Nos résultats ont montré une bonne concordance entre les différentes mesures bronchiques à la TDM et à l'IRM. En outre, des corrélations significatives ont été retrouvées avec la fonction respiratoire et les scores cliniques visuelles, de façon comparable à celles retrouvées avec la TDM. Ainsi les informations morphologiques sur la sévérité de l'atteinte structurales semblent être les mêmes entre TDM et IRM. Cependant, la mise en évidence d'une sous-estimation systématique des mesures bronchiques à l'IRM pourrait être expliquée par une moins bonne résolution spatiale de l'IRM 3DUTE comparativement au scanner. Notre étude présentait quelques limitations. Une intervention manuelle était nécessaire afin de déconnecter la segmentation de la paroi bronchique du vaisseau adjacent et ceci pour les deux modalités. Nous avons analysé seulement 4 bronches du fait que l'arbre bronchique extrait des images IRM 3DUTE était moins fourni. Cependant, nos résultats ont montré des corrélations significatives avec la sévérité de l'atteinte

structurale. Les acquisitions IRM duraient plus longtemps que les acquisitions TDM mais les nouvelles séquences 3DUTE ont vu leur durée d'acquisition diminuer de moitié.

L'étape suivante serait d'appliquer la méthode de quantification du remodelage bronchique dans les autres maladies obstructives chroniques des voies aériennes. La mise en place d'une étude prospective incluant des patients BPCO et asthmatiques (Clinical Trial : PIMABOD) est imminente. Il serait également intéressant d'étudier les signaux de la paroi bronchique de façon similaire à celle déjà rapportée au scanner (68).

#### *Etude de l'atteinte destructive et inflammatoire des voies aériennes à l'IRM 3DUTE*

Les bronchectasies, les sacculations et l'emphysème qui correspondent à l'atteinte destructive des voies aériennes peuvent se traduire par des hyposignaux à l'IRM. Les phénomènes inflammatoires responsables des épaissements des parois bronchiques, de consolidations et d'impactions mucoides se traduisent par des hypersignaux à l'IRM. L'objectif de notre étude [Publication n°6] était d'étudier la pertinence de la quantification de ces hypo et hyper signaux IRM dans l'évaluation de la sévérité de l'atteinte structurale des voies aériennes dans la mucoviscidose. Nos résultats ont montré des corrélations significatives avec les quantifications TDM des hypo et hyper densités. Ces données quantitatives corrélaient de façon similaire avec la fonction respiratoire. Egalement les scores visuels de sévérité avaient le même niveau de corrélation avec la fonction respiratoire que les données quantitatives. Ces résultats appuient la validité de la quantification des hypo et hyper signaux comme biomarqueurs de la sévérité de l'atteinte structurale des voies aériennes. Cependant, seule la variation des hyper signaux, à un an, présentait des corrélations significatives avec la variation du volume expiratoire maximal en une seconde. Ceci peut suggérer que les hypo signaux peuvent correspondre à une atteinte fixée cicatricielle des altérations et les hyper signaux à une atteinte plus variable de la maladie. L'étude présente quelques limites à discuter. Les biomarqueurs quantifiés sont des paramètres globaux de l'atteinte cependant une quantification régionale par lobe reste possible. La quantification des hyper signaux est biaisée par l'inclusion des vaisseaux pulmonaires normaux, par conséquent une évaluation de ces biomarqueurs dans une population dont le degré de sévérité est modéré s'impose. Enfin, les altérations ventilatoires et/ou perfusionnelles n'ont pas pu être évaluées sur les images acquises seulement en volume résiduel fonctionnel, néanmoins des acquisitions dynamiques permettant une étude fonctionnelle du poumon existent (33,115) et peuvent être proposées afin de combiner les biomarqueurs morphologiques et fonctionnels dans les études à venir.

*Quantification spécifique de l'inflammation des voies aériennes à l'IRM*

La validité du rationnel d'associer les hypersignaux T2 de l'IRM à des phénomènes inflammatoires potentiellement réversibles est basée sur les études récentes dont les résultats montrent une capacité de ces hypersignaux T2 à établir le diagnostic d'exacerbation et à régresser sous traitement dans le contexte de mucoviscidose (29,132). Ainsi dans notre étude (133)[Publication n°7] nous avons développé une méthode automatique de quantification de ces hypersignaux T2 comme marqueurs de l'atteinte inflammatoire des voies aériennes potentiellement réversible sous traitement. Les résultats de notre étude ont montré une capacité de notre méthode à quantifier de façon spécifique l'atteinte inflammatoire des voies aériennes et ceci sans contamination vasculaire grâce aux propriétés de la séquence IRM T2 utilisée. De plus, une diminution des hypersignaux T2 a été observée après traitement ce qui suggère que notre méthode pourrait être utilisée dans la surveillance de ces malades. En outre, le biomarqueur combinant le volume des hypersignaux et leur valeur T2 était le seul qui a présenté des corrélations significatives avec la variation après traitement du volume expiratoire maximal en une seconde. Ceci suggère que la valeur du signal T2 peut apporter une information fonctionnelle supplémentaire au volume lésionnel des hypersignaux. Notre étude présente quelques limites. Le nombre de malades atteints de mucoviscidose inclus dans notre étude était réduit. Cependant, ce travail était une étude de faisabilité et une preuve de concept technique. Ainsi, d'autres études avec un effectif plus important sont en cours de préparation. Notre méthode de quantification ne peut évaluer que les atteintes inflammatoires ce qui exclut les atteintes fibrotiques et destructives, néanmoins l'histoire naturelle de l'atteinte des voies aériennes commence par des phénomènes inflammatoires accessible avec notre méthode. De plus, l'utilisation dans un même protocole IRM de séquence 3DUTE permet d'évaluer qualitativement et quantitativement les phénomènes destructifs. Egalement, l'atteinte fonctionnelle ventilatoire et perfusionnelle n'ont pas été évaluées mais l'utilisation d'IRM multiparamétrique est envisageable pour une évaluation exhaustive des atteintes des voies aériennes proximales et distales.

Cette nouvelle méthode de quantification des hypersignaux T2 nous permettra dans les études à venir de repérer et de quantifier le remodelage bronchique notamment dans l'asthme pour évaluer la réponse aux thérapeutiques nouvellement développées.

# CONCLUSION

L'imagerie quantitative prend de plus en plus de place dans l'étude des modifications structurales et fonctionnelles des maladies bronchiques obstructives chroniques. Les limites de l'analyse visuelle qualitative ont poussé au développement de nouvelles méthodes quantitatives objectives, fiables et reproductibles. Ainsi, dans une nouvelle ère de développement thérapeutique, le rôle de l'imagerie a changé et l'on doit non seulement, indiquer la sévérité globale de l'atteinte pulmonaire mais également évaluer les modifications subtiles de cette atteinte sous traitement. Les travaux menés dans le cadre de cette thèse et les nouvelles méthodes développés apportent de nouveaux outils pour la compréhension et l'évaluation des maladies obstructives chroniques des voies aériennes.

Ainsi, dans la BPCO les mesures non-invasives des remodelages bronchique et vasculaire permettent d'identifier des phénotypes spécifiques de la maladie où il existe des interactions entre les systèmes cardiovasculaire et respiratoire. Aussi, grâce à l'IRM 3DUTE, la quantification de la sévérité de l'extension de l'emphysème devient possible et permet de distinguer entre des malades qui souffrent d'une atteinte fonctionnelle respiratoire variable.

Dans l'atteinte pulmonaire de la mucoviscidose, les méthodes quantitatives développées permettent de suivre et d'évaluer la sévérité de la maladie. Ainsi, la transposition des techniques des mesures bronchiques de la TDM à l'IRM 3DUTE permet de quantifier le remodelage bronchique et de distinguer entre les atteintes fonctionnelles respiratoires sévères des non sévères. Egalement, la quantification des phénomènes destructifs et inflammatoires à l'IRM 3DUTE permet d'évaluer de façon fiable la sévérité de l'atteinte structurale et de la suivre dans le temps sans aucune irradiation. Enfin, l'évaluation plus spécifique des processus inflammatoires actives des voies aériennes permet une détection précoce des atteintes pulmonaires dans la mucoviscidose et un suivi sous traitement fiable et objectif.

En outre, la quantification de l'atteinte des voies aériennes distales reste un défi important à l'IRM comme au scanner. En effet, le développement d'une méthode semi-automatique dans le cadre de cette thèse représente une première étape. Une validation de cette méthode dans les maladies bronchiques obstructive chroniques, et notamment dans l'asthme, ainsi qu'une évaluation de sa pertinence dans le phenotypage et le suivi de ces malades feront l'objet des études à venir.

En conclusion, nous espérons que ces travaux contribuent à l'amélioration et au développement des méthodes d'évaluation des différents compartiments atteints dans les maladies obstructives chroniques des voies aériennes ainsi qu'à une meilleure compréhension des phénomènes physiopathologiques sous-jacents permettant une meilleure prise en charge des patients.

# **REFERENCES**

1. (GOLD). Global Initiative for Chronic Obstructive Lung Disease. Global Strategy for the Diagnosis, Management and Prevention of Chronic Obstructive Pulmonary Disease. NIH Publication (updated 2016) 1998: <http://www.goldcopd.org>.
2. Global Initiative for Asthma. Global Strategy for Asthma Management and Prevention, 2016. Available from: [www.ginasthma.org](http://www.ginasthma.org).
3. Adeloye D, Chua S, Lee C, Basquill C, Papan A, Theodoratou E, et al. Global and regional estimates of COPD prevalence: Systematic review and meta-analysis. *J Glob Health* [Internet]. 5(2). Disponible sur: <https://www.ncbi.nlm.nih.gov/pmc/articles/PMC4693508/>
4. Atsou K, Chouaid C, Hejblum G. Variability of the chronic obstructive pulmonary disease key epidemiological data in Europe: systematic review. *BMC Med*. 18 janv 2011;9:7.
5. Lozano R, Naghavi M, Foreman K, Lim S, Shibuya K, Aboyans V, et al. Global and regional mortality from 235 causes of death for 20 age groups in 1990 and 2010: a systematic analysis for the Global Burden of Disease Study 2010. *Lancet Lond Engl*. 15 déc 2012;380(9859):2095-128.
6. Masoli M, Fabian D, Holt S, Beasley R. The global burden of asthma: executive summary of the GINA Dissemination Committee Report. *Allergy*. 2004;59(5):469-78.
7. Chung KF, Godard P, Adelroth E, Ayres J, Barnes N, Barnes P, et al. Difficult/therapy-resistant asthma: the need for an integrated approach to define clinical phenotypes, evaluate risk factors, understand pathophysiology and find novel therapies. ERS Task Force on Difficult/Therapy-Resistant Asthma. European Respiratory Society. *Eur Respir J*. mai 1999;13(5):1198-208.
8. Global Initiative for Chronic Obstructive Lung Diseases. GINA-GOLD. Diagnosis of diseases of chronic airflow limitation: asthma, COPD and asthma-COPD overlap syndrome (ACOS). (Available at:); 2015 <http://ginasthma.org/asthma-copd-and-asthma-copd-overlap-syndrome-acos/>.
9. Jain M, Goss CH. Update in cystic fibrosis 2013. *Am J Respir Crit Care Med*. 15 mai 2014;189(10):1181-6.
10. McCormick J, Mehta G, Olesen HV, Viviani L, Macek M, Mehta A, et al. Comparative demographics of the European cystic fibrosis population: a cross-sectional database analysis. *Lancet Lond Engl*. 20 mars 2010;375(9719):1007-13.
11. O'Sullivan BP, Freedman SD. Cystic fibrosis. *Lancet Lond Engl*. 30 mai 2009;373(9678):1891-904.
12. Kuehn BM. Progress in treating cystic fibrosis means that many patients may now reach midlife and beyond. *JAMA*. 24 sept 2014;312(12):1182-3.
13. Regamey N, Jeffery PK, Alton EFW, Bush A, Davies JC. Airway remodelling and its relationship to inflammation in cystic fibrosis. *Thorax*. 1 juill 2011;66(7):624-9.

14. Kostikas K, Greulich T, Mackay AJ, Lossi NS, Aalamian-Mattheis M, Nunez X, et al. Treatment response in COPD: does FEV1 say it all? A post hoc analysis of the CRYSTAL study. *ERJ Open Res.* 1 févr 2019;5(1):00243-2018.
15. Grenier PA, Beigelman-Aubry C, Fétita C, Prêteux F, Brauner MW, Lenoir S. New frontiers in CT imaging of airway disease. *Eur Radiol.* mai 2002;12(5):1022-44.
16. Lynch DA, Austin JHM, Hogg JC, Grenier PA, Kauczor H-U, Bankier AA, et al. CT-Definable Subtypes of Chronic Obstructive Pulmonary Disease: A Statement of the Fleischner Society. *Radiology.* 11 mai 2015;277(1):192-205.
17. Coxson HO, Leipsic J, Parraga G, Sin DD. Using pulmonary imaging to move chronic obstructive pulmonary disease beyond FEV1. *Am J Respir Crit Care Med.* 15 juill 2014;190(2):135-44.
18. Wenzel S. Severe Asthma in Adults. *Am J Respir Crit Care Med.* 15 juill 2005;172(2):149-60.
19. Lynch DA, Newell JD, Tschomper BA, Cink TM, Newman LS, Bethel R. Uncomplicated asthma in adults: comparison of CT appearance of the lungs in asthmatic and healthy subjects. *Radiology.* 1 sept 1993;188(3):829-33.
20. Gupta S, Siddiqui S, Haldar P, Raj JV, Entwisle JJ, Wardlaw AJ, et al. Qualitative Analysis of High-Resolution CT Scans in Severe Asthma. *Chest.* déc 2009;136(6):1521-8.
21. Horsley AR, Davies JC, Gray RD, Macleod KA, Donovan J, Aziz ZA, et al. Changes in physiological, functional and structural markers of cystic fibrosis lung disease with treatment of a pulmonary exacerbation. *Thorax.* juin 2013;68(6):532-9.
22. Tiddens HAWM, Stick SM, Davis S. Multi-modality monitoring of cystic fibrosis lung disease: the role of chest computed tomography. *Paediatr Respir Rev.* mars 2014;15(1):92-7.
23. Wild JM, Marshall H, Bock M, Schad LR, Jakob PM, Puderbach M, et al. MRI of the lung (1/3): methods. *Insights Imaging.* août 2012;3(4):345-53.
24. Biederer J, Beer M, Hirsch W, Wild J, Fabel M, Puderbach M, et al. MRI of the lung (2/3). Why ... when ... how? *Insights Imaging.* 13 févr 2012;3(4):355-71.
25. Mayo JR, MacKay A, Müller NL. MR imaging of the lungs: value of short TE spin-echo pulse sequences. *AJR Am J Roentgenol.* nov 1992;159(5):951-6.
26. Dournes G, Grodzki D, Macey J, Girodet P-O, Fayon M, Chateil J-F, et al. Quiet Submillimeter MR Imaging of the Lung Is Feasible with a PETRA Sequence at 1.5 T. *Radiology.* juill 2015;276(1):258-65.
27. Lutterbey G, Gieseke J, von Falkenhausen M, Morakkabati N, Schild H. Lung MRI at 3.0 T: a comparison of helical CT and high-field MRI in the detection of diffuse lung disease. *Eur Radiol.* févr 2005;15(2):324-8.

28. Puderbach M, Eichinger M. The role of advanced imaging techniques in cystic fibrosis follow-up: is there a place for MRI? *Pediatr Radiol.* juin 2010;40(6):844-9.
29. Renz DM, Scholz O, Böttcher J, Maurer MH, Denecke T, Schwarz C, et al. Comparison between magnetic resonance imaging and computed tomography of the lung in patients with cystic fibrosis with regard to clinical, laboratory, and pulmonary functional parameters. *Invest Radiol.* oct 2015;50(10):733-42.
30. Dournes G, Menut F, Macey J, Fayon M, Chateil J-F, Salel M, et al. Lung morphology assessment of cystic fibrosis using MRI with ultra-short echo time at submillimeter spatial resolution. *Eur Radiol.* nov 2016;26(11):3811-20.
31. Veldhoen S, Weng AM, Knapp J, Kunz AS, Stüb D, Wirth C, et al. Self-gated Non-Contrast-enhanced Functional Lung MR Imaging for Quantitative Ventilation Assessment in Patients with Cystic Fibrosis. *Radiology.* 6 oct 2016;283(1):242-51.
32. Kaireit TF, Gutberlet M, Voskrebenezv A, Freise J, Welte T, Hohlfeld JM, et al. Comparison of quantitative regional ventilation-weighted fourier decomposition MRI with dynamic fluorinated gas washout MRI and lung function testing in COPD patients. *J Magn Reson Imaging JMRI.* 2018;47(6):1534-41.
33. Bondesson D, Schneider MJ, Gaass T, Kühn B, Bauman G, Dietrich O, et al. Nonuniform Fourier-decomposition MRI for ventilation- and perfusion-weighted imaging of the lung. *Magn Reson Med.* 1 oct 2019;82(4):1312-21.
34. Yi CA, Lee KS, Han J, Chung MP, Chung MJ, Shin KM. 3-T MRI for Differentiating Inflammation- and Fibrosis-Predominant Lesions of Usual and Nonspecific Interstitial Pneumonia: Comparison Study with Pathologic Correlation. *Am J Roentgenol.* 1 avr 2008;190(4):878-85.
35. Vogel-Claussen J, Renne J, Hinrichs J, Schönfeld C, Gutberlet M, Schaumann F, et al. Quantification of Pulmonary Inflammation after Segmental Allergen Challenge Using Turbo-Inversion Recovery-Magnitude Magnetic Resonance Imaging. *Am J Respir Crit Care Med.* 8 janv 2014;189(6):650-7.
36. Grenier P, Mourey-Gerosa I, Benali K, Brauner MW, Leung AN, Lenoir S, et al. Abnormalities of the airways and lung parenchyma in asthmatics: CT observations in 50 patients and inter- and intraobserver variability. *Eur Radiol.* 1996;6(2):199-206.
37. Lynch DA, Murphy JR, Crapo JD, Criner GJ, Galperin-Aizenberg M, Jacobson FL, et al. A combined pulmonary -radiology workshop for visual evaluation of COPD: study design, chest CT findings and concordance with quantitative evaluation. *COPD.* avr 2012;9(2):151-9.
38. Calder AD, Bush A, Brody AS, Owens CM. Scoring of chest CT in children with cystic fibrosis: state of the art. *Pediatr Radiol.* déc 2014;44(12):1496-506.
39. Moss RB, Rodman D, Spencer LT, Aitken ML, Zeitlin PL, Waltz D, et al. Repeated adeno-associated virus serotype 2 aerosol-mediated cystic fibrosis transmembrane regulator gene transfer to the lungs of patients with cystic fibrosis: a multicenter, double-blind, placebo-controlled trial. *Chest.* févr 2004;125(2):509-21.

40. Robinson TE, Goris ML, Zhu HJ, Chen X, Bhise P, Sheikh F, et al. Dornase alfa reduces air trapping in children with mild cystic fibrosis lung disease: a quantitative analysis. *Chest*. oct 2005;128(4):2327-35.
41. Müller NL, Staples CA, Miller RR, Abboud RT. « Density mask ». An objective method to quantitate emphysema using computed tomography. *Chest*. oct 1988;94(4):782-7.
42. Madani A, Zanen J, de Maertelaer V, Gevenois PA. Pulmonary emphysema: objective quantification at multi-detector row CT--comparison with macroscopic and microscopic morphometry. *Radiology*. mars 2006;238(3):1036-43.
43. Hackx M, Bankier AA, Gevenois PA. Chronic obstructive pulmonary disease: CT quantification of airways disease. *Radiology*. oct 2012;265(1):34-48.
44. Lynch DA, Al-Qaisi MA. Quantitative computed tomography in chronic obstructive pulmonary disease. *J Thorac Imaging*. sept 2013;28(5):284-90.
45. Gevenois PA, de Maertelaer V, De Vuyst P, Zanen J, Yernault JC. Comparison of computed density and macroscopic morphometry in pulmonary emphysema. *Am J Respir Crit Care Med*. août 1995;152(2):653-7.
46. Gevenois PA, De Vuyst P, de Maertelaer V, Zanen J, Jacobovitz D, Cosio MG, et al. Comparison of computed density and microscopic morphometry in pulmonary emphysema. *Am J Respir Crit Care Med*. juill 1996;154(1):187-92.
47. Bankier AA, De Maertelaer V, Keyzer C, Gevenois PA. Pulmonary emphysema: subjective visual grading versus objective quantification with macroscopic morphometry and thin-section CT densitometry. *Radiology*. juin 1999;211(3):851-8.
48. Nakano Y, Muro S, Sakai H, Hirai T, Chin K, Tsukino M, et al. Computed tomographic measurements of airway dimensions and emphysema in smokers. Correlation with lung function. *Am J Respir Crit Care Med*. sept 2000;162(3 Pt 1):1102-8.
49. Coxson HO, Dirksen A, Edwards LD, Yates JC, Agusti A, Bakke P, et al. The presence and progression of emphysema in COPD as determined by CT scanning and biomarker expression: a prospective analysis from the ECLIPSE study. *Lancet Respir Med*. avr 2013;1(2):129-36.
50. Regan EA, Hokanson JE, Murphy JR, Make B, Lynch DA, Beaty TH, et al. Genetic epidemiology of COPD (COPDGene) study design. *COPD*. févr 2010;7(1):32-43.
51. Heussel CP, Herth FJF, Kappes J, Hantusch R, Hartlieb S, Weinheimer O, et al. Fully automatic quantitative assessment of emphysema in computed tomography: comparison with pulmonary function testing and normal values. *Eur Radiol*. oct 2009;19(10):2391-402.
52. Newell JD, Sieren J, Hoffman EA. Development of quantitative computed tomography lung protocols. *J Thorac Imaging*. sept 2013;28(5):266-71.
53. Wang Z, Gu S, Leader JK, Kundu S, Tedrow JR, Sciruba FC, et al. Optimal Threshold in CT Quantification of Emphysema. *Eur Radiol*. avr 2013;23(4):975-84.

54. Dirksen A, Friis M, Olesen KP, Skovgaard LT, Sørensen K. Progress of emphysema in severe alpha 1-antitrypsin deficiency as assessed by annual CT. *Acta Radiol Stockh Swed* 1987. sept 1997;38(5):826-32.
55. Stolk J, Dirksen A, van der Lugt AA, Hutsebaut J, Mathieu J, de Ree J, et al. Repeatability of lung density measurements with low-dose computed tomography in subjects with alpha-1-antitrypsin deficiency-associated emphysema. *Invest Radiol*. nov 2001;36(11):648-51.
56. Dirksen A. Monitoring the progress of emphysema by repeat computed tomography scans with focus on noise reduction. *Proc Am Thorac Soc*. 15 déc 2008;5(9):925-8.
57. Madani A, De Maertelaer V, Zanen J, Gevenois PA. Pulmonary emphysema: radiation dose and section thickness at multidetector CT quantification--comparison with macroscopic and microscopic morphometry. *Radiology*. avr 2007;243(1):250-7.
58. Mets OM, Willeminck MJ, de Kort FPL, Mol CP, Leiner T, Oudkerk M, et al. The effect of iterative reconstruction on computed tomography assessment of emphysema, air trapping and airway dimensions. *Eur Radiol*. 1 oct 2012;22(10):2103-9.
59. Nishio M, Koyama H, Ohno Y, Negi N, Seki S, Yoshikawa T, et al. Emphysema Quantification Using Ultralow-Dose CT With Iterative Reconstruction and Filtered Back Projection. *AJR Am J Roentgenol*. juin 2016;206(6):1184-92.
60. Berger P, Perot V, Desbarats P, Tunon-de-Lara JM, Marthan R, Laurent F. Airway wall thickness in cigarette smokers: quantitative thin-section CT assessment. *Radiology*. juin 2005;235(3):1055-64.
61. Nakano Y, Wong JC, de Jong PA, Buzatu L, Nagao T, Coxson HO, et al. The prediction of small airway dimensions using computed tomography. *Am J Respir Crit Care Med*. 15 janv 2005;171(2):142-6.
62. Achenbach T, Weinheimer O, Brochhausen C, Hollemann D, Baumbach B, Scholz A, et al. Accuracy of automatic airway morphometry in computed tomography-correlation of radiological-pathological findings. *Eur J Radiol*. janv 2012;81(1):183-8.
63. Senéterre E, Paganin F, Bruel JM, Michel FB, Bousquet J. Measurement of the internal size of bronchi using high resolution computed tomography (HRCT). *Eur Respir J*. mars 1994;7(3):596-600.
64. King GG, Müller NL, Whittall KP, Xiang Q-S, Paré PD. An Analysis Algorithm for Measuring Airway Lumen and Wall Areas from High-Resolution Computed Tomographic Data. *Am J Respir Crit Care Med*. 1 févr 2000;161(2):574-80.
65. Brillet PY, Fetita CI, Beigelman-Aubry C, Saragaglia A, Perchet D, Preteux F, et al. Quantification of bronchial dimensions at MDCT using dedicated software. *Eur Radiol*. juin 2007;17(6):1483-9.
66. Montaudon M, Berger P, de Dietrich G, Braquelaire A, Marthan R, Tunon-de-Lara JM, et al. Assessment of airways with three-dimensional quantitative thin-section CT: in vitro and in vivo validation. *Radiology*. févr 2007;242(2):563-72.

67. Montaudon M, Lederlin M, Reich S, Begueret H, Tunon-de-Lara JM, Marthan R, et al. Bronchial measurements in patients with asthma: comparison of quantitative thin-section CT findings with those in healthy subjects and correlation with pathologic findings. *Radiology*. déc 2009;253(3):844-53.
68. Lederlin M, Laurent F, Dromer C, Cochet H, Berger P, Montaudon M. Mean bronchial wall attenuation value in chronic obstructive pulmonary disease: comparison with standard bronchial parameters and correlation with function. *AJR Am J Roentgenol*. avr 2012;198(4):800-8.
69. Dournes G, Laurent F, Coste F, Dromer C, Blanchard E, Picard F, et al. Computed tomographic measurement of airway remodeling and emphysema in advanced chronic obstructive pulmonary disease. Correlation with pulmonary hypertension. *Am J Respir Crit Care Med*. 1 janv 2015;191(1):63-70.
70. Montaudon M, Berger P, Cangini-Sacher A, de Dietrich G, Tunon-de-Lara JM, Marthan R, et al. Bronchial measurement with three-dimensional quantitative thin-section CT in patients with cystic fibrosis. *Radiology*. févr 2007;242(2):573-81.
71. Murphy K, Pluim JPW, van Rikxoort EM, de Jong PA, de Hoop B, Gietema HA, et al. Toward automatic regional analysis of pulmonary function using inspiration and expiration thoracic CT. *Med Phys*. mars 2012;39(3):1650-62.
72. Schroeder JD, McKenzie AS, Zach JA, Wilson CG, Curran-Everett D, Stinson DS, et al. Relationships Between Airflow Obstruction and Quantitative CT Measurements of Emphysema, Air Trapping, and Airways in Subjects With and Without Chronic Obstructive Pulmonary Disease. *Am J Roentgenol*. 23 août 2013;201(3):W460-70.
73. Matsuoka S, Kurihara Y, Yagihashi K, Hoshino M, Watanabe N, Nakajima Y. Quantitative assessment of air trapping in chronic obstructive pulmonary disease using inspiratory and expiratory volumetric MDCT. *AJR Am J Roentgenol*. mars 2008;190(3):762-9.
74. Eda S, Kubo K, Fujimoto K, Matsuzawa Y, Sekiguchi M, Sakai F. The relations between expiratory chest CT using helical CT and pulmonary function tests in emphysema. *Am J Respir Crit Care Med*. avr 1997;155(4):1290-4.
75. O'Donnell RA, Peebles C, Ward JA, Daraker A, Angco G, Broberg P, et al. Relationship between peripheral airway dysfunction, airway obstruction, and neutrophilic inflammation in COPD. *Thorax*. oct 2004;59(10):837-42.
76. Bommart S, Marin G, Bourdin A, Molinari N, Klein F, Hayot M, et al. Relationship between CT air trapping criteria and lung function in small airway impairment quantification. *BMC Pulm Med*. 28 févr 2014;14:29.
77. Galbán CJ, Han MK, Boes JL, Chughtai KA, Meyer CR, Johnson TD, et al. Computed tomography-based biomarker provides unique signature for diagnosis of COPD phenotypes and disease progression. *Nat Med*. nov 2012;18(11):1711-5.
78. Kim EY, Seo JB, Lee HJ, Kim N, Lee E, Lee SM, et al. Detailed analysis of the density change on chest CT of COPD using non-rigid registration of inspiration/expiration CT scans. *Eur Radiol*. févr 2015;25(2):541-9.

79. Arakawa H, Webb WR. Air trapping on expiratory high-resolution CT scans in the absence of inspiratory scan abnormalities: correlation with pulmonary function tests and differential diagnosis. *AJR Am J Roentgenol.* mai 1998;170(5):1349-53.
80. Bhatt SP, Soler X, Wang X, Murray S, Anzueto AR, Beaty TH, et al. Association between Functional Small Airway Disease and FEV1 Decline in Chronic Obstructive Pulmonary Disease. *Am J Respir Crit Care Med.* 15 2016;194(2):178-84.
81. Minai OA, Chaouat A, Adnot S. Pulmonary hypertension in COPD: epidemiology, significance, and management: pulmonary vascular disease: the global perspective. *Chest.* juin 2010;137(6 Suppl):39S-51S.
82. Chaouat A, Naeije R, Weitzenblum E. Pulmonary hypertension in COPD. *Eur Respir J.* 1 nov 2008;32(5):1371-85.
83. Said SI, Hamidi SA, Bosc LG. Asthma and pulmonary arterial hypertension: do they share a key mechanism of pathogenesis? *Eur Respir J.* 1 avr 2010;35(4):730-4.
84. Rydell-Törmänen K, Uller L, Erjefält JS. Remodeling of extra-bronchial lung vasculature following allergic airway inflammation. *Respir Res.* 2008;9(1):18.
85. Rydell-Törmänen K, Uller L, Erjefält JS. Allergic Airway Inflammation Initiates Long-Term Vascular Remodeling of the Pulmonary Circulation. *Int Arch Allergy Immunol.* 2009;149(3):251-8.
86. Vonk-Noordegraaf A, Haddad F, Chin KM, Forfia PR, Kawut SM, Lumens J, et al. Right heart adaptation to pulmonary arterial hypertension: physiology and pathobiology. *J Am Coll Cardiol.* 24 déc 2013;62(25 Suppl):D22-33.
87. Ando K, Kuraishi H, Nagaoka T, Tsutsumi T, Hoshika Y, Kimura T, et al. Potential Role of CT Metrics in Chronic Obstructive Pulmonary Disease with Pulmonary Hypertension. *Lung.* déc 2015;193(6):911-8.
88. Coste F, Dournes G, Dromer C, Blanchard E, Freund-Michel V, Girodet P-O, et al. CT evaluation of small pulmonary vessels area in patients with COPD with severe pulmonary hypertension. *Thorax.* 2016;71(9):830-7.
89. Ma J, Yu N, Shen C, Wang Z, He T, Guo Y-M. A three-dimensional approach for identifying small pulmonary vessels in smokers. *J X-Ray Sci Technol.* 2017;25(3):391-402.
90. Wells JM, Iyer AS, Rahaghi FN, Bhatt SP, Gupta H, Denney TS, et al. Pulmonary Artery Enlargement is Associated with RV Dysfunction and Loss of Blood Volume in Small Pulmonary Vessels in Chronic Obstructive Pulmonary Disease. *Circ Cardiovasc Imaging* [Internet]. avr 2015;8(4). Disponible sur: <https://www.ncbi.nlm.nih.gov/pmc/articles/PMC4392846/>
91. Washko GR, Nardelli P, Ash SY, Vegas Sanchez-Ferrero G, Rahaghi FN, Come CE, et al. Arterial Vascular Pruning, Right Ventricular Size, and Clinical Outcomes in Chronic Obstructive Pulmonary Disease. A Longitudinal Observational Study. *Am J Respir Crit Care Med.* 15 août 2019;200(4):454-61.

92. Ash SY, Rahaghi FN, Come CE, Ross JC, Colon AG, Cardet-Guisasola JC, et al. Pruning of the Pulmonary Vasculature in Asthma. The Severe Asthma Research Program (SARP) Cohort. *Am J Respir Crit Care Med.* 1 juill 2018;198(1):39-50.
93. Matsuoka S, Washko GR, Dransfield MT, Yamashiro T, San Jose Estepar R, Diaz A, et al. Quantitative CT measurement of cross-sectional area of small pulmonary vessel in COPD: correlations with emphysema and airflow limitation. *Acad Radiol.* janv 2010;17(1):93-9.
94. Scharf SM, Iqbal M, Keller C, Criner G, Lee S, Fessler HE, et al. Hemodynamic characterization of patients with severe emphysema. *Am J Respir Crit Care Med.* 1 août 2002;166(3):314-22.
95. Blanco I, Piccari L, Barberà JA. Pulmonary vasculature in COPD: The silent component. *Respirol Carlton Vic.* 2016;21(6):984-94.
96. Matsuoka S, Washko GR, Yamashiro T, Estepar RSJ, Diaz A, Silverman EK, et al. Pulmonary hypertension and computed tomography measurement of small pulmonary vessels in severe emphysema. *Am J Respir Crit Care Med.* 1 févr 2010;181(3):218-25.
97. Iyer AS, Wells JM, Vishin S, Bhatt SP, Wille KM, Dransfield MT. CT Scan-Measured Pulmonary Artery to Aorta Ratio and Echocardiography for Detecting Pulmonary Hypertension in Severe COPD. *Chest.* avr 2014;145(4):824-32.
98. Wells JM, Farris RF, Gosdin TA, Dransfield MT, Wood ME, Bell SC, et al. Pulmonary artery enlargement and cystic fibrosis pulmonary exacerbations: a cohort study. *Lancet Respir Med.* août 2016;4(8):636-45.
99. Coste F, Benlala I, Dournes G, Girodet P-O, Laurent F, Berger P. Assessing pulmonary hypertension in COPD. Is there a role for computed tomography? *Int J Chron Obstruct Pulmon Dis.* 2019;14:2065-79.
100. Ma W, Sheikh K, Svenningsen S, Pike D, Guo F, Etemad-Rezai R, et al. Ultra-short echo-time pulmonary MRI: evaluation and reproducibility in COPD subjects with and without bronchiectasis. *J Magn Reson Imaging JMRI.* mai 2015;41(5):1465-74.
101. Zhang W-J, Hubbard Cristinacce PL, Bondesson E, Nordenmark LH, Young SS, Liu Y-Z, et al. MR Quantitative Equilibrium Signal Mapping: A Reliable Alternative to CT in the Assessment of Emphysema in Patients with Chronic Obstructive Pulmonary Disease. *Radiology.* 7 janv 2015;275(2):579-88.
102. Roach DJ, Crémillieux Y, Serai SD, Thomen RP, Wang H, Zou Y, et al. Morphological and quantitative evaluation of emphysema in chronic obstructive pulmonary disease patients: A comparative study of MRI with CT. *J Magn Reson Imaging JMRI.* 2016;44(6):1656-63.
103. Meier-Schroers M, Sprinkart AM, Becker M, Homsy R, Thomas D. Quantitative and Qualitative Assessment of Pulmonary Emphysema with T2-Weighted PROPELLER MRI in a High-Risk Population Compared to Low-Dose CT. *RöFo - Fortschritte Auf Dem Geb Röntgenstrahlen Bildgeb Verfahr.* août 2018;190(08):733-9.

104. Benlala I, Laurent F, Dournes G. T2-weighted PROPELLER MRI is not suitable for pulmonary emphysema quantification. *ROFO Fortschr Geb Rontgenstr Nuklearmed.* 2018;190(12):1169-70.
105. Pennati F, Quirk JD, Yablonskiy DA, Castro M, Aliverti A, Woods JC. Assessment of Regional Lung Function with Multivolume 1H MR Imaging in Health and Obstructive Lung Disease: Comparison with 3He MR Imaging. *Radiology.* 15 juin 2014;273(2):580-90.
106. Pennati F, Roach DJ, Clancy JP, Brody AS, Fleck RJ, Aliverti A, et al. Assessment of pulmonary structure–function relationships in young children and adolescents with cystic fibrosis by multivolume proton-MRI and CT. *J Magn Reson Imaging.* 2018;48(2):531-42.
107. Nyilas S, Bauman G, Sommer G, Stranzinger E, Pusterla O, Frey U, et al. Novel magnetic resonance technique for functional imaging of cystic fibrosis lung disease. *Eur Respir J.* 1 déc 2017;50(6):1701464.
108. Thomen RP, Walkup LL, Roach DJ, Cleveland ZI, Clancy JP, Woods JC. Hyperpolarized 129Xe for investigation of mild cystic fibrosis lung disease in pediatric patients. *J Cyst Fibros Off J Eur Cyst Fibros Soc.* mars 2017;16(2):275-82.
109. Altes TA, Mugler JP, Ruppert K, Tustison NJ, Gersbach J, Szentpetery S, et al. Clinical correlates of lung ventilation defects in asthmatic children. *J Allergy Clin Immunol.* mars 2016;137(3):789-796.e7.
110. Woods JC, Choong CK, Yablonskiy DA, Bentley J, Wong J, Pierce JA, et al. Hyperpolarized 3He diffusion MRI and histology in pulmonary emphysema. *Magn Reson Med.* 2006;56(6):1293-300.
111. Ley S, Zaporozhan J, Morbach A, Eberle B, Gast K, Heussel C, et al. Functional Evaluation of Emphysema Using Diffusion-Weighted 3Helium-Magnetic Resonance Imaging, High-Resolution Computed Tomography, and Lung Function Tests. *Invest Radiol.* juill 2004;39(7):427-34.
112. McMahon CJ, Dodd JD, Hill C, Woodhouse N, Wild JM, FICHELE S, et al. Hyperpolarized 3helium magnetic resonance ventilation imaging of the lung in cystic fibrosis: comparison with high resolution CT and spirometry. *Eur Radiol.* nov 2006;16(11):2483-90.
113. Ohno Y, Hatabu H, Takenaka D, Van Cauteren M, Fujii M, Sugimura K. Dynamic oxygen-enhanced MRI reflects diffusing capacity of the lung. *Magn Reson Med.* juin 2002;47(6):1139-44.
114. Jobst BJ, Triphan SMF, Sedlacek O, Anjorin A, Kauczor HU, Biederer J, et al. Functional lung MRI in chronic obstructive pulmonary disease: comparison of T1 mapping, oxygen-enhanced T1 mapping and dynamic contrast enhanced perfusion. *PloS One.* 2015;10(3):e0121520.
115. Bauman G, Scholz A, Rivoire J, Terekhov M, Friedrich J, de Oliveira A, et al. Lung ventilation- and perfusion-weighted Fourier decomposition magnetic resonance imaging:

- in vivo validation with hyperpolarized  $^3\text{He}$  and dynamic contrast-enhanced MRI. *Magn Reson Med.* janv 2013;69(1):229-37.
116. Zhang W-J, Niven RM, Young SS, Liu Y-Z, Parker GJM, Naish JH. T1-weighted Dynamic Contrast-enhanced MR Imaging of the Lung in Asthma: Semiquantitative Analysis for the Assessment of Contrast Agent Kinetic Characteristics. *Radiology.* mars 2016;278(3):906-16.
  117. Reiter U, Reiter G, Fuchsjäger M. MR phase-contrast imaging in pulmonary hypertension. *Br J Radiol.* juill 2016;89(1063):20150995.
  118. Coste F, Benlala I, Dournes G, Dromer C, Blanchard E, Girodet P-O, et al. Quantitative CT assessment of bronchial and vascular alterations in severe precapillary pulmonary hypertension. *Int J Chron Obstruct Pulmon Dis.* 2019;14:381-9.
  119. Seeger W, Adir Y, Barberà JA, Champion H, Coghlan JG, Cottin V, et al. Pulmonary hypertension in chronic lung diseases. *J Am Coll Cardiol.* 24 déc 2013;62(25 Suppl):D109-116.
  120. Chaouat A, Bugnet A-S, Kadaoui N, Schott R, Enache I, Ducloné A, et al. Severe pulmonary hypertension and chronic obstructive pulmonary disease. *Am J Respir Crit Care Med.* 15 juill 2005;172(2):189-94.
  121. van den Berge M, Ten Hacken NHT, Cohen J, Douma WR, Postma DS. Small airway disease in asthma and COPD: clinical implications. *Chest.* févr 2011;139(2):412-23.
  122. Tatsis G, Kotsifas K, Filaditaki V, Makrantonis G, Bouliou S. Efficacy of beclomethasone dipropionate HFA 200 microg once daily in chronic obstructive pulmonary disease and bronchial asthma. *J Int Med Res.* juin 2007;35(3):361-73.
  123. Hub M, Karger CP. Estimation of the uncertainty of elastic image registration with the demons algorithm. *Phys Med Biol.* 7 mai 2013;58(9):3023-36.
  124. Small JH, Flower CD, Traill ZC, Gleeson FV. Air-trapping in extrinsic allergic alveolitis on computed tomography. *Clin Radiol.* oct 1996;51(10):684-8.
  125. Zúñiga SG, Hernández JS, Toledo HM, Ávila MM, Gochicoa-Rangel L, Reyes JLM, et al. Small airway dysfunction in chronic hypersensitivity pneumonitis. *Respirology.* 2017;22(8):1637-42.
  126. Austin JH, Müller NL, Friedman PJ, Hansell DM, Naidich DP, Remy-Jardin M, et al. Glossary of terms for CT of the lungs: recommendations of the Nomenclature Committee of the Fleischner Society. *Radiology.* août 1996;200(2):327-31.
  127. Oguma T, Niimi A, Hirai T, Jinnai M, Matsumoto H, Ito I, et al. Assessment of Small Airways with Computed Tomography: Mosaic Attenuation or Lung Density? *Respir Int Rev Thorac Dis.* 2015;89(6):539-49.
  128. Dournes G, Yazbek J, Benhassen W, Benlala I, Blanchard E, Truchetet M-E, et al. 3D ultrashort echo time MRI of the lung using stack-of-spirals and spherical k-Space coverages: Evaluation in healthy volunteers and parenchymal diseases. *J Magn Reson Imaging JMRI.* 2018;48(6):1489-97.

129. Benlala I, Berger P, Girodet P-O, Dromer C, Macey J, Laurent F, et al. Automated Volumetric Quantification of Emphysema Severity by Using Ultrashort Echo Time MRI: Validation in Participants with Chronic Obstructive Pulmonary Disease. *Radiology*. juill 2019;292(1):216-25.
130. Alamidi DF, Kindvall SSI, Hubbard Cristinacce PL, McGrath DM, Young SS, Naish JH, et al. T1 Relaxation Time in Lungs of Asymptomatic Smokers. *PLoS ONE* [Internet]. 9 mars 2016;11(3). Disponible sur: <https://www.ncbi.nlm.nih.gov/pmc/articles/PMC4784914/>
131. Alamidi DF, Morgan AR, Hubbard Cristinacce PL, Nordenmark LH, Hockings PD, Lagerstrand KM, et al. COPD Patients Have Short Lung Magnetic Resonance T1 Relaxation Time. *COPD*. 2016;13(2):153-9.
132. Wielpütz MO, Puderbach M, Kopp-Schneider A, Stahl M, Fritzsching E, Sommerburg O, et al. Magnetic resonance imaging detects changes in structure and perfusion, and response to therapy in early cystic fibrosis lung disease. *Am J Respir Crit Care Med*. 15 avr 2014;189(8):956-65.
133. Benlala I, Hocke François, Macey J, BUI stéphanie, Berger P, Laurent F, et al. Quantification of MRI T2 High Signal Volume in Cystic Fibrosis: A Pilot Study. *Radiology* [Internet]. Disponible sur: <https://doi.org/10.1148/radiol.2019190797>